



**DEVELOPMENT OF A NOVEL
SINGLE INPUT BI-DIRECTIONAL CANNULA
FOR EXTRACORPOREAL MEMBRANE OXYGENATION**

By

Anon Jantanukul

**This thesis is submitted in partial fulfilment of the requirements for
the degree of Doctor of Philosophy in Biomedical Engineering**

Department of Biomedical Engineering

University of Strathclyde

2024

DECLARATION

This thesis is the result of the author's original research. It has been composed by the author and has not been previously submitted for examination, which has led to the award of a degree.

The copyright of this thesis belongs to the author under the terms of the United Kingdom Copyright Acts as qualified by University of Strathclyde Regulation 3.50. Due acknowledgement must always be made of the use of any material contained in, or derived from, this thesis.

Signed:

A handwritten signature in black ink, appearing to be 'G. J. ...' with a flourish at the end.

Date: ~~10 December 2022~~

ABSTRACT

Backgrounds: Arterial cannulation for peripheral veno-arterial extracorporeal membrane oxygenation (VA-ECMO) causes a risk of disrupting blood flow, which can lead to neurological injury or limb ischaemia. The current arterial bi-directional cannula presents risks for both haematological and vascular injury. This study aims to develop a new bi-directional cannula designed for improving perfusion and reducing associated complications.

Methods: Six bi-directional cannulae were tested, each with a primary diameter of 4.33 millimetre (mm) and a secondary distal lumen of 1.80 mm, had three radius curve (R) features (1.40 mm: 1st iteration, 1.00 mm: 2nd iteration, and 0.85 mm: 3rd iteration, respectively), and three underpart features (sinus: 4th iteration, ramp: 5th iteration, and sinus-ramp: 6th iteration, respectively). These cannulae were evaluated with computational fluid dynamics (CFD) to characterise blood flow and wall shear stress (WSS), dye and particle tracking to visualise flow, haemodynamic performance to identify pressure-flow relationship and volume distribution, and haematological response to define blood components depletion and haemolysis status.

Results: In CFD, there were no differences in the flow path regarding the primary lumen outflow. Secondary lumen flow of 1st iteration was found to direct flow to the vessel wall with highest WSS. Others improved flow and reduced WSS impacts, especially in 6th iteration. Dye injection showed a symmetrical, central flow trajectory in 2nd, 5th, and 6th iteration. Furthermore, particle tracking verified this in 2nd and 6th iterations. Pressure-flow relationship found that at 3 LPM provided pressure gradient less than 100 mmHg in all cannulae. Volume flow distribution, the 6th iteration showed higher output volumes at secondary lumen than 1st and 2nd iteration. The red blood cells, haemoglobin, white blood cells and platelets in all groups had decreased. Notably 2nd iteration was superior result in haemolysis analysis as significant lower plasma-free haemoglobin, and normalised index of haemolysis.

Conclusion: Findings of the *in-silico* and *in-vitro* experiments indicate that the 2nd and 6th iterations effectively demonstrated to centreline and lower risk of jet impact to vessel wall. Additionally, 2nd iteration demonstrate possibility of improving arterial cannulation in peripheral VA-ECMO as shown in haematological evidence.

Keywords: ECMO, Limb ischemia, Bi-directional cannula, Distal perfusion

ACKNOWLEDGMENTS

A PhD during the COVID-19 pandemic was challenging. This journey would not have been possible and would not have succeeded without the invaluable help of many people.

First and foremost, I would like to express my appreciation to Professor Terry Gourlay, my advisor, for his suggestions and encouragement during this project. I also express my thankfulness to the second supervisor, Dr Craig Robertson, for his assistance in the laboratory and for his valuable guidance. I also thank Dr Monica Kerr for her suggestion on CFD and all colleagues at the Wolfson Centre for their technical assistance.

I am grateful for PhD funding from Chulabhorn International College of Medicine (CICM), Thammasat University, Thailand. Thanks to my colleagues at the Department of Cardiovascular and Thoracic Technology for their hard work during my study periods.

I sincerely thank my family, especially my wife and son, Poy and Pau, for their understanding, patience, and support throughout this journey.

this study is dedicated to my patients, 'the great teacher'.

Anon Jantanukul

CONTENTS

DECLARATION	i
ABSTRACT	ii
ACKNOWLEDGMENTS	iv
CONTENTS	v
LIST OF FIGURES	ix
LIST OF TABLES	xiv
LIST OF ABBREVIATIONS	xv
CHAPTER 1 LITERATURE REVIEW.....	1
1.1 INTRODUCTION	1
1.2 BRIEF HISTORY OF ECMO.....	3
1.3 PRINCIPLE OF ECMO.....	11
1.3.1 Type of ECMO	11
1.3.2 Indication and Contraindication.....	12
1.3.3 Circuit Components	15
1.4 ECMO CANNULATION.....	22
1.4.1 Central Cannulation	25
1.4.2 Peripheral Cannulation	27
1.5 BLOOD FLOW AND OXYGEN DELIVERY BY ECMO.....	31
1.6 OVERALL COMPLICATIONS IN ECMO	33
1.7 CANNULATION-RELATED VASCULAR COMPLICATIONS IN PERIPHERAL ECMO	35
1.7.1 Carotid artery cannulation and neurological complications	36
1.7.2 Femoral cannulation and limb ischemia	37
1.8 CURRENT CANNULATION TECHNIQUES TO SUPPORT DISTAL PERFUSION	38
1.8.1 Modified T-graft	38
1.8.2 Distal perfusion.....	40
1.8.3 Small arterial cannula	41

1.9 THE BI-DIRECTIONAL CANNULA	43
1.9.1 Self-expanding bi-directional cannula	43
1.9.2 Bi-directional cannula with the side hole	45
1.10 CHAPTER SUMMARY	51
CHAPTER 2 THESIS AIMS AND OBJECTIVES	54
2.1 CLINICAL RATIONALE	54
2.2 HYPOTHESIS AND OBJECTIVES	55
CHAPTER 3 BI-DIRECTIONAL ARTERIAL CANNULAE DESIGN	58
3.1 INTRODUCTION	58
3.2 THE 1 ST ITERATION	60
3.2.1 MATERIALS AND METHODS	62
3.2.2 RESULTS	66
3.2.3 The 1 st ITERATION SUMMARY	68
3.3 CHANGING THE SECONDARY LUMEN RADIANT CURVE	69
3.3.1 MATERIALS AND METHODS	69
3.3.2 RESULTS	71
3.3.3 SECOND AND THIRD ITERATION SUMMARY	73
3.4 CHANGING UNDERPART OF THE SECONDARY LUMEN	74
3.4.1 MATERIALS AND METHODS	74
3.4.2 RESULTS	78
3.4.3 4 th , 5 th and 6 th ITERATIONS SUMMARY	81
3.5 WALL SHEAR STRESS AND FLOW	82
3.5.1 MATERIALS AND METHODS	82
3.5.2 RESULTS	83
3.6 CHAPTER SUMMARY	86
CHAPTER 4 FLOW VISUALISATION	88
4.1 INTRODUCTION	88
4.2 DYE INJECTION	91
4.2.1 MATERIALS AND METHODS	91

4.2.2 RESULTS	97
4.3. PARTICLE TRACKING.....	104
4.3.1 MATERIALS AND METHODS	104
4.3.2 RESULTS	109
4.4 CFD VALIDATION.....	113
4.4.1 MATERIALS AND METHODS	113
4.4.2 RESULTS	114
4.5 LIMITATIONS	117
4.6 CHAPTER SUMMARY	118
CHAPTER 5 PRESSURE-FLOW PROPERTIES.....	120
5.1 INTRODUCTION	120
5.2 PRESSURE-FLOW MEASUREMENT.....	121
5.2.1 MATERIAL AND METHODS.....	121
5.2.2 RESULTS	127
5.3 VOLUMETRIC MEASUREMENT	130
5.3.1 MATERIAL AND METHODS.....	130
5.3.2 RESULTS	131
5.4 CHAPTER SUMMARY	134
CHAPTER 6 HAEMATOLOGICAL RESPONSES	136
6.1 INTRODUCTION	136
6.2 MATERIALS AND METHODS.....	137
6.3 RESULTS	146
6.4 LIMITATIONS	153
6.5 CHAPTER SUMMARY	153
CHAPTER 7 DISCUSSION	155
7.1 INTRODUCTION	155
7.2 CFD SERVES AS A TOOL IN THE DESIGN PROCESS	156
7.3 VALIDATION DESIGN WITH FLOW VISUALISATION	159

7.4 HAEMODYNAMIC MEASUREMENT TO ASSESS THE PERFORMANCE OF THE CANNULA.....	162
7.5 HAEMATOLOGICAL RESPONSE TO BLOOD HANDLING TEST	165
CHAPTER 8 CONCLUSION AND FUTURE WORK	168
8.1 CONCLUSION	168
8.2 LIMITATIONS	168
8.3 FUTURE WORK.....	169
REFERENCES.....	171

LIST OF FIGURES

Figure 1.1 Comparison of CPB (a) and ECMO (b) circuit components.	2
Figure 1.2 DG Melrose performs his heart-lung machine as a prolonged circulatory support in the intensive care unit.	6
Figure 1.3 Silicone membrane oxygenator.	8
Figure 1.4 International Summary of Statistics: The number of ECMO Centre and cases that register to ELSO from 2009 to 2022.	10
Figure 1.5 Diagram of VA-ECMO parallel with native circulation.	11
Figure 1.6 Diagram of Venovenous ECMO and right-side heart.	12
Figure 1.7 Components and blood flow of ECMO circulation.	16
Figure 1.8 Illustrate access or venous cannula.	18
Figure 1.9 Return or arterial cannula.	19
Figure 1.10 Blood pump for extracorporeal circulation.	20
Figure 1.11 Portable ECMO system designed for use in ambulances or helicopters.	20
Figure 1.12 The structure of oxygenator and hollow fibre membrane.	21
Figure 1.13 The common cannulation approaches for ECMO.	23
Figure 1.14 The central cannulation approaches for ECMO.	26
Figure 1.15 Neck cannulation for VA-ECMO.	28
Figure 1.16 Axillary artery cannulation.	28
Figure 1.17 Femoro-femoral VA-ECMO cannulation.	29
Figure 1.18 Percutaneous cannulation approach by Seldinger's technique.	31
Figure 1.19 Cannulation approach to carotid artery in VA-ECMO.	36
Figure 1.20 Arterial cannula inserted in the femoral artery.	37

Figure 1.21 Illustration of cannulation performed by the T-graft technique.	39
Figure 1.22 Distal perfusion technique.	40
Figure 1.23 Clot formation in distal perfusion technique.	41
Figure 1.24 Self-expanding bi-directional cannula.	44
Figure 1.25 Circumferential side holes bi-directional cannula.	45
Figure 1.26 Side holes bi-directional cannula.	46
Figure 1.27 Bi-flow, commercial bi-directional cannula by Liva-Nova™.	47
Figure 1.28 Internal structure of the bi-directional cannula designed by Prof. T Gourlay	49
Figure 2.1 The algorithm to determine the conceptual framework of this study.	57
Figure 3.1 Illustrated the structure of a bi-directional cannula (1 st iteration cannula).	61
Figure 3.2 Cannula in the vascular structure for the CFD test.	63
Figure 3.3 Vascular mesh generation for the CFD test with the near wall inflation layers.	64
Figure 3.4 Grid-independent tests (GIT) for mesh generation.	64
Figure 3.5 Flow path and velocity magnitude of 1 st iteration cannula.	66
Figure 3.6 Wall Shear stress at the inferior vessel wall from 1 st iteration cannula.	67
Figure 3.7 The wall shears values from the outflow of secondary lumens.	67
Figure 3.8 Wall Shear at the superior vessel wall from the bi-directional cannula, 1 st iteration cannula.	68
Figure 3.9 Internal structure of 2 nd and 3 rd iteration.	70
Figure 3.10 Streamline and magnitude across of flow velocity of 2 nd and 3 rd iteration.	71
Figure 3.11 The shear stress from blood distribution to the inferior wall vessel.	72
Figure 3.12 The superior wall shear stress from 2 nd and 3 rd iteration.	73

Figure 3.13	The underpart of the secondary lumen for adjusted to 4-6 iterations.	75
Figure 3.14	Illustrated the underpart in the ramp cannula (4 th iteration).	76
Figure 3.15	Diagram of the secondary lumen of the sinus cannula (5 th iteration).	76
Figure 3.16	The underpart of the secondary outlet 6 th iteration.	77
Figure 3.17	Flow path and velocity magnitude across the 4 th iteration.	78
Figure 3.18	Flow path and velocity magnitude across the 5 th iteration.	78
Figure 3.19	Flow path and velocity magnitude across the 6 th iteration.	79
Figure 3.20	The shear stress from blood distribution to the inferior wall vessel.	80
Figure 3.21	The shear stress from blood distribution to the superior wall vessel.	81
Figure 3.22	Wall shear measurement from both outlets.	82
Figure 3.23	Inferior wall shear stress measured from the secondary lumen.	83
Figure 3.24	Inferior wall shear stress measured from the primary lumen.	84
Figure 3.25	Cross-sectional flow velocity at the secondary lumen.	85
Figure 3.26	3D print of all cannula version prototypes.	87
Figure 4.1	Dye and particle dislodgment patterns from the different cannulae tips.	89
Figure 4.2	Illustrated vectors of flow pattern and velocity mapping from PIV.	90
Figure 4.3	Calibration of a roller pump using volumetric measurement.	91
Figure 4.4	Illustrated the water volumetric measure from 0.5-6 LPM and pump speed.	92
Figure 4.5	Schematic of experimental circuit for dye injection.	93
Figure 4.6	Illustrated dye injection experiment set up.	94
Figure 4.7	Measurement of dye distribution, upper (α) and lower (β) angles of central line contours.	96
Figure 4.8	The dye visualisation in the 1 st iteration cannula.	97

Figure 4.9 The dye visualisation in the 2 nd iteration.	98
Figure 4.10 The dye distribution visualised in the 3 rd iteration.	99
Figure 4.11 The dye visualisation in the ramp version (4 th iteration).	100
Figure 4.12 The dye visualisation in the 5 th iteration.	101
Figure 4.13 The dye visualisation in the 6 th iteration.	102
Figure 4.14 Prototype cannula aligned with an acrylic square tube.	105
Figure 4.15 Schematic of set up for particle tracking experiments.	106
Figure 4.16 Illustrated the set up for particle tracking experiments.	107
Figure 4.17 Calibration ruler for particle tracking analysis.	109
Figure 4.18 Velocity magnitude and vector field at secondary lumen of the 1 st iteration cannula.	110
Figure 4.19 Velocity magnitude and vector field at secondary lumen of the R 1.00 version.	110
Figure 4.20 Velocity magnitude and vector field at secondary lumen of the R 0.85 version.	111
Figure 4.21 Velocity magnitude and vector field at secondary lumen of the ramp version.	111
Figure 4.22 Velocity magnitude and vector field at secondary lumen of the sinus version.	112
Figure 4.23 Velocity magnitude and vector field at secondary lumen of the sinus-ramp version.	112
Figure 4.24 Indicated the plane for the velocity measurement in CFD and particle tracking.	113
Figure 4.25 Compared the Velocity ratio (V_x/V_{max}) at centreline (D/2).....	115
Figure 4.26 Compared the Velocity ratio (V_x/V_{max}) at near inferior line (D/5).....	115

Figure 4.27 Comparison of flow magnitude in CFD and flow visualization.....	116
Figure 4.28 Comparison of the picture of particle shape in 0.5 vs. 4.0 LPM.	117
Figure 5.1 Cable tie to prevent leakage.....	122
Figure 5.2 Schematic and assembly of the experiment set up in pressure-flow relation.	123
Figure 5.3 The experiment set up with BioPac system.....	124
Figure 5.4 Illustrated calibration and dynamic pressure wave.....	125
Figure 5.5 Pressure and flow relationship.....	127
Figure 5.6 Pressure gradient of all prototypes compared with 1 st iteration cannula.	128
Figure 5.7 Calculated M-number of all prototypes compared with 1 st iteration cannula.	129
Figure 5.8 Schematic and assembly of volumetric measurements circuit.	130
Figure 5.9 The experiment was set up to measure the actual volume of both outlets. ...	131
Figure 5.10 Volume output from the primary lumen compared with 1 st iteration cannula.	132
Figure 5.11 Volume output from the secondary lumen compared with the 1 st iteration cannula.....	133
Figure 6.1 Circuit diagram for haematological test.	139
Figure 6.2 Circuit preparation for haematological test.	140
Figure 6.3 Blood-based priming solution.	141
Figure 6.4 Illustrated blood sample collection and preparation process.	142
Figure 6.5 Spectrophotometer and 96 well plate.	143
Figure 6.6 Red blood cell depletion over 30 min under four protocols.	146
Figure 6.7 Depletion of haemoglobin over 30 min under four protocols.	147

Figure 6.8 Depletion of white blood cells over 30 min under four protocols.....	148
Figure 6.9 Depletion of platelets over 30 min under four protocols.....	149
Figure 6.10 Compared the haemolysed plasma colour.	150
Figure 6.11 Compared the haemolysed in plasma.	151
Figure 6.12 Compared the normalised index of haemolysis.....	152

LIST OF TABLES

Table 1.1 ECMO survival rate (Per 1000 ECMO Hours), 2017–2022.	10
Table 1.2 Indication for cardiac ECMO.	13
Table 1.3 Indication for respiratory ECMO.	14
Table 1.4 Contraindication of ECMO.	15
Table 1.5 The essential features of cannulas.	17
Table 1.6 Characteristics of commercial cannulae for ECMO.	24
Table 1.7 ECMO Complications (Per 1000 ECMO Hours), 2017–2022.	34
Table 1.8 Demonstrate Cannulation-Related Complication and Survival Rate.	35
Table 1.9 Summary of current techniques for distal perfusion.	42
Table 1.10 Summary of current design in bi-directional cannula.	50
Table 3.1 Summary of the 1 st iteration canula.	69
Table 3.2 Summary of the 2 nd and 3 rd iteration.	74
Table 3.3 Summary of the 4 th , 5 th , and 6 th iteration.	82
Table 4.1 Comparison of the ratio of the upper (α) and lower (β) angles of the dye distribution at secondary lumen.	103
Table 4.2 Correlation of velocity measured in CFD and PIV at D/2 and D/5.	114

LIST OF ABBREVIATIONS

3D	3-Dimension
a.	Artery
AHA	American Heart Association
AMI	Acute Myocardial Infraction
ANOVA	Analysis of Variance
AOI	Age-Adjusted Oxygenation Index
APSS	Acute Physiology of Stroke Score
ASTM	American Society for Testing and Materials
BF	Blood Flow
BSA	Body Surface Area
CDH	Congenital Diaphragmatic Hernia
CESAR	Conventional Ventilatory Support Versus Extracorporeal Membrane Oxygenation for Severe Adult Respiratory Failure
CFD	Computational Fluid Dynamics
CHF	Congestive Heart Failure
CI	Cardiac Index
CLAHE	Contrast Limited Adaptive Histogram Equalization
CNS	Central Nervous System
CO	Cardiac Output
CO ₂	Carbon Dioxide
COVID	Corona Virus Disease
CPB	Cardiopulmonary Bypass
CT	Computed Tomography
dL	Decilitre
DO ₂	Oxygen Delivery
ECC	Extracorporeal Circuit
ECLS	Extracorporeal Life Support

ECMO	Extracorporeal Membrane Oxygenation
ECPR	Extracorporeal Cardiopulmonary Resuscitation
EDTA	Ethylenediaminetetraacetic Acid
EEG	Electroencephalogram
ELSO	Extracorporeal Life Support Organisation
FFT	Fast Fourier Transform
FiO ₂	Fraction Of Inspired Oxygen
FPS	Frames Per Second
GI	Gastrointestinal
GIT	Grid-Independent Tests
Hb	Haemoglobin
Hct	Haematocrit
IABP	Intraaortic Pump
ID	Internal Diameter
IVC	Inferior Vena cava
kg/m ³	Kilogram Per Cubic Metre
kg/m-s	Kilogram Per Meter-Second
kg/s	Kilogram Per Second
LA	Left Atrium
LED	Light-Emitting Diode
LPM	Litre Per Minute
LV	Left Ventricle
m/s	Matre Per Second
m ²	Square Metre
MAS	Meconium Aspiration Syndrome
MCS	Mechanical Circulatory Support
mg	Milligram
mg/dl	Milligrams Per Decilitre
mg/L	Milligram Per Litre

ml/min	Millilitre/minute
mm	Millimetre
mmHg	Millimetre of Mercury
MRI	Magnetic Resonance Imaging
Nd:YAG	Neodymium-doped yttrium aluminium garnet
NIH	Normalised index of haemolysis
O ₂	Oxygen
°C	Degree Celsius
OD	Outer Diameter
OI	Oxygenation Index
Pa	Pascals
PaO ₂	Partial Pressure of Oxygen in the Arterial Blood
PFH	Plasma-Free Haemoglobin
PIV	Particle Image Velocimetry
PLT	Platelet
PMP	Polymethyl Pentene
PP	Polypropylene
PTV	Particle Tracking Velocimetry
PVC	Polyvinyl Chloride
px	Pixels
RA	Right Atrium
RBC	Red Blood Cell
ROI	Region of Interest
RV	Right Ventricle
SaO ₂	Oxygen Saturation
SD	Standard Deviation
SIMPLE	Semi-Implicit Method for Pressure-Linked Equations
SST	Shear Stress Transport Turbulent
SVC	Superior Vena cava

US	Ultrasound
VA-ECMO	Venoarterial Extracorporeal Membrane Oxygenation
VV-ECMO	Venovenous Extracorporeal Membrane Oxygenation
WBC	White Blood Cell
WSS	Wall Shear Stress
μm	Micron

CHAPTER 1

LITERATURE REVIEW

1.1 INTRODUCTION

Extracorporeal membrane oxygenation (ECMO) is the deployment of artificial circulation technology that takes over the heart and lungs, to permit adequate perfusion and gas exchange for patients with cardiorespiratory failure. This procedure is also recognised as extracorporeal life support (ECLS) and mechanical circulatory support for resuscitation or extracorporeal cardiopulmonary resuscitation (ECPR) (Guglin et al., 2019; Makdisi & Wang, 2015).

Extracorporeal membrane oxygenation vs Cardiopulmonary bypass

The main components of cardiopulmonary bypass (CPB) and ECMO are similar as they consist of the drainage (or venous, or access) cannula, blood pump, membrane oxygenator, heat exchanger, and return (or arterial) cannula, all connected by a tubing system. CPB is used for short term deployment, whereas ECMO can be used for more than two weeks. The CPB circuit can be combined with the delivery set for cardioplegia, venting system, suction system, and venous reservoir, while these components can be excluded in ECMO (Gehrmann et al., 2015; Punjabi & Taylor, 2013).

The CPB procedure aims to support the patient undergo cardiac surgery. Pumpless heart in cardiac surgery is induced by providing the cardioplegic solution. The arrested heart can be reduced metabolism demand in the myocardium and avoiding excessive blood on the surgical view. Also, the CPB circuit is usually an open extracorporeal circuit that blood to drain to the reservoir by the siphoning effect. The venous reservoir ‘made from a hard-shell container’ is the main component that plays role to eliminate air bubbles and debris that enter the circuit from the venous drainage line and excessive volume from venting and suction pumps. In addition, the arterial filter is applied to CPB which aims to filtrating microbubble and clot before return to patient (Ailawadi & Zacour, 2009).

In contrast, the ECMO is a continued supporting circulation without stop cardiac contraction. The flow runs through the closed circuit without siphoning effect. Therefore, unnecessary components used in CPB which are cardioplegic delivery system, arterial filter, and hardshell venous reservoir have been excluded from circuit. Because the complexity of the circuit is possibly related to mechanical complications, inflammatory response, thromboembolism, and air embolism. However, the main feature of the circuit remains requires specific equipment, material, and procedure to ensure all processes perform perfectly for long-term support (Ailawadi & Zacour, 2009; Gehrman et al., 2015; Makdisi & Wang, 2015).

In figure 1.1 demonstrated the overall setting of the CPB and ECMO circuit components that are used in the current clinical practice.

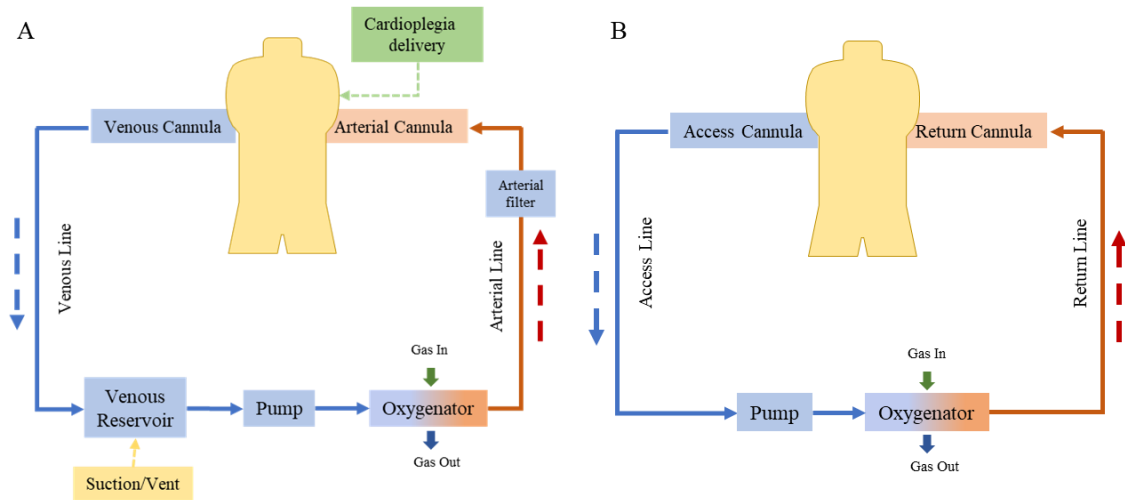


Figure 1.1 Comparison of CPB (a) and ECMO (b) circuit components.

--- Dash arrows refer to blood flow direction (modified from Makdisi and Wang (2015); Ruszel et al. (2021)).

1.2 BRIEF HISTORY OF ECMO

During the latter half of the 20th century, extracorporeal circulation has been the focus of conceptual research, development, and clinical study. This work has proven the efficacy and efficiency of CPB, and latterly, the technology associated with ECMO. Notable developments, including the concept of outside body perfusion, heart-lung machine and oxygenator development, prolonged circulatory support, high-performance membrane oxygenator development, and the ECMO era, will be described the following sections of this chapter.

The concept of outside of body perfusion support

The initial concept of using artificial circulation for organ preservation was presented by several investigators. Le Gallois (1812) demonstrated the possibility to inject oxygenated blood to perfuse to organ. This concept had been further developed and demonstrated in a number of laboratories (Boettcher et al., 2003).

A key event in the development cycle of extracorporeal support systems was the discovery of heparin, extracted from dog liver, by Jay McClen in 1916. The discovery of an effective anti-clotting agent stimulated progress in a number of medical areas. Additionally, it enabled the further development of extracorporeal perfusion techniques (McLean, 1959).

An extreme example of the potential for isolated organ perfusion was successfully carried out in the 1930s by Sergei Brukhonenko, using cross-connected circulation to support the isolated canine head, and maintained its function for about 40 minutes. The study demonstrated to some degree the possibility to use extracorporeal circulation to support patient perfusion in cardiac surgery (Krementsov, 2009).

Heart-lung machine and oxygenator development

During the late 1940s to early the 1950s, there were numerous designs of CPB machines that were developed with various types of bubble, film, and membrane oxygenators (Iwahashi et al., 2004).

The film and bubble oxygenators are direct-contact extracorporeal oxygenators. Film oxygenators expose a thin layer of deoxygenated blood to a single rotating disc or stationary screen and gas exchange occurs by introducing oxygen directly to red blood cells. The efficacy of gas exchange was dependent on surface area and duration of contact (Iwahashi et al., 2004).

Bubble oxygenators expose venous blood in a mixing chamber and when gas is introduced, bubbles form that enable oxygen to enter the blood cells. The factor that influences gas exchange are the volume of the bubbles introduced to blood. Bubble-type oxygenators have a higher risk of air embolism, especially when small, less buoyant bubbles remain in suspension and do not rise spontaneously. In current practice, the perfusionist needs to ensure to de-airing before return the oxygenated blood to patient (Iwahashi et al., 2004).

The father of artificial organs, Willem Kolff, introduced the concept of membrane oxygenators in 1943 in the first working artificial kidney. The report highlighted that the system transforms deoxygenated blood into oxygenated blood. These findings indicated the possibility of utilising membranes as artificial lungs; however, their efficacy may need more advancements in materials and oxygen delivery techniques (Kolff et al., 1997; Kolff et al., 1956; Stanley, 2013).

CPB was developed using animal experiments until the first successful use in human cardiac surgery by John Gibbon in 1953. During that year, four surgical procedures were performed to close an atrial septal defect. However, there was only one surviving case, an 18-year-old female patient (Hessel, 2014; Hill, 1982; Kurusz, 2012; Stoney, 2009).

In the same period, heart-lung machine system support in cardiac procedures was published in a British Medical Journal. The author presented the conceptual framework of the mechanical heart-lung system, which includes the pump, oxygenator, circuit, and monitoring strategies for the operative procedure (Melrose, 1953). Furthermore, an experiment was conducted by Melrose and colleagues in animal research to validate their mechanical heart-lung system. Subsequently, this system proved effective in clinical settings within a few years (Cleland & Melrose, 1955). In 1958, Melrose and Gerbode reported the efficacy of elective cardiac arrest using potassium citrate solution in open heart surgery. This discovery has proven to be advantageous in surgical outcomes and continues to be utilised for heart preservation in open-heart surgeries until the present day (Bradić et al., 2023; Gerbode & Melrose, 1958).

Additionally, cross-circulation heart surgery was introduced by C Walton Lillehei in 1954. The operation was to repair a 3-year old's ventricular septal defect, the opening in ventricle wall, using the 25-year-old father's circulation for support the children. Both circulations connected by tubing system and process blood flow and gas exchange. However, this high-risk procedure was soon terminated as it threatened a 200% donor to recipient mortality rate (Boettcher et al., 2003; Punjabi & Taylor, 2013).

Prolonged circulatory support

Prolonged circulatory support suggests a procedure in which CPB is used to assist the failing heart and/or lungs, generally in post-cardiac surgery cases. Such a procedure requires support over an extended period, beyond normal CPB deployment. However, this procedure was not defined as ECMO because membrane oxygenators were not available at that time. The oxygenator during that time consisted mainly of a bubble-type design. There were two significant animal experiments that related to the development of this procedure.

In an early study by Melrose and colleagues (1953), the physiologic status was measured in anoxic dogs with a heart-lung machine. This experiment attempted to investigate the

applicability of this procedure in resuscitation and circulatory failure. The study utilised different cannulation modalities, taking venous blood and returning to the venous or arterial circulation. The authors suggested that the return catheter should be applied to a central vein or aorta and confirmed that extrapulmonary oxygenation was a reasonable method of support circulatory failure cases (Melrose et al., 1953).

In another early study, Reed and Kittle's performed the extracorporeal perfusion on 15 canines using bubble oxygenators for two hours. The results of their study included observations concerning metabolic acidosis and neurological issues. Moreover, 14 out of 15 animals survived the procedures. The authors, reflecting on this success, suggested that further experimentation should be carried out to further extend duration of CPB support (Reed & Kittle, 1958).



Figure 1.2 DG Melrose performs his heart-lung machine as a prolonged circulatory support in the intensive care unit.

(Taken from Lynn CJ, 2012 referred to Prof. T. Gourlay's personal library)

Attempts were made to use extended circulatory support in the early period of the clinical development of CPB, shown in Figure 1.2. However, these studies highlighted several

issues that limited the application of the procedure. The main observed adverse effect was red blood cell trauma associated with the blood oxygenation method and system. As a result, complications resulting from direct blood gas interaction, and oxygen toxicity from uncontrolled excessive oxygenation were observed (Iwahashi et al., 2004).

High performance membrane oxygenator

In 1958, Clowes and colleagues developed a permeable ethylcellulose layered oxygenator that was the first to be used in animal experiments and clinical cases. The early technologies often experienced plasma leakage via the membrane pores during prolonged operation. These problems occurred because hydrophilic membrane pore size had reformed and allowed fluid moveout to the gas pathway. Therefore, membrane material has been changed to hydrophobic polymers such as polytetrafluoroethylene and silicone. Later designs ameliorated this by using the stronger, more resilient membrane materials (Clowes Gh Jr Fau - Hopkins & Neville, 1956; Clowes et al., 1956; Clowes & Neville, 1957; Kammermeyer, 1957; Lim, 2006).

Silicone membranes were introduced as a permeable material for blood-gas exchange. However, the limitations in manufacturing technology can result in the occurrence of pinholes in thin silicone films. Until the membrane was improved by Burn in 1959 (Lim, 2006), and had continuous improvement and developed to the disposable device, single use oxygenator, as reported in 1965 by Bramson ML et al (Bramson, Osborn, Beachley Main, et al., 1965), and proven in the cardiac surgical cases as in the report in 1969 (Bramson et al., 1969). Theodor Kolobow improved an oxygenator by including a spiral configuration of a silicone membrane, which was inspired by Kolff's oxygenator. The new membrane oxygenator is compact and offers a greater surface area. Kolobow introduced a new membrane oxygenator to animal experiments in 1971, and studied the extracorporeal membrane lung to support lamb circulation without anaesthesia for 16 days (Kolobow et al., 1971). More efficient oxygenator configurations for extracorporeal techniques improved surgical outcomes and were more durable and resilient for prolonged support than those used in cardiac surgery. The Kolobow's oxygenator

received continuous improvements and was later launched into the market and has been widely utilised in the ECMO for several years (Featherstone & Ball, 2018; Kolobow & Bowman, 1963; Lim, 2006). In Figure 1.3 shown the oxygenator by Medtronic company which is the silicone membrane type oxygenator.



Figure 1.3 Silicone membrane oxygenator.

The ECMO era

In 1971, the first adult patient to survive ECMO treatment presented with post-traumatic respiratory failure and required support for prolonged gas exchange, and the peripheral cannulation with the Bramson-membrane heart-lung machine was maintained for 72 hr. (Hill et al., 1972). Then, in 1975, the first surviving neonatal case was reported. However, insufficient guidelines and knowledge gaps on ECMO deployment in these early years had limited its usage and clinical acceptant globally (Bartlett, 2005, 2017a).

The Extracorporeal Life Support Organisation (ELSO) was established in 1989. The organisation aimed to support medical ECMO specialists for clinical practice, conduct research and establish a centre for ECMO in several countries (Vuylsteke et al., 2017). The significant growth in case numbers and service centres available registered with ELSO (Tonna et al., 2024). As reported by ELSO, clinical outcomes compared with early period of ECMO are gradually improved through advancements in ECMO

technologies and by 2022, 50% of patients that underwent ECMO were discharged or transferred to further treatment such as treated by standard care (Tonna et al., 2024).

In 2006, a study was purposed by Peek and colleagues on the efficacy of conventional ventilatory support versus extracorporeal membrane oxygenation for severe adult respiratory failure (CESAR). This study demonstrated that ECMO significantly improves outcomes in ECMO. This study presents the findings of a multicentre trial conducted in the UK, focusing on the treatment of respiratory failure using conventional methods and ECMO. The results of the study, a higher percentage of patients treated by ECMO (63%) survived without disability for six months compared to those who received conventional management (47%). Consequently, CESAR became the standard criteria of ECMO for respiratory failure cases. (Peek et al., 2006; Peek et al., 2009).

The rise in case numbers of overall ECMO started in 2009 can be related to the H1N1 influenza pandemic. ECMO was being indication as a potential treatment option for patients suffering from ARDS caused by influenza A (H1N1) (ANZECMO, 2009; Roch et al., 2010). Then in 2015, American Heart Association (AHA) guideline recommended ECMO for cardiopulmonary resuscitation (CPR) in circulatory arrest patients, in a procedure known as ECPR (Extracorporeal Cardiopulmonary Resuscitation) (Link et al., 2015; Mosier et al., 2015). Additionally, the COVID-19 pandemic increased ECMO deployment in patients with cardiac and respiratory failure. The use of ECMO during the COVID-19 pandemic has been shown to greatly help the patients and became a standard guideline. (National Institutes of Health, 2024).

Based on the ELSO data, in Table 1.1, the overall mortality rate differs between ECMO techniques (October 2023), which was between 29.5 and 57.7% for cardiac ECMO and ECPR, and between 57.3 and 68.5% for respiratory ECMO. Although still showing high mortality, the survival to discharge was significant improved from the previous periods (before the year 2017) (Extracorporeal Life Support Organization, 2023; Tonna et al., 2024).

Table 1.1 ECMO survival rate (Per 1000 ECMO Hours), 2017–2022.

Age Group	Support Type	Runs	Survival to 24 Hours After ECMO Decannulation*	Survival to Hospital Discharge**
Adult	Respiratory	48,338	67.2% (32,008/47,663)	57.3% (27,701)
	Cardiac	45,830	62.6% (28,138/44,927)	44.2% (20,264)
	ECPR	14,097	44% (6,124/13,910)	29.5% (4,162)
Paediatric	Respiratory	8,495	74.5% (6,214/8,342)	63.8% (5,423)
	Cardiac	11,504	76.9% (8,621/11,213)	57.7% (6,636)
	ECPR	5,740	58.9% (3,311/5,617)	41.0% (2,355)
Neonatal	Respiratory	11,511	82.7% (9,327/11,277)	68.5% (7,888)
	Cardiac	6,911	71.5% (4,827/6,750)	48.3% (3,337)
	ECPR	2,142	67.5% (1,411/2,091)	44.3% (949)

**This excludes run records in which the patient was not reported as being discharged alive to home and for which the patient’s time of death/discharge was not recorded.*

***This is the percentage of patients discharged alive and off ECMO.*

(Modified from; Tonna et al. (2024))

Due to an ECMO is optional to treat the selected severe cases with failing circulation and respiratory. The number of ECMO centre and case number that register to ELSO since 2009 to 2022 are significantly increase as illustrated in Figure 1.4. (Tonna et al., 2024).

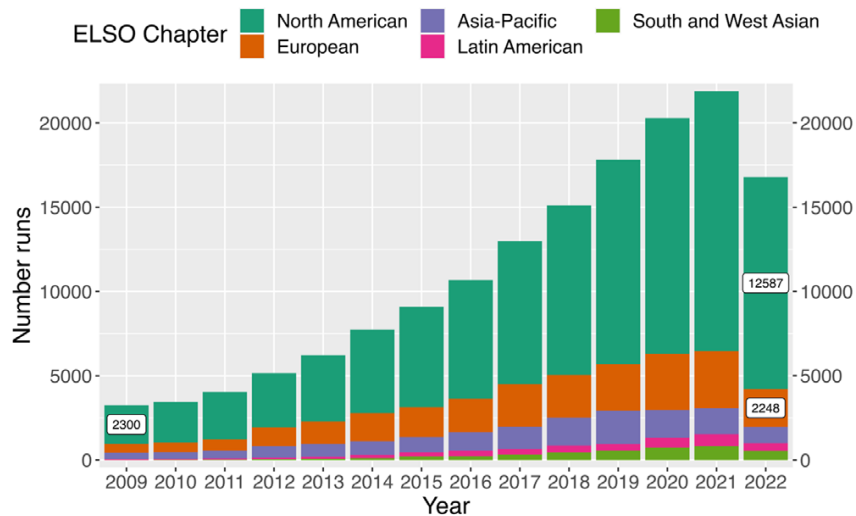


Figure 1.4 International Summary of Statistics: The number of ECMO Centre and cases that register to ELSO from 2009 to 2022.

(Taken from Tonna et al. (2024))

1.3 PRINCIPLE OF ECMO

1.3.1 Type of ECMO

Venoarterial (VA) and venovenous (VV) ECMO are classified based on the location of the return cannula (respectively VA or VV-ECMO). The technique in which the cannula returns to the arterial system is known as VA-ECMO. This treatment is for both respiratory and haemodynamic support by supplying oxygenated blood to the systemic circulation (Figure 1.5) and connected in parallel to the lungs and heart. In contrast, VV-ECMO is appropriate for patients with respiratory failure and is configured to allow delivery of oxygenated blood to the vein that connects to the pulmonary system (Figure 1.6) (Makdisi & Wang, 2015; Pavlushkov et al., 2017).

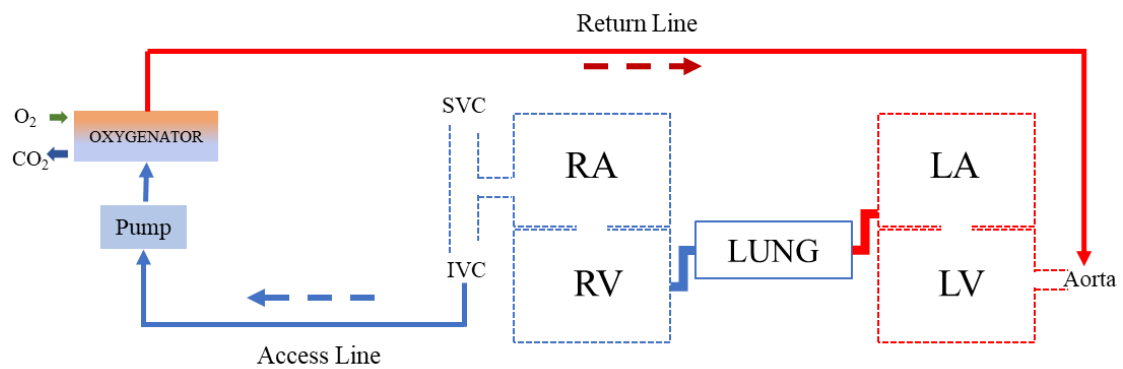


Figure 1.5 Diagram of VA-ECMO parallel with native circulation.

(SVC, superior venacava; IVC inferior venacava; RA, right atrium; RV, right ventricle; LA, left atrium; LV, left ventricle; O₂, Oxygen; CO₂, Carbon dioxide) (modified from Pavlushkov et al. (2017))

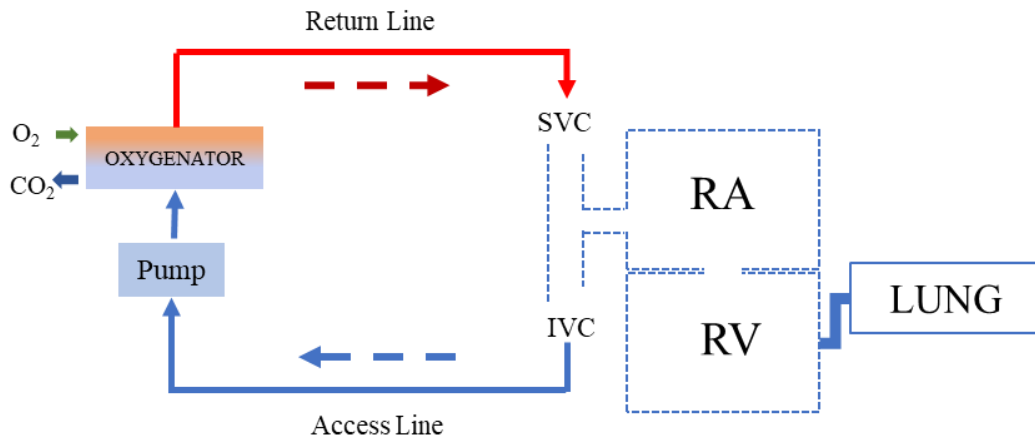


Figure 1.6 Diagram of Venovenous ECMO and right-side heart.

(SVC, superior venacava; IVC inferior venacava; RA, right atrium; RV, right ventricle; LA, left atrium; LV, left ventricle; O₂, Oxygenator; CO₂, Carbondioxide) (modified from Pavlushkov et al. (2017))

1.3.2 Indication and Contraindication

In recent years, the majority of the institutions engaged in the delivery of ECMO utilize protocols developed following the ELSO recommendations. These include the key indication for establishing ECMO, categorised by either cardiac or respiratory complications.

In general, the conditions for respiratory ECMO support include severe hypoxic respiratory failure, severe air leakage, diaphragmatic hernia, meconium aspiration or severe pulmonary hypertension (Maratta et al., 2020; Tonna et al., 2021; Wild et al., 2020). The cases for support in cardiac cases include cardiogenic shock, preoperative haemodynamic unstabilisation, weaning CPB failure and resuscitation. The following tables highlight the inclusion and exclusion criteria for ECMO support, summarised from ELSO guidelines and related publications (Brown et al., 2021; Lorusso et al., 2021; Roeleveld & Mendonca, 2019).

Table 1.2 Indication for cardiac ECMO.

<p>Neonatal (Roeleveld & Mendonca, 2019) And Paediatric (Brown et al., 2021)</p>	<p>Catheterization and surgical procedure related to:</p> <ul style="list-style-type: none"> - Preoperative hemodynamic instability - Difficulty to wean cardiopulmonary bypass - Elective support for high-risk procedure - Post-operative circulatory failure <p>Bridge to cardiac transplantation or ventricular assist device Shock (e.g., cardiogenic, distributive, obstructive) In hospital cardiac arrest with unstable hemodynamic Extracorporeal cardiopulmonary resuscitation</p>
<p>Adult (Lorusso et al., 2021)</p>	<p>Cardiogenic shock associated with:</p> <ul style="list-style-type: none"> - Inadequate tissue perfusion due to hypotension and low cardiac output - Shock with failure to respond to maximal treatment (e.g., inotropic, vasoconstrictor, IABP) - AMI, Myocarditis, Peripartum cardiomyopathy, Decompensated CHF, Post-operative circulatory failure <p>Septic shock Difficulty to wean cardiopulmonary bypass Post-operative circulatory failure Preoperative hemodynamic instability Bridge to cardiac transplantation or ventricular assist device Extracorporeal cardiopulmonary resuscitation</p>

Table 1.3 Indication for respiratory ECMO.

<p>Neonatal (Wild et al., 2020)</p>	<p>Congenital diaphragmatic hernia (CDH) Meconium aspiration syndrome (MAS) Persistent pulmonary hypertension Potential recovery of severe respiratory +/- circulatory with one or more of:</p> <ul style="list-style-type: none"> - Inadequate tissue perfusion - Hypoxic respiratory failure with acute decompensation ($\text{PaO}_2 < 40$ mmHg) - Oxygenation Index (OI) > 40 for > 4 hr - Severe pulmonary hypertension with right or left ventricular dysfunction
<p>Paediatric (Maratta et al., 2020)</p>	<p>Acute severe respiratory failure with treated by high level setting of ventilator from one or more following conditions.</p> <ul style="list-style-type: none"> - Acute respiratory distress syndrome - Viral or bacterial pneumonia - Aspiration pneumonia - Status asthmaticus - Mediastinal masses - Pulmonary haemorrhage - Severe air leak <p>Bridge to lung transplantation Perioperative support to airway surgery Temporary lung nonfunction (e.g., extensive bronchoalveolar lavage)</p>
<p>Adult (Tonna et al., 2021)</p>	<p>Hypoxic respiratory failure CO₂ retention on mechanical ventilation with high support Severe air leak syndromes Bridge to lung transplantation Cardiac or respiratory collapse (e.g., Pulmonary emboli, Airway obstruction)</p>

OI = ((mean airway pressure x FiO₂)/ Post ductal PaO₂) x 100; 50% mortality risk, consider starting ECMO (PaO₂/FiO₂ < 150 on FiO₂ > 90% and/or Murray score 23 1, AOI score 602, or APSS score 3); 90% mortality risk, strong indication to start ECMO (PaO₂/FiO₂ < 100 on FiO₂ > 90% and/or Murray score 3-4(1), AOI >80 (2), APSS 8 (3) despite optimal care for 6 hours or less).

Table 1.4 Contraindication of ECMO.

Absolute	Prolonged mechanical ventilation support and irreversible respiratory failure Genetic abnormalities Irreversible cardiac disease Irreversible cerebral injury End stage malignancy Uncontrol bleeding
Relative	End stage organ failure Low birth weight (< 2 kilograms) Preterm birth (<34 weeks) or Advance aging

The absolute and relative contraindication which summarised from Brown et al. (2021); Lorusso et al. (2021); Maratta et al. (2020); Tonna et al. (2021); Wild et al. (2020)

1.3.3 Circuit Components

The basic ECMO components contain cannulae, a pump and oxygenator, all in series and connected by tubing of varying diameter. The blood flow direction in the ECMO circuit starts from the access cannula, which receives deoxygenated blood from the patient. Deoxygenated blood enters the pump and is directed to the oxygenator where gas exchange occurs through the membrane. Then, oxygenated blood from the oxygenator outlet is returned turn to the patient via a return cannula (Lequier et al., 2013). The direction of blood flow through the basic ECMO circuit is shown in Figure 1.7.

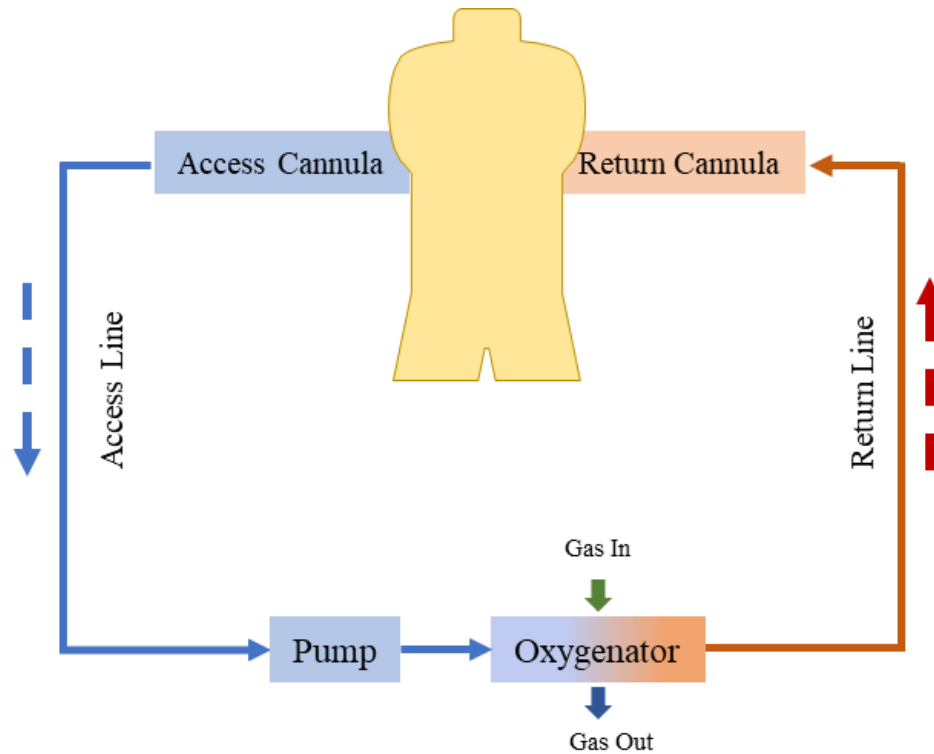


Figure 1.7 Components and blood flow of ECMO circulation.

The main components are drainage and return cannulae, a pump, and an oxygenator. Blood flows begin at the access cannula, pass through the pump, continue to the oxygenator, and finally return to the patient. (--- Dash arrows refer to blood flow direction) (modified from Lequier et al. (2013); Pavlushkov et al. (2017))

Cannulae

A cannula is a catheter that primarily functions to connect the circuit and the patient. Cannula and circuit configurations are based on the organ that needs to be supported. There are two types of cannulae based on their position in the circuit; the access and return cannulae. In Table 1.5 outlines characteristic for important features to design the cannulas for ECMO.

Table 1.5 The essential features of cannulas.

Features	Requirement	Characteristics
Materials	Flexibility and consistency of shape	Polyurethane Wire-reinforced Malleable
Surface coating	Reduced artificial surfaces activates the coagulation and complement cascades	Biocompatible coatings
Length and Shape	Venous cannulae: Enough drainage flows, does not collapse vessel from negative pressure Arterial cannulae: Provide adequate flow, low pressure gradient and jet	Slim shape and thin wall Side holes in venous cannula Diffuser tip in arterial cannula Short catheter for Central cannulation Long catheter for Peripherals cannulation
Double lumen	Combine both drainage and return into one catheter	Suitable for VV-ECMO
Additional features	Insertion kit, Malleable Sidearms or luer port	For percutaneous insertion For additional reperfusion catheter

(modified from Kohler et al. (2012); Pavlushkov et al. (2017))

Access Cannulae

An access (or venous) catheter directs deoxygenated blood through the ECMO system by bypassing the heart and artificially oxygenating the blood. For this reason, the venous cannula feature usually includes the side holes, drainage opening at the cannula body. The side holes function to assist more significant blood drainage to the circuit. Single or dual venous cannulae are used based on ECMO deployment. The venous cannulation can be inserted to the right atrium, femoral vein, subclavian vein, or internal jugular vein. Single venous cannula is usually used in peripheral and central approaches which insert for VV and VA-ECMO which is separated from the return cannula. In contrast, the dual cannula which combines both drainage and return into one catheter, can be access to the peripheral venous, served for the VV-ECMO (Kohler et al., 2012; Pavlushkov et al., 2017).

In Figure 1.8 displays a long venous cannula designed for the femoral vein, which has a tip with side holes and an end hole.

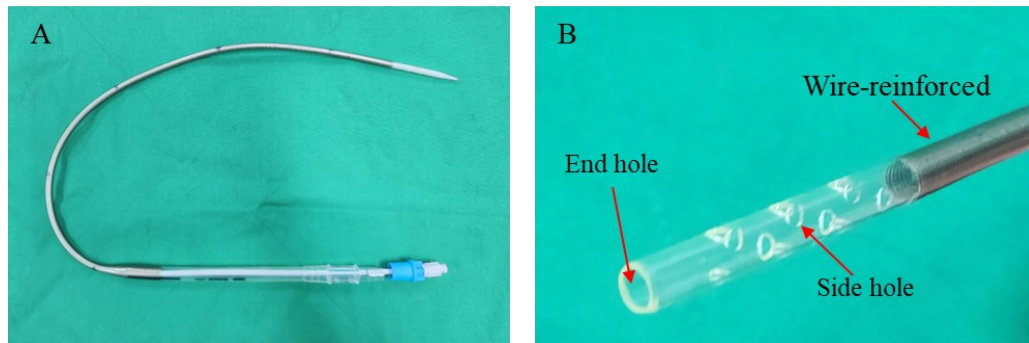


Figure 1.8 Illustrate access or venous cannula.

(A: Femoral venous cannula; B: Cannula tip with side holes and end hole)

Return Cannulae

The return (arterial) cannula is a catheter that delivers oxygenated blood to the patient from the ECC. The position of this cannula is located beyond the blood pump and oxygenator and is known as the arterial cannula in VA-ECMO. Importantly, the cannula is designed to accommodate high pressures and dampen the impact of high flow that is responsible for haemolysis. The cannulation site is again selected in accordance with the specific procedure. For example, in the VA-ECMO case, the return catheter could be placed at the aorta, femoral artery, axillary artery or carotid artery (Kohler et al., 2012; Pavlushkov et al., 2017).



Figure 1.9 Return or arterial cannula.

(A: Femoral arterial cannula; B: Different cannula tip for aortic cannulation)

Blood Pump

The blood pump functions to establish flow through the ECMO circuit and to also support flow through the native circulation. This device is located between the oxygenator and access cannula. There are two types of blood pump in the ECMO: roller and centrifugal pump. The roller pump created blood flow by compressing a section of tubing with two rollers, facilitating its forward movement. The centrifugal pump uses rotating cones to create a vortex, which then applies an outward centrifugal force that drives the blood forward to exit through an outlet (Naruka et al., 2022). The roller pump (Figure 1.10 A) is required to force blood flow throughout the circuit and is suitable for silicone sheets oxygenator, which has a high resistance than the hollow fibres oxygenator (Nikkole Haines et al., 2009; Horton et al., 2004). However, there were reports of red blood cell trauma (haemolysis), and circuit malfunctions during prolonged support (Kaluza et al., 2022; Peek et al., 1999).

Recent commercial ECMO circuits often use a centrifugal pump (Figure 1.10 B) to eliminate issues most related to roller pumps, such as the risk of tubing rupture, shorter circuit lengths, and complex calibration. Modern oxygenators and pumps in Figure 1.11 utilised in ECMO enable the design of compact and portable circuits, facilitating the transportation of patients between different departments and hospitals (Fiusco et al., 2022; Johnson et al., 2022; O'Brien et al., 2017; Ündar et al., 2018).

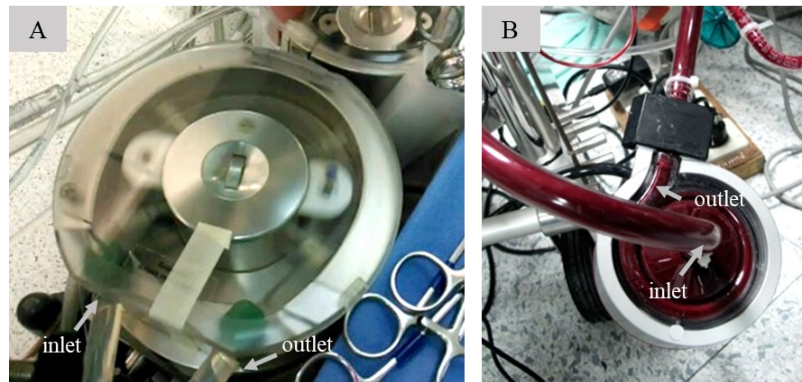


Figure 1.10 Blood pump for extracorporeal circulation.

(A: Roller pump; B: Centrifugal pump)



Figure 1.11 Portable ECMO system designed for use in ambulances or helicopters.

(Taken from Berndtson and Doucet (2021))

Oxygenator

The oxygenator for ECMO gas exchange is located downstream of the blood pump. The blood inlet port receives deoxygenated blood from the pump, and an outlet port delivers oxygenated blood to a return cannula.

The membrane oxygenator utilised in an ECMO system may consist of several biomaterials, such as silicone rubber, polypropylene (PP) or the more recent polymethylpentene (PMP). The oxygenator is comprised of thousands of hollow fibres encased in a hard outer shell, and blood flows around the outside of these fibres. Oxygen rich gas flows on the inside lumen of these fibres and oxygen is able to diffuse through the fibres from the oxygen side to the blood side, from the oxygen rich inner wall (oxygen gas side) to the oxygen poor outer wall (blood side), and carbon dioxide actively transfers in the other direction. The use of PMP material in the oxygenator resulted in reduced priming volume, decreased pressure gradient across oxygenator, and minimised plasma leakage as compared to the conventional silicone and PP membrane oxygenator. The gas exchange surface area of PMP fibre oxygenators ranges from 0.3 to 1.8 m² (D. A. Berdajs et al., 2011; Daniel et al., 2018; N. Haines et al., 2009; Lequier et al., 2013; Ündar et al., 2018).

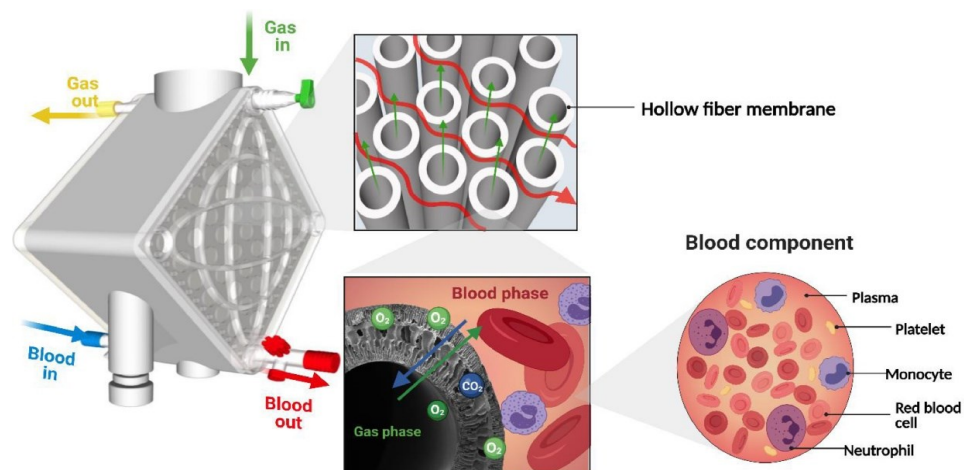


Figure 1.12 The structure of oxygenator and hollow fibre membrane.

(Taken from Nguyen Thi et al. (2022))

Additionally, modern oxygenators (Figure 1.12) contain integrated heat exchangers to control patient core temperature. The heater-cooler machine is connected to the heat exchanger, supplying both cold and warm water. The water pathway is separate from the blood pathway, with a close link to the gas exchanger. The compact design, oxygenator integrated with heat exchanger, benefits from minimising haemodilution caused by a large priming solution and reducing contact activation due to short-circuiting (Bramson, Osborn, Main, et al., 1965; Ficial et al., 2021; Horton et al., 2004).

1.4 ECMO CANNULATION

The cannulation procedure is the initial step in establishing ECMO and is critical to the successful deployment of the technique. The access and return, appropriate catheters are inserted into various vessels depending on the ECMO configuration being applied, VV or VA-ECMO, and these are then connected to the ECMO circuit. It is critical, under all ECMO techniques, to select appropriate cannula and cannulation sites to ensure adequate drainage and return to support the patient undergoing ECMO support and to minimize pathophysiological impacts. ECMO canulae can be deployed using either direct surgical insertion or a percutaneous approach, but it is necessary that vessels of appropriate size and location are selected to ensure adequate blood flow during the procedure. The site for cannulation is illustrated in Figure 1.13, while the characteristics of commercial cannulae for ECMO are described in Table 1.6.

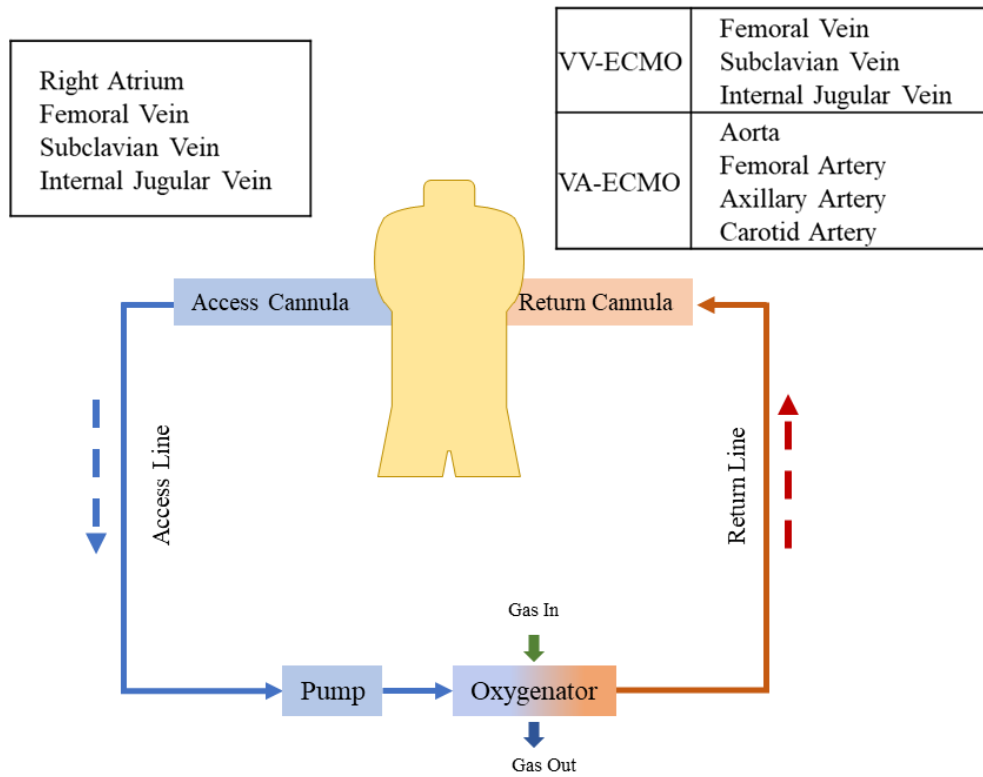


Figure 1.13 The common cannulation approaches for ECMO.

The central cannulation mainly approaches to the great vessels, while the peripheral procedure involves to varies vessel depended on modality (VV-ECMO, veno-venous ECMO; VA-ECMO, veno-arterial ECMO) (modified from Pavlushkov et al. (2017))

Table 1.6 Characteristics of commercial cannulae for ECMO.

Model	Insertion Site	Size (circumference; Fr)	Features
Medtronic/Crescent RA Jugular ¹	Venous cannula Jugular vein	13, 15,19	Dual Lumen Wire-reinforced
Medtronic/Crescent Jugular ¹	Venous cannula Jugular vein	24, 26, 28, 30, 32	Dual Lumen Wire-reinforced
Medtronic/Bio-Medicus Life Support Flex ¹	Arterial and Venous cannula Jugular artery or vein Femoral artery or vein	15, 17, 19, 21, 23, 25	Biocoated Wire-reinforced
Medtronic/Bio-Medicus Life Support Flex XL ¹	Arterial and Venous cannula Jugular artery or vein Femoral artery or vein	15, 17, 19, 21, 23, 25	Biocoated Long length Wire-reinforced
Medtronic/Bio-Medicus Life Support Multi ¹	Venous cannula Jugular or Femoral vein	21, 23, 25	Side hole Wire-reinforced
Medtronic/Bio-Medicus Life Support Multi XL ¹	Venous cannula Jugular or Femoral vein	21, 23, 27, 29	Side hole Long length Wire-reinforced
Medtronic/Bio-Medicus Life Support Mini return ¹	Arterial cannula Carotid artery or distal perfusion	9, 11, 13, 15	Percutaneous Wire-reinforced
Medtronic/Bio-Medicus Life Support Mini Drainage ¹	Venous cannula Jugular vein	9, 11, 13, 15	Side hole Wire-reinforced
Getinge/Arterial HLS Cannulae (short and long) ²	Arterial cannula Carotid or Femoral artery	13, 15, 17, 19 ,21, 23	Biocoated Side hole tip Short and Long length Wire-reinforced
Getinge/Venous HLS Cannulae (short and long) ²	Venous cannula Jugular or Femoral vein	19, 21, 23, 25, 27, 29	Biocoated Side hole along cannula Short and Long length Wire-reinforced
Getinge/Avalon Elite ³	Venous cannula Jugular vein	13, 16, 19, 20, 23, 27, 30	Dual Lumen Wire-reinforced
Edwards Lifesciences/OptiSite ⁴	Arterial cannula Aorta, femoral, axillary and subclavian artery	16, 18, 20, 22	Side hole tip Wire-reinforced
Euroset/Revas universal venous cannula ⁵	Venous cannula Jugular or Femoral vein	18, 20, 22	Biocoated Side hole tip Wire-reinforced
Euroset/Revas femoral venous cannula ⁵	Venous cannula Femoral vein	22, 24, 26	Biocoated Side hole along cannula Wire-reinforced

Model	Insertion Site	Size (circumference; Fr)	Features
Euroset/Revas arterial cannula ⁵	Arterial cannula Femoral artery	16, 18, 20, 22, 24	Biocoated Side hole tip Wire-reinforced

(modified from Kohler et al. (2012); Pavlushkov et al. (2017))

¹ <https://www.medtronic.com/content/dam/medtronic-wide/public/united-states/medical-specialties/cardiac-surgery/extracorporeal-life-support-ecls-product-catalog.pdf>

² https://www.getinge.com/dam/hospital/documents/english/hls-cannulae-brochure-en-non_us_japan.pdf

³ https://www.getinge.com/dam/hospital/documents/english/avalon-elite-brochure-en-non_us.pdf

⁴ https://assets-us-01.kc-usercontent.com/6239a81e-8f0f-0040-a1df-b4932a10f6ae/64f6200f-950e-4719-b7d2-c70fb2ddd4e6/PP--US-1555v3.0-CSS_OptiSite_8.5x11_A1LRtablet%20%281%29.pdf

⁵ <https://eurosets.com/products/ecls/ecls-cannulae/>

1.4.1 Central Cannulation

The central cannulation technique is frequently applied in post-cardiac procedures or in cases in which it is difficult to achieve cannula placement using less invasive methods, for example, in small or tortuous vessels (Pavlushkov et al., 2017). In post-cardiac surgery, the central cannulation, already in place to deliver CPB, can be disconnected from the CPB circuit and switched to the new ECMO circuit. New cannulae are therefore unnecessary. Using the CPB canulae also offers the capability to maximize blood flow during ECMO due to their connection to the great vessels, avoiding flow limitations associated with the use of smaller, more peripheral vessels and cannulae. Moreover, the flow associated with central cannulation in VA-ECMO is in an antegrade direction with the return cannula providing a return flow to the ascending aorta. However, as the sternum remains open, this technique introduces an increased risk of infection and bleeding (Pavlushkov et al., 2017; Radakovic et al., 2021).

The great vessels in the thoracic chamber are the aorta, superior vena cava, inferior vena cava and pulmonary artery. The aortic root originates from the outflow tract of the left ventricle, separated by the aortic valve. At this point the vessel becomes an arch, in which the ascending aorta curves to create the descending aorta which provides blood

flow to the inferior organs system. The major veins, the inferior vena cava and superior vena cava, carry deoxygenated blood from the upper and lower part of the body respectively. The deoxygenated blood is drained from the major veins into the right atrium (Manole et al., 2013).

The surgical approach for central cannulation generally requires opening of the chest by the sternotomy technique. The sternum is divided to expose the heart and the great vessels. The aortic cannula is placed directly to the aortic root. In the same way, the venous cannula is inserted using the bi-caval or the right atrium approach. All cannulae are secured using purse-string sutures and then de-aired and connected to an ECMO circuit. After cannulation, the chest remains open and covered by a sterile sheet (Garcia-Rinaldi et al., 1983; Reeb et al., 2016). In Figure 1.14 shown central cannulation approaches for VA and VV ECMO.

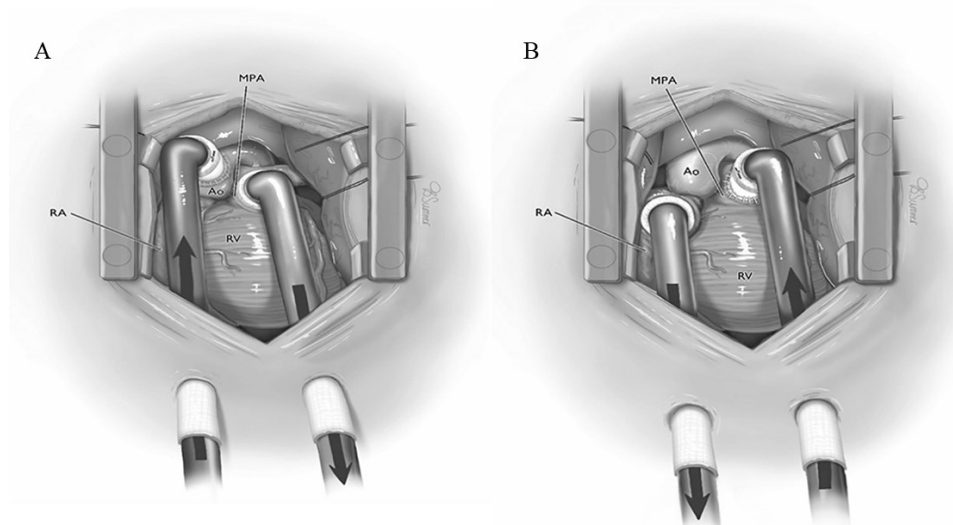


Figure 1.14 The central cannulation approaches for ECMO.

(A: VA-ECMO and B: VV-ECMO configuration; Cannulae are placed in the MPA (venous) and ascending aorta (arterial). RA, Right atrium; MPA, main pulmonary artery; Ao, aorta; RV, right ventricle) (Taken from Stephens et al. (2023))

1.4.2 Peripheral Cannulation

Peripheral cannulation is suitable for unexposed sternotomy cases, for example, cardiopulmonary resuscitation or emergency. In VA-ECMO, the venous cannulation is generally inserted into the femoral vein but returns to a variety of arteries, for example the femoral, carotid, and axillary artery. A carotid artery is a commonly used option for the arterial return, usually combined with the femoral vein in adults. However, the carotid artery and internal jugular vein are commonly used in a neonatal case due to the vascular size when compared to the femoral region. The axillary artery is an alternative route for arterial cannulation in some conditions, such as severe aortic calcification (C. Banfi et al., 2016; Pavlushkov et al., 2017).

In VV-ECMO, the cannulation sites usually employed are the femoral vein and the internal jugular vein. The jugular vessel is generally used for the return catheter, while the femoral vein is the access catheter. Recently, due to the development of the dual lumen catheter, which combines the inlet and outlet lumen in one deployable catheter, is recommended for VV-ECMO. This catheter allows for cannulation through a single site, providing advantages such as increased mobility, easier participation in physical therapy, improved patient comfort after extubation, and reduced risk of infection with only one cannulation site. (C. Banfi et al., 2016; Bazan et al., 2021; Pavlushkov et al., 2017; Reeb et al., 2016).

Carotid, subclavian and axillary artery

Three arterial branches split from the aortic arch, the brachiocephalic artery, left common carotid artery and left subclavian artery. The brachiocephalic artery contributes to the right carotid artery and subclavian artery. The common carotid artery is parallel on both sides but has a different origin. The right vessel emerges from the trunk while the left side connects directly to the aortic arch. These bilateral vessels provide blood flow from the chest region to the brain. Finally, the left subclavian artery has the primary function of supplying the left arm and associated tissues. (Hager et al., 2002; Manole et al., 2013). In Figure 1.15 and 1.16 illustrates the cannulation at carotid and axillary artery.

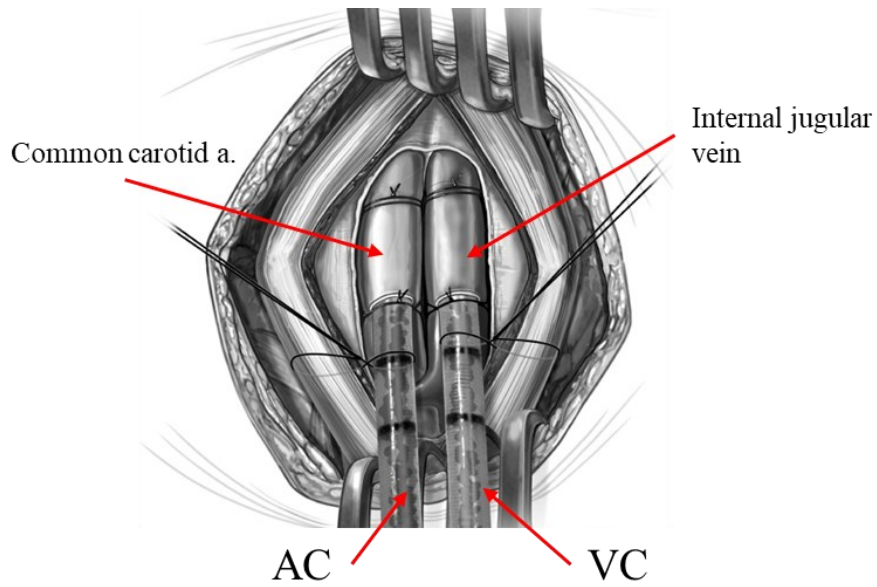


Figure 1.15 Neck cannulation for VA-ECMO.

(AC, arterial cannula; VC, venous cannula. (taken from Imamura and Caldarone (2019))

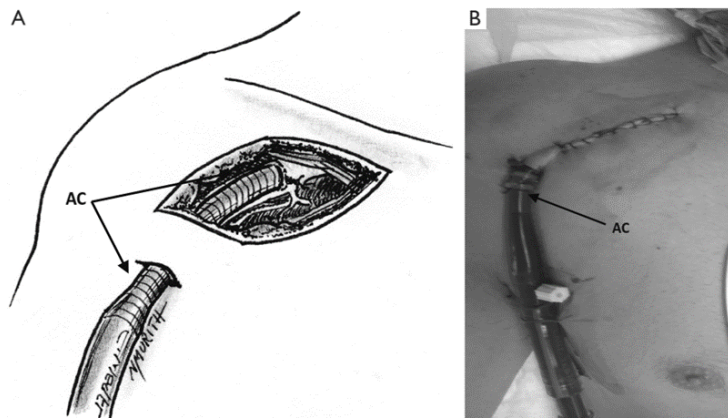


Figure 1.16 Axillary artery cannulation.

(AC, arterial cannula. (taken from Carlo Banfi et al. (2016))

Femoral Artery

Inferior extremity is supplied with blood by an external iliac artery which originates at the bifurcation of the abdominal aorta, becoming the femoral artery when this vessel enters the thigh region. The femoral artery provides a branch called the deep femoral

artery to support the pelvis and deep thigh muscles. The main femoral artery continues to the knee region, becomes a popliteal artery and is divided into the anterior and posterior tibial arteries. Both are supplied to a lower part of the leg regions and join at the area around the foot as the dorsal pedis, dorsal arch and plantar arch, which provides branches to supply the foot and toes (Crişan, 2012a; Hwang, 2017).

Femoral Vein

Four major branches of the external iliac vein drain deoxygenated blood via common femoral veins. Beginning from the plantar vein and dorsal arch, accumulate from the foot, digits, and toe and enter the venous system. Then, deoxygenated blood travels back via the anterior and posterior tibial to the popliteal vein. The great saphenous vein receives blood from the lower extremity region including superficial tissues, with the deep femoral vein collects blood from the thigh (Crişan, 2012a; Hwang, 2017). Femoro-femoral cannulation is shown in figure 1.17.

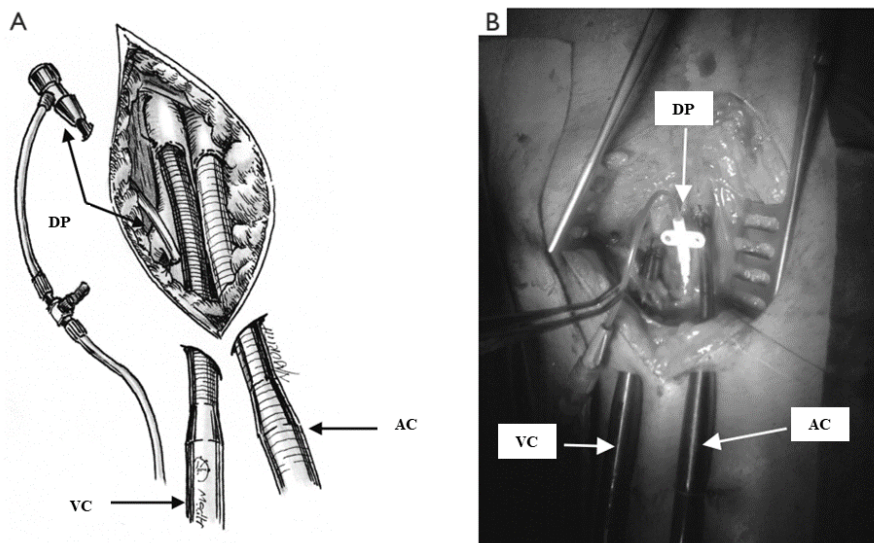


Figure 1.17 Femoro-femoral VA-ECMO cannulation.

(AC, arterial cannula; VC, venous cannula; RR, retrograde reperfusion. (taken from Carlo Banfi et al. (2016)

The technique for peripheral cannulation

Surgical technique

There are two cannulation techniques by surgery, direct insertion or placing the cannula with extended grafts. The direct insertion technique requires opening the skin and then inserting the catheter into the vessel (Kemaloğlu, 2018). In contrast, prosthetic vessels are required to attach the vessel, and the cannula will be inserted through the graft lumen. After the cannulation is performed, the surgical silk will snug around the cannula to secure the position (Calderon et al., 2015; Chamogeorgakis et al., 2013).

The technique to perform peripheral cannulation for this region can be approached by the surgical or percutaneous method. Usually, the open method with an end-to-side (T-graft) connection applies in an axillary artery, while the percutaneous or semi-open technique may apply to a carotid artery (Bauer & Malone, 2022; Chamogeorgakis et al., 2013; Hedayati et al., 2004).

Percutaneous technique

The Seldinger's technique usually applies percutaneous cannulation (Seldinger, 1953). This method also utilizes several operations: for example, device insertion for blood pressure monitoring. The minimally invasive procedure results in reduced infection and bleeding compared with open technique. However, well-trained physicians and teams need to perform the procedure (Carlo Banfi et al., 2016; Burrell et al., 2018).

Regarding the modified Seldinger's technique, needle, dilator, and guidewire are prepared. The needle punctures the skin to the vessel then a guidewire is introduced through the needle lumen. Next, the needle withdraws and then the cannula with the dilator is introduced through the guidewire. After that, the guidewire and dilator are removed, and the cannula remains intravascularly placed. Air bubbles are cleared to minimise blockage ischemia. Ultrasound guidance has recently been deployed (Carlo Banfi et al., 2016; Burrell et al., 2018). In Figure 1.18 shown the percutaneous approached by the Seldinger's technique.

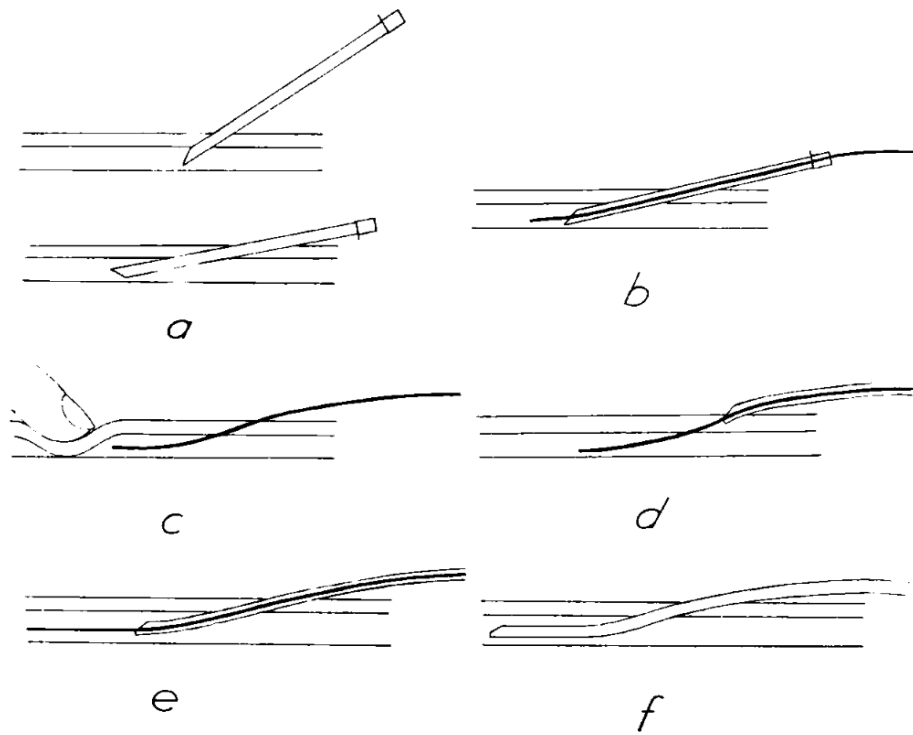


Figure 1.18 Percutaneous cannulation approach by Seldinger's technique.

(a: The vessel punctured, then a needle pushed upwards; b: The guide-wire inserted; c: The needle withdrawn and the vessel compressed; d: The catheter threaded on to the guide-wire; e: The catheter inserted into the vessel; d: The guide-wire withdrawn) (taken from Seldinger (1953))

1.5 BLOOD FLOW AND OXYGEN DELIVERY BY ECMO

In many ways ECMO is a simplified variant on the human physiological cardiopulmonary system but is not generally responsive to the physiological response to blood flow and pressure under physiological feedback. For example, ECMO is generally a non-pulsatile flow modality, which has been shown to be associated with a number of pathophysiological complications, such as peripheral occlusion, renal and adrenal impairment and regional ischaemia (Brain et al., 2022). The cardiac output is influenced by and varies with the body surface area, in response to the oxygen demand. The relationship between these two parameters can be determined by the cardiac index, which is a measure commonly used to assess the heart's function (Jegier et al., 1963).

In the absence of techniques to compensate for these normal physiological responses, or reliable and truly pulsatile flow generation systems, it is imperative that the adequacy of ECMO delivery is monitored in terms of the metabolic impact to ensure that the support is adequate and meets the metabolic demand (Brain et al., 2022). A fundamental aspect of this approach is to ensure that blood flow and oxygen delivery are at a level that is appropriate for the patient being treated based upon predicted metabolic consumption. This critical factor may be computed from the relation of body surface area and cardiac index (Jegier et al., 1963).

$$\text{Physiological concept; } CO = BSA \times CI \quad (1)$$

Where: CO is the cardiac output, BSA is the body surface area and CI is the cardiac index.

Since the blood flow in CPB and ECMO is referred to as the cardiac output in normal physiology, therefore the ECMO flow can be calculated by;

$$\text{ECMO flow; } BF = BSA \times CI \quad (2)$$

Where: BF is the ECMO blood flow, BSA is the body surface area and CI is the cardiac index (Condello et al., 2020).

Adequate ECMO flow is estimated by using number of cardiac index and can be increased 2.4 to 3 L/m²/min. Alternatively, it also estimated by the oxygen consumption number which in the neonate is 100-120 cc/kg/min, in the paediatric patient is 80-100 cc/kg/min, and in the adult is 60-80 cc/kg/min. The results of both formulae are likely to be similar numbers. Critically, it is essential to monitor patient mean arterial pressure, and maintain a mixed venous saturation 70% as in the normal range (Brown et al., 2021; Lorusso et al., 2021) as a minimum indicator of adequate perfusion support.

In terms of oxygenation, in the modern ECMO, hollow fibres oxygenators are generally employed. In these devices, blood gas exchange is achieved at the fibre interface in a counter current diffusion exchange process in which oxygen is transferred to the

desaturated blood and carbon dioxide is removed from the venous blood. Control of both oxygen and carbon dioxide exchange is controlled through a combination of gas flow rate and gas oxygen concentration. In modern practice, oxygenators are highly efficient, despite having a relatively small surface exchange area compared with the previous design. Oxygen delivery in ECMO can be also described by a relationship of cardiac output and arterial oxygen content using the following equation (Bartlett, 2017b; Brain et al., 2022; Ficial et al., 2021; Severinghaus, 1979).

$$DO_2 = [CO \times Hb \times SaO_2 \times 1.34] + [0.003 \times PaO_2] \quad (3)$$

Where: DO₂ is oxygen delivery, CO is cardiac output, Hb is Haemoglobin concentration, SaO₂ is oxygen saturation and PaO₂ is arterial tension.

1.6 OVERALL COMPLICATIONS IN ECMO

Various sources of complications in ECMO have been reported as in Table 1.7, including clot formation, cannula problem and air in the circuit. Common non-system complications include embolic events, bleeding, neurologic injury, renal insufficiency, and limb ischemia (Extracorporeal Life Support Organization, 2023). However, as this study's primary focus is on peripheral VA-ECMO cannula design, the cannulae associated issues are of primary significance and these will be reviewed in more detail in the following section.

Table 1.7 ECMO Complications (Per 1000 ECMO Hours), 2017–2022.

Complications	Adult			Paediatric			Neonatal		
	Respirator y	Cardiac	ECPR	Respirator y	Cardiac	ECPR	Respirator y	Cardiac	ECPR
Cannula problems	0.155	0.206	0.377	0.534	0.424	0.748	0.666	0.589	0.718
Air in circuit	0.025	0.051	0.083	0.152	0.171	0.202	0.146	0.173	0.23
Circuit change	0.258	0.177	0.18	0.636	0.621	0.554	0.862	0.767	0.761
Clots and air emboli	0.006	0.008	0.016	0.025	0.025	0.016	0.074	0.031	0.029
Thrombosis/clots	0.103	0.225	0.282	0.545	0.816	0.775	1.242	0.977	1.069
RRT	0.574	1.655	1.924	0.875	1.515	2.074	0.907	1.772	2.175
Cannula site bleeding	0.123	0.751	1.059	0.343	1.006	1.097	0.37	1.019	1.522
Surgical site bleeding	0.156	0.871	0.643	0.227	0.85	0.631	0.294	0.902	0.811
GI haemorrhage	0.136	0.272	0.392	0.123	0.137	0.264	0.073	0.074	0.122
Tamponade (blood)	0.02	0.212	0.171	0.064	0.175	0.136	0.051	0.166	0.194
Seizures	0.019	0.068	0.241	0.134	0.311	1.283	0.524	0.749	1.084
Brain death	0.024	0.072	0.433	0.054	0.094	0.492	0.108	0.191	0.301
Haemolysis (all types)	0.16	0.282	0.351	1.039	0.983	1.017	0.352	0.556	1.342
Limb Ischemia	0.021	0.241	0.41	0.021	0.102	0.13	0.005	0.037	0.057
Compartment syndrome	0.005	0.053	0.092	0.009	0.031	0.064	1.222	1.2	1.629
Fasciotomy	0.01	0.156	0.232	0.021	0.066	0.104	0.013	0.05	0.022
Amputation	0.004	0.042	0.052	0.01	0.023	0.013	0.001	0.006	0.014

CNS, central nervous system; CT, computed tomography; dL, decilitre; ECPR, extracorporeal cardiopulmonary resuscitation; EEG, electroencephalogram; RRT, Renal replacement therapy; GI, gastrointestinal; mg, milligram; MRI, magnetic resonance imaging; US, ultrasound; WBC, white blood cell. (modified from Tonna et al. (2024))

1.7 CANNULATION-RELATED VASCULAR COMPLICATIONS IN PERIPHERAL ECMO

The data in Table 1.8 from the 2017 ELSO registration presents the case number and survival rate linked with cannula complications. Patient groups' survival rate in respiratory cases was higher than in cardiac and ECLS cases. The data does not indicate whether VA or VV-ECMO, and cannulation site was deployed (Extracorporeal Life Support Organization, 2017).

Table 1.8 Demonstrate Cannulation-Related Complication and Survival Rate.

Patient		Reported (Case, %)	Survived (%)
Neonatal	Respiratory	536 (13.2)	59
	Cardiac	204 (7.9)	36
	ECLS	65 (8)	28
Paediatric	Respiratory	490 (14)	63
	Cardiac	303 (6.5)	53
	ECLS	172 (7.3)	35
Adult	Respiratory	818(4.7)	50
	Cardiac	636(3.2)	37
	ECLS	253(3.9)	17

A retrospective study by Wong et al. (2017) compared peripheral VA-ECMO cannulation site (carotid, femoral or axillary artery) complications to survival rate in a single centre. There was no difference in mortality between patients' numbers with cannulation-related problems and non-problem groups. Notably, over-perfusion was higher in the axillary approach, and most of the vascular issues were found in the femoral cannulation group, primarily exhibiting limb ischemia. The authors stated that the institute's protocol allowed a cannulation site changeover when complications occurred, and it is possible that this switch approach may have an impact on the results. Additionally, Lo Coco et al. (2018) classified the common complications in peripheral VA-ECMO into four groups: bleeding, neurological, vascular, and infection. In general, most arterial cannulation concerns are related to inadequate perfusion, possibly leading to limb ischemia and neurological complications.

1.7.1 Carotid artery cannulation and neurological complications

The carotid artery is a bilateral vessel that arises in both sides of the neck and supplies blood to the brain (Figure 1.19). Carotid or subclavian artery cannulation for ECMO is usually performed in neonates and paediatric patients due to the small femoral artery size in these patients (Harvey, 2018; McGough et al., 1993). Carotid cannulation may lead to the interruption of blood flow to the brain via the cannulated vessel. Previous studies argue that adequate compensation due to cannula obstruction may be achieved via the Circle of Willis' circulatory anastomosis from the opposing uncannulated vessel, but that there is a high risk of neurological complications (Kazmi et al., 2018; Shoskes et al., 2020). Moreover, there is some evidence that the carotid artery cannulation approach may be associated with interrupted neurodevelopment in neonatal ECMO patients (Kozik, 2020; Polito et al., 2013). However, the factors leading to neurological sequelae of ECMO are numerous and such complications have been identified independently of the cannulation approach employed. These contributing factors include flow obstruction, mobilization of calcification, thromboembolism and haemorrhage (Migdady et al., 2020; Shoskes et al., 2020).

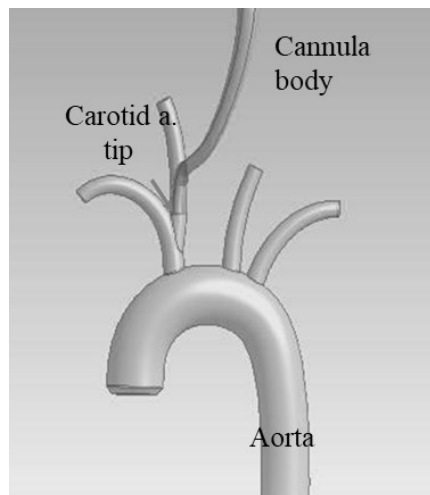


Figure 1.19 Cannulation approach to carotid artery in VA-ECMO.

This cannulation approach provides antegrade blood flow to the Aorta via Carotid artery, however the cannula body can be disrupting blood supply to the brain due to obstruction of the cannulated vessel.

1.7.2 Femoral cannulation and limb ischemia

Limb ischemia can develop during and after the ECMO procedure. These are related to the cannula size, haemodynamic status, venous compression, vascular disease and percutaneous cannulation (Yeo et al., 2015; Zimpfer et al., 2006).

The femoral artery (Figure 1.20) approach impairs distal perfusion when the cannula obstructs blood flow to the inferior portion of the limb and may result in ischaemia and compartment syndrome. Ischaemia ultimately leads to reduced adenosine triphosphate (ATP), anaerobic respiration, mitochondrial breakdown, and cell death (Simon et al., 2018). Compartment syndrome is caused when intra-compartmental pressure increases to within 10-30 mmHg of the patient's baseline diastolic blood pressure (Singh et al., 2004). This reflects insufficient perfusion and extremity ischaemia lead to functional impairment and limb deformity if untreated through fasciotomy or amputation (Bonicolini et al., 2019; Park et al., 2022).

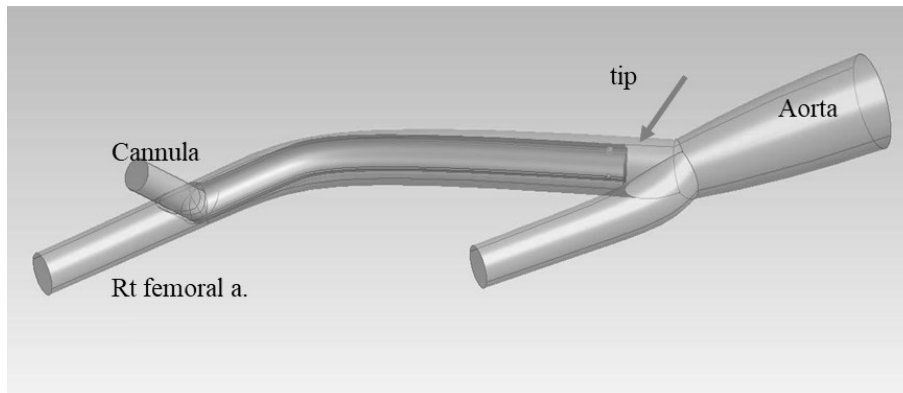


Figure 1.20 Arterial cannula inserted in the femoral artery.

Tip of catheter place in the proximal part of vessel to provide blood supply to systemic part, while the distal part of vessel is obstructed by cannula's body itself.

1.8 CURRENT CANNULATION TECHNIQUES TO SUPPORT DISTAL PERFUSION

Generally, the femoral cannula for peripheral VA-ECMO is similar to its use in open-heart surgery. A conventional issue is backward cannulation flow to the distal part of the lower limb. Since there is less likelihood of limb ischaemia during general cardiac surgery (Jayaraman et al., 2017; Raffa et al., 2019). To preserve distal perfusion in peripheral VA-ECMO, there are a number of techniques deployed including operating a modified T-graft, adding a distal catheter, and inserting a smaller-size of the cannula (Fraser et al., 2019).

1.8.1 Modified T-graft

In Figure 1.21, the modified T-graft procedure refers to the connection of a long, straight cannula to a prosthetic vascular graft, which is then anastomosed to a native blood vessel. The femoral artery is frequently employed in this procedure in clinical practice to ensure a secure graft attachment using the appropriate suturing method. The arterial return cannula is inserted into the graft to facilitate blood circulation from the ECMO system (C. Banfi et al., 2016; Fraser et al., 2019; Makdisi et al., 2017). The modified T-graft procedure usually performed in the axillary and subclavian artery, inadequate perfusion was a rare problem, possibly due to the flow direction being similar to the normal physiological direction (Ahmed et al., 2020; C. Banfi et al., 2016; Hedayati et al., 2004). Additionally, it can be applied to femoral artery approached.

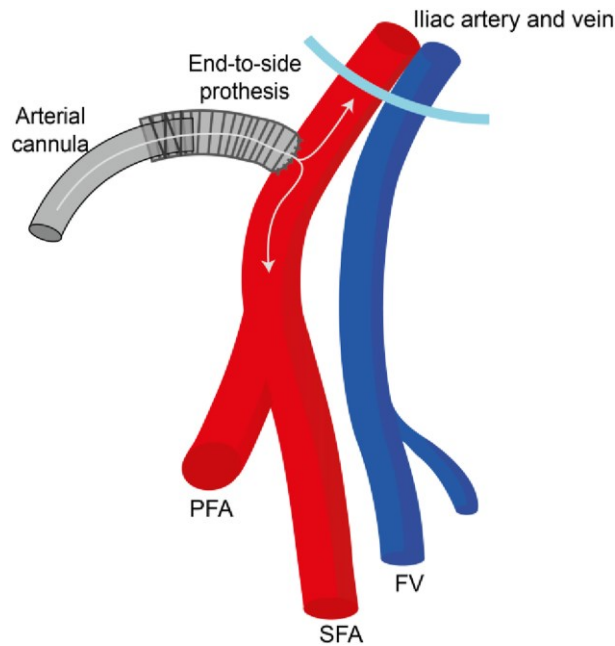


Figure 1.21 Illustration of cannulation performed by the T-graft technique.

End to side technique connects the vascular graft to the native vessel and the cannula is inserted via a graft lumen. (taken from Simons et al. (2024))

However, this approach requires open surgery to access the subclavian region and connect the cannula using an extended vascular graft. As a result, vascular injury and bleeding remain the main complications of this technique (C. Banfi et al., 2016; Chamogeorgakis et al., 2013). Furthermore, it has been found that the extended graft technique was linked to excess flow and hyperperfusion, which may lead to injury to the vessel wall (Chamogeorgakis et al., 2013).

Additionally, the procedure may prolong the preparation time for the ECMO process due to associated complications, and critically, the preparation of an effective graft branch connection requires the expertise of a skilled physician (Bauer & Malone, 2022; Calderon et al., 2015; Kemaloğlu, 2018; Mosquera et al., 2014; Reeb et al., 2016).

1.8.2 Distal perfusion

Another approach to preserving distal perfusion involves the insertion of a secondary catheter to provide support to the distal region of the limb (Figure 1.22). An extension line is required in this procedure to separate the blood from the perfusion circuit connected to the distal catheter. This extension line is necessary to provide blood flow to the inferior part of the legs (C. Banfi et al., 2016; Huang et al., 2004; Makdisi et al., 2017). Recently, the reports have demonstrated favourable results using prophylaxis distal perfusion catheter, thus supporting the recommendation of ELSO to utilise this technique in ECMO cases. Therefore, several centres prioritise using this procedure to enhance distal perfusion in peripheral VA-ECMO (Gajkowski et al., 2022).

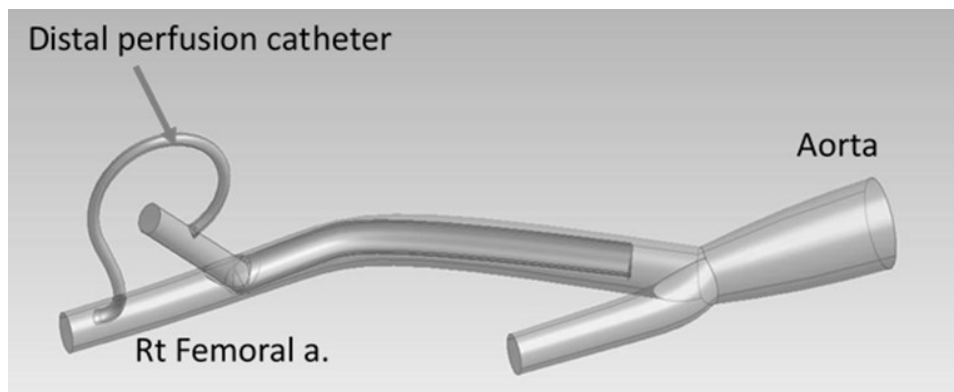


Figure 1.22 Distal perfusion technique.

Second catheter required to insert to the opposite direction to provide blood supply distally.

Distal perfusion remains a significant complication, as reported in several studies. The proper placement of prophylactic catheter cannulation requires the skill of a trained physician, as it has been observed to be vessel perforation and incorrectly placed (Rupprecht et al., 2015; Wang et al., 2023). Also, there have been reports of complications related to the haematological status, including bleeding and clotting formation at the cannulation site. The management of bleeding at cannulation sites involved sewing and applying local pressure. However, in cases of serious bleeding, the administration of blood components may be necessary (Nguyen et al., 2022). Clot

formation may occur more often in the low-flow space segment due to the limited blood flow between the arterial cannula and the distal perfusion cannula as shown in Figure 1.23. Consequently, limb ischemia caused by thrombosis can remain elevated even after decannulation (Au et al., 2019; Trieu et al., 2023).

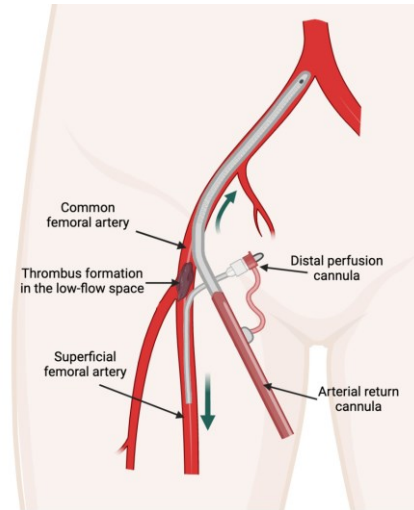


Figure 1.23 Clot formation in distal perfusion technique.

(taken from Trieu et al. (2023))

The multiple cannulations related to blood stream infection as found in several ECMO reports. This issue is associated with decreasing of survival rated in ECMO. (Allou et al., 2019; Lee et al., 2022). There were no direct reports of infection associated with the distal perfusion catheter. However, using secondary insertion sites were possible found the catheter-related blood stream infection.

1.8.3 Small arterial cannula

Large arterial cannulas are usually placed into the femoral artery to ensure adequate perfusion. However, it can be tight around the vessel and can obstruct blood flow distally. Therefore, smaller arterial cannula sizes for femoral cannulation have been introduced to clinical practice. This technique uses a cannula with a smaller diameter than the native artery and aims to permit blood flow to leak in a retrograde direction to the distal aspects of the extremities. Kim and colleagues (2019) reported that the limb

ischemia during ECMO associated with the ratio of cannula diameter to BSA more than 11, therefore using the small cannula possibly reduced the limb ischemia (Kim et al., 2019; Takayama et al., 2015).

Small cannulas also provide superior bleeding outcomes compared to larger cannulas. However, this procedure also has negative results, including infection and leg ischemia, which may require the cannula to be repositioned (Takayama et al., 2015). In addition, most patients on ECMO are administered drugs that cause vasoconstriction to maintain acceptable haemodynamic, which therefore disallows retrograde flow. As such, restricted blood vessel diameters affect blood flow and may contribute to ischaemia (Moller et al., 2019).

Table 1.9 Summary of current techniques for distal perfusion.

Technique	Description	Possible Site	Limitation
T-graft (Calderon et al., 2015)	Connect end of the vascular graft to side of a native blood vessel Insert the long straight cannula into a vascular graft	Axillary a. Subclavian a. Femoral a.	Need to expose skin Site graft bleeding/leakage Thrombus formation Site infection Overflow Skilled physician Extend duration
Distal catheter (Makdisi et al., 2017)	Catheter inserting to preserve the legs' inferior part. Split blood from the circuit to distal part	Femoral a.	Two sites of insertion Higer risk of infection Bleeding Clotting formation Skilled physician Extend duration
Smaller arterial cannula (Takayama et al., 2015)	Using smaller diameter than native blood vessel	Axillary a. Femoral a.	Vasoconstrictor cause obstruction

1.9 THE BI-DIRECTIONAL CANNULA

A bi-directional cannula features a single inlet that bifurcates and allows blood flow in two directions and is used to prevent the restricted perfusion to distal sites. It eliminates the side effects of two insertion sites and decreases the likelihood of ischaemic events. In addition, the procedure time for initiating ECMO can be reduced by minimising the time required to insert two catheters. The present design categorises the bi-directional cannula into two groups based on the presence or absence of side-hole features.

1.9.1 Self-expanding bi-directional cannula

The cannula called Smartcannula® LLC (Lausanne, Switzerland) was developed by von Segesser and colleagues as reported in 2002. The main features include the tip with a self-expanding mesh made from memory alloy. This cannula was initially developed in CFD for venous cannulation to enhance venous drainage during cardiopulmonary bypass procedures, then has been proven in animal experiments and clinical use (Berdajs et al., 2010; Mueller et al., 2002).

Self-expanding cannula has been extensively utilised in bi-directional arterial cannula applications. Figure 1.24 demonstrates that the mesh allows the retrograde blood flow into the distal segment. This cannula has been tested in animal models undergoing cardiopulmonary bypass. The authors claim that the cannula supports better flow to the distal segment than the additional catheter technique. However, the cannulation method requires fastening and securing by the 45-degree angle ring which causes lack of flexibility (D. Berdajs et al., 2011).

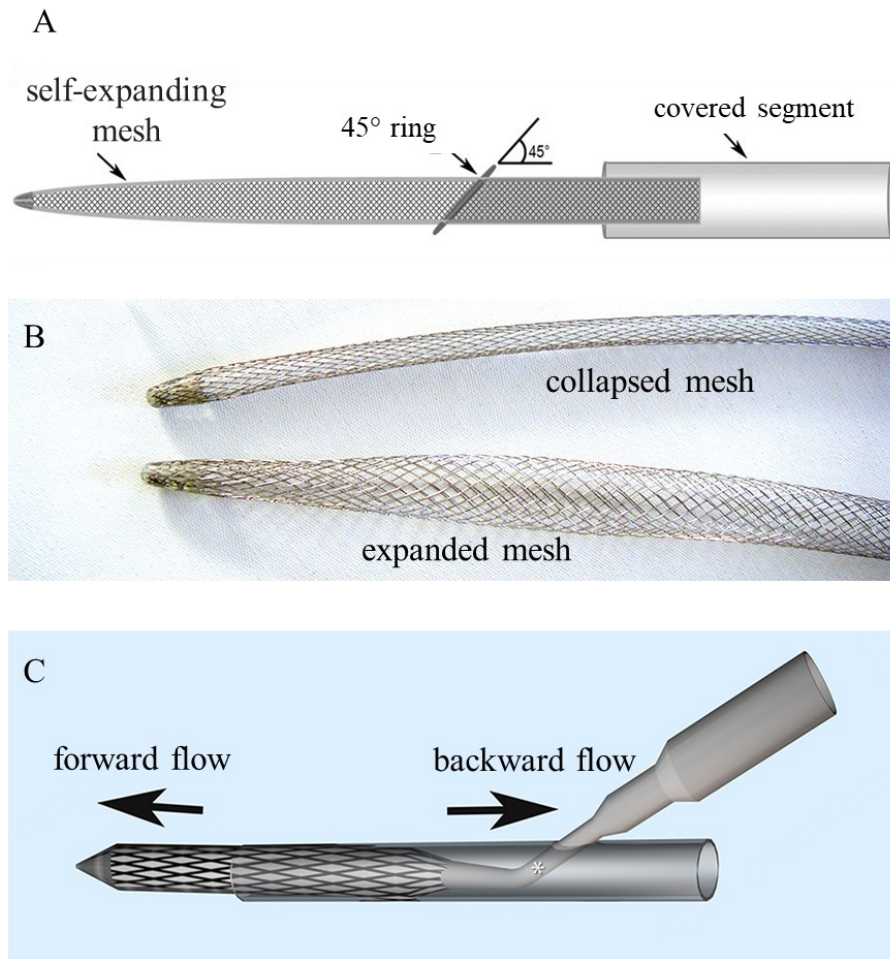


Figure 1.24 Self-expanding bi-directional cannula.

(A: Cannula structure; B: Demonstrated collapsed and expanded mesh; C: Diagram of cannula configuration in the blood vessel. (Taken from Berdajs et al. (2010); von Segesser et al. (2016).

The cannula was suggested for potential use in ECMO for the prevention and treatment of leg ischemia during H1N1 pandemics (von Segesser et al., 2016). Furthermore, the cannula received ongoing improvements in different versions and was later evaluated by *in-vitro* experimentation. These tests aimed to examine cannulas' efficacy in the pressure-flow relationship and both directional flow performance. The cannula demonstrated favourable flow and pressure properties as compared to the standard cannula. This finding suggested that the bidirectional cannula offers a potential solution for addressing lower leg ischemia. The authors propose conducting *in-vivo* investigations to validate

these results prior to using them in clinical situations (Abdel-Sayed et al., 2020; Abdel-Sayed et al., 2021).

1.9.2 Bi-directional cannula with the side hole

In contrast, design of a bi-directional cannula with a side hole, the main component includes end opening combined with another opening on cannula's side wall. These openings will be delivered blood to the systemic and distal part, respectively. There are two previous designs of bi-directional cannulae, demonstrated in a CPB and ECMO, with circumferential, multi- and single side- hole.

The cannula design by Magovern and colleagues in 2005 utilised circumferential holes and a gap between the cannula and the vessel allowed blood flow to pass through the cannula to the distal part. In animal experiments, using a two-hour cardiopulmonary bypass period, they found a significantly higher flow to distal femoral aspects when compared to the standard single mono-directional cannula technique. However, the experiment was not performed under prolonged support conditions as in the clinical setting (Magovern et al., 2005).

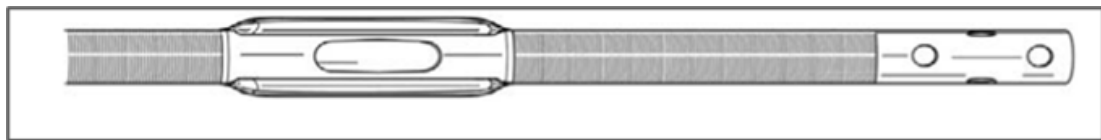


Figure 1.25 Circumferential side holes bi-directional cannula.

(Taken from Magovern et al. (2005))

In 2006, Matsui and colleagues carried out animal and clinical studies of a novel cannula configuration in which the body of the femoral arterial cannula incorporated two small side holes. These holes are positioned at distances of 103 and 110 mm from the tip of the cannula, each 2 mm in diameter (Figure 1.26). The cannula underwent validation in the animal model, demonstrating a flow rate of 1.5 LPM and a separate flow to the distal part corresponding to 5-6% of the systemic flow. Then the cannula confirmed in clinical studies, ECMO was run for between 1-12 days in six patients. The authors claimed that

this cannula can be provide the distal and systemic flow in both experiments. However, there were three participants in clinical trial required repositioning the cannula body to improve blood flow to the distal. The authors suggested that the size of the side holes may need to be further defined in future studies (Matsui et al., 2006).

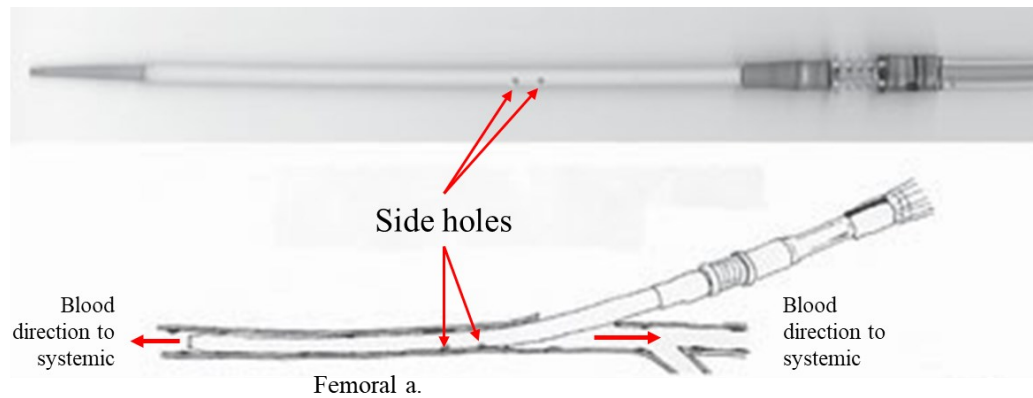


Figure 1.26 Side holes bi-directional cannula.

(Taken from Matsui et al. (2006))

The Bi-Flow femoral arterial cannula by Liva-Nova company is the only available commercial bi-directional cannula for cardiopulmonary bypass (Liva Nova's Bi-Flow™ femoral arterial cannula: Liva Nova PLC, London, United Kingdom). The structure is similar to the standard femoral arterial cannula but includes two orifices at the tip and side of the cannula. Therefore, it allows cannulation by the modified Seldinger technique. Initially, this approach was investigated in animal models (Chen et al., 2017). In 2018, Maraco and colleagues applied this cannula design to fifteen patients who underwent open-heart surgery. The duration of the cardiopulmonary bypass was between 50 to 228 minutes. Although it demonstrated that a newly designed cannula can provided blood to the distal part with minor complications, there was evidence of endothelial damage due to the sandblasting impact of the side-hole jet on the arterial wall, cannulation site bleeding, haematoma, and infection in some participants (Marasco et al., 2018).

More recently, the efficacy of this cannula was demonstrated in a larger clinical trial involving 64 patients undergoing cardiopulmonary bypass. Conventional cannulation

and bi-directional cannula were compared in the randomised control study. Seroma on the femoral region, superficial wound infection, and pseudo-haematoma were found in the bidirectional cannula group. In contrast, the conventional cannula group had femoral embolectomy and artery repair, wound infection, and cannulation site haematoma. However, this study validated the effectiveness of the novel cannula in maintaining a consistent flow to the limb (Gunaydin et al., 2021).

In 2023, the first clinical trial on this cannula with 22 patients underwent VA-ECMO and there were no reports of compartment syndrome. However, one patient reported limb ischemia and two patients experienced significant bleeding (Simons et al., 2023).

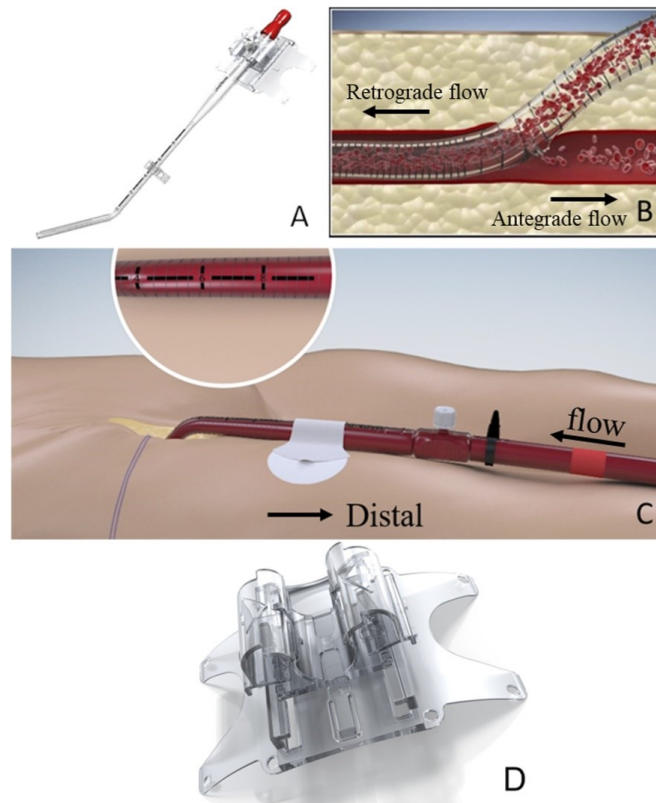


Figure 1.27 Bi-flow, commercial bi-directional cannula by Liva-Nova™.

(A: Cannula panel; B: Flow directions and configuration with blood vessel; C: Fixation and position method; D: Fixation device. (Taken from Simons et al. (2023))

A bi-directional cannula has been investigated in the Department of Biomedical Engineering at the University of Strathclyde in recent times. As shown in Figure 1.31, the cannula has single input bi-directional output and has a right-angled configuration. In this device, the inlet port receives blood flow from the ECMO system and separates the flow into two streams using an internal flow diverter which proportionately splits the blood flow to the proximal and distal outlets. The two outlets sit in the horizontal plane in the vasculature and provides blood to systemic and distal parts. This design potential aligns with the ideal bi-directional cannula featuring the following two characteristics.

1. One inlet and two outlets, this feature allows:
 - Enables the use of a single cannulation site.
 - Reduces the risks linked to the deployment of an isolated distal cannula.
2. Internal split barrier, this feature allows:
 - Proportionately divide blood flow to the proximal and distal part.

However, abnormal flow conditions demonstrated in animal experiments may result in haemolysis and possibly vessel injury. The present work will continue to improve the design with the objective of addressing these issues (Gourlay T et al.).

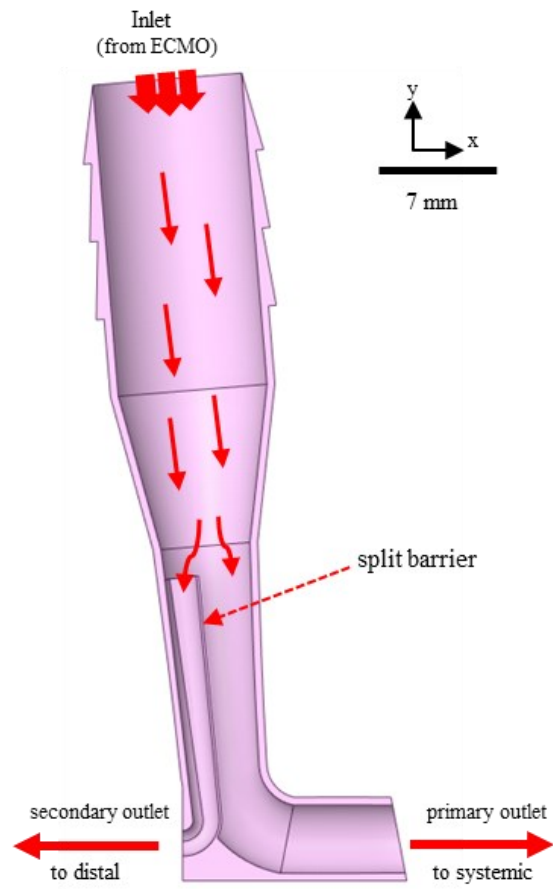


Figure 1.28 Internal structure of the bi-directional cannula designed by Prof. T Gourlay

Table 1.10 Summary of current design in bi-directional cannula.

Model	Feature	Experiment	Limitations	References
Self-expanding	Cone-shaped tip with a self-expanding mesh body and the distal segment 45-degree angle ring	Animal <i>in-vitro</i>	Lack of flexibility to change position. Need to validate the application as a bi-directional arterial cannula.	Mueller XM, et al., (2002) Berdajs et al. (2011) von Segesser, L. et al. (2016) Abdel-Sayed et al. (2020, 21)
Circumferential side holes	Circumferential holes and gap between the cannula and the vessel	Animal	CPB duration is shorter than in the ECMO case. Rail crest designed might cause a perforated vessel during insertion.	Magovern et al. (2005)
Two small side holes	Straight femoral arterial cannula integrated with two small side holes	Animal and Human	Half of the participants need to reposition to release blood flow to the distal	Matsui Y et al (2016)
Bi-Flow femoral arterial cannula	Straight femoral arterial cannula includes two orifices at the tip and side of the cannula	Animal and Human	Provided blood to the distal part with minor complication, but risk of perforated vessel	Chen et al. (2017) Maraco et al (2018) Gunaydin et al. (2021) Simons et al., (2023)
Prof. Gourlay's bi-directional cannula	Right-angle shape includes one inlet, and two outlet features with split wall	Animal <i>in-vitro</i> <i>in-silico</i>	Possible vessel injury and haemolysis	Gourlay T et al.

1.10 CHAPTER SUMMARY

- ECMO is a mechanical cardiopulmonary support technique used to treat critical patients suffering from circulatory and/or respiratory failure and insufficiency.
- In a manner similar to CPB, ECMO transfers deoxygenated blood from the patient, exchanges it throughout the extracorporeal circuit and returns it to the native circulation in an oxygenated state. The artificial circulation provided by the ECMO system results in a reduced left ventricle and lung workload, permitting these to recover under less functional stress.
- The components of an ECMO circuit include an artificial oxygenator, blood pump, tubing system and cannulae. The patient's deoxygenated blood will be drained through the venous (or access) cannula and pumped through the artificial gas exchange system and back to the patient via the arterial (or return) cannula.
- The monitoring and management plan in ECMO is associated with the patient's pathophysiology and the ECMO component employed, and common complications generally relate to either the patient's condition or circuit component issues.
- The cannulation is critical to the success of the ECMO outcome. The cannula connects the native circulation and the ECMO circuit. In clinical practice, the insertion sites for VA-ECMO can be classified into two groups, central and peripheral cannulation. Access cannulation can be employed using the right atrium, superior and inferior vena cava, femoral vein, subclavian vein, or internal jugular vein. In contrast, return catheter is generally inserted into the aorta, femoral artery, axillary artery, or carotid artery. The peripheral VA-ECMO for emergency support the arterial cannula is commonly deployed via the femoral artery or carotid artery (Pavlushkov et al., 2017).

- The peripheral arterial cannulation approach is associated with an increased risk of ischemia events. The arterial cannula in peripheral VA-ECMO causes blood vessel obstruction and reduces blood supply to the distally to the insertion site. These episodes can lead to a lack of oxygen and nutrient support to the distal organs. In patients undergoing VA-ECMO using the femoral artery, the distal limb ischaemia can lead to fasciotomy or amputation. Using the carotid artery for arterial return introduced a risk of post-ECMO cerebral complications (ELSO, 2017, 2019).
- Recently, it has been recognized that an approach to mitigating these complications is required for safe ECMO deployment. One option is to deliver two arterial cannulae, one of which provides distal blood flow. Another approach, which has gained some clinical traction, is to deploy a single cannula using an end-side graft. However, complications associated with these approaches including bleeding, vessel perforation, and infection have been identified in clinical practice (Napp et al., 2016, Pavlushkov et al., 2017, Hendrickson and Glower, 1998, Matsui et al., 2006). Attempts to deploy an arterial cannula with bi-directional flow have been made in cardiovascular surgery cases, in procedures far shorter in duration than ECMO, however, investigations have found problems associated with the insertion of the cannula. (Marasco et al., 2018).
- The review of the literature in the context of the present work suggests that the ideal arterial cannulation solution should the following critical characteristics.
 1. One inlet and two outlets - this allows a single cannulation site to be employed and eliminates the risks associated with deploying an isolated distal cannulae to provide distal flow.
 2. The flow distribution of this cannula should not raise the risk of vascular wall and blood damage. The blood flow from this cannula should be predictable.

3. The cannula's size should fit to the vessel diameter, directing blood flow along the central line. Tangential flow jetting from a poorly designed cannula in the arterial position can lead to vessel wall damage and embolic risk.
4. The cannula should provide adequate systematic and distal perfusion. This is the most important feature, blood flow from cannula is not only predictable but also given appropriate ratio to support organ perfusion in both flow directions.

CHAPTER 2

THESIS AIMS AND OBJECTIVES

2.1 CLINICAL RATIONALE

The incidence of ECMO use continues to rise in modern clinical practice, generally employing peripheral cannulation techniques despite the known complications associated with this approach. To overcome some of these complications, the present work is focused on the design of a single inlet bi-directional cannula for use in ECMO situations. Much of this work will focus on the cannula design and validation using laboratory and *in-silico* techniques.

It is recognised that utilising an additional cannula to support distal perfusion during ECMO requires two insertion sites, increasing the risk of cannulation site complications, and indeed, some associated systemic complications, such as infection and vascular injury. Therefore, any ideal bi-directional cannula should have a single inlet and the capability to provide blood flow in two directions.

Blood flow distribution in the proximal and distal parts is a significant concern in avoiding over-perfusion in T-graft cannulation methods. The novel design should incorporate a mechanism or structure to split the flow into proximal and distal elements and to provide these in proportion to flow demand, thereby providing adequate flow in both directions to support metabolic demand.

Ideally, flow from both outflows should be aligned with the central line of the insertion vessel to protect from sandblasting effects caused by directing blood flow at the vessel wall, a common cause of vascular damage in previous designs. Additionally, when utilising the carotid artery approach, for ECMO support, a bi-directional cannula is capable for providing essential cerebral perfusion rather than relying on collateral flow. The provision of cerebral support during ECMO, particularly when the carotid approach

is employed remains a clinical concern that may be somewhat addressed through the deployment of bi-directional flow cannulae.

This thesis proposes that a cannulae design, utilising a novel bi-directional flow structure, could successfully reduce complications associated with peripheral ECMO, particularly vascular and haemodynamic complications.

2.2 HYPOTHESIS AND OBJECTIVES

Objectives of the Research

The overall objective of this work is to develop a prototype bi-directional cannula for single port peripheral access in patients undergoing ECMO. The validity of the technology will be assessed under laboratory and *in-silico* conditions. In particular, the work will address the following associated objectives:

1. To design and produce a single input bi-directional cannula with adequate and proportional flow distribution profile.
2. To ascertain that the cannula, designed for the single input bi-directional approach to cannulation has acceptable fluid dynamic properties without issues of jetting to the vascular wall in either output aspect.
3. To demonstrate that the cannula design has acceptable haemodynamic properties.

This work proposes the design and development of a novel single-input bi-directional cannula with the ultimate objective of minimising some of the complications associated with peripheral ECMO, specifically in relation to vascular access and impact. The planned flow of the research is as follows and is outlined in Figure 2.1.

Phase 1 - To utilise computational fluid dynamics (CFD) to conduct an *in-silico* study and observe the flow distribution of the previous version of the bi-directional cannula used in VA-ECMO (Chapter 3).

Phase 2 - To improve the bi-directional arterial cannula, investigate flow distribution *in-silico* study, and then produce the cannulae prototype (Chapter 3).

Phase 3 - To validate each version through flow visualisation using dye injection and particle tracking (Chapter 4).

Phase 4 - To investigate haemodynamics via the pressure-flow characteristics of the cannula prototype, and proportional flow distribution (Chapter 5).

Phase 5 - To investigate haematological responses in an *in-vitro* experiment using animal blood (Chapter 6).

Figure 2.1 illustrates the algorithm employed in this study. This thesis project will analyse flow distribution using CFD. This experiment highlights and discusses the potential problems for developing a new design. The most appropriate bi-directional cannula geometry will be evaluated and refined using CFD until the ideal model is reached. After that, a 3D printing prototype of the suitable model will be produced. Each prototype will be tested under laboratory conditions with a focus on haemodynamics and flow distribution and vectoring.

Hypothesis

The hypothesis is that is possible to produce a single input bi-directional cannula for ECMO applications with acceptable haemodynamics and proportional flow distribution.

Null Hypothesis

It is not possible to produce a single input bi-directional cannula for ECMO applications with acceptable haemodynamics and proportional flow distribution.

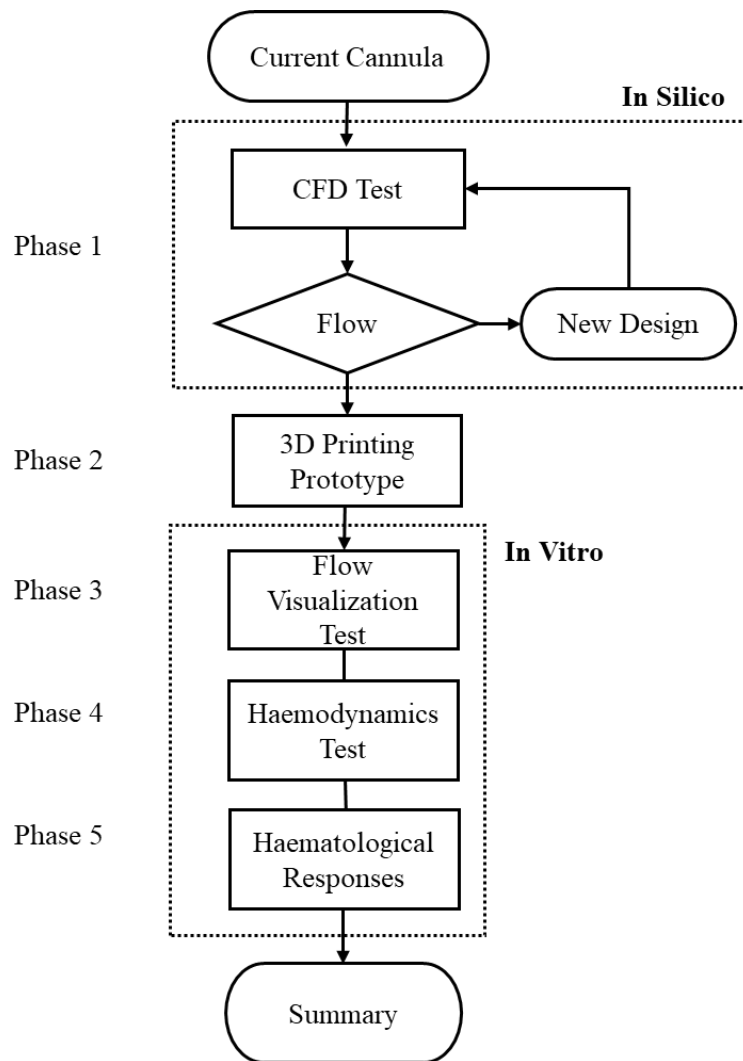


Figure 2.1 The algorithm to determine the conceptual framework of this study.

CHAPTER 3

BI-DIRECTIONAL ARTERIAL CANNULAE DESIGN

3.1 INTRODUCTION

The arterial cannula is the catheter that links the circuit and the patient. This component is crucial in ensuring sufficient blood flow through the ECMO, which is essential for achieving successful outcomes. The cannula features and their impact on flow are critical for designing an appropriate cannula (Kohler et al., 2012). Computational fluid dynamics (CFD) is widely recognised for its ability to estimate blood flow characteristics and vascular wall shear (Kumar et al., 2023; Schwarz et al., 2023). This technique also offers advantages over experimental methods in terms of cost and time efficiency (Kohler et al., 2012; Sotiropoulos, 2012).

CFD is utilised to examine the flow of CPB and ECMO to understand the physiological changes that occur during procedures. Additionally, CFD is a valuable tool for the design of flow circuit components. Different cannula tips and configurations have been investigated to determine the jet flow characteristics and predict its impact on the vessel wall. Neidlin and colleagues (2014) compared the jet flow characteristics from six cannula designs, which have differences in the internal features and tips. The addition of swirl and side holes in these features was meant to reduce the impact of the cannula jet on the aortic wall and distribute the blood flow. The finding found that the cannula features influence the flow distribution and its impact jet on the aortic wall stress.

These similar results found by Thomas and colleagues (2017), who performed CFD to guide the design of the aortic cannula feature and tip by comparing different cannula tips. An internal spiral flow inducer was used to decrease velocity and minimise the impact of the jet flow on the vessel wall. The cannula with spiral flow inducer found better in velocity factors compared with the standard cannula. This suggests that a lower jet velocity may potentially decrease the sandblasting effect on the blood vessel wall.

(Thomas et al., 2017). Additionally, Gramigna and colleagues (2023) investigated the flow and wall shear stress from two cannulas, straight and angled tips, for ascending aorta cannulation. The study highlighted the benefits of utilising CFD providing valuable understandings and recommendations for physicians based on the cannula selection (Gramigna et al., 2023).

Nezami and colleagues (2021) performed CFD to assess the peripheral ECMO at the femoral cannulation in relation to various heart conditions during every stage of the ECMO support, from the full support until the weaning process. The results showed that oxygenated blood from ECMO cannot be provided to the upper region of the body when cardiac contraction has recovered. This issue occurs because the cardiac output can resist the ECMO flow. The study's findings suggest that CFD can be used to estimate ECMO flow and predict potential complications. (Nezami et al., 2021). A study also analysed the haemodynamic status of two different ECMO options, central and peripheral cannulation. The authors stated that, whilst peripheral ECMO may achieve better upper limb and brain perfusion compared to central ECMO, it is most associated with lower limb ischemia. Central ECMO cannulation complications are more likely to be wall shear stress in the ascending aorta region (Gu et al., 2016).

Regarding the CFD for study distal perfusion in ECMO, Brockaert and colleagues (2023) investigated the different sizes of the main and distal cannula for peripheral ECMO. The arterial cannula size was 21 Fr, 19 Fr, 17 Fr, and 15 Fr with distal perfusion of 10 Fr, 8 Fr, and 6 Fr. They suggested that the size of the distal catheter was related to the size of the main arterial catheter. The optimal combination was identified as using a 17 Fr arterial cannula with 8 Fr and 10 Fr distal catheter. These findings demonstrated that the proportional blood supply to the systemic and distal regions is essential to preserve the whole body and organs (Brockaert et al., 2023).

As demonstrated in the aforementioned studies, CFD can provide insights into haemodynamic in different situations and cannulae design. Moreover, it offers the advantage of the operating plan to enhance the outcome of ECMO. However, achieving

model accuracy and taking physiological factors into account remain significant challenges in CFD. This enables the simplification of unnecessary model complexity, striking a balance between computing speed and accuracy, leading to discrepancies between calculated results and true values (Lee, 2011; Morris et al., 2016).

In this study, the CFD is utilised as an initial step to analyse the newly designed cannula. This chapter presents the findings of the CFD analysis, which aimed to determine the flow trajectory and the impact of each novel cannula configuration on the vasculature. These data aimed to guide prototype development for further testing, as stated in phase 1 and 2 of the planned flow of the research (Session 2.2).

3.2 The 1st ITERATION

The Initial Design and 1st iteration Cannula

The bi-directional cannula was reconstructed from an initial design. The ideal design for a peripheral ECMO cannula is a right-angled shape with a bi-directional flow featuring a single input and two outlets. The original design has an external diameter of 14 French (Fr) (4.66 mm). A partitioning wall separates the blood flow from the main inlet into two separate outflows, referred to as the primary and secondary lumens. The outlet lumens are intended to supply blood to the systemic and distal regions of the cannula body. The primary outlet is responsible for supplying blood to the systemic circulation, while the secondary outlet supplies blood to the distal region. The cannula used in the initial design of this study will be referred to as the 1st iteration cannula. Figure 3.1 illustrates the internal structure of the 1st iteration cannula of the bi-directional cannula.

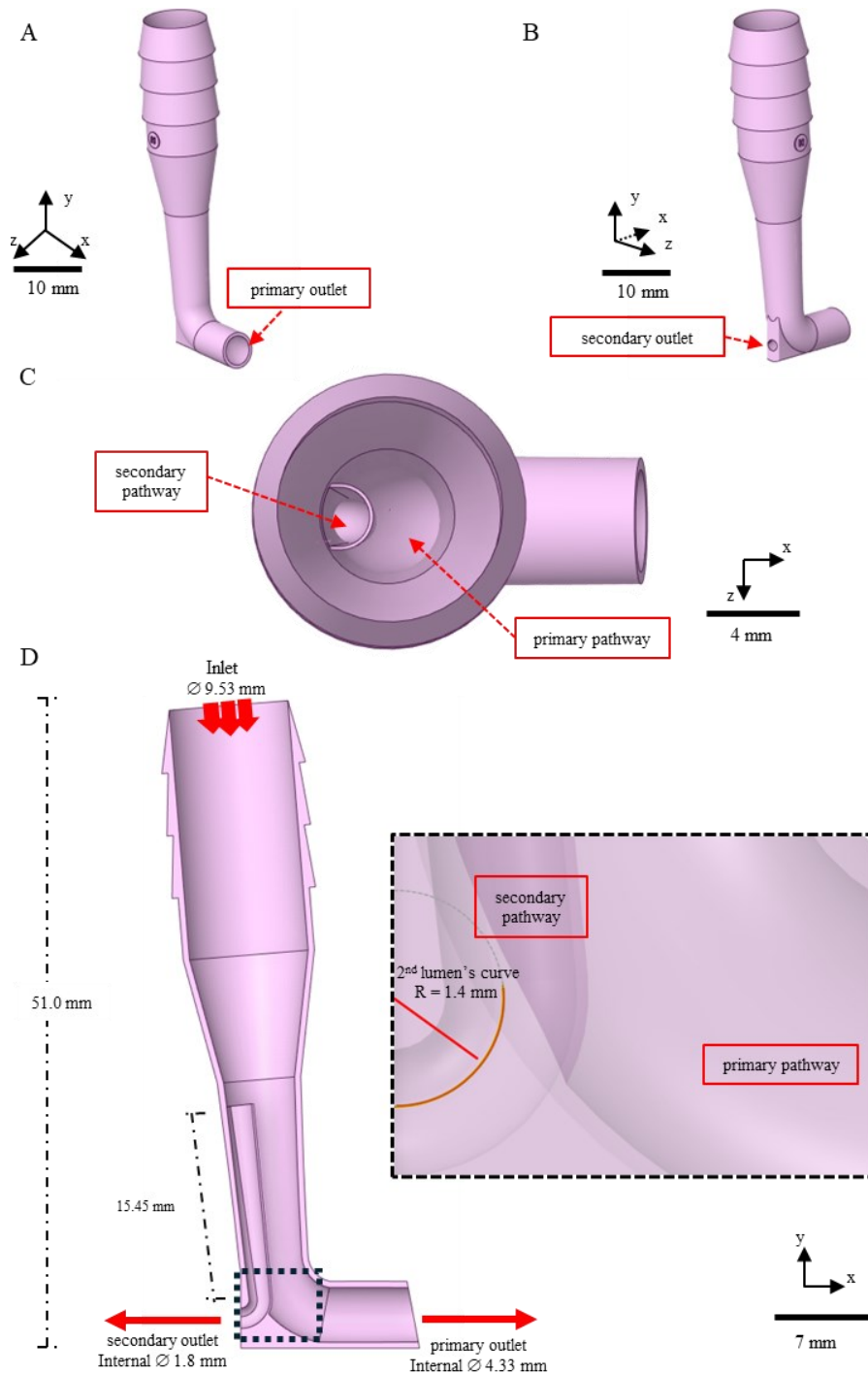


Figure 3.1 Illustrated the structure of a bi-directional cannula (1st iteration cannula).

(A: Front view shows the primary outlet; B: Rear view shows the secondary outlet; C: Top view shows the cannula's inlet; also see through on the top presented the primary and secondary lumen; D: Internal structure from a long sectional view, curvature and underpart of the secondary lumen is 1.40 mm.)

The 1st iteration cannula geometry was created in the design software (Space Claims, ANSYS Inc, USA and Creo Parametric 3.0, PTC Inc, Boston, USA) regarding the original version. The outer diameter was increased to 5.33 mm (16 Fr), aiming to be suitable for patients weighing about 40-50 kg. The cannula is expected to provide blood flow at about 3-4 litre per minute (60-80 ml/kg/min) (Brown et al., 2021; Gajkowski et al., 2022; Pooboni & Gulla, 2021).

The cannula body's overall wall thickness is fixed at 1.00 mm. The secondary lumen has a diameter of 1.80 mm (5.4 Fr) and a radius curve of 1.40 mm, whereas the internal diameter profile of the primary lumen is 4.33 mm. The diameter of the secondary lumen is estimated based on the distal catheter size utilised in previous studies that utilised 5.0 Fr catheter for support distal perfusion (Elmously et al., 2018; Lamb et al., 2017). In addition, the cannula body is integrated with the connector part, which is prepared for joining with a 3/8-inch tube (internal diameter), as generally used for an arterial line in the ECMO clinical procedures (Gajkowski et al., 2022).

3.2.1 MATERIALS AND METHODS

Computational Fluid Dynamics

Geometry preparation

A cannula geometric model was assembled into the 7.00 x 120 mm vascular pipe identical to common femoral artery dimensions, as shown in Figure 3.2.(Brockaert et al., 2023; Crişan, 2012b; Gu et al., 2016; Hwang, 2017), and then the file was imported into Ansys workbench to edit the geometry and CFD process (Ansys fluent 2022 R1, ANSYS Inc, USA). The connector part was excluded due to minimising the complexity of model meshing.

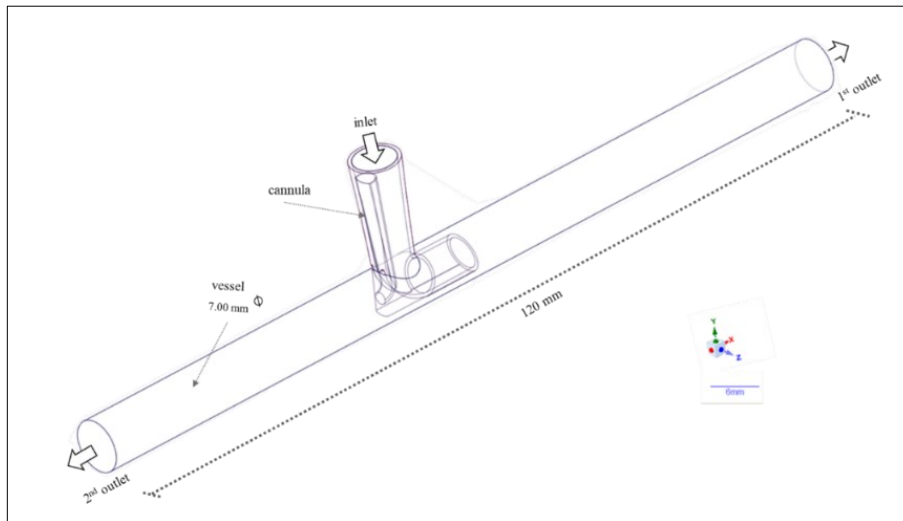


Figure 3.2 *Cannula in the vascular structure for the CFD test.*

The geometric model of a cannula is compiled into a 7.00 x 120 mm vascular model. The cannula connector has been excluded from the model to eliminate complexity in mesh generation. One inlet and two outlets of the bi-directional cannula are determined for the CFD test.

Mesh preparation

Mesh generation on the fluid domain was prepared using the patch-conforming tetrahedron method. Inflation boundary layer grids were generated regarding the near-wall boundary of vascular geometry. The velocity at the cannula tip was in accordance with the literature (Foltan et al., 2019; Thomas et al., 2017). Inflation layers were implemented to achieve a y^+ value of approximately 1. Therefore, 0.077 mm was used as the first layer thickness. The inflation layer growth factor rate of 1.2 progressively increases to 5 layers (Figure 3.3). After applying the inflation layers, the mesh element size was adjusted from coarse to fine. Then, the mesh-independent tests or grid-independent tests (GIT), were conducted to confirm the acceptability of element number and maximum velocity in the CFD was approximately 6.35 m/s, which resulted in the grid number of about $2.5 - 3.5 \times 10^6$ elements being used in this study (Figure 3.4).

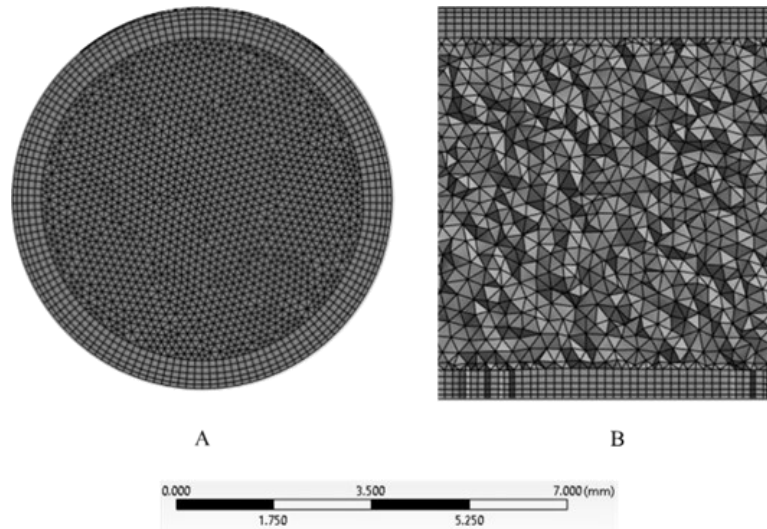


Figure 3.3 Vascular mesh generation for the CFD test with the near wall inflation layers.

The inflated layers were created to mimic the impact of boundary region flow near the vessel wall. (A: Cross-sectional view; B: Long-sectional view)

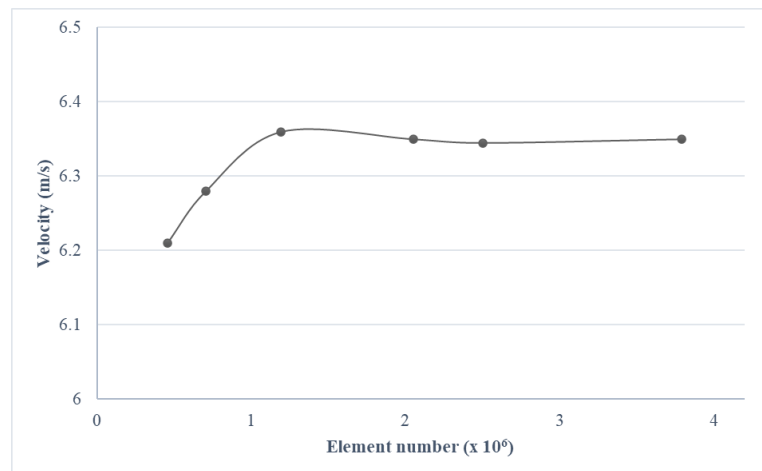


Figure 3.4 Grid-independent tests (GIT) for mesh generation.

The graph of adjusted mesh size and maximum velocity that measured from CFD. The study's utilization of $2.5\text{--}3.5 \times 10^6$ elements showed that the highest velocity was approximately 6.35 m/s.

Fluid properties

CFD in the cardiovascular system can be performed using either Newtonian or non-Newtonian fluid models. The non-Newtonian fluid model is determined as a shear rate

layer of viscosity. This fluid property is recommended for use in small artery simulations, such the cases that involving coronary and cerebral arteries and complex geometries, because it can provide more accurate outcomes for wall shear stress (WSS) (Hippelheuser et al., 2014; Rabby et al., 2014). In addition, for vessels with a diameter larger than 1.0 mm, it is reasonable to assume that blood exhibits the characteristics of a Newtonian fluid (Bessonov et al., 2016). Thus, for this study, Newtonian and incompressible fluids were utilised in the CFD simulation. The constant density and viscosity were set at 1060 kg/m^3 and 0.0035 kg/m-s , respectively, with the transition-SST turbulence model (Gramigna et al., 2023; Kaufmann et al., 2014; Menon et al., 2013; Nezami et al., 2021).

Boundary Condition

An estimated mass-flow condition of 4.0 LPM (0.07 kg/s) with pressure of 100 mmHg (13,333 Pa) was used to set the boundary at the inlet (Brodman et al., 1985; Neidlin et al., 2014). The outlet flow parameters were set up with a primary to secondary lumen outflow cross sectional area ratio of 0.83:0.17, estimated to be the flow supplied to the lower limb and systemic (Elmously et al., 2018; Lamb et al., 2017; Neidlin et al., 2014). The semi-implicit method for pressure-linked equations (SIMPLE) was an algorithm used with a scaled residual of 1,500 iterations. Then, the target of convergence was calculated using a criterion below $10\text{E-}4$ (Gramigna et al., 2023; Kaufmann et al., 2014; Nezami et al., 2021).

Post-processing

The flow characteristics including path and velocity magnitude were assessed to identify blood flow characteristics. Then, velocity magnitudes were taken at distances of 1.0, 7.5, and 14.0 mm from the 2nd lumen to verify the direction of the jet flow. In addition, the WSS in the superior and inferior regions of the vessel model was evaluated to assess the effect of jet flow on the blood vessel wall.

3.2.2 RESULTS

Flow Characteristic

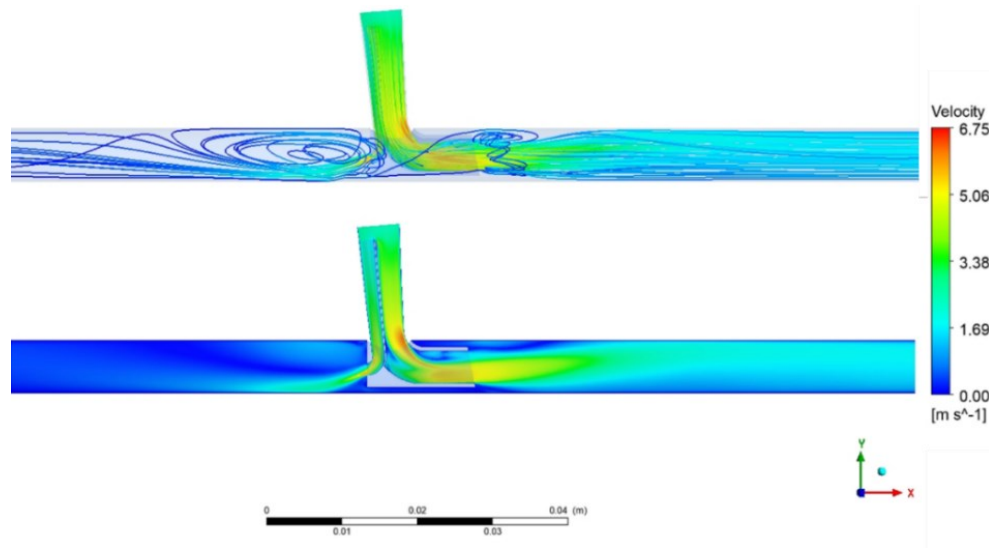


Figure 3.5 Flow path and velocity magnitude of 1st iteration cannula.

The magnitude of the flow velocity corresponds to the streamline in the value. The image clearly shows that the jet is flowing directly to the inferior vessel wall. (A: streamline of the cannula; B: velocity magnitude of the cannula)

Figure 3.5 shows the flow distribution measured via the bi-directional cannula to the vessel. The highest velocity is found at the primary pathway angle, and flow turbulence appears towards the lumen's end then returns to laminar flow at the exit. At the secondary lumen, the flow path is projected to the inferior vessel wall and causes the streamline to recirculate to the superior aspect of the vessel. The direction of velocity magnitude and streamlined distribution detects the end of the second lumen at the vessel wall.

Wall Shear Stress

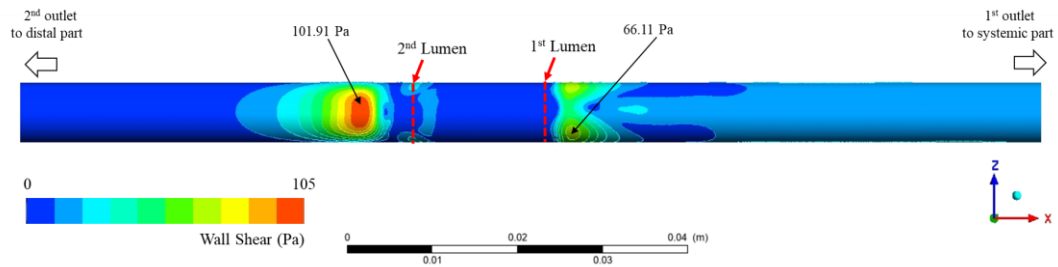


Figure 3.6 Wall Shear stress at the inferior vessel wall from 1st iteration cannula.

Significant shear is seen in the red zone after the secondary lumen.

The flow on each outlet of the cannula affected the wall shear stress, as shown in Figure 3.6. High shear at the lateral wall at the primary lumen is first caused by the turbulent flow, then gradually decreases up to the exit. However, wall shearing was higher at the secondary lumen compared to the primary lumen due to shearing stress from the blood flow projected directly to the vascular surface (101.91 vs 66.11 Pa, respectively).

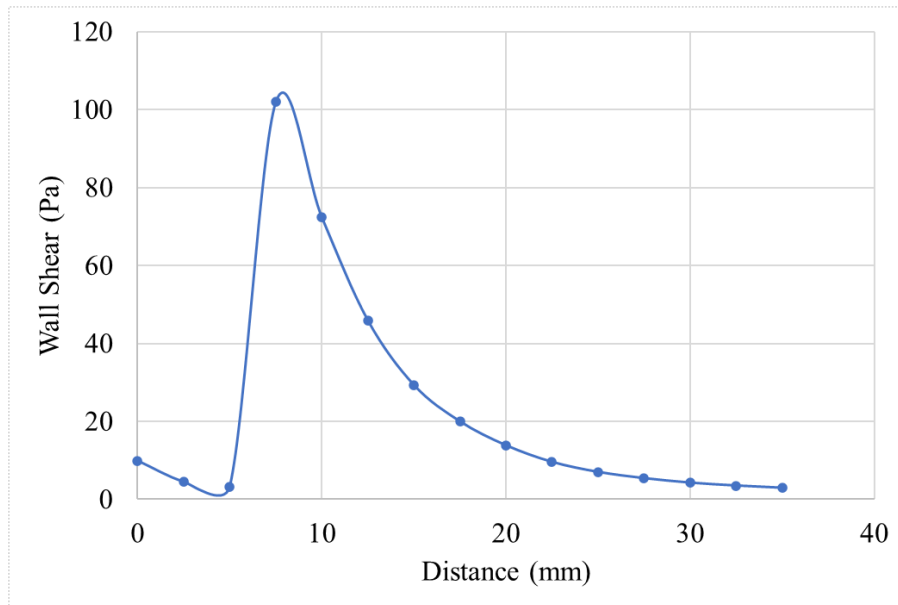


Figure 3.7 The wall shears values from the outflow of secondary lumens.

The highest WSS was found approximately 7.5 mm from the secondary lumen outlet, X-axis distance from the secondary lumen, and Y-axis wall shear value (Pa).

The graph in Figure 3.7 illustrates wall shear at a distance from the secondary lumen outflow. The most significant wall shear was found approximately 7.5 mm (101.91 Pa) from the outlet, associated with the flow directed to the vessel wall, then decrease to 2.9 Pa at 35 mm.

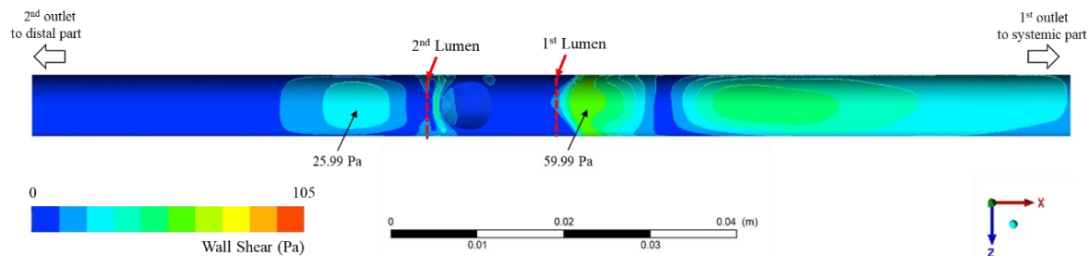


Figure 3.8 Wall Shear at the superior vessel wall from the bi-directional cannula, 1st iteration cannula.

The wall shear stress, influenced by blood flow, is measured at the superior vessel wall, with the highest shear observed at the primary outflow region and a lower shear at the secondary lumen region.

The wall shear stress resulting from the blood flow of the 1st iteration cannula was measured at the superior vessel wall, as seen in Figure 3.8. The highest shear occurred at the initial part of the primary outflow (59.99 Pa), whereas the lower zone is found at the secondary lumen (25.99 Pa). This finding is related to the previous results, in which the high turbulence at the primary lumen opening and flow path is projected directly to the inferior vessel wall.

3.2.3 The 1st ITERATION SUMMARY

The first part of this study utilised a CFD approach to investigate the flow distribution of a first iteration of a bi-directional cannula VA-ECMO (phase 1, see Session 2.2). The bi-directional cannula with a radius of 1.40 mm can provide flow in each direction. The flow directions of the secondary lumen in the 1.40 mm cannula control model resulted in greater flow velocity to the vessel wall and increased shear stress. The flow direction and extent of shear are likely to cause vascular and blood cell damage, as discussed in session 1.7.

Therefore, the flow distribution of this cannula should reduce the potential for vascular wall and blood damage, as well as excessive shear stress on red blood cells, particularly from the secondary lumen. As in the initial design results, the secondary lumen required to be improved for observing the flow direction and velocity jet into the vessel's central line, located left from the wall. The following step in this chapter will investigate an improved iteration of the bi-directional cannula based on the CFD work and will conduct *in-silico* flow distribution prior to development of the cannula prototype (see Session 2.2, phase 2).

Table 3.1 Summary of the 1st iteration canula.

Cannula	Characteristic of ideal canula		Requires improvement	
	Design	Aims	From CFD finding	Characteristic need
1 st iteration	<ul style="list-style-type: none"> - One inlet and two outlets - Internal split barrier 	<ul style="list-style-type: none"> - Single cannulation site - Proportionately divide blood flow 	<ul style="list-style-type: none"> - Flow direction of 2nd outlet to vessel wall - Jet flow with high velocity - High wall shear stress at inferior vessel wall 	<ul style="list-style-type: none"> - to improved flow direction of 2nd outlet

3.3 CHANGING THE SECONDARY LUMEN RADIANT CURVE

3.3.1 MATERIALS AND METHODS

Geometry of 2nd and 3rd iteration

In the next design step, the radiant curve was modified, leading to a shift in the arc to a sharper angle. The adjustment was made to redirect blood direction towards the centre of the vessel, thus avoiding any impact of the jet on the arterial wall.

The second and third iterations were adjusted from the control model by changing the secondary lumen radiant curve (R) of 1.00 and 0.85 mm, respectively. All structures, including internal and exterior diameters, remain the exact dimensions as in the 1st iteration cannula, except for the secondary pathway length. The secondary track was

extended from 15.45 mm to 15.80 due to adjusting the curve to 1.00 and 0.85 mm. The dimensions of the 2nd and 3rd iteration are presented in Figure 3.9.

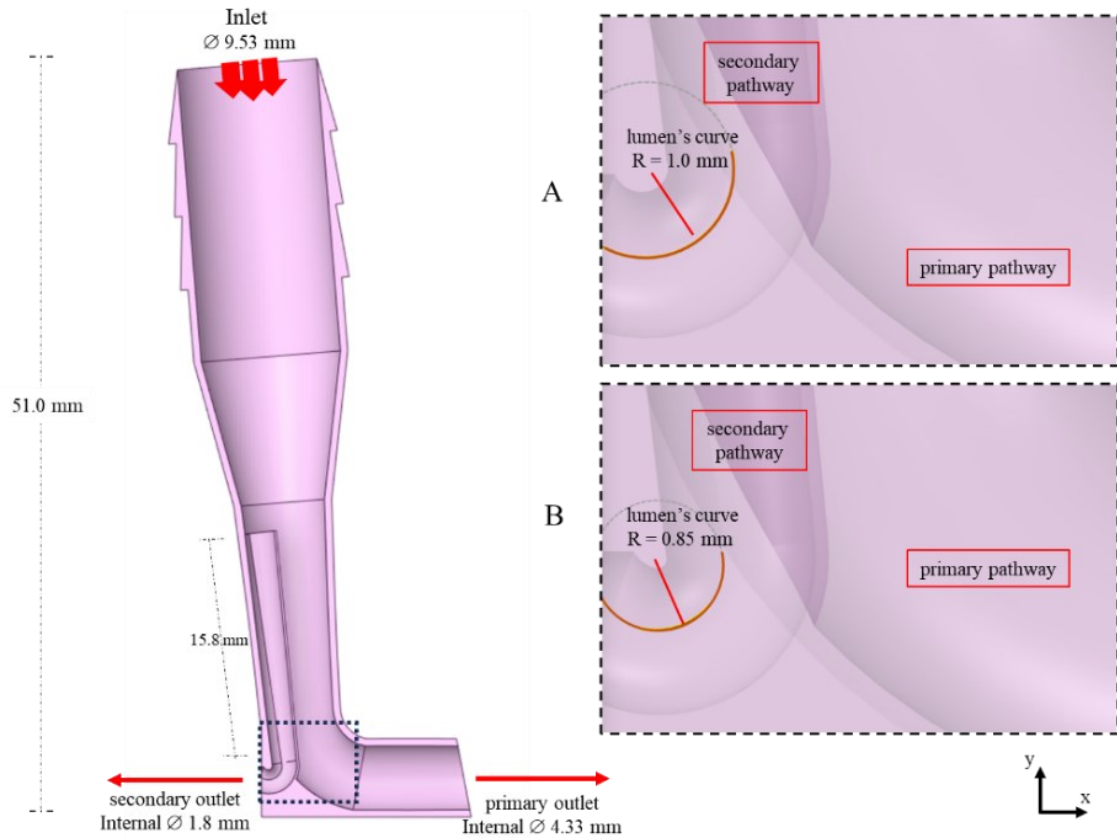


Figure 3.9 Internal structure of 2nd and 3rd iteration.

The long sectional view displays curvature and the underpart of the secondary lumen in the zoomed picture; the radius curve's lumens were adjusted to A: $R = 1.00$ mm and B: $R = 0.85$ mm, respectively.

All parameters' settings and conditions for CFD simulation were similar to those in the 1st iteration cannula (Session 3.2.1). The findings of blood flow characteristics and wall stress were evaluated for future modification phases.

3.3.2 RESULTS

Flow Characteristics

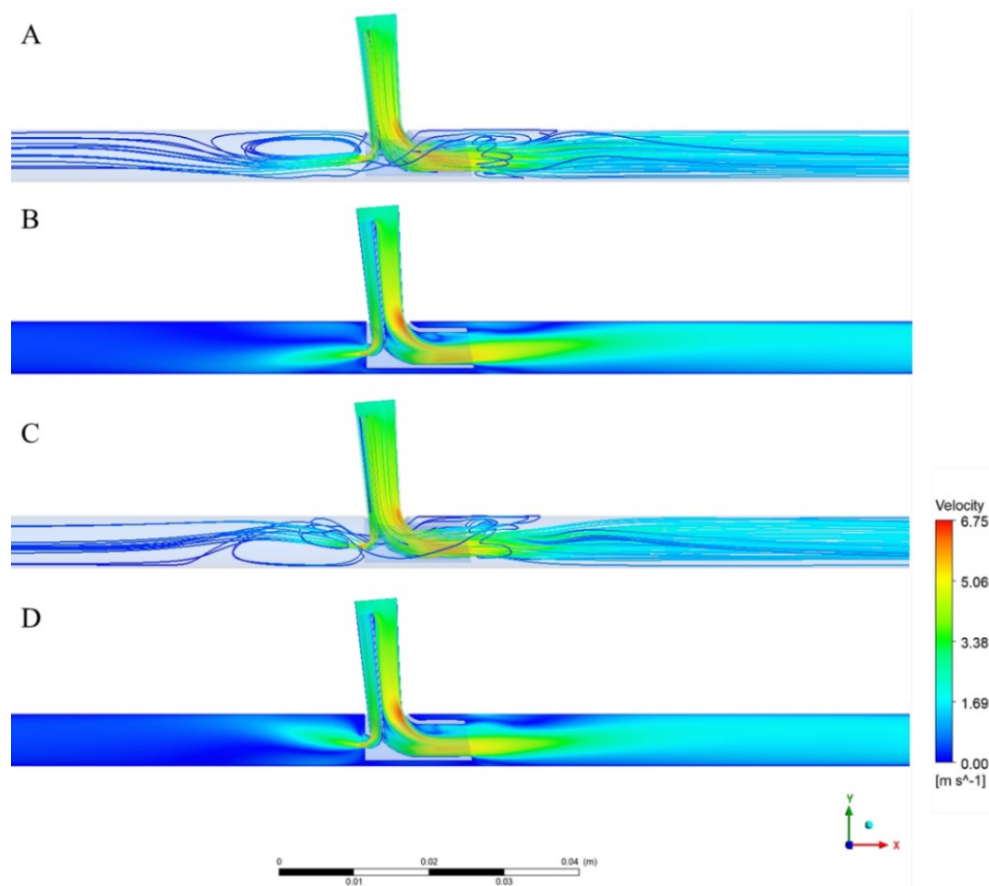


Figure 3.10 Streamline and magnitude across of flow velocity of 2nd and 3rd iteration.

The streamline pattern in both versions is similar at the primary lumen, while at the secondary lumen, the velocity magnitude of both R 1.00 and R 0.85 cannula were found to move away from the inferior wall but in different angle directions. (A: Streamline in 2nd iteration; B: Velocity magnitude in 2nd iteration ; C: Streamline in 3rd iteration ; D: Velocity magnitude in 3rd iteration)

Streamlines of flow in the 2nd and 3rd iterations, with a radian curve of 1.00 mm and 0.85 mm, are present in Figure 3.10 A and C, respectively. The flow characteristic of the 2nd and 3rd iterations found a similar pattern at the primary outlet. While, turbulence in flow is observed near the end of the lumen, transitioning back to laminar flow at the exit.

At the secondary lumen of both versions, turbulence occurred in both cases, the flow path was found to project to the inferior vessel wall in the 2nd iteration (Figure 3.10 A). This flow was closer to the middle line of the vessel compared to the 3rd iteration, which was likely project to the superior wall (Figure 3.10 C).

As well as the flow path, the velocity profile at the primary lumen of the 2nd and 3rd iteration were similar (Figure 3.10 B and D, respectively). The highest velocity point in this lumen occurs at the curve of about 6.75 m/s, a behaviour also found in the 1st iteration cannula. In addition, the velocity magnitude profile at the secondary lumen is similar in pattern to that of the streamline.

Wall Shear Stress

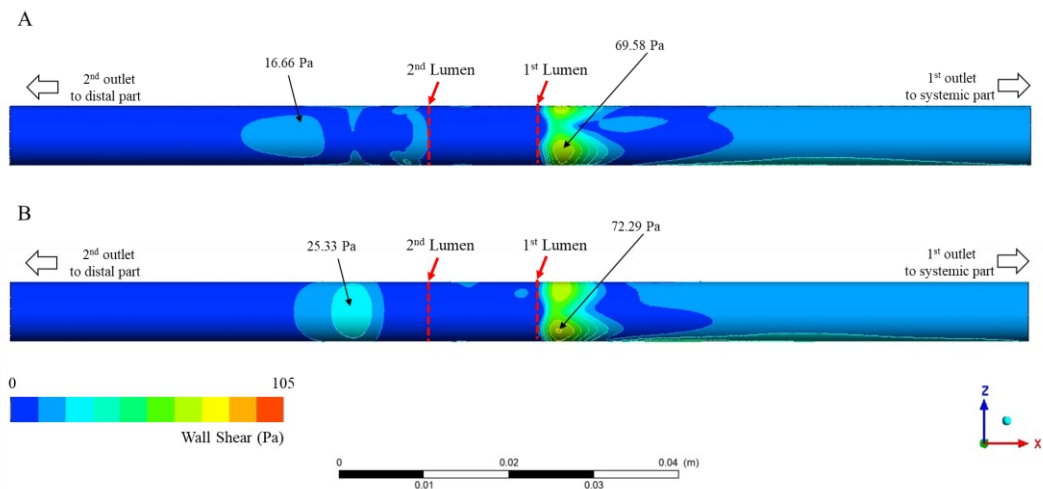


Figure 3.11 The shear stress from blood distribution to the inferior wall vessel.

CFD wall shear measurements identified a higher region from the 2nd outlet in the R 0.85 version compared with R 1.00 version. (A: 2nd iteration, radial = 1.00 mm; B: 3rd iteration, radial = 0.85 mm).

In Figure 3.11 illustrates that the pattern of wall shear stress around the primary lumen of both cannulae were similar, reflecting the turbulent region in the flow path at near the end of the lumen. In the 2nd iteration, the flow tends to shift towards the superior wall (Figure 3.11A), while the vessel on the inferior wall was found in the 3rd iteration. This

suggests that the angle of flow direction may be responsible for flow direction and the higher values of WSS (Figure 3.11B).

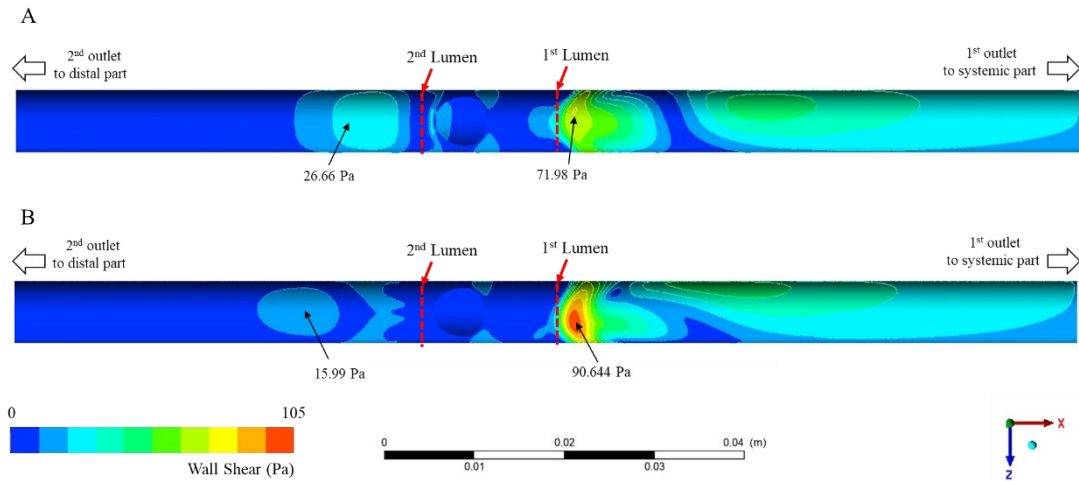


Figure 3.12 The superior wall shear stress from 2nd and 3rd iteration.

Compared with R 1.00 version, R 0.85 version has a lower shear at the secondary outlet but a more significant shear at the primary outlet (A: 2nd iteration, radial = 1.00 mm; B: 3rd iteration, radial = 0.85 mm).

Figure 3.12 shows wall shear measured at the superior vessel. The more shear stress was spotted at the primary outlet in the 3rd iteration. However, the lower shear at the secondary lumen showed lower in this version.

3.3.3 SECOND AND THIRD ITERATION SUMMARY

This design step produced two cannula configurations in an effort to resolve the issue of optimizing velocity profiles and flow direction using CFD techniques. The findings confirmed that the flow from the primary lumen of both cannulae were similar to the 1st iteration cannula, whereas adjusting the secondary lumen radian curve of 1.00 and 0.85 mm can improve flow direction and WSS. It was suggested that the angle of flow direction play a role in determining flow direction and the higher values of WSS.

Although WSS from the primary outlet flow, in 2nd iteration found higher than those in 1st iteration cannula it found lower than those in 3rd iteration. Moreover, the secondary

outlet, flow direction to centre line was notably superior in the 2nd iteration. This finding possibly will minimise the risk of blood cell and vascular adverse effects. With this in mind, the following step will focus on designing suitable secondary lumen features to improve the flow direction and effect.

Table 3.2 Summary of the 2nd and 3rd iteration.

Cannulae	Characteristic of ideal canula		Requires improvement	
	Additional features	Aims	From CFD finding	Characteristic need
2 nd iteration	- 2 nd lumen radian curve of 1.00 mm	- Convert flow direction from inferior vessel wall	- The flow direction is closer to the centre line compared to the 1 st iteration	- Improve flow direction - Reduced the velocity
3 rd iteration	- 2 nd lumen radian curve of 0.85 mm	- Convert flow direction from inferior vessel wall	- The flow direction is likely to move towards the superior wall.	- This cannula was excluded in the following step of the design process, due to flow direction to superior wall.

3.4 CHANGING UNDERPART OF THE SECONDARY LUMEN

3.4.1 MATERIALS AND METHODS

Geometry of 4th, 5th and 6th iteration

The secondary lumen of subsequent iterations was adjusted in response to the results of the investigation of the control, 2nd and 3rd iterations. As shown in Figure 3.13, the lumen curve's underpart was transformed from 2nd iteration (R 1.00). The internal lumen features were added aim to provided flow direction to centre line and reduced and impact of velocity jet flow to vessel wall as using in the previous studies (Gramigna et al., 2023; Thomas et al., 2017).

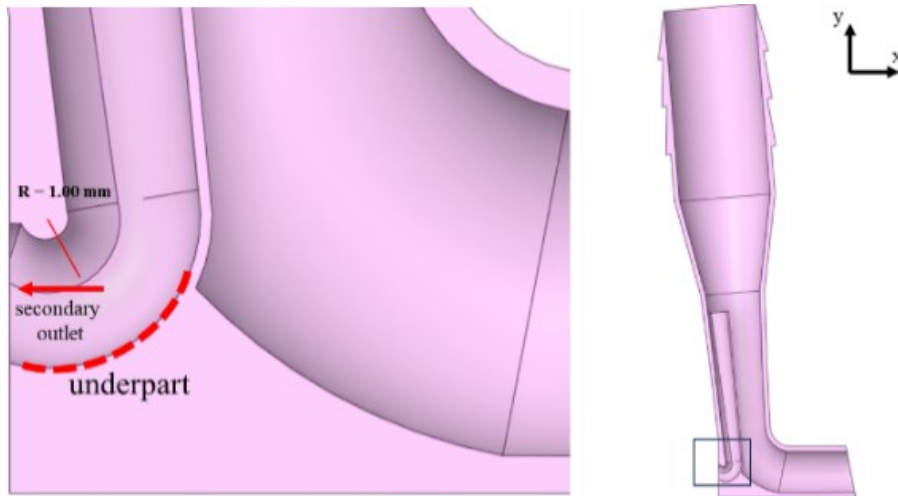


Figure 3.13 *The underpart of the secondary lumen for adjusted to 4-6 iterations.*

The improved design aims to convert the flow direction into the vessel's central line by adding the feature on the underpart of the secondary lumen.

Three different iterations were developed with varying configurations of these as the following reasons.

- 4th iteration: An outlet ramp or flow director was added to provide flow direction towards the centre line.
- 5th iteration: A sinus or small groove was added to decrease outward flow and minimise the velocity of the jet.
- 6th iteration: The sinus and ramp functions were combined to take advantage of the benefits of both features.

The feature in the 4th iteration of the cannula design was altered by adding a 20 - degree ramp at the outlet, and the 0.12 mm small groove, scallop or sinus was incorporated into 5th iteration. Thus, the 4th iteration is known as the ramp version and the 5th iteration as the sinus version. Finally, 6th iteration was designed that combined both of these features and was named the sinus-ramp version. Details of the underpart and its adjustment of 4th, 5th and 6th iteration design can be seen in Figures 3.14 to 3.16.

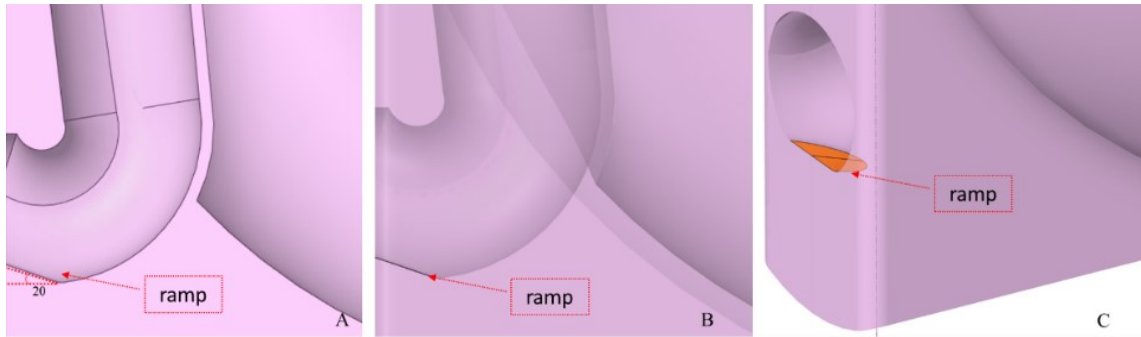


Figure 3.14 Illustrated the underpart in the ramp cannula (4th iteration).

The small 20-degree ramp was added to the opening of the secondary lumen to direct the flow to the middle line of the vessel. (A: the 20 - degree ramp on the underpart, B and C: Highlighted the ramp in different views)

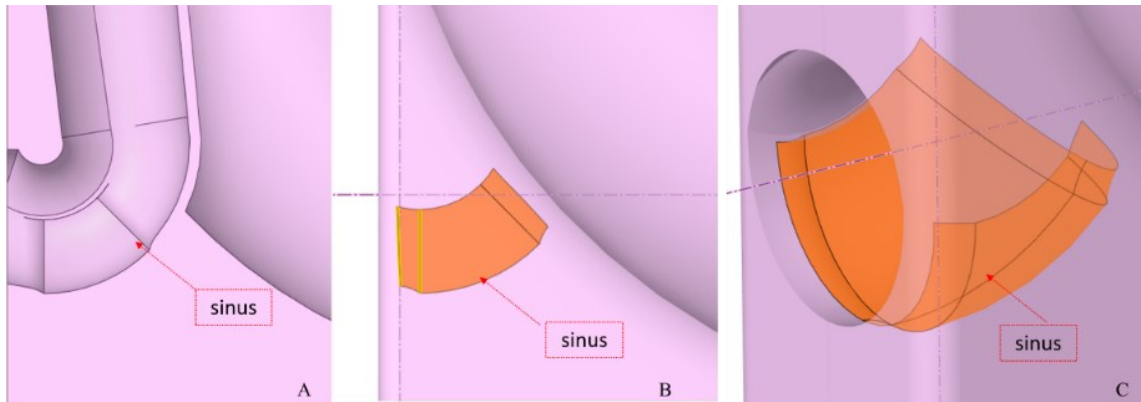


Figure 3.15 Diagram of the secondary lumen of the sinus cannula (5th iteration).

A small groove (0.12 mm), sinus, was added to the underpart in this version to transform blood direction before exiting the vessel. (A: The small groove or sinus on the underpart, B and C: Highlighted the groove in different views)

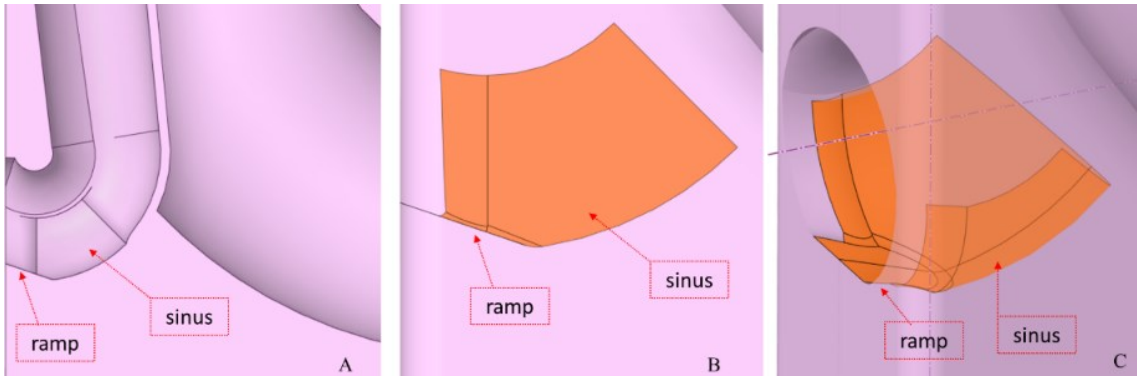


Figure 3.16 *The underpart of the secondary outlet 6th iteration.*

The features of the two previous versions were combined in this cannula, which is intended to gain advantages from the ramp and sinus. (A: Remark the 20-degree ramp combined with sinus on the underpart of the secondary lumen, B and C: Highlighted an adapted feature in different views)

In all these versions, the CFD test was performed in accordance with the methodology in the Session 3.2.1. Once again, blood flow and wall shear were evaluated to compare with the previous designs.

3.4.2 RESULTS

Flow Characteristics

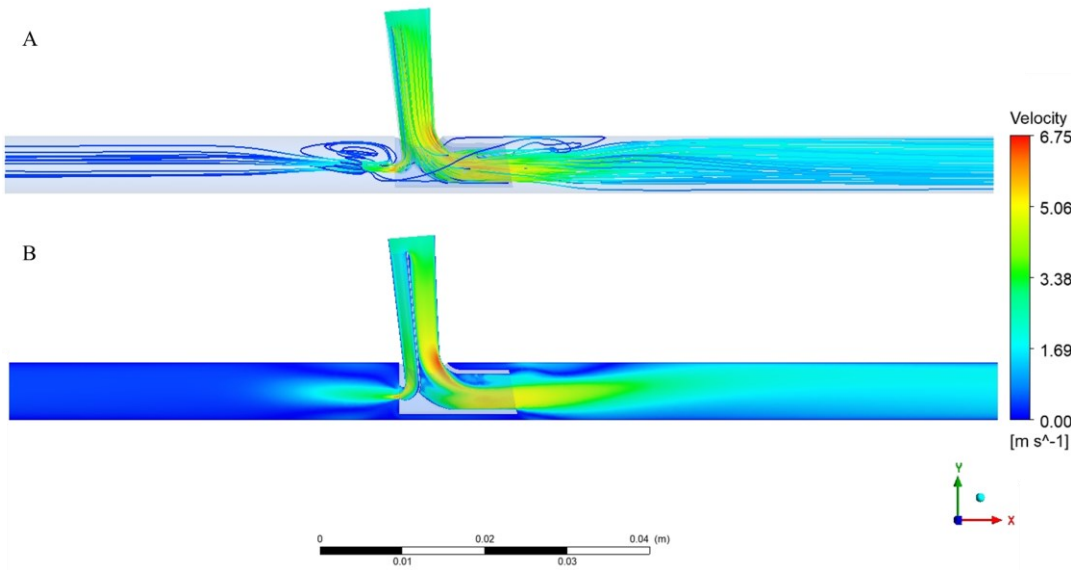


Figure 3.17 Flow path and velocity magnitude across the 4th iteration.

(A: Streamline; B: Velocity magnitude)

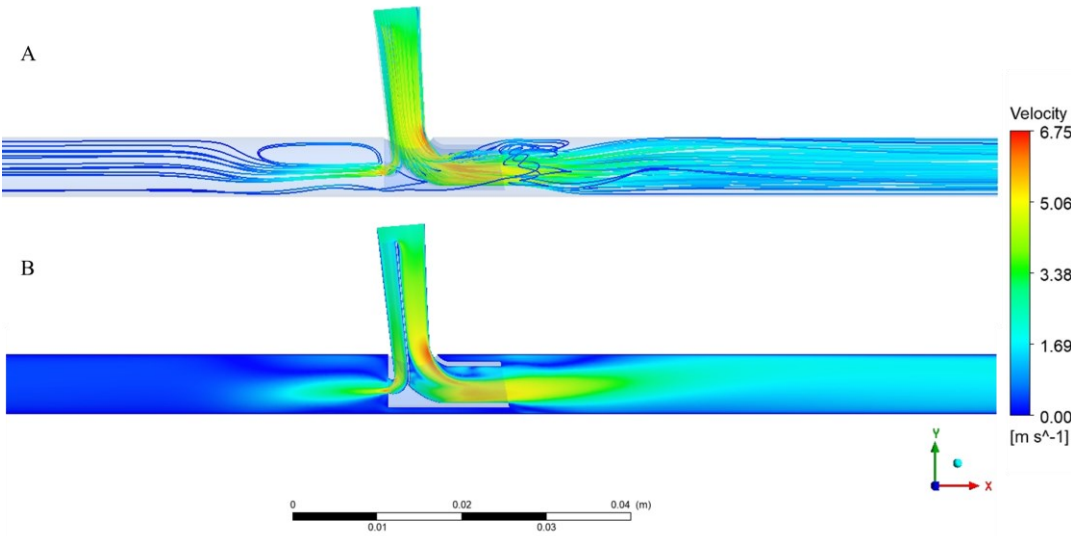


Figure 3.18 Flow path and velocity magnitude across the 5th iteration.

(A: Streamline; B: Velocity magnitude)

The blood flow path of the 4th and 5th iterations are shown in Figure 3.17A and 3.18A. The blood flow direction magnitude in these cannulae were closer were more central to the vessel lumen when compared to the first three iterations to the central line than in the central and both second iteration versions.

There were no evident differences in the primary lumen streamlines compared to 1st, 2nd and 3rd iterations. The maximum velocity in both models is approximately 6.75 m/s in the angle of primary pathway. In addition, the velocity magnitude in Figure 3.17 B and 3.18 B showed that both versions have a similar flow direction. The flow direction from the secondary outlet was more centrally directed than those in the 1st, 2nd and 3rd iterations. However, the upper region of the vessel shows turbulent elements associated with the secondary lumen in 4th and 5th iterations.

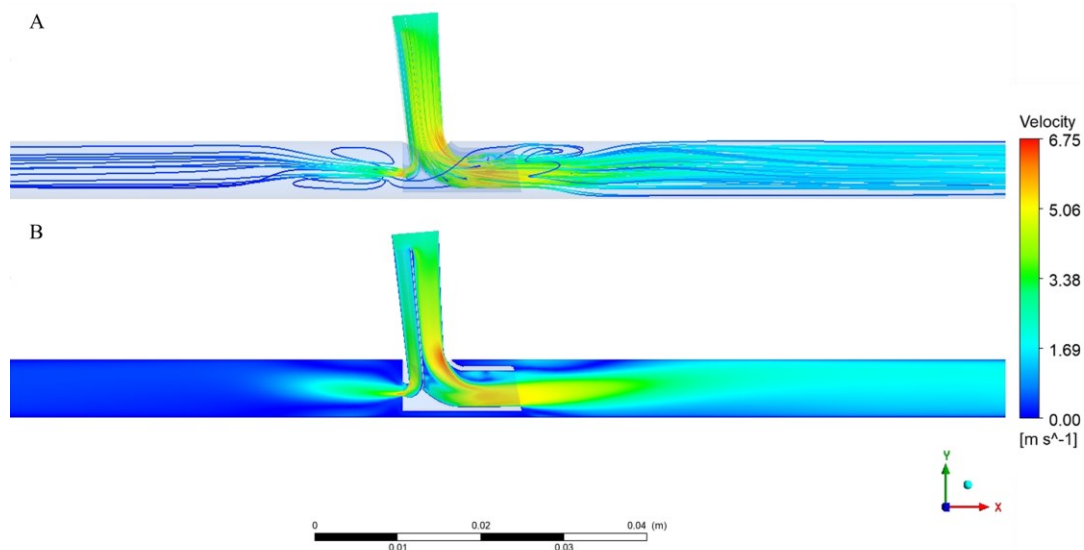


Figure 3.19 Flow path and velocity magnitude across the 6th iteration.

The blood flow direction magnitude in these cannulae were closer were more central to the vessel lumen when compared to the previous iterations (A: Streamline; B: Velocity magnitude)

In Figure 3.19, the flow path and velocity magnitude from primary outlet in the 6th iteration have been found to remain the same as in the 1st - 5th iteration, which a similar flow and velocity pattern provides the maximum value at primary outflow. Furthermore, the flow direction at the secondary lumen indicated that flow is directed to the vessel's

midline. However, there were a little turbulent current at the superior and inferior areas of the vessel.

Wall Shear Stress

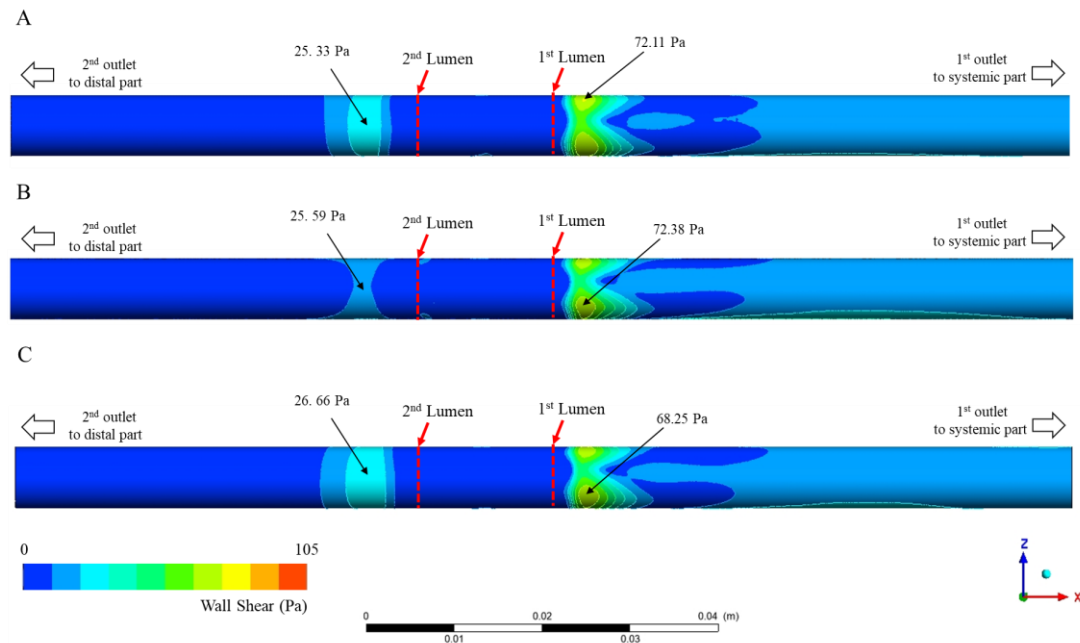


Figure 3.20 The shear stress from blood distribution to the inferior wall vessel.

The pattern of wall shear at the inferior wall is very similar in all versions, with one having a higher area at the primary lumen. (A: Ramp version; B: Sinus version; C: Sinus-ramp version)

In Figure 3.20 A and B, the colour mapping outlines the wall shear stress applied to the inferior vessel wall from the 4th, 5th and 6th iterations, respectively. The shear rate area was similarly placed with near identical values at the primary lumen (72.11 Pa vs 72.38 Pa vs 68.25 Pa, 4th, 5th and 6th iterations, respectively). A higher shear area at the secondary lumen was presented in the sinus-ramp version, however it very similarly value compared to 4th and 5th iterations (25.33 Pa vs 25.59 Pa vs 26.66 Pa, 4th, 5th and 6th iterations, respectively).

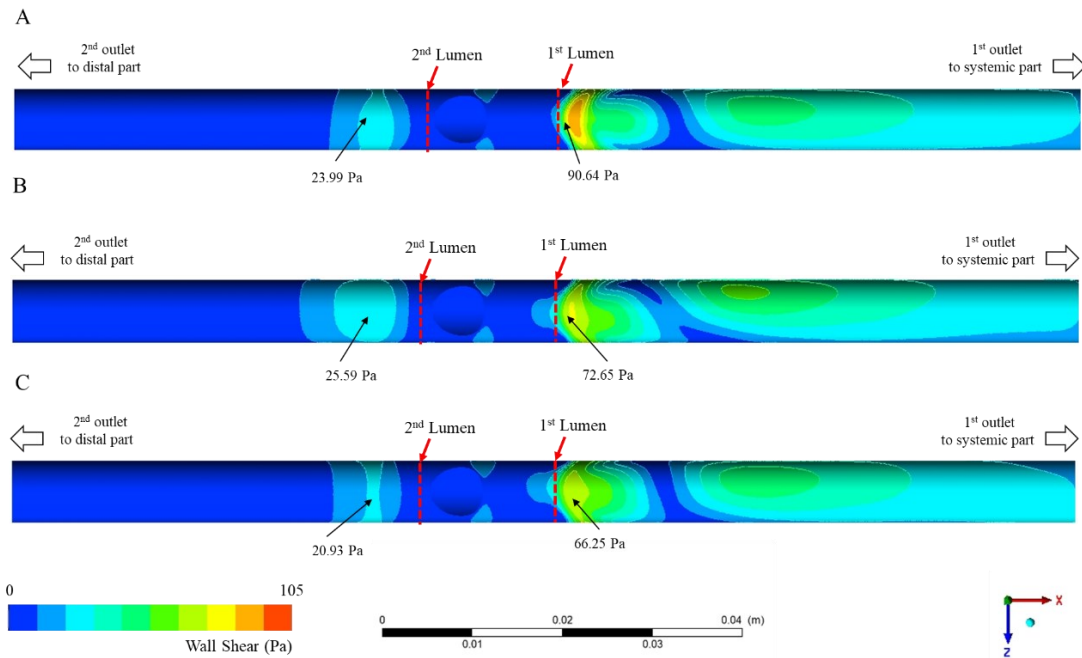


Figure 3.21 The shear stress from blood distribution to the superior wall vessel.

High shear spot in the ramp version. (A: Ramp version; B: Sinus version; C: Sinus-ramp version)

The wall shear at the superior vessel is shown in Figure 3.21. The ramp version produced a significant region of wall shear immediately after the 1st lumen outlet (90.64 Pa). However, there are similar shear patterns across the profile.

Although the highest shear was found in the ramp version, a similar profile is presented in all models as an increased shear spot found at the primary lumen and a minor shear point at the secondary lumen.

3.4.3 4th, 5th and 6th ITERATIONS SUMMARY

The CFD experimented with three improved cannula configurations. These were characterised as; ramp cannula, sinus cannula and sinus-ramp cannula. In all modelling analysis the performance of these iterations was compared to the original cannula design. The primary lumen’s flow characteristics and wall shear remain relatively unchanged from the previous iterations analysis. The flow direction from 2nd outlet indicated that the sinus-ramp version was most appropriate, followed by ramp and sinus, respectively.

Table 3.3 Summary of the 4th, 5th, and 6th iteration.

Cannulae	Characteristic of ideal canula		CFD finding
	Additional features	Aims	
4 th iteration	- Adding ramp at 2 nd lumen	- To provide flow direction towards the centre line.	<ul style="list-style-type: none"> - In comparison to previous iterations, the flow direction and wall shear from the 2nd outlet has shown improvements across all versions. - A reduction in velocity from the 2nd outlet was observed when compared to the 1st iteration, particularly notable in the 6th iteration (also see figure 3.25)
5 th iteration	- Adding sinus at 2 nd lumen	- To decrease outward flow and minimise the velocity of the jet.	
6 th iteration	- Adding sinus and ramp at 2 nd lumen	<ul style="list-style-type: none"> - To provide flow direction towards the centre line. - To decrease outward flow and minimise the velocity of the jet. 	

3.5 WALL SHEAR STRESS AND FLOW

3.5.1 MATERIALS AND METHODS

Wall shear stress

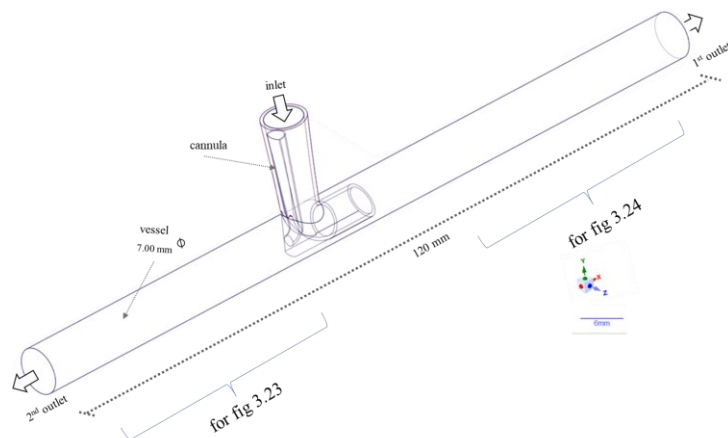


Figure 3.22 Wall shear measurement from both outlets.

The probe in the CFD programme was used to measure the inferior wall shear, 0 to 35.00 mm from each outlet. Then the value was plotted to evaluate the stress on the vessel wall influenced by the blood flow. Figure 3.22 describes the diagrams of shear measurement followed by the comparable graph in Figure 3.23 and 3.24.

Cross-sectional velocity

Measurements of the magnitude of the cross-sectional flow velocity were performed at distances of 1.0, 7.5, and 14.0 mm from the secondary lumen. The purpose of these measurements was to identify the various flow patterns that may affect the vessel wall, as well as the velocity profile associated with each position.

3.5.2 RESULTS

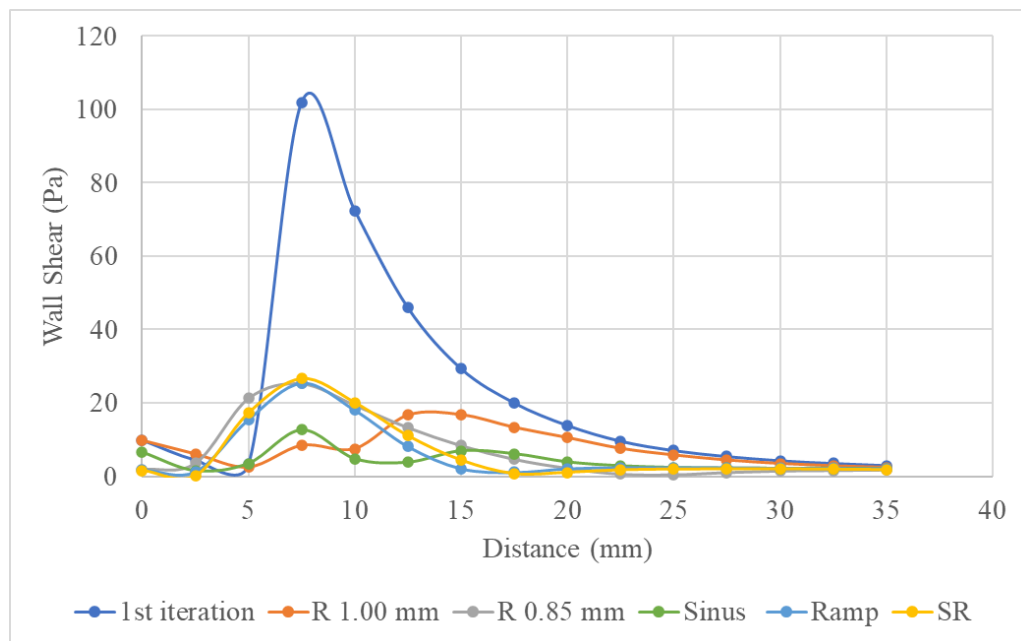


Figure 3.23 Inferior wall shear stress measured from the secondary lumen.

SR; Sinus-ramp version

The wall shear along the 35.0 mm from the secondary outlet is shown in Figure 3.23. Regarding the results in previous session, most cannulae that delivered blood flow outward from the inferior wall showed shear of less than 30 Pa. However, the 1st iteration cannula has the highest peak, reaching to 101.9 Pa.

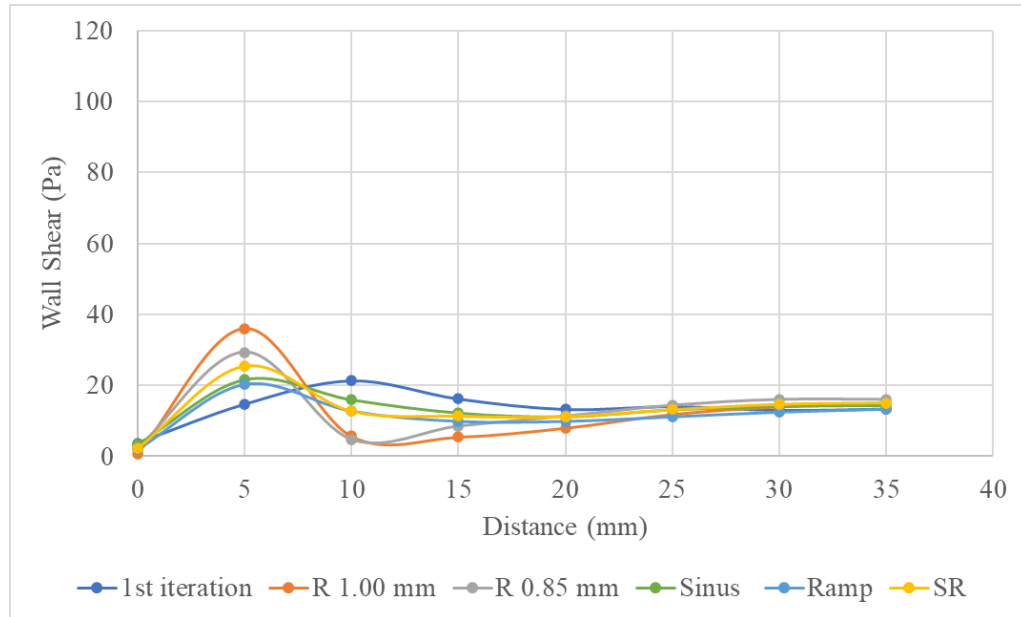


Figure 3.24 Inferior wall shear stress measured from the primary lumen.

SR; Sinus-ramp version

As seen in Figure 3.24, the highest shear from the primary lumen at inferior vessel wall was found higher than 20 Pa at 5.0 mm for all iteration, except to the ramp cannula. All reached a similar value at 25 mm with approximately range 11.2 to 14.4 Pa (Ramp and R 0.85, respectively).

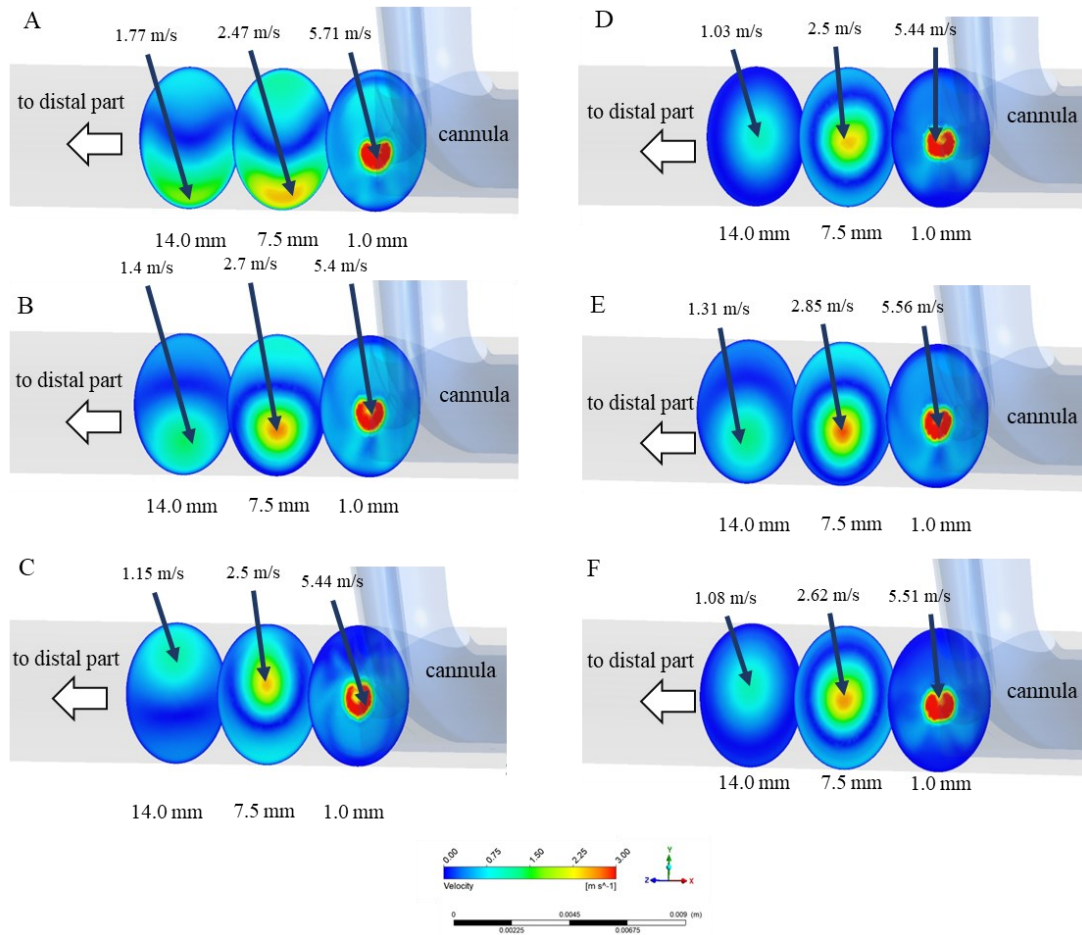


Figure 3.25 *Cross-sectional flow velocity at the secondary lumen.*

The flow magnitudes at all three locations, 1.0 mm, 7.5 mm and 14.0 mm indicate the direction and decline of velocity at the secondary lumen. (A: 1st iteration (R 1.4 mm), B: 2nd iteration (R 1.00 mm), C: 3rd iteration (R 0.85 mm), D: 4th iteration (Ramp), E: 5th iteration (sinus) and F: 6th iteration (sinus-ramp), respectively)

In Figure 3.25A, the direction and velocity declined of blood flow at the secondary lumen is illustrated by a series of velocity magnitudes in cross-section. The highest velocity was measured at 1.0 mm (5.71 m/s) and gradually declined to 2.47 m/s at 7.5 mm and 1.77 m/s at 14.0 mm, respectively; significantly, the flow path is projected to the inferior part of the vessel.

The comparison of flow magnitudes in 2nd and 3rd iteration is presented in Figure 3.25 B and C. In both cannulae, the highest velocity was seen at 1.0 mm, decreasing until the third. In addition, these findings are demonstrated in Figure 3.12 A that the flow direction in 2nd iteration is directed towards to the inferior wall. In contrast, the 3rd iteration shifted flow direction towards the superior aspect of the vessel.

In addition, the central line of flow magnitude is presented in Figure 3.25 D, E and F. The ramp and sinus-ramp cannula versions (4th and 6th iteration) were associated with improved results when compared to the previous iterations. In both cannula the high velocity magnitude were located in the middle of the vessel cross-section. In the 5th iteration, the flow travels towards the inferior wall as presented in Figure 3.25E.

3.6 CHAPTER SUMMARY

This chapter demonstrated the methodology adopted in the design of a number of cannula configurations to optimise a pre-existing cannula design. Flow simulation using CFD was employed to guide the development and to ensure that progressive design iterations were associated with performance improvements. The primary focus of this aspect of the work was optimising flow direction and minimising vessel wall impact. The findings confirm that the novel cannulae is associated with improved flow direction at the critical secondary lumen and has the potential to reduce some common complications of ECMO.

The first stage of this chapter analysed the flow paths of a single input bi-directional cannula featuring a secondary lumen with a 1.4 mm radian curve. The finding showed that flow increased velocity and sandblasting against the vessel wall, resulting in greater shear stress. Then, in the 2nd and 3rd iterations, the 2nd lumen radian curve underwent modifications of 1.00 mm and 0.85 mm, respectively. On this stage, the 2nd iteration significantly improved the flow direction toward the centre line. After that, the 2nd lumen was added features to improve the flow direction. Three versions were available, featuring ramp, sinus, and sinus-ramp, respectively. The results at this point suggested

that the sinus-ramp configuration was the most suitable. This finding may reduce the risk of adverse effects on blood cells and vessels.

Following this modelling, the thesis will focus on creating the cannulae using 3-dimensional printing. This will enable the assessment of the physical performance of the various prototypes, Figure 3.26, and concurrently, validate the *in-silico* performance results. In moving the investigation forward we will utilise. The flow visualisation with a mock circulation set-up module to validate results from the *in-silico* study.

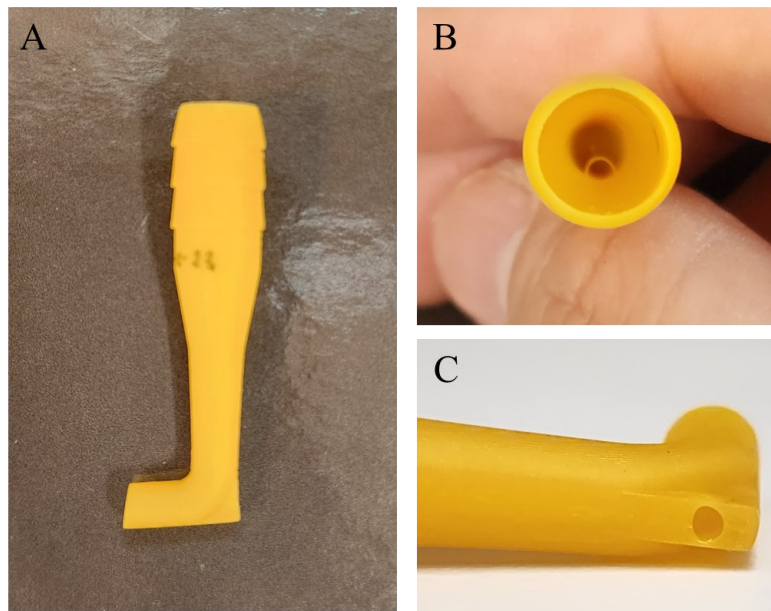


Figure 3.26 3D print of all cannula version prototypes.

(A: Whole cannula body; B: Split wall; C: Secondary lumen)

CHAPTER 4

FLOW VISUALISATION

4.1 INTRODUCTION

Flow visualisation is an experimental technique utilized for measuring the movement of fluids around physical objects, and can be conducted in an actual or a simulated environment (Merzkirch, 2007). Experimental flow visualization often involves the introduction of heat or foreign elements, such as particles or ink, into a fluid. An analytical method of flow can be performed with or without the assistance of complex computations. Parameters used to illustrate the flow behaviour are vectors, path lines, or tangents illustrating the velocity field (Merzkirch, 2007; Post & van Walsum, 1993). It is typically used in developing and validating novel designs, including using wind tunnels in the design process for automobiles or aircraft. Furthermore, it has recently been increasingly used to validate CFD simulations, specifically in diagnosing complex diseases and designing medical devices (Post & van Walsum, 1993; Pozo Álvarez, 2021b).

In cardiovascular disease, flow visualisation can be measured by specific equipment such as echocardiography, magnetic resonance imaging (MRI) or ultrasound. The *in-vitro* flow techniques such as particle tracking are being used to investigate the structure and function of the heart and vessel in cardiovascular diseases, including using echocardiography to examine the flow through the heart valve (Pozo Álvarez, 2021a).

The dye injection technique using methylene blue was used to compare the flow pattern distribution and velocity jet from two arterial cannula tips. Methylene blue was introduced into the cannula, and images of dye distribution were captured. This study also simulated an impact of jet flow on the vessel wall (sandblasting). Also, the atherosclerotic aorta was simulated using transparency sheet coated with charcoal granules. The dislodgement of atheroemboli was evaluated by observing the presence of

a clear region of charcoal granules on the sheet, which was caused by the flow of a high-velocity jet. In the Figure 4.1 shown flow characteristics between the two cannula tips and their jet flow result in the formation of a clear area of charcoal granules (White et al., 2009).

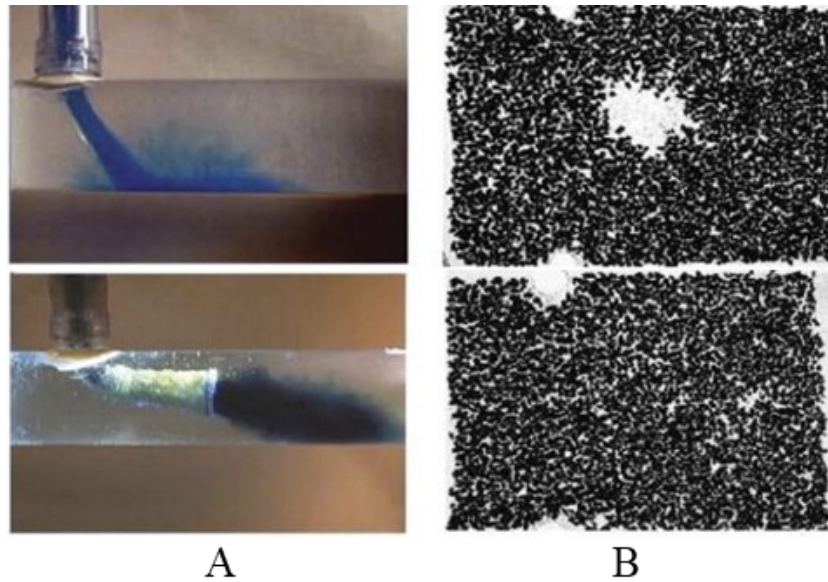


Figure 4.1 Dye and particle dislodgment patterns from the different cannulae tips.

(A: dye pattern; B: particle dislodgment patterns, taken from White et al. (2009))

McDonald and colleague compared the flow patterns of 19 arterial cannulae for cardiopulmonary bypass (CPB) using particle image velocimetry (PIV). Additionally, Haymet and colleague used the same technique to evaluate the flow patterns of femoral cannulae for ECMO. Both investigations have shown that the particle tracking technique is able to predict the sandblasting impact on the endothelium caused by the high-velocity jet from the cannula. The PIV technique can visually represent flow patterns and map velocities using a colour gradient, as shown in Figure 4.2 (Haymet et al., 2021; McDonald et al., 2016).

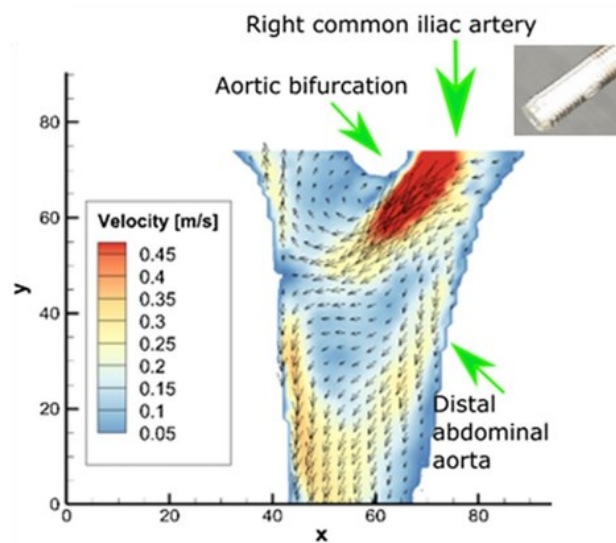


Figure 4.2 Illustrated vectors of flow pattern and velocity mapping from PIV.

(taken from Haymet et al. (2021))

In addition, particle tracking, and dye injection can be used as a quantitative test to validate the simulation results from the CFD, such as ink-stain distribution compared with the PIV and CFD for CPB arterial cannulation (Hugenroth et al., 2021). The vector fields were obtained and compared PIV experiment and CFD simulation in neonatal arterial cannula. Correlation coefficient between velocity profile from PIV and CFD was useful to verify both technique (Rasooli & Pekkan, 2019). The CFD results in the novel cannula are also verified through dye visualisation. Measuring and verifying the angle of dye distribution and CFD was demonstrated by Menon and colleagues. Their study demonstrated that the dimensions and outflow features are essential components of arterial cannula design for adult patients undergoing cardiac surgery. (Menon et al., 2013).

In this chapter, the study used particle tracking and ink dye injection techniques to assess the optimal cannula configuration and investigate the effects of alterations to the fluid pathway from the cannula in a simulated circulation. The findings were compared and verified with CFD to investigate the cannula flow direction and distribution at the secondary lumen.

4.2 DYE INJECTION

4.2.1 MATERIALS AND METHODS

Roller pump calibration

A roller pump (Stockert/Shiley CAPS multiflow roller pump, Stockert GmbH, German) was calibrated by pumping water at different flow rates through 1/2-inch silicone tubing (inner diameter of 12 mm, outer diameter of 18 mm). The pump flow was then compared to the flow calculated from the volumetric collection at the outlet within 1 minute to determine the flow in litres per minute (LPM). Figures 4.3 and 4.4 show the volume measure ranging from 0.5-6 LPM used for the flow visualisation test.

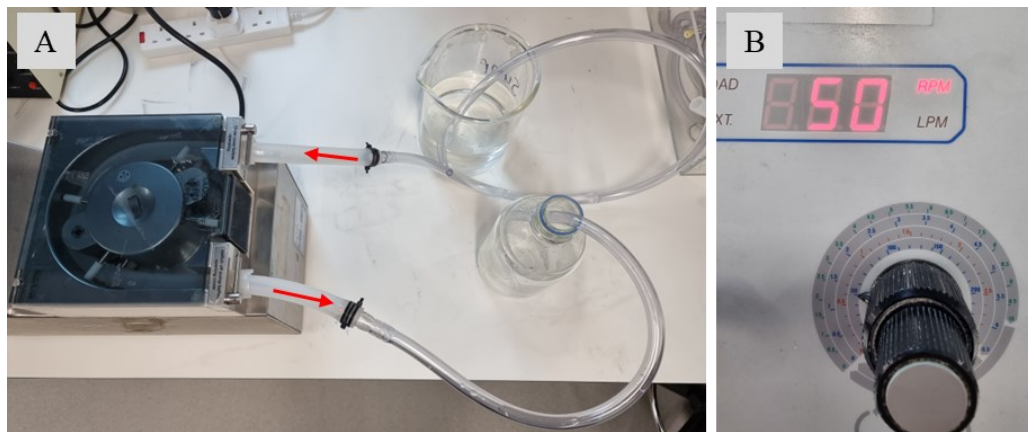


Figure 4.3 Calibration of a roller pump using volumetric measurement.

The water travels from the pump's inlet to its outlet, and the volume of water output is then compared to the pump's speed in revolutions per minute. (A: the calibration set up; B: pump's display in RPM.)

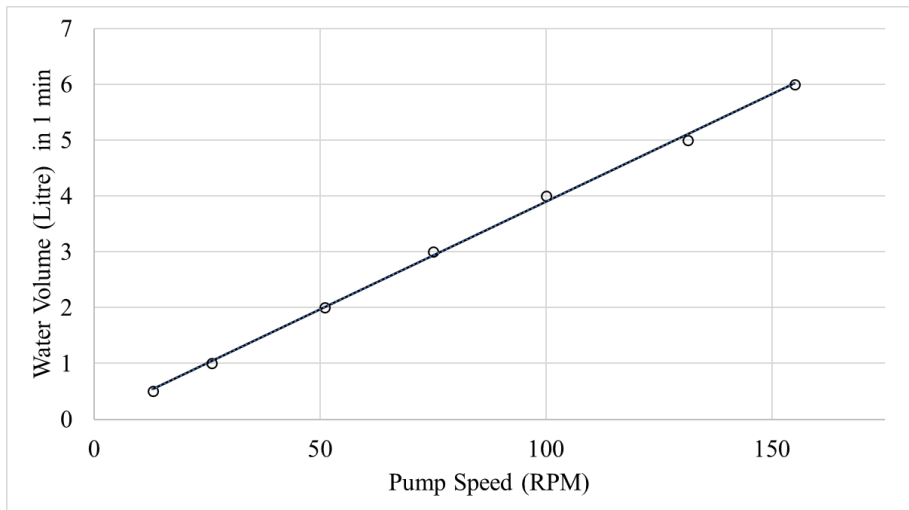


Figure 4.4 Illustrated the water volumetric measure from 0.5-6 LPM and pump speed.

Correlation (r^2) of volume from the roller pump outlets compared to the pump speed was 0.998.

Circuit preparation

An open circuit was developed for conducting dye injection experiments (Figure 4.5 and 4.6). The components of the phantom circuit consisted of a roller pump, an upstream reservoir, a drainage reservoir, and a prototype cannula. Each prototype cannula was attached to a PVC circular tube with an internal diameter of 7.00 mm (outer diameter of 9.00 mm), using cyanoacrylate. The diameter is determined based on the average measurement of the adult femoral artery in prior research, also based on using the CFD set up in session 3.2.1 (Crişan, 2012b; Gu et al., 2016; Hwang, 2017).

A luer port connector was attached upstream of the cannula inlet and dye injection was visualized through the extended tube. The recording system applied a high-speed camera (Photron FASTCAM SA4, Photron (Europe) Limited, UK) with a 100 mm f/2.8 lens (Tokina 100 mm f 2.8 macro, Tonika, Japan) positioned perpendicular to the cannula. LED lights (GS Vitec GmbH Lighting, USA) illuminated the motion of the dye when passing through the bi-directional cannula.

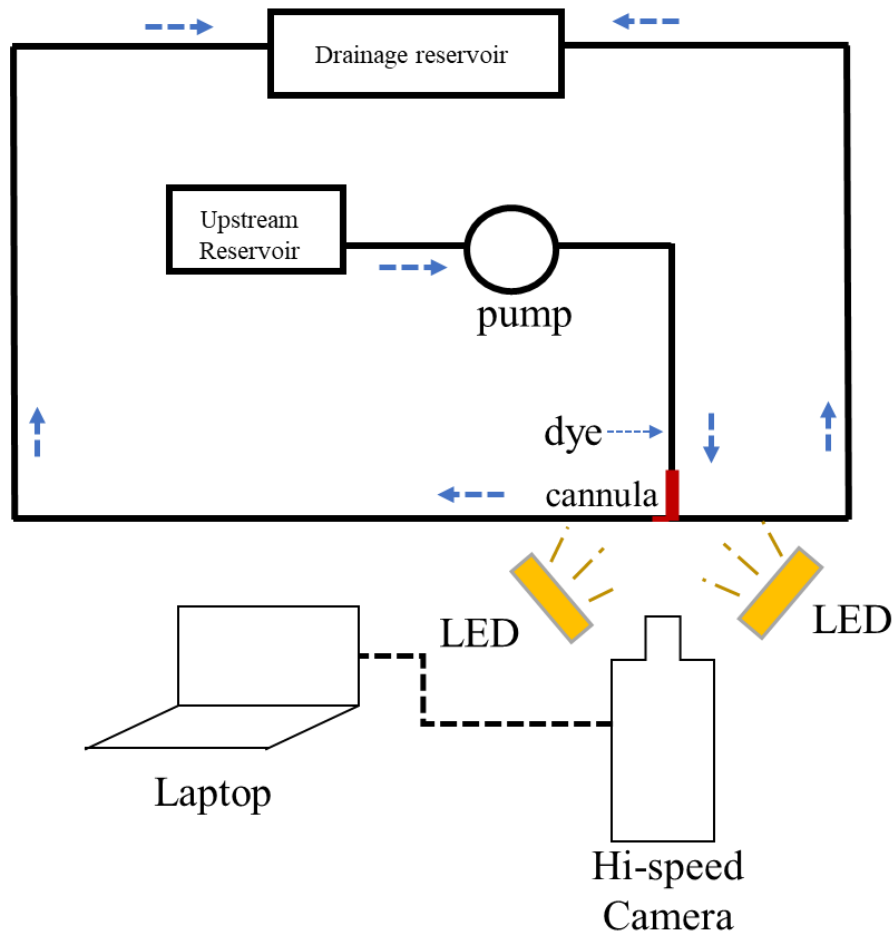


Figure 4.5 Schematic of experimental circuit for dye injection.

Circuit components with hi-speed camera and lighting system prepared for dye injection set up. Dash arrow: flow direction.

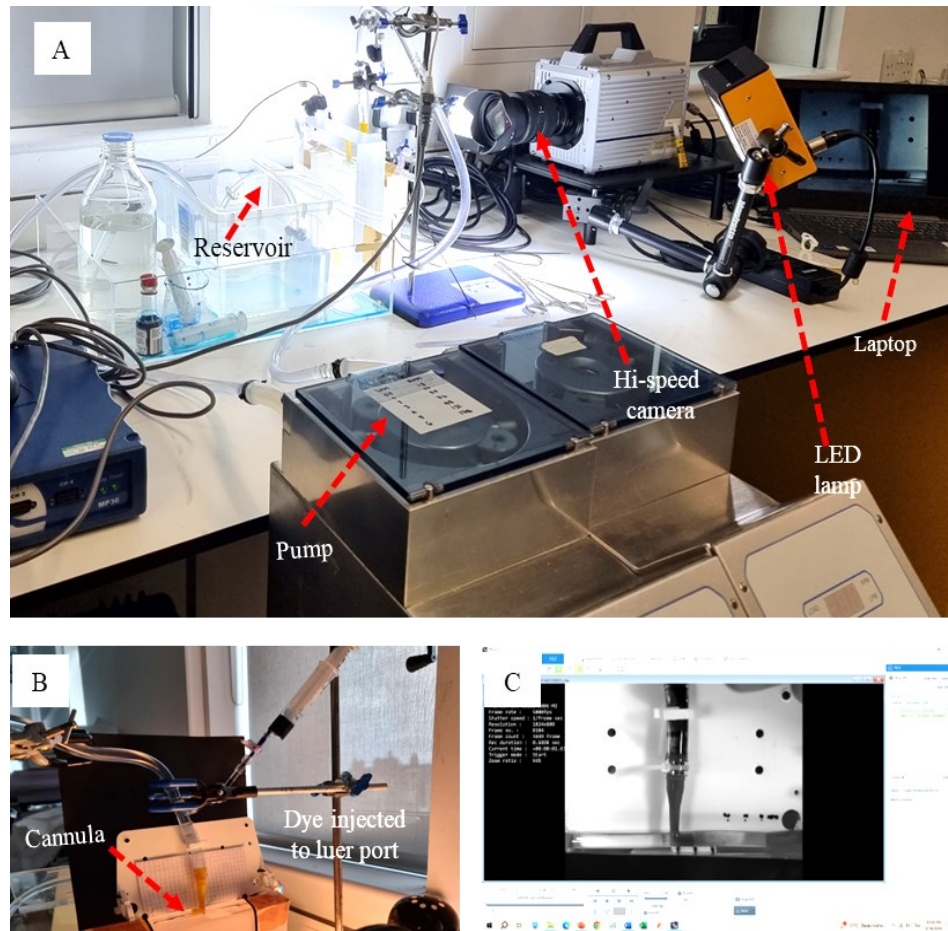


Figure 4.6 Illustrated dye injection experiment set up.

(A: The dye injection experiment set up with a hi-speed camera and lighting system; B: An extended line attached to a luer at the proximal to cannula inlet food dye ink; C: The screenshot window from the laptop.)

Dye injection and image acquisition

The circuit was primed with tap water at approximately 22 degrees Celsius. After debubbling the circuit, the flow rate driven from an upstream reservoir through a roller pump gradually increased until it reached 4 litres per minute as defined in the CFD (Session 3.2.1) (Neidlin et al., 2014). These parameters are recommended for patients with a weight of approximately 50 kg (60-80 ml/kg/min) (Brown et al., 2021; Gajkowski et al., 2022). Once establishing a constant flow, 10 ml of concentrated food dye was injected into the inlet luer port to evaluate the flow through the prototype cannula and vascular phantom and into the drainage reservoir (Figure 4.6). The image acquisition operates with a high-speed camera, which records the motion of the dye ink at a rate of 5000 frames per second.

Dye distribution analysis

The images captured at the outflow contour were analysed using FASTCAM Viewer software (Photron Fast CAM Viewer version 4.0, Photron Limited, UK). The data was collected in 100 frames, corresponding to a period of 20 milliseconds. For the subsequent phase of analysis, frame numbers were chosen at intervals of 5 milliseconds (frame number 0, 25, 50, 75, and 100, respectively). Therefore, time stamps of the picture set were T_0 , $T_1 = 5$, $T_2 = 10$, $T_3 = 15$ and $T_4 = 20$ milliseconds, respectively. Throughout this time, dye ink was dispersed and transmitted through an opening until it fully traversed the vascular phantom. The arrows were manually inserted to determine the characteristics through dye distribution using FASTCAM Viewer software.

Symmetrical measurements

At T_{0-4} , the upper (α) and lower (β) angle of dye distribution measured using FASTCAM Viewer software (Photron Fast CAM Viewer version 4.0, Photron Limited, UK). The central line contours at the secondary lumen are presented in Figure 4.7. The value of angle and ratio were compared to observe the balance of dye distribution to the superior and inferior region of tube wall and represented the access vessel. Therefore, the

presence of an imbalance angle indicates a shift of the jet direction trend to one side of the tubing wall resulting in potential vessel injury. The α angle represents the flow directed towards the superior vessel wall, while the β angle represents the flow directed towards the inferior vessel wall. The distribution of dye is referred to as the α angle equal to β angle. Thus, ratio of α and β is expected to be approximately one, indicating a symmetrical distribution of dye from the 2nd lumen.

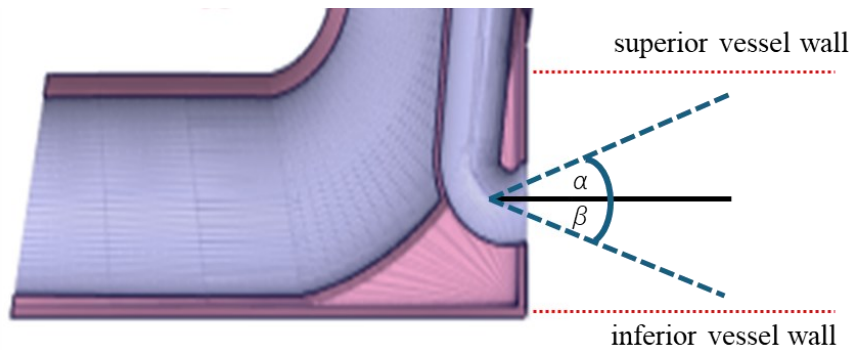


Figure 4.7 Measurement of dye distribution, upper (α) and lower (β) angles of central line contours.

4.2.2 RESULTS

4.2.2.1 Dye distribution

1st iteration cannula

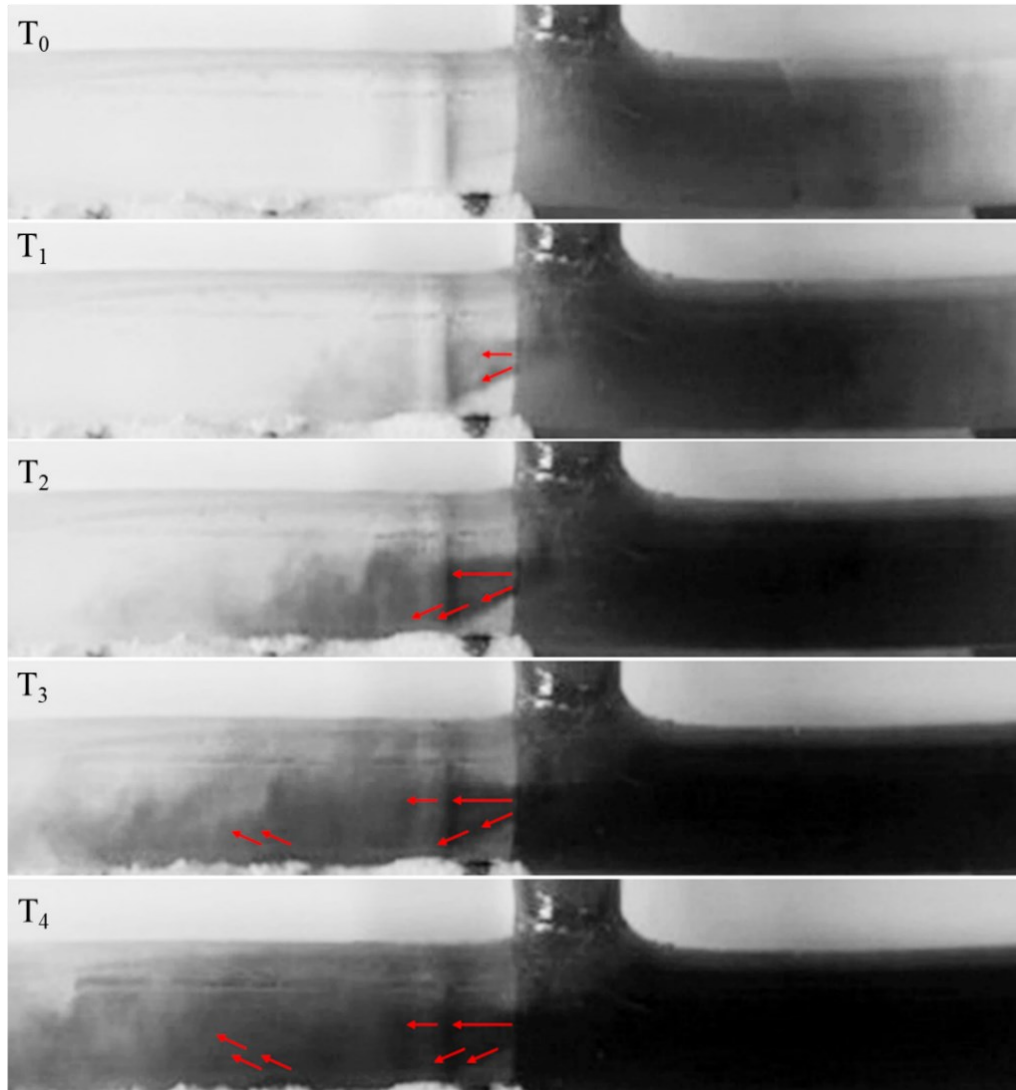


Figure 4.8 The dye visualisation in the 1st iteration cannula.

(Arrows: flow direction; T_0 = initial time, and $T_1 = 5$, $T_2 = 10$, $T_3 = 15$ and $T_4 = 20$ milliseconds)

Figure. 4.8 illustrates the dye distribution in the 1st iteration cannula. At an interval of 10 ms, dye distribution was detected towards the inferior wall and redirected to the central aspect of the outlet of the tubing at 15 and 20 ms (T_3 and T_4 , respectively).

Version R 1.00 (2nd iteration)

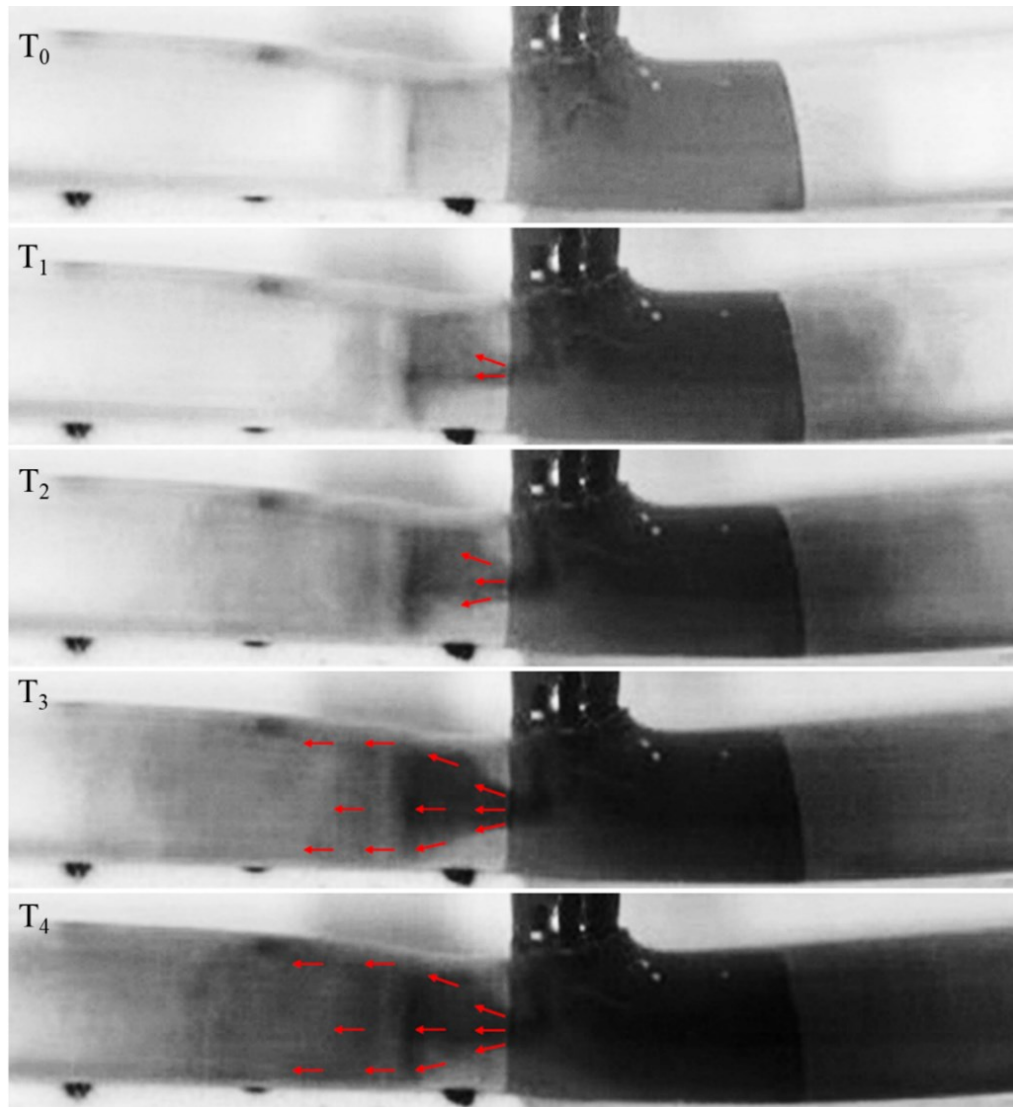


Figure 4.9 The dye visualisation in the 2nd iteration.

(Arrows: flow direction; T₀ = initial time, and T₁ = 5, T₂ = 10, T₃ = 15 and T₄ = 20 milliseconds)

Figure. 4.9 demonstrates the dispersion of dye in the R 1.00 version. The dye is centrally dispersed initially (T₁) and then extends towards the tubing walls from T₂ onwards.

Version R 0.85 (3rd iteration)

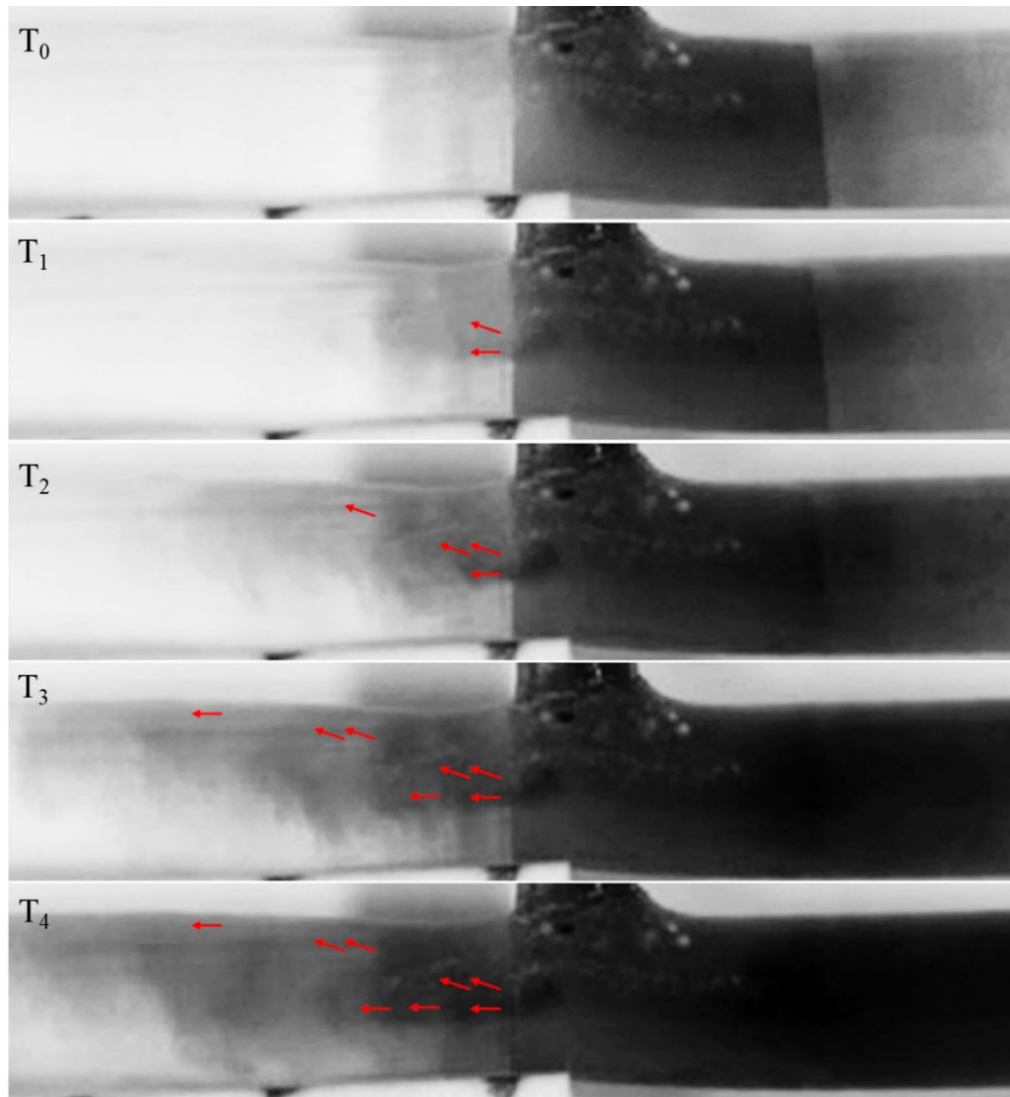


Figure 4.10 The dye distribution visualised in the 3rd iteration.

(Arrows: flow direction; T_0 = initial time, and $T_1 = 5$, $T_2 = 10$, $T_3 = 15$ and $T_4 = 20$ milliseconds.)

The dye distributes to the top aspect of the tubing (superior wall). The dye continues to direct towards the superior wall (T_2 and T_3) before eventually spreading inferiorly at T_4) (Figure 4.10).

Ramp Version (4th iteration)

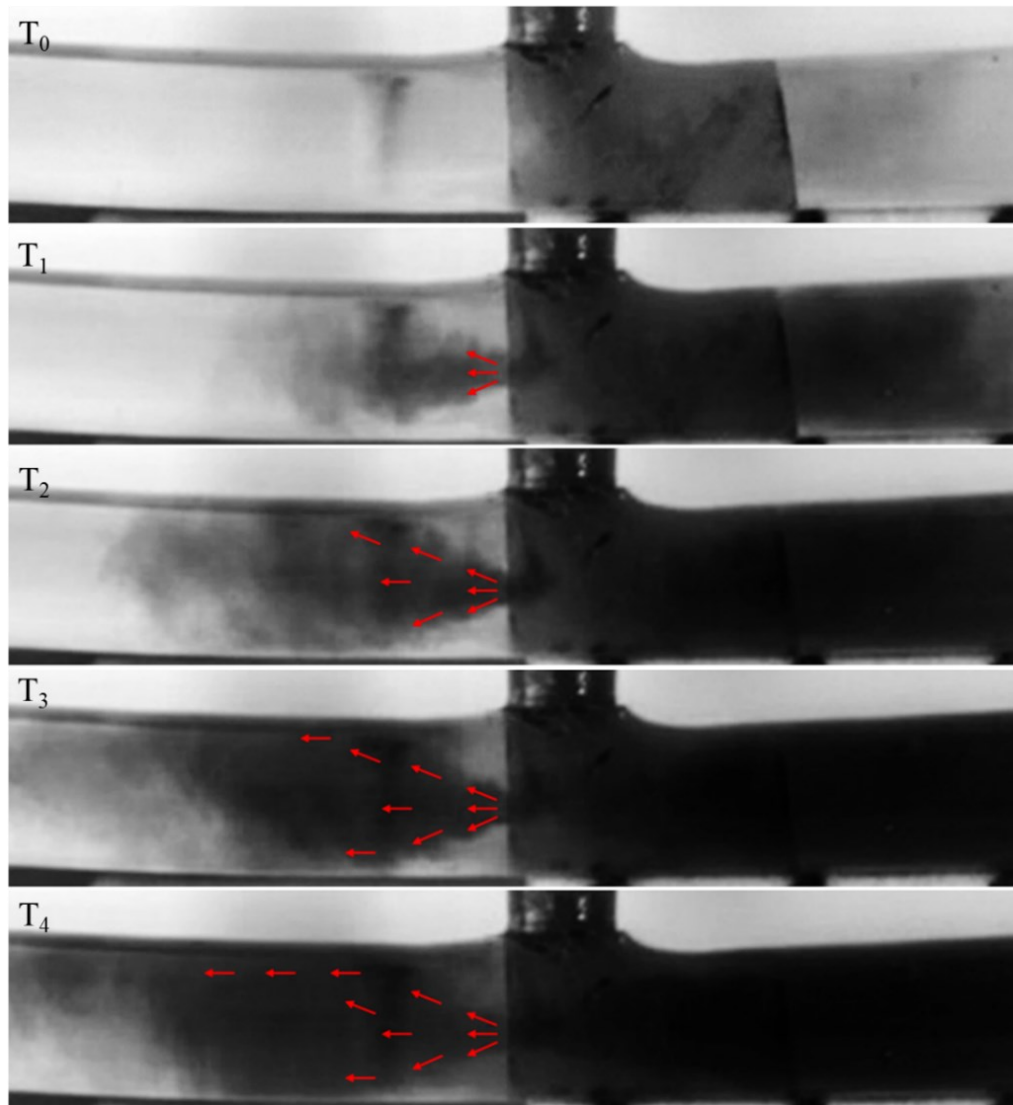


Figure 4.11 The dye visualisation in the ramp version (4th iteration).

(Arrows: flow direction; T₀ = initial time, and T₁ = 5, T₂ = 10, T₃ = 15 and T₄ = 20 milliseconds)

The dye distribution in the ramp version generally demonstrates symmetrical dispersion towards the superior and inferior regions of vessel wall. The observed trend was continually present in the image captured within 10 ms to 20 ms (Figure 4.11).

Sinus Version (5th iteration)

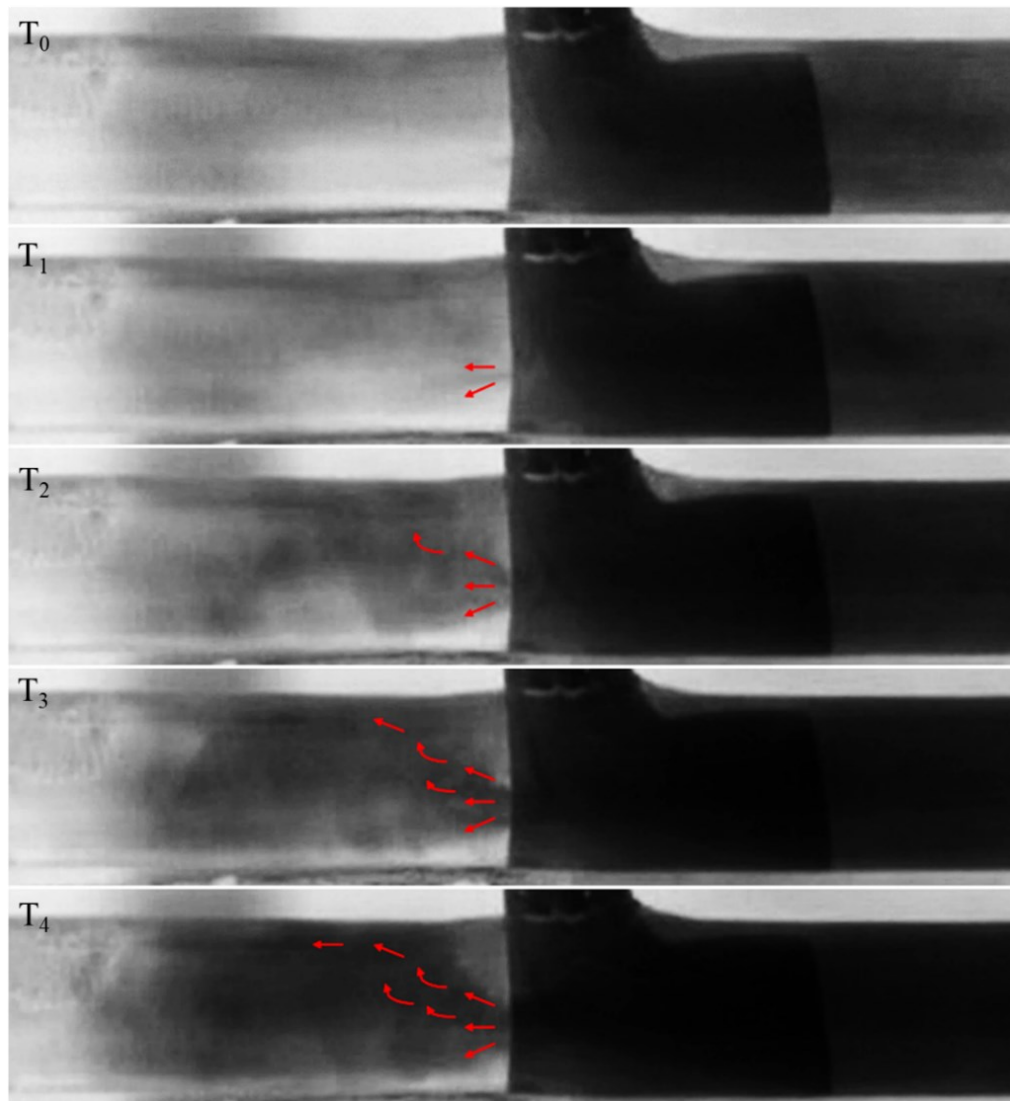


Figure 4.12 The dye visualisation in the 5th iteration.

(Arrows: flow direction; T_0 = initial time, and $T_1 = 5$, $T_2 = 10$, $T_3 = 15$ and $T_4 = 20$ milliseconds)

In Figure. 4.12, the result in the sinus version found that the dye distribution initially distributes inferiorly before ascending to the superior aspect of the tubing wall. Notably, this abnormal flow occurs within the time range of 10 ms to 20 ms.

Sinus-ramp Version (6th iteration)

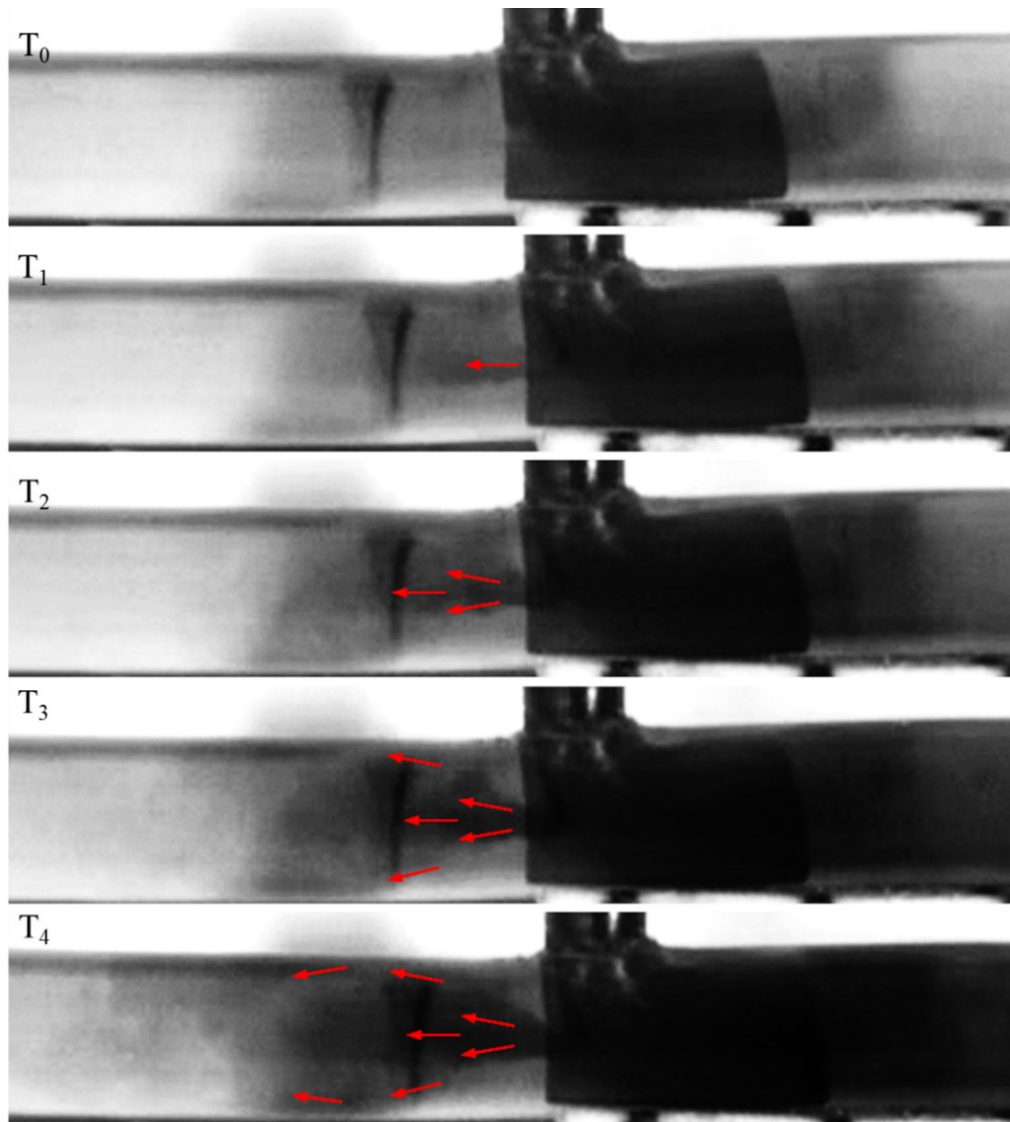


Figure 4.13 The dye visualisation in the 6th iteration.

(Arrows: flow direction; T₀ = initial time, and T₁ = 5, T₂ = 10, T₃ = 15 and T₄ = 20 milliseconds)

Figure 4.13 illustrates the distribution of dye in the sinus-ramp version. Dye dispersal appears relatively symmetrical, and this profile is maintained throughout.

In this session, the artefact in some pictures were found according to the presence of a shadow in the background. However, it did not affect the overall visual of flow distribution.

4.2.2.2 Symmetrical measurements.

Table 4.1 Comparison of the ratio of the upper (α) and lower (β) angles of the dye distribution at secondary lumen.

Cannula	Time (ms)	α	β	Ratio
R 1.40 (1 st iteration)	5	14.82 \pm 3.23	24.67 \pm 1.75	0.6
	10	16.36 \pm 3.86	25.85 \pm 1.99	0.63
	15	17.72 \pm 3.68	28.36 \pm 0.54	0.62
	20	19.01 \pm 0.12	29.5 \pm 1.70	0.64
R 1.00 (2 nd iteration)	5	26.96 \pm 1.61	19.67 \pm 2.52	1.37
	10	33.1 \pm 2.50	23.6 \pm 0.14	1.4
	15	36.41 \pm 3.18	25.96 \pm 6.38	1.4
	20	38.56 \pm 5.73	31.24 \pm 6.60	1.23
R 0.85 (3 rd iteration)	5	21.98 \pm 12.71	14.01 \pm 0.74	1.57
	10	42.05 \pm 4.18	14.73 \pm 0.98	2.85
	15	47.74 \pm 2.35	16.49 \pm 1.00	2.9
	20	49.04 \pm 0.76	18.56 \pm 3.34	2.64
Ramp (4 th iteration)	5	24.36 \pm 0.30	17.94 \pm 0.69	1.36
	10	27.14 \pm 1.93	20.97 \pm 0.28	1.29
	15	25.92 \pm 1.84	21.03 \pm 2.25	1.23
	20	28.85 \pm 3.22	21.76 \pm 2.04	1.33
Sinus (5 th iteration)	5	17.37 \pm 9.32	23.5 \pm 6.23	0.74
	10	18.62 \pm 6.48	30.99 \pm 0.48	0.6
	15	19.38 \pm 5.83	31.94 \pm 0.96	0.61
	20	26.77 \pm 1.71	31.71 \pm 0.69	0.84
Sinus-ramp (6 th iteration)	5	23.68 \pm 2.66	22.94 \pm 0.98	1.03
	10	24.23 \pm 0.01	22.03 \pm 1.66	1.1
	15	24.58 \pm 0.88	23.29 \pm 0.95	1.06
	20	25.56 \pm 2.26	23.14 \pm 0.87	1.1

The ratio of the angles was calculated from the average α to β angles which were measured and averaged over two cycles (table 4.1) to assess the symmetrical movement of dye injection. The dye distribution in the 1st iteration cannula showed higher levels of β than α from the beginning. The angle ratio remains approximately 0.6 from the initial to the final frame.

In version R 1.00, a wider distribution was present on both α and β throughout the recorded period, showing final upper-to-lower angle proportions of 1.37, 1.40, 1.40, and 1.23, respectively. Moreover, α in the R 0.85 version was wider than β , leading to an angle ratio of 1.57 to 2.64.

The dye distribution angle in the ramp version assessment was higher in both α and β , and was distributed relatively symmetrically. The angle ratio of the selected frame was consistently around 1.30. Analysis of the sinus version revealed a higher β than α , resulting in a final angle ratio of around 0.84. Furthermore, regarding the distribution of dye in the sinus-ramp version, the ratio remained stable at around 20 - 25 degrees for 10 - 20 milliseconds, showing a tendency towards balance with a value of 1.10.

4.3. PARTICLE TRACKING

4.3.1 MATERIALS AND METHODS

Cannula preparation

This study used a 6.3 x 6.3 mm acrylic square tube aligned with a prototype cannula to minimise the visual distortion effects caused by the curvature of circular tube. As shown in Figure 4.14, the square tube cross sectional area is very similar to the cross-sectional area of the 7.00 mm circular tube (38.48 vs 39.69 mm², square tube vs circular tube, respectively). An adhesive putty was used to block the gap and prevent leak between the cannula body and internal tube. Then, the prototype cannulae and square tube section was connected to the mock circuit for further investigation.

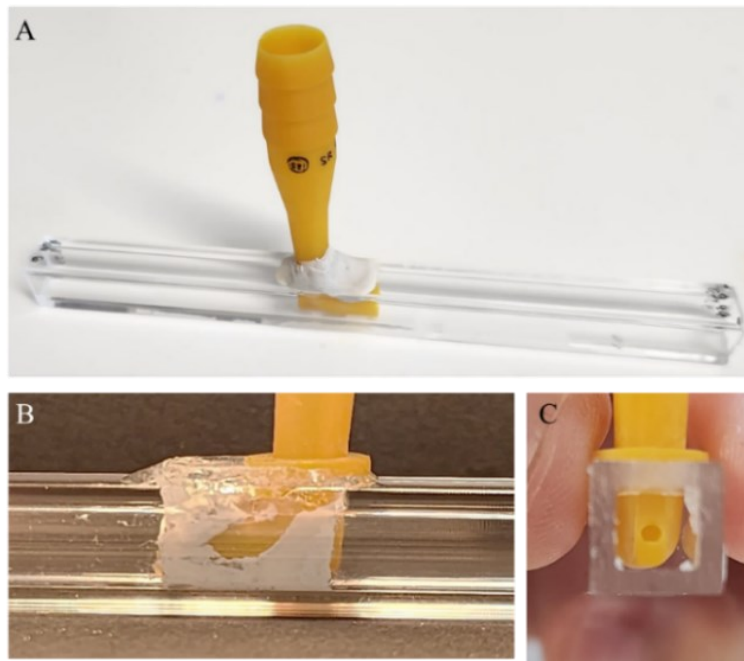


Figure 4.14 Prototype cannula aligned with an acrylic square tube.

(A: Overall view; B: Zoom in; Adhesive putty applied to the gap between the cannula body and tube C: Zoom in cross sectional view shows the secondary outlet.)

Circuit preparation

In Figure 4.15 and 4.16, the particle tracking was performed using a closed-loop system consisting of a roller pump, reservoir, and cannula to facilitate the circulation of fluid-seeded particles. This study used the high-speed camera and lighting systems described in section 4.2.1 to record the particle dispersion across the region of interest.

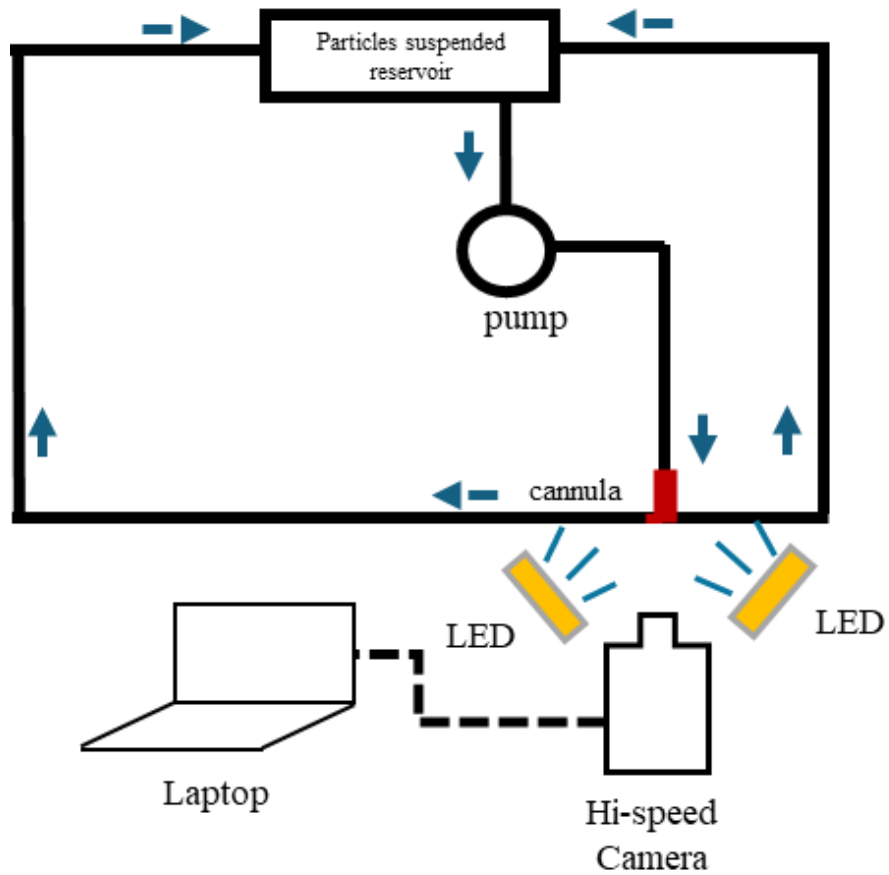


Figure 4.15 Schematic of set up for particle tracking experiments.

Circuit components with hi-speed camera and lighting system for particles tracking test; Dash arrow: flow direction.

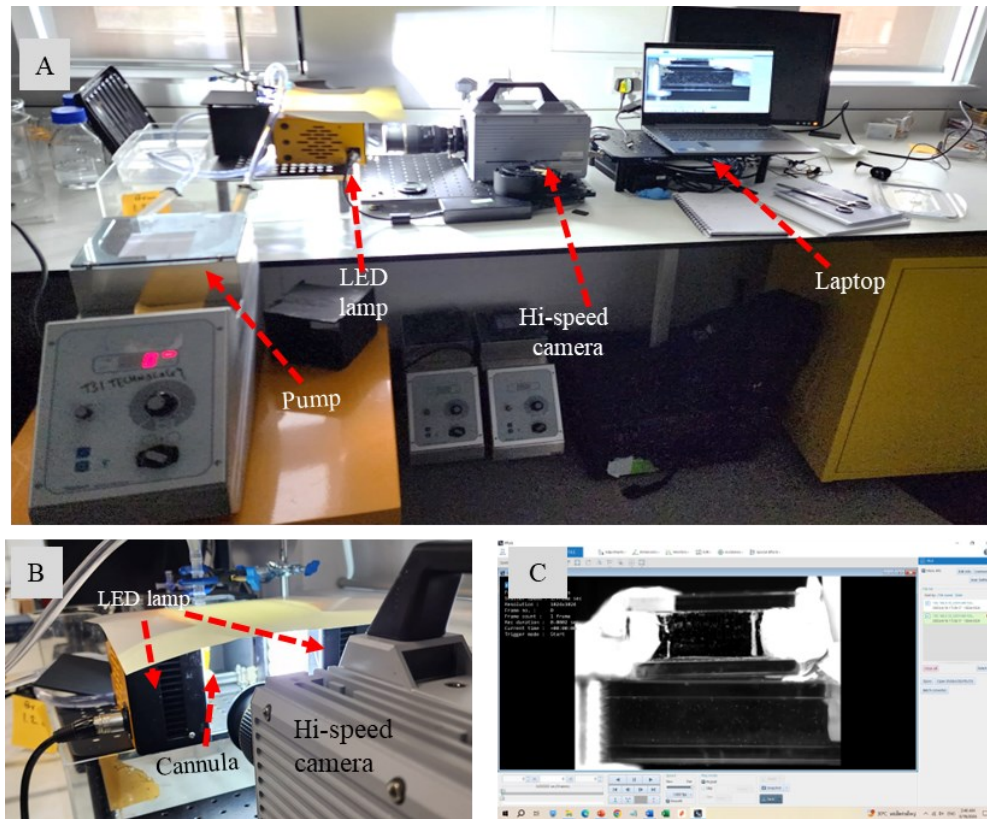


Figure 4.16 Illustrated the set up for particle tracking experiments.

(A: The particle tracking experiment set up with a hi-speed camera and lighting system; B: The cannula and tube observed from behind the camera; C: The screenshot window from the laptop)

Microspheres preparation and prime

The priming solution consists of white polyethene microspheres ranging in size from 10 to 90 μm , suspended in a 0.1% tween solution (Cospheric LLC, CA, USA) (https://www.cospheric.com/tween_solutions_density_marker_beads.htm). This solution was then diluted with 1200 ml of deionised water and was then used as the priming solution. The temperature of the priming solution was approximately 22°C. The priming solution containing microspheres was added to the circuit. Then, the pump flow was gradually increased until the fluid completely filled the circuit, and any air bubbles were removed from the system.

Image acquisition

In this study, pump flow through the circuit was set at 0.5 LPM instead of 4 LPM to improve visual perception. This issue is described in session 4.5. The image acquisition was performed in accordance with section 4.2.1. The calibrating scale was captured at the initiation of the recording process, using a ruler in the square tube solution as shown in Figure 4.17. The high-speed camera recorded at 5000 frames per second at a resolution of 1024 x 800 pixels. The camera was aimed and magnified at the secondary lumen to observe the flow to the vessel wall.

Particle tracking analysis

Particle tracking analysis was processed using the PIVLab tool (version 2.6, T William & R Sonntag, 2021) on MATLAB (Version R2023b, MathWorks, USA) (Thielicke & Sonntag, 2021). After the recording, a picture sequence of 2000 frames were selected for further analysis. The time resolved image sequencing process was used to indicate the particle movement across the picture frame, resulting to a series of 1000 image pairs.

The region of interest (ROI) window was cropped at 800 x 230 pixels (px), covering approximately 20 mm from the opening of secondary lumen. The particle size in each picture was approximately 2-3 px. Image pre-processing used contrast limited adaptive histogram equalization (CLAHE) with window size of 64 px and background subtraction was performed to eliminate the noise and improve the particle detected. The PIV algorithm employed Fast Fourier Transform (FFT) window deformation to analyse the interrogation area, in which the smallest window was 16 x 16 px.

Calibration

As in Figure 4.17, the ruler was submerged in the square tube contained with tween solution. This ruler was used for a calibration scale used in the processing program. The calibration scale was measured to indicate the reference length (in px) and converted to meters using the pre-recorded image. The time step was set at 0.2 msec which was equal

to the time across frame to frame of a 5000-fps high-speed camera. The velocity-based validation was selected velocity scatterplot in the program to indicate the vector direction from the secondary lumen.

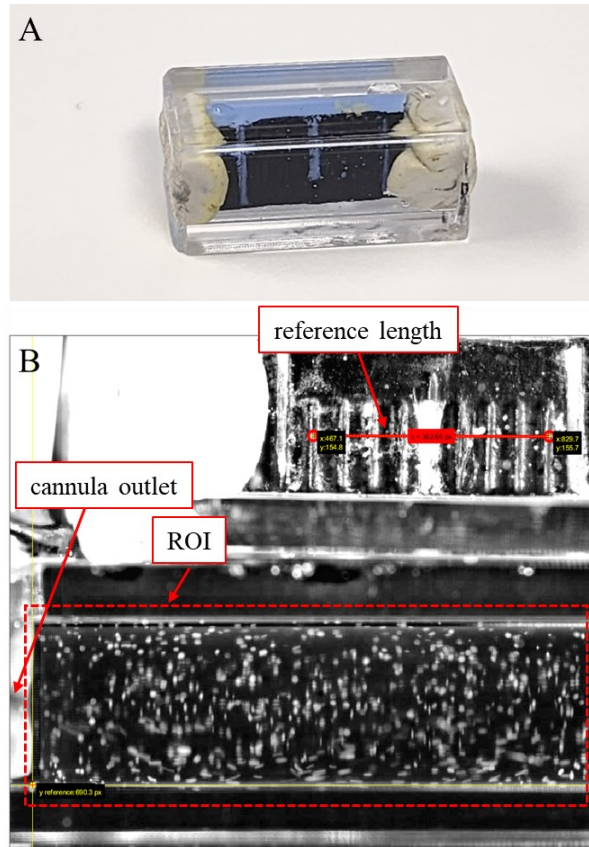


Figure 4.17 Calibration ruler for particle tracking analysis.

(A: Ruler in the square tube with tween solution prepared for calibration; B: Calibration image from PIVLab) (ROI: Region of interest)

4.3.2 RESULTS

The directional flow vectors produced from the secondary lumen of each cannula version were investigated to assess the flow direction towards the central vessel in different versions of the cannula. These findings were used to confirm their impact on the distribution of the vessel wall.

R 1.40 (1st iteration)

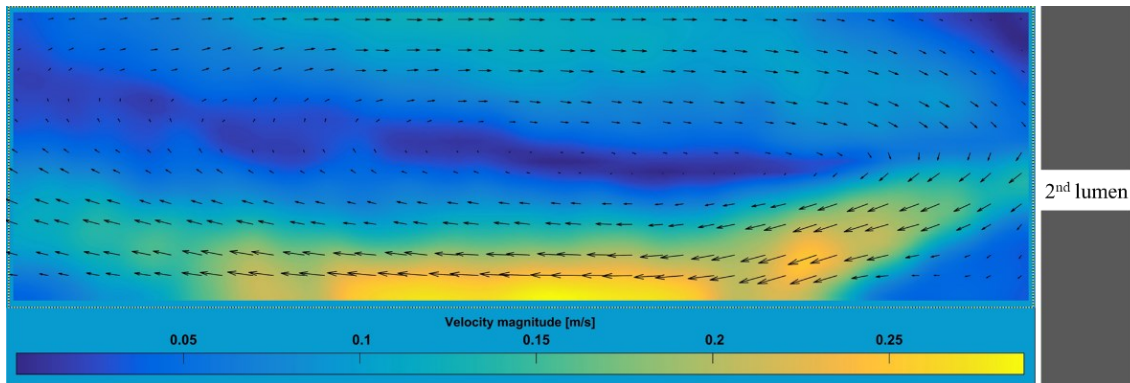


Figure 4.18 Velocity magnitude and vector field at secondary lumen of the 1st iteration cannula.

Figure 4.18 displays the flow distribution vectors that arise from the secondary lumen of the 1st iteration cannula. The flow vectors found projection onto the inferior wall and a subsequent reversal towards the superior region. The average velocity magnitude was gathered in the inferior section of the picture.

R1.00 and R 0.85 versions (2nd and 3rd iterations)

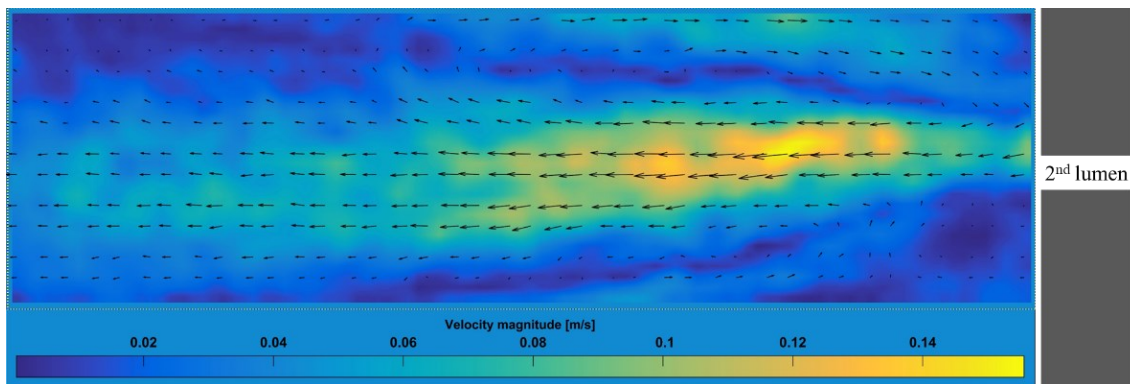


Figure 4.19 Velocity magnitude and vector field at secondary lumen of the R 1.00 version.

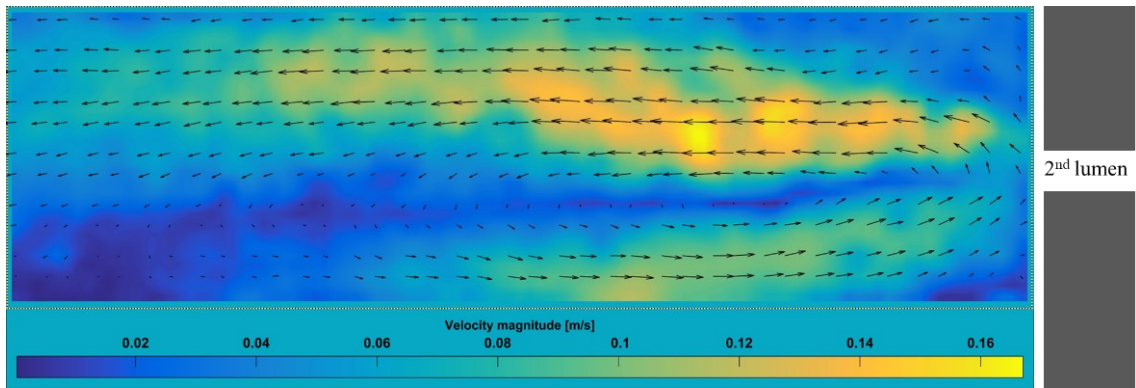


Figure 4.20 Velocity magnitude and vector field at secondary lumen of the R 0.85 version.

The velocity magnitude and vectors of version R 1.00 are displayed in Figure 4.19. Flow reversal was observed in the superior region. However, most of the flow vectors were found to be directed centrally, representing a potential reduction in the possibility of vessel damage. In comparison, a version with radian curve of 0.85 mm, the magnitude and vector of mean velocity tended towards the superior region. The reverse flow was observed in the opposite direction, as shown in Figure 4.20.

Ramp and Sinus Versions (4th and 5th iterations)

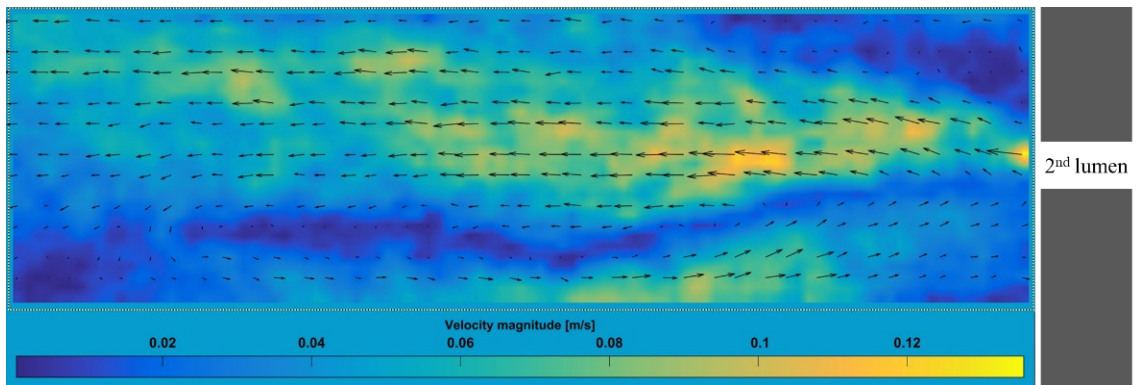


Figure 4.21 Velocity magnitude and vector field at secondary lumen of the ramp version.

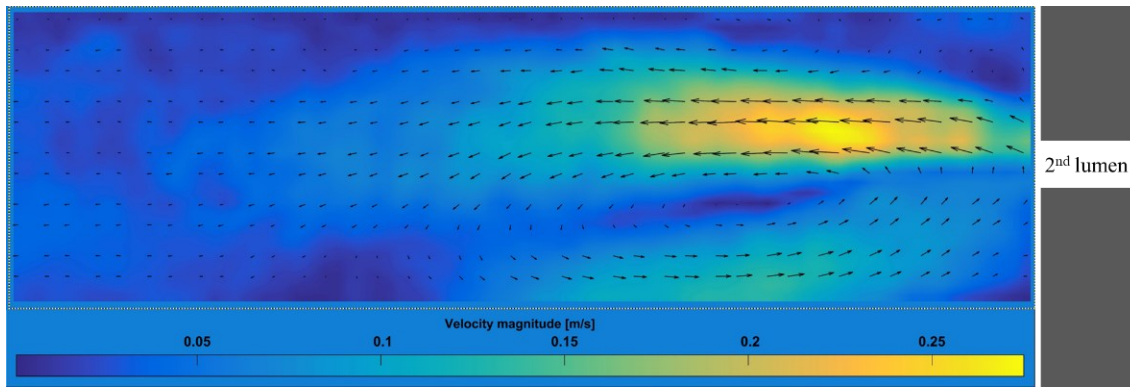


Figure 4.22 *Velocity magnitude and vector field at secondary lumen of the sinus version.*

The flow vectors of the fourth and fifth version are displayed in Figure 4.21 and 4.22. Compared to the earlier versions, the flow vector and magnitude from a secondary exit are more centrally aligned. In comparison to the sinus version, the ramp version had a higher mean velocity.

However, both versions of the flow direction observed in the picture were directed towards the superior region, while the bottom part exhibited reverse current. In addition, the upward flow was found earlier in the sinus version.

Sinus-ramp Version (6th iteration)

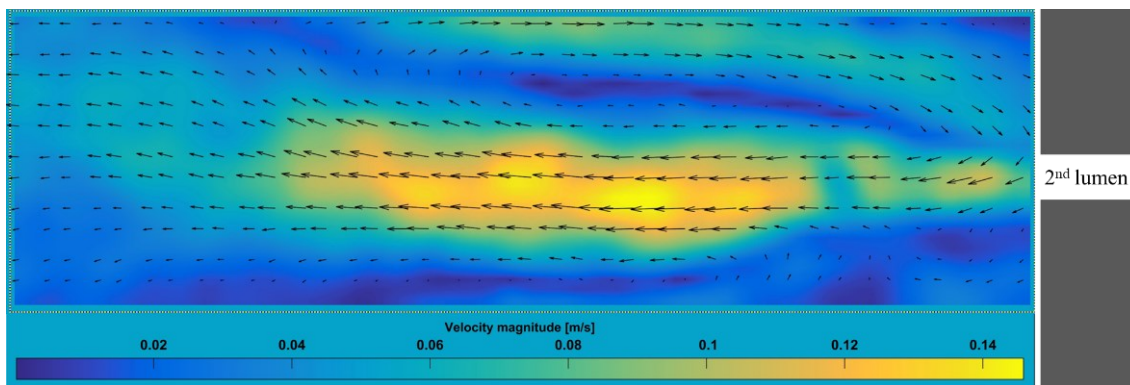


Figure 4.23 *Velocity magnitude and vector field at secondary lumen of the sinus-ramp version.*

Figure 4.23 illustrates the flow characteristics of the sinus-ramp version. The velocity vector pattern appears centralised, with a presence of reverse current in the upper region. Additionally, a major mean velocity magnitude has been found to remain in the central

line potentially. This result suggested that this iteration may offer a decreased chance of vessel damage.

4.4 CFD VALIDATION

In this section, outcomes from dye injection and particle tracking are compared with CFD outcomes. An investigation was carried out to establish the flow direction based on the dye injection outcomes and the traversing angle of the dye through the cannula outlet. Particle tracking was conducted to validate the CFD in the 1st iteration cannula and to determine flow direction and magnitude in all cannula variations. A comparison was then drawn between CFD and flow visualization with these methods.

4.4.1 MATERIALS AND METHODS

The 1st iteration cannula of the bi-directional cannula was used for quantitative validation of CFD techniques. The velocity contours of mid-plane and near inferior wall of the particle tracking and CFD were compared as correspond to the same axis scale. The horizontal velocity measurements were recorded at two distinct points along the velocity magnitude which are a set distance from the secondary lumen. At D/2 plane represents the centreline of horizontal velocity while D/5 represents the near inferior wall horizontal velocity (Figure 4.24).

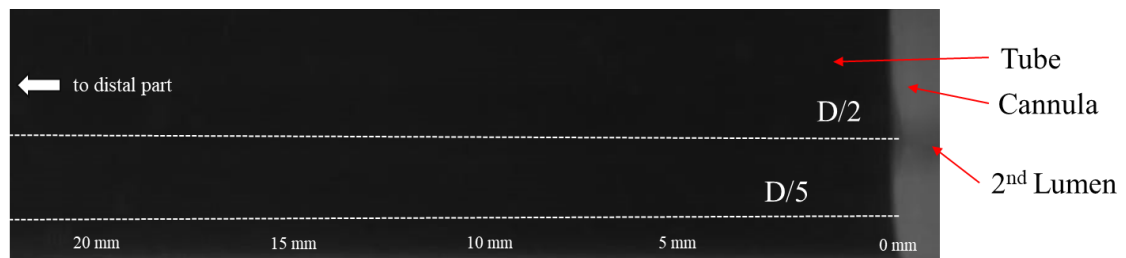


Figure 4.24 Indicated the plane for the velocity measurement in CFD and particle tracking.

(D/2: the centreline; D/5: the near inferior line; 2nd lumen: secondary lumen)

The findings on the velocity ratio at specific locations velocity (V_x) over the maximum velocity (V_{max}) were obtained from the PIVlab software and CFD. The following equation was used for determining the ratio throughout the test.

$$\text{Velocity ratio} = V_x/V_{max}$$

Where: V_x is a velocity at specific locations and V_{max} is a maximum velocity that measured from all areas of interest

Statistical analysis

As shown in Figure 4.24, the distances from the secondary lumen were measured at 0, 5, 10, 15, and 20 mm, respectively. The statistical test for correlation coefficient (r^2) of V_x/V_{max} from particle tracking experiments was used to validate and compare the trajectory against the CFD results, using Minitab statistical software (Minitab Statistical Software ver. 20, Minitab, LLC, USA).

4.4.2 RESULTS

CFD VS Particle Tracking

Table 4.2 Correlation of velocity measured in CFD and PIV at D/2 and D/5.

Distance (mm)	D/2				D/5			
	V_x		Velocity ratio		V_x		Velocity ratio	
	CFD	PIV	CFD	PIV	CFD	PIV	CFD	PIV
0	3.02	0.11	1	1	0.31	0.03	0.11	0.14
5	0.44	0.017	0.15	0.15	2.72	0.22	1	1
10	0.2	0.02	0.07	0.18	1.66	0.216	0.61	0.98
15	0.096	0.046	0.03	0.42	1.28	0.14	0.47	0.64
20	0.31	0.07	0.1	0.64	1.01	0.07	0.37	0.32

r^2 0.81

r^2 0.9

r^2 : correlation; D/2: measured at centre line; D/5: measured at inferior line.

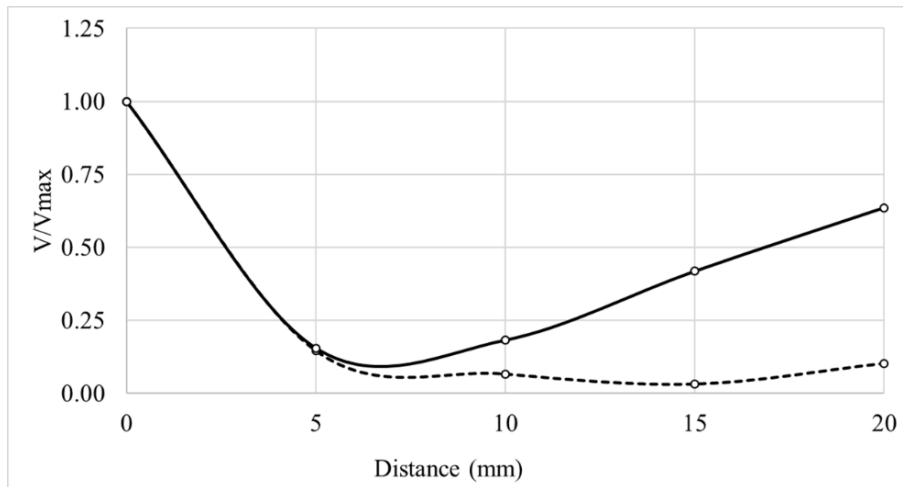


Figure 4.25 Compared the Velocity ratio (V_x/V_{max}) at centreline ($D/2$)

$r^2=0.81$ (Dash line: CFD; Solid line: Particle tracking)

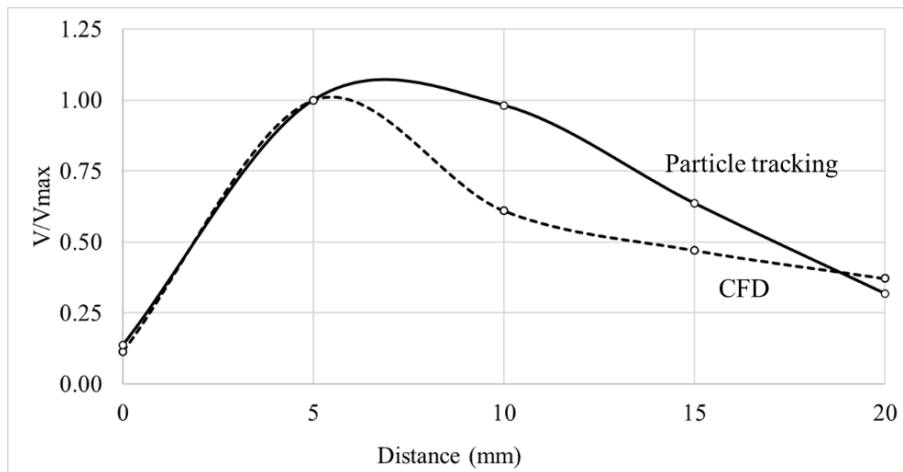


Figure 4.26 Compared the Velocity ratio (V_x/V_{max}) at near inferior line ($D/5$)

$r^2=0.9$ (Dash line: CFD; Solid line: Particle tracking)

The correlation of proportion of the velocity (V_x/V_{max}) between CFD and particle tracking studies was compared and shown in table 4.2 and Figure 4.25 and 26. At the centre line ($D/2$), the proportion of the velocity trend decreased between 5 and 15 mm and then reversed at 20 mm. While the velocity magnitude trend at near inferior line ($D/5$) found an initial increase of 5 to 10 mm, followed by a subsequent decrease from

about 15 to 20. The correlation (r^2) of V_x/V_{\max} between CFD and particle tracking at $D/2$ was 0.81, while at $D/5$ it was 0.9.

CFD vs Flow visualization

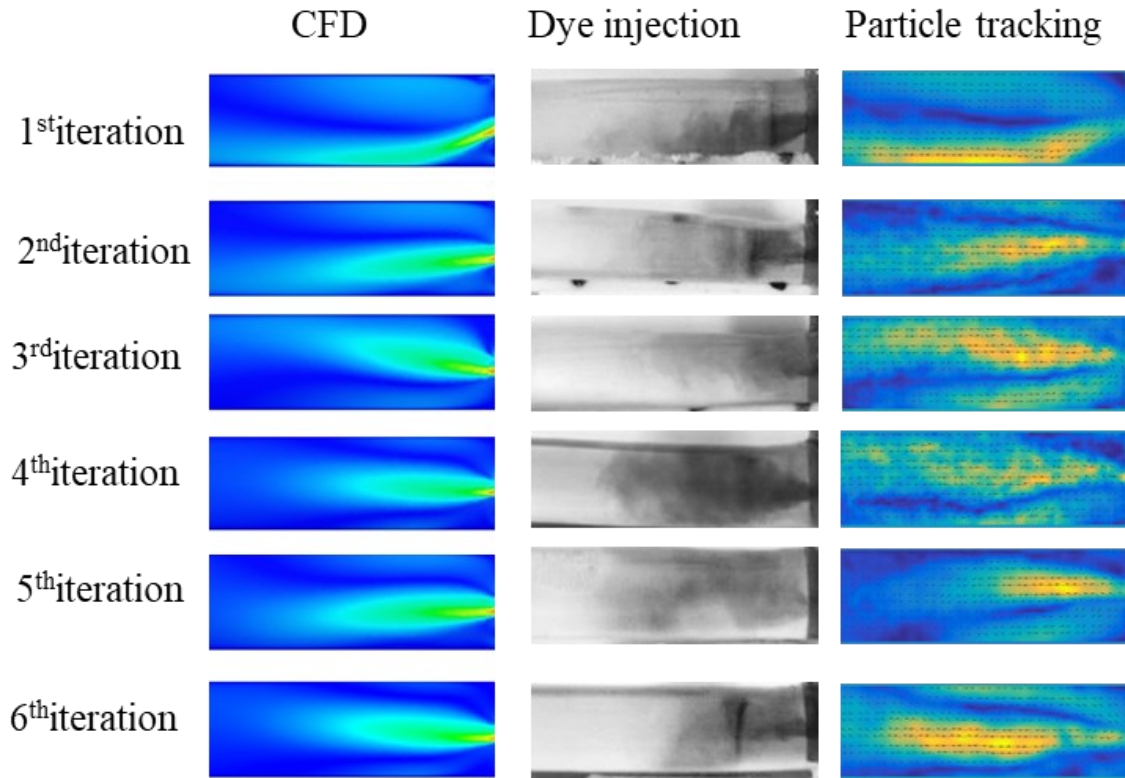


Figure 4.27 Comparison of flow magnitude in CFD and flow visualization.

Comparison of flow characteristics with the use of CFD analysis and flow visualisation tests are shown in Figure 4.27. Notably, the particle tracking result had a flow pattern very similar to those observed in dye injection test. Also, the velocity magnitude results of the CFD simulations showed a similarity to flow visualisation throughout all versions of the cannulae. In the sinus and R 1.00, the flow magnitude in CFD were different compared with both flow visualisation tests. However, dye injection and particle tracking experiment exhibited similar dispersion characteristics.

4.5 LIMITATIONS

The limitation of this study was that the experiment used LED as a light source instead of the synchronised laser sheet system to create visualisation. The illumination areas cannot be controlled and possibly skips out of the field due to the unspecific visualisation plane. Moreover, the high flow rate (4.0 LPM) caused some particles to become non-circular shaped and invisible, particularly at the opening of the secondary lumen, as presented in Figure 4.28. These problems interfered with the PIV processing, especially when measuring the velocity and related parameters (Nobach & Bodenschatz, 2009). As a result, the velocity in this study is unsuitable for directly comparing the experiment results with the earlier computational model. Therefore, to improve the visual perception of particles, the experimental procedure was repeated at a flow rate of 0.5 LPM.

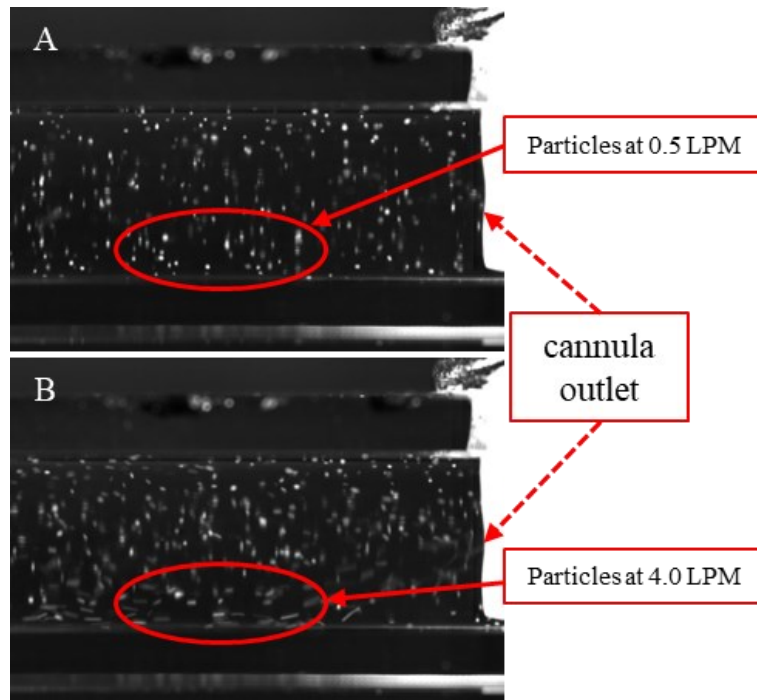


Figure 4.28 Comparison of the picture of particle shape in 0.5 vs. 4.0 LPM.

The image that was taken from the flow 0.5 LPM shown more circular shaped than the flow 4.0 LPM, which were suit for process with the PIV processing program. (A: Particle shape at 0.5 LPM; B: Particle shape at 4.0 LPM)

4.6 CHAPTER SUMMARY

This chapter demonstrates the results of the distribution of dye and particles at the secondary lumen in different cannula versions to validate the CFD test as purposed in phase 3 (see Chapter 2, Session 2.2).

- The 1st iteration cannula, flow visualisation experiments found flow movement towards the inferior wall. This suggests an increase chance of vessel damage as well found in CFD. Additionally, the CFD validation in the 1st iteration cannula compares the velocity magnitude trends at different distances and offers favourable correlation.
- In version R 0.85, flow distribution found consistent upward movement towards the superior region, while version R 1.00 shows rapid movement centrally and superiorly.
- The sinus-ramp versions show more central flow vectors, and the ramp version shows symmetrical movement towards the superior and inferior regions. However, the sinus version initially distributes to the inferior region before ascending to the superior wall.
- The study assessed symmetrical movement of dye injection and showed varying distributions in all versions. The 1st iteration cannula showed higher β levels, whereas the sinus-ramp version shows central velocity vector patterns and a consistent ratio range of angles.
- The CFD velocity magnitude in version sinus and version R 1.00 found slightly different patterns from the flow visualization test, however a similar distribution was found in both the dye injection and particle tracking experiment.

The findings in this chapter indicate that the use of dye injection and particle tracking is an effective method for understanding flow properties and validating CFD. The experimental work then focused on haemodynamic properties by measuring the flow-pressure relationship of the prototype for each version. The work used a mimicking extracorporeal flow setup module to address phase 4 (chapter 2). Additionally, a volumetric measurement was conducted to verify proportional flow distribution from the cannula.

CHAPTER 5

PRESSURE-FLOW PROPERTIES

5.1 INTRODUCTION

Mechanical properties and performance in extracorporeal circulation are usually determined by monitoring the haemodynamic response. The main parameters measured in extracorporeal circulation are flow rate, circuit pressure and haemodynamic energy. Evaluation of these parameters is an essential method for assessing characteristics and performance of each components in ECMO circuit (Patel et al., 2023).

Adequate blood flow is key to positive ECMO outcomes. Normally, the flow can generate pressure throughout the circuit component. Therefore, pressure monitoring in ECMO is identified by the position of pressure measurement on the circuit. The pressure gradient across components of the circuit is commonly used in several research and clinical practices to simplify procedural efficacy and to minimise complications (Broman et al., 2019). For example, a calculated gradient pressure between pre- and post-oxygenator is transoxygenator pressure, and is a useful parameter to observe presence of clots in the hollow fibres and the oxygenator performance (Gourlay et al., 1990; Wang et al., 2018).

Regarding arterial cannulae, the pressure gradient can be determined by comparing the pressures at the inlet and outlet ports in relation to different given flow rates. This parameter is an essential indicator for assessing the performance and safety margin of the arterial cannula design. The turbulence of flow and excessive gradient pressure from the arterial cannula can lead to endothelial trauma, red blood cell haemolysis, and impairment of platelet function. A pressure gradient which is greater than 100 mmHg is not recommended for use in CPB and ECMO (Brodman et al., 1985; Broman et al., 2019).

The M-number, which is derived from the gradient pressure, can be used to assess the pressure-flow characteristics of the arterial cannula. This number is calculated based on the pressure gradient parameter, viscosity, and cannula diameter. Several studies have compared the M-number of the commercial arterial cannula in the market to verify their performance. A higher M-number is strongly correlated with increased pressure gradient and complications resulting from elevated resistance and turbulence flow (Sinard et al., 1991).

In addition, volumetric measurement of blood is present in the flow rate examined by the ultrasound doppler in clinical practice (Blanco, 2015). This method can monitor the adequate blood supply to the organ, which is related to adequate perfusion and organ preservation. Sufficient blood flow is related to ischemic consequences and organ dysfunction. So therefore, in order to develop a novel bi-directional arterial cannula for ECMO, this parameter is evaluated to ensure that the cannula can provide adequate blood flow to both the systemic and distal sites (Abdel-Sayed et al., 2021).

This chapter investigated haemodynamic properties via the pressure-flow characteristics of each cannula version. Furthermore, volumetric measurements were performed at the primary and secondary exits to verify the volume output at both outlets. These tests are a part of phase 4 of this study (see Chapter 2).

5.2 PRESSURE-FLOW MEASUREMENT

5.2.1 MATERIAL AND METHODS

Cannula preparation and pump calibration

The prototype of bi-directional cannula was prepared with a 7.0 mm tube as use in dye injection test in session 4.2.1. A cable tie was fastened around the tube to avoid flow and pressure leak across the gap between the tube and cannula (Figure 5.1). Moreover, before experiments started, the roller pump was calibrated as described in session 4.2.1.

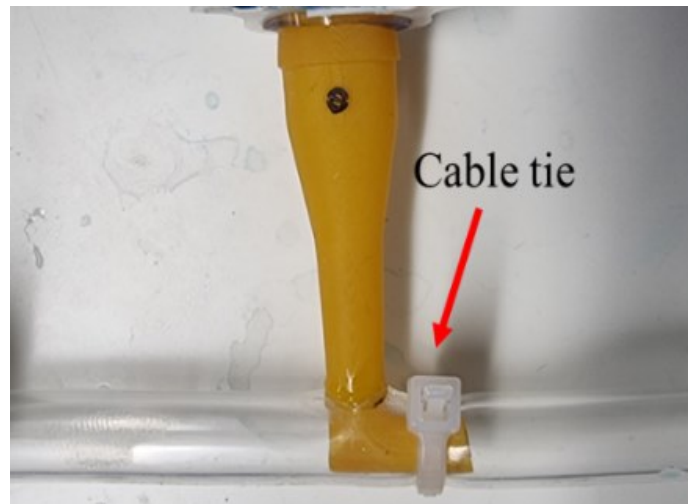


Figure 5.1 Cable tie to prevent leakage.

A cable tie was used to prevent reverse flow from the outlet, protecting against pressure and fluid leakage.

Circuit and prime

The closed-loop system was established as a mock circulation for pressure and flow measurement. The components of the circuit included a reservoir, pump (Stockert/Shiley CAPS multiflow roller pump, Stockert GmbH, German), and prototype cannula. All components were connected and primed with water at room temperature. The water was pumped from the reservoir and through the prototype cannula, which bifurcated flow and drained back to the reservoir.

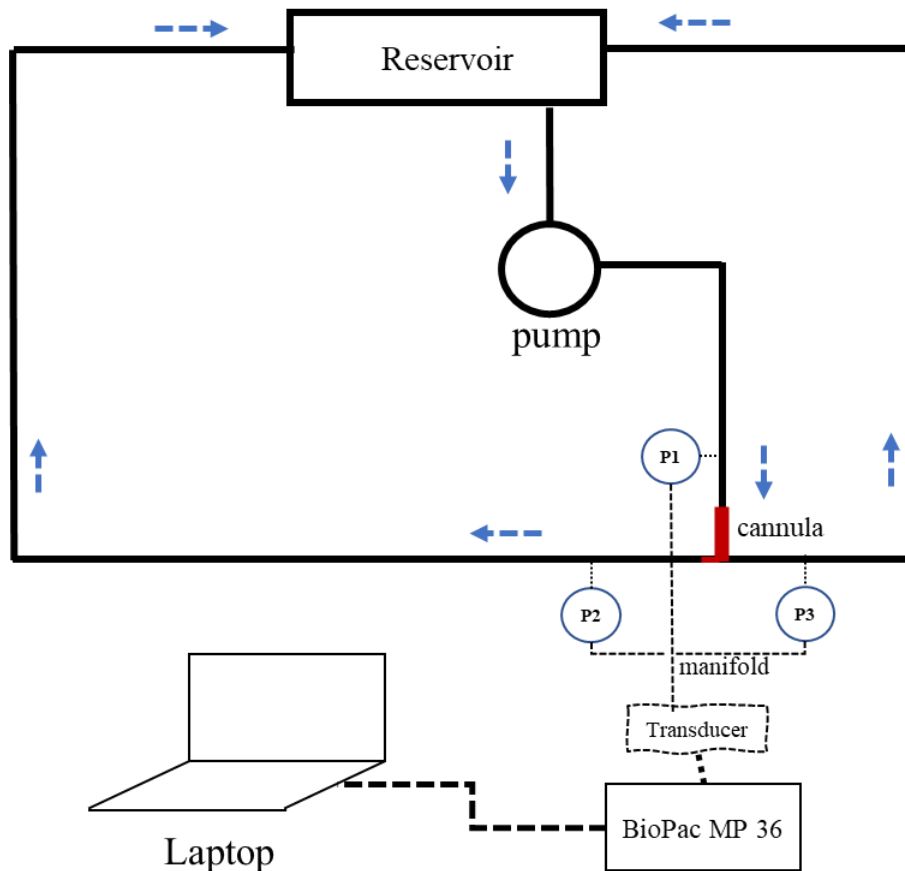


Figure 5.2 Schematic and assembly of the experiment set up in pressure-flow relation.

Mock circulation connected to the Biopac System utilised for pressure measurement, Dash arrow represents the flow direction, P1 is a pre-cannula pressure, P2 is a primary lumen pressure and P3 is a secondary lumen pressure.

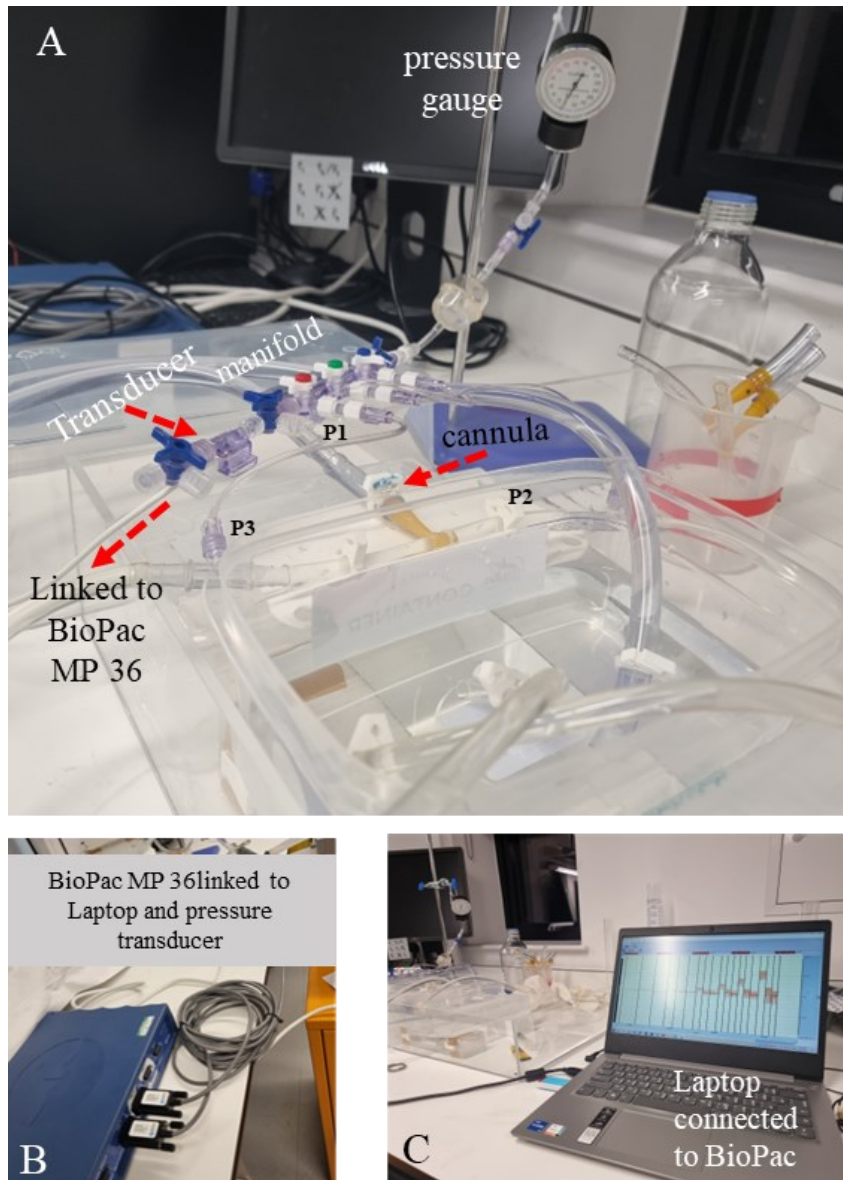


Figure 5.3 *The experiment set up with BioPac system.*

The experiment was set up in pressure-flow relation, using BioPac system. P1 is a precannula pressure, P2 is a primary lumen pressure and P3 is a secondary lumen pressure. (A: Transducer with pressure gauge used in this experiment; B: The BioPac MP 36 Module; C: Laptop linked with the system)

Pressure data acquisition

Pressure tube attached to the proximal and two sides of the distal luer-port. Also, it was connected to manifold and pressure transducers, which then linked to the Biopac module (MP-36, Biopac Systems Inc, US) and the laptop for further analysis. The pressure signal has been obtained through the use of the Biopac system. The experiment recorded the pre-cannula pressure, primary lumen pressure and a secondary lumen pressure at given pump flow rates ranging to 0.5, 1, 2, 3, 4, and 5 LPM, respectively.

The pressure values were measured via AcqKnowledge software (version 5.0, Biopac Systems Inc, US) for real-time data capture. The pressure was calibrated and compared with a pressure gauge to confirm the actual value that was measured in the Biopac system. A pressure signal was recorded for approximately 10 seconds for each provided flow rate (Figure 5.3 and 5.4). The average pressure values of each test were calculated (Vieira, Jr., et al. 2012). These measurements were repeated six cycles (n=6).

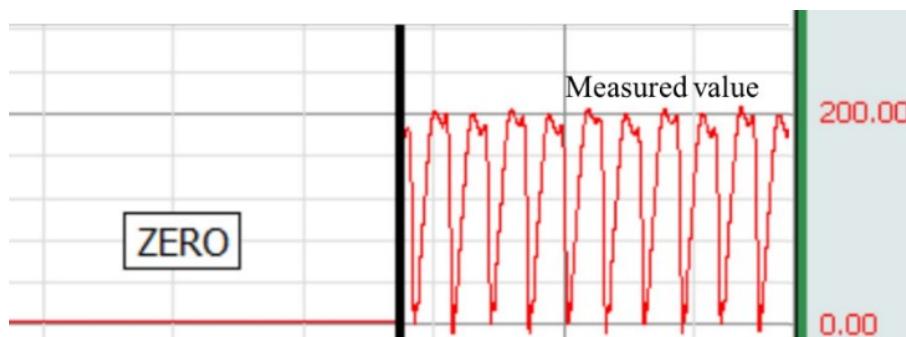


Figure 5.4 Illustrated calibration and dynamic pressure wave.

Recorded waveform in the AcqKnowledge software, zero-pressure set up (left), and measured pressure during running circuit (right).

Pressure gradient calculation

The pressure difference between the inlet and outlets establishes the pressure gradient along the cannula. The calculation of the pressure gradient in the arterial cannula is as follows.

$$\text{Pressure gradient (mmHg)} = \text{Pre-cannula pressure} - \text{post-cannula pressure}$$

Therefore, the pressure gradient calculated in the cannula was calculated using the following equation.

$$\Delta P = P1 - (P2 + P3)$$

Where: ΔP is pressure gradient, $P1$ is the pre-cannula pressure, $P2$ is the primary lumen pressure and $P3$ is the secondary lumen pressure.

Furthermore, the M-number was calculated for all prototype versions using the following equation based on the calculated pressure gradient (Montoya et al., 1991).

$$M = \text{Log} (7.161 \times 10^6 \mu^{-0.25} \Delta P F^{-1.75})$$

Where: P is the pressure gradient across the cannula, F is the given flow rate, and μ is the viscosity of the priming solution; regarding the water used as the priming solution, the viscosity is approximately 1.0016 mPa at the room temperature.

Statistical analysis

The pressure-flow relation analysis was compared by conducting a one-way ANOVA with Dunnett multi-comparison using Minitab Statistical Software ver. 20 (Minitab, LLC, USA), except for the M-number which used the Kruskal-Wallis's test. The significant differences at p-value < 0.05 were determined by changes from the 1st iteration cannula. This statistical test involved calculating the mean and standard deviation (mean \pm SD) of the pressure gradient and M-number.

5.2.2 RESULTS

This chapter presents two key findings: the relationship between pressure and flow, and the measurement of volume from both outlets. And the pressure-flow relationship and the M-number resulted in a pressure gradient of the inlet and outlets, shown in Figure 5.5-5.7.

Pressure gradient at different given flow.

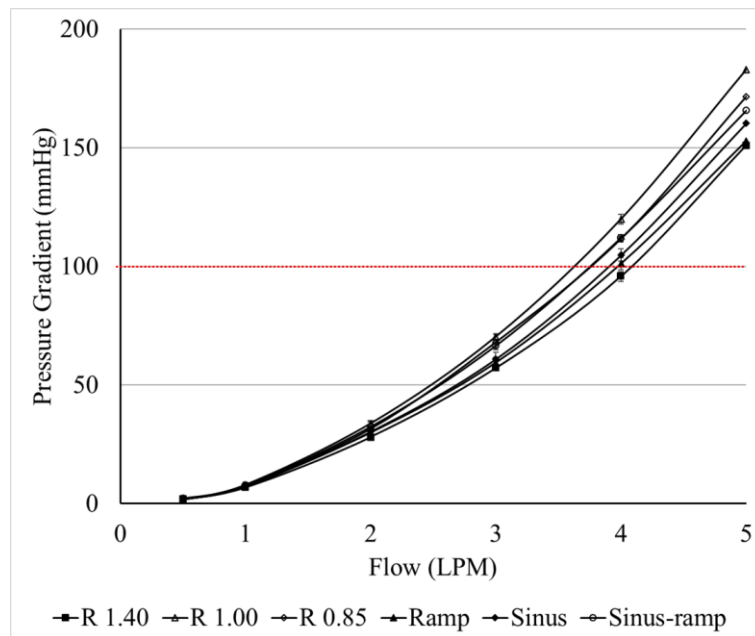


Figure 5.5 Pressure and flow relationship.

The 1st iteration cannula has a maximum flow rate of 4 LPM with a cut-off of 100 mmHg, whereas the others have a flow rate of 3 LPM. (1st iteration: R 1.40 mm; 2nd iteration: R 1.00 mm; 3rd iteration: R 0.85 mm; 4th iteration: Ramp; 5th iteration: Sinus and; 6th iteration: Sinus-ramp)

In Figure 5.5, the mean pressure was plotted against flow in all versions tested. The pressure gradient of all cannula versions increases proportionally as the pump flow increases from 0.5 to 6 LPM. The range of gradients pressure of these versions at 0.5 LPM were 1.6 to 2.3 mmHg, at 1.0 LPM were 6.9 to 7.9 mmHg, at 2.0 LPM were 28 to 34 mmHg, at 3.0 LPM were 57 to 70 mmHg, at 4.0 LPM were 95 to 120 mmHg, and at 5.0 LPM were 150 to 183 mmHg, respectively.

The 1st iteration cannula (R 1.40) observed a drop in pressure of less than 100 mmHg at a flow rate of 4 LPM, whereas other versions of the cannula noted this difference at flow rates of 3-4 LPM. These finding suggests that the 1st iteration cannula has a maximum flow rate of 4 LPM, whereas the other versions have maximum flow rates ranging from 3 to 4 LPM.

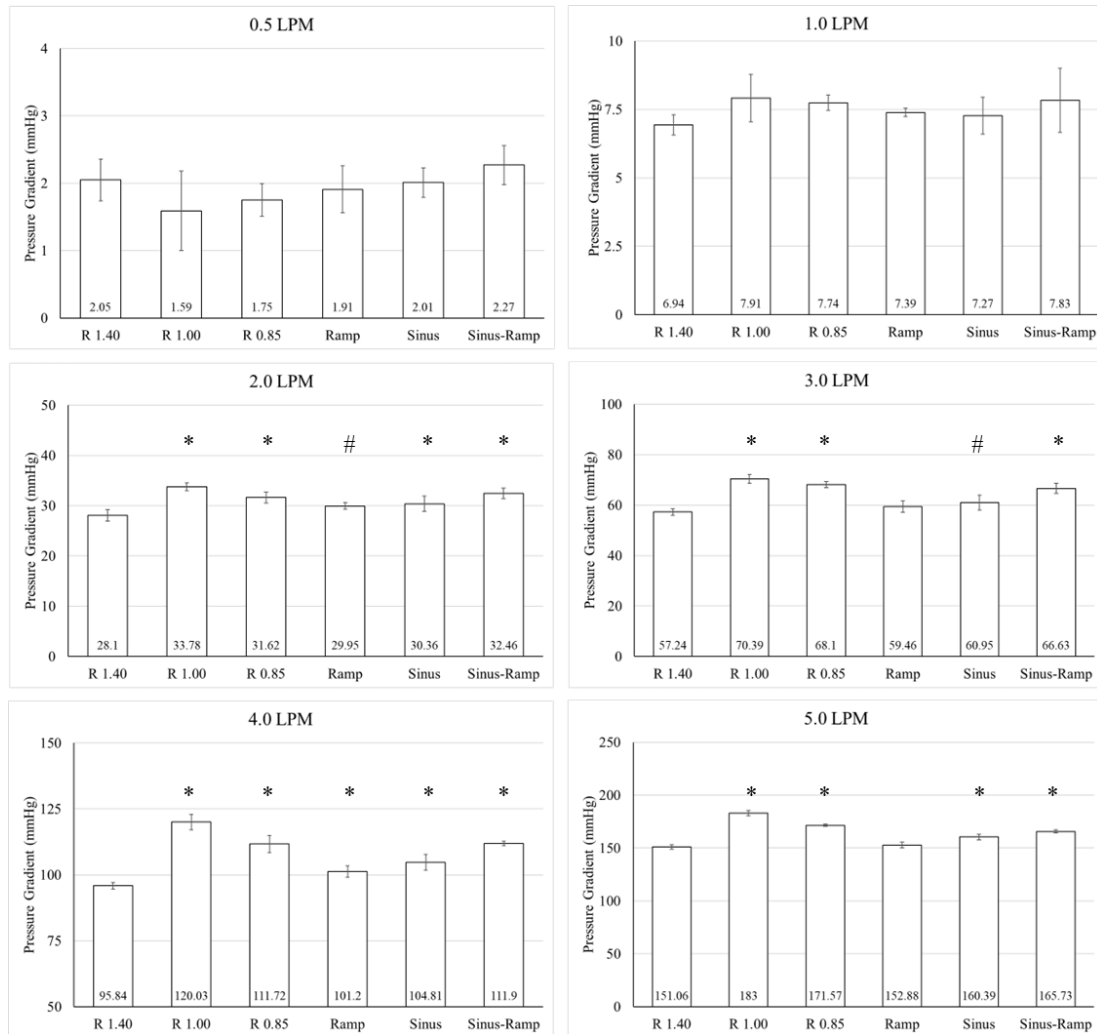


Figure 5.6 Pressure gradient of all prototypes compared with 1st iteration cannula.

n = 6: data presents in mean ± SD: # significant p-value < 0.05, * significant p-value < 0.01 (1st iteration: R 1.40 mm; 2nd iteration: R 1.00 mm; 3rd iteration: R 0.85 mm; 4th iteration: Ramp; 5th iteration: Sinus and; 6th iteration: Sinus-ramp)

In Figure 5.6, the bar graph compares the pressure gradient of each cannula at each given flow, and there were no significant differences in the pressure gradient observed among the different prototypes at flow rates of 0.5 and 1 LPM. At 2 to 5 LPM flow rates, the gradient pressures found were higher in all new cannula versions compared to the 1st iteration cannula (R 1.40). Pressure gradients at 2 to 5 LPM flow significantly increased ($p < 0.01$) in R 1.00, R 0.85, and the sinus-ramp version. These results were followed by a significant difference in pressure gradient in flow rates at 2, 4, and 5 LPM (p -value < 0.01) and 3 LPM ($p < 0.05$). In addition, the ramp version had a significant difference in pressure gradient at 2 and 4 LPM ($p < 0.05$ and < 0.01 , respectively).

M-number

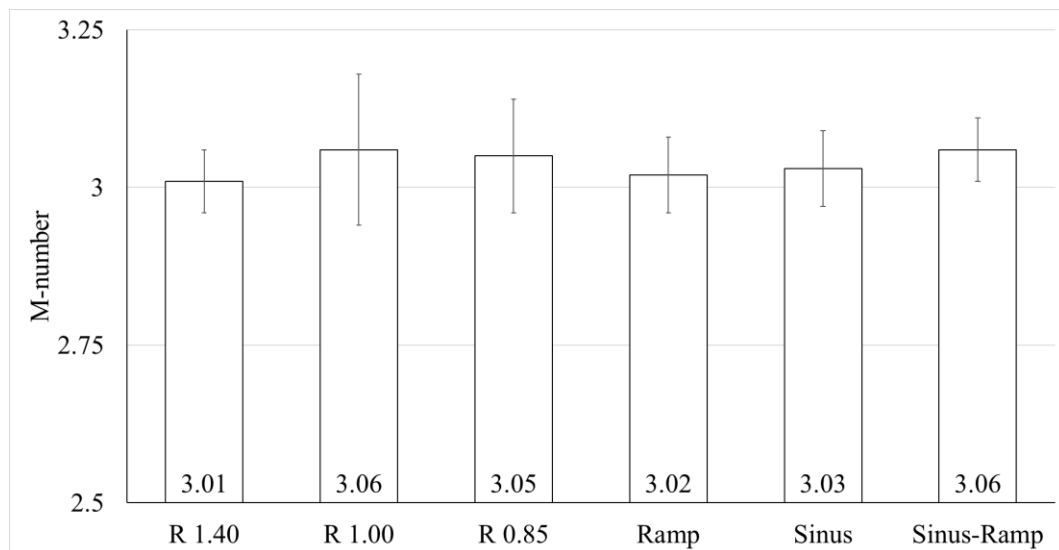


Figure 5.7 Calculated M-number of all prototypes compared with 1st iteration cannula.

The Kruskal-Wallis test for M-number was conducted, with no statistical differences observed: Data presents in mean \pm SD; n = 6 (1st iteration: R 1.40 mm; 2nd iteration: R 1.00 mm; 3rd iteration: R 0.85 mm; 4th iteration: Ramp; 5th iteration: Sinus; and: 6th iteration: Sinus-ramp)

The M-number value shown in Figure 5.7 in mean \pm SD. The results found for all cannula versions were 3.01 ± 0.05 , 3.06 ± 0.12 , 3.05 ± 0.09 , 3.03 ± 0.06 , 3.02 ± 0.06 and 3.06 ± 0.05 , respectively. No significant differences were observed when compared with the 1st iteration cannula.

5.3 VOLUMETRIC MEASUREMENT

5.3.1 MATERIAL AND METHODS

Circuit and prime

The mock circuit used in volumetric measurement consisted of the upstream reservoir, pump, and two drainage reservoirs on a weighing scale (Figure 5.5 and 5.6). After connecting each component with the testing cannula, the circuit was primed with water. The direction of solution was moved from the upstream reservoir via a roller pump (Stockert/Shiley CAPS multifold roller pump, Stockert GmbH, German) and delivered to the testing cannula. The water was finally separated into each downstream reservoir.

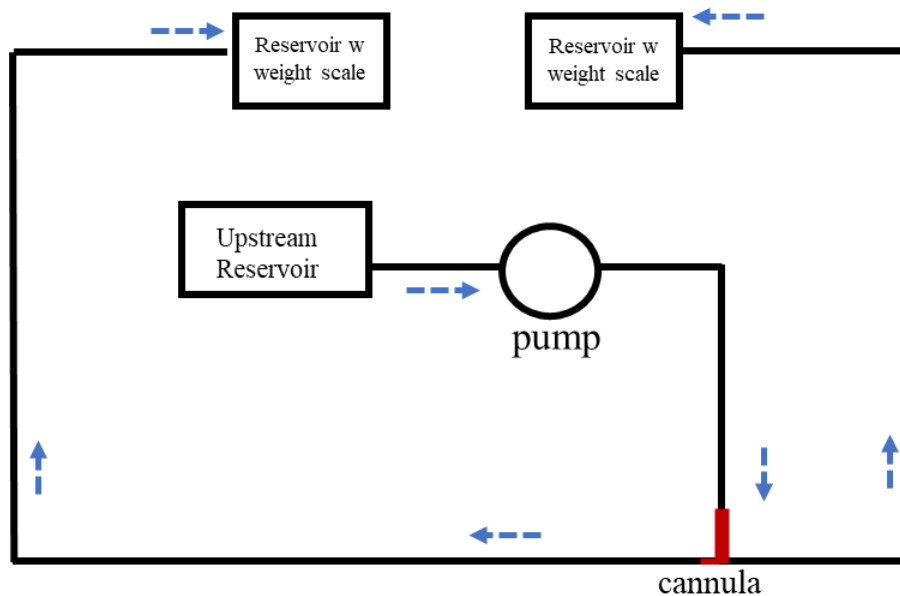


Figure 5.8 Schematic and assembly of volumetric measurements circuit.

Dash arrow represents the flow direction, which were bifurcated by the cannula.

Volume measurement

The volume passing through the cannula outlet in one minute was measured using the weighing scale to estimate the actual output volume at each site. The experiment was carried out at a total inlet flow of 0.5, 1, 2, 3, 4, and 5 LPM six cycles (n=6).

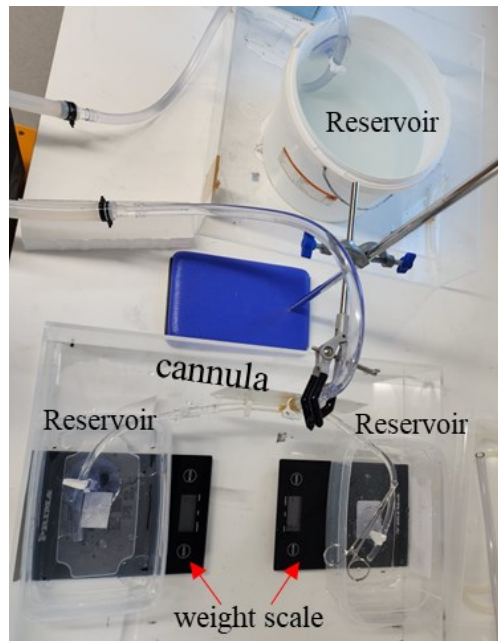


Figure 5.9 The experiment was set up to measure the actual volume of both outlets.

Statistical analysis

A statistical analysis to significant differences at p -value < 0.05 . was conducted to compare the mean and standard deviation. One-way ANOVA with post hoc analysis (Dunnett comparison) was performed to identify any differences from the 1st iteration cannula using Minitab statistical software (Minitab Statistical Software ver. 20, Minitab, LLC, USA).

5.3.2 RESULTS

The volumetric measurements from both sites of the prototype cannula are shown in Figures 5.10 and 11 were compared to the 1st iteration cannula. In general, the volume of each cannula version increased correspondingly to the given flow rate.

Primary lumen output

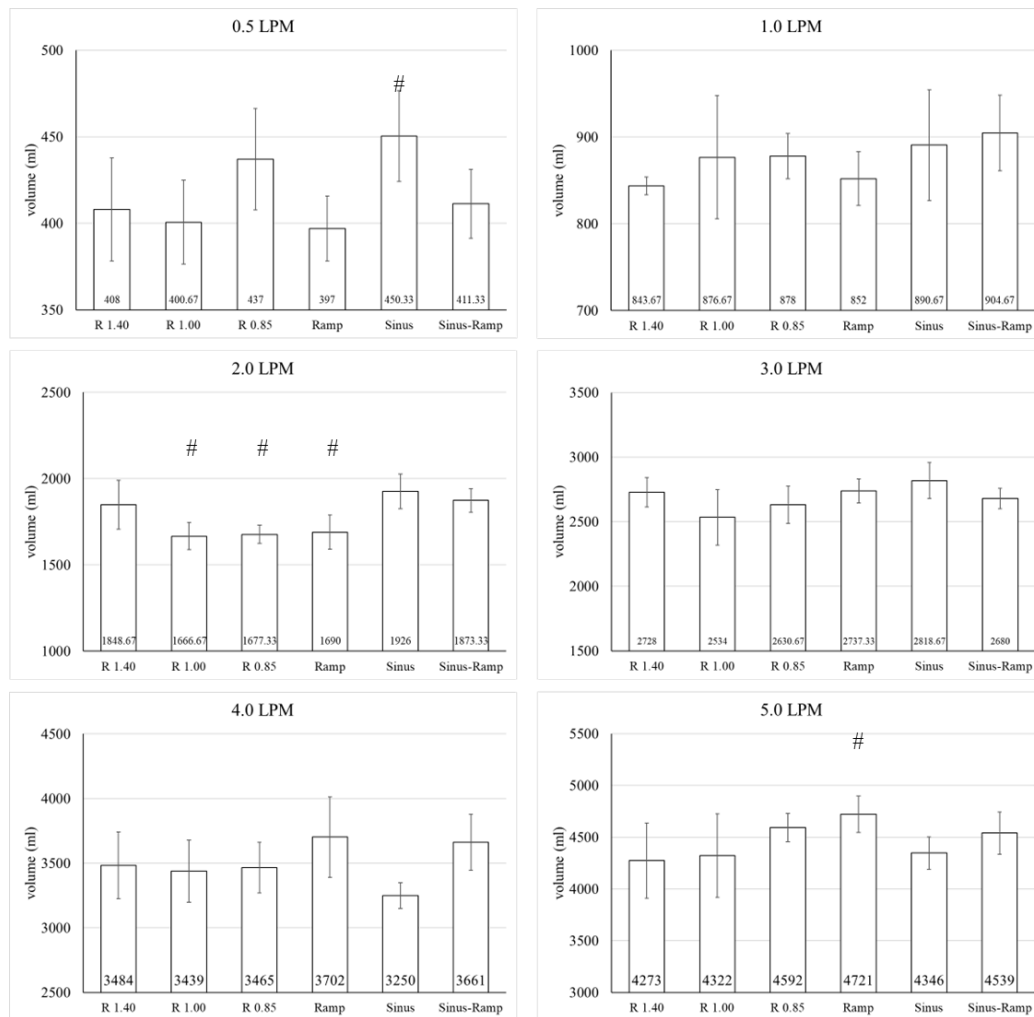


Figure 5.10 Volume output from the primary lumen compared with 1st iteration cannula.

One-way ANOVA with post-test comparison tested for the volume output: Data presents in mean \pm SD: # significant p -value < 0.05 , $n = 6$. (1st iteration: R 1.40 mm; 2nd iteration: R 1.00 mm; 3rd iteration: R 0.85 mm; 4th iteration: Ramp; 5th iteration: Sinus and; 6th iteration: Sinus-ramp)

In figure 5.10, the primary lumen output volume from most of the prototypes compared with the R 1.40 cannula (1st iteration) demonstrated no significant differences. Notably, there was an increase in output at a flow rate of 0.5 LPM for the sinus versions, with a statistically significant difference (408 ± 29.8 ml vs 450.33 ± 26.21 ml, p -value < 0.05 , respectively). Similarly, the ramp version showed higher output at 5 LPM compared to

the 1st iteration cannula (4273 ± 363.55 ml vs 4721 ± 175.64 ml, respectively, $p < 0.05$). A significant decrease in volume was observed at 2 LPM with the R 1.00, R 0.85, and ramp versions ($p < 0.05$).

Secondary lumen output

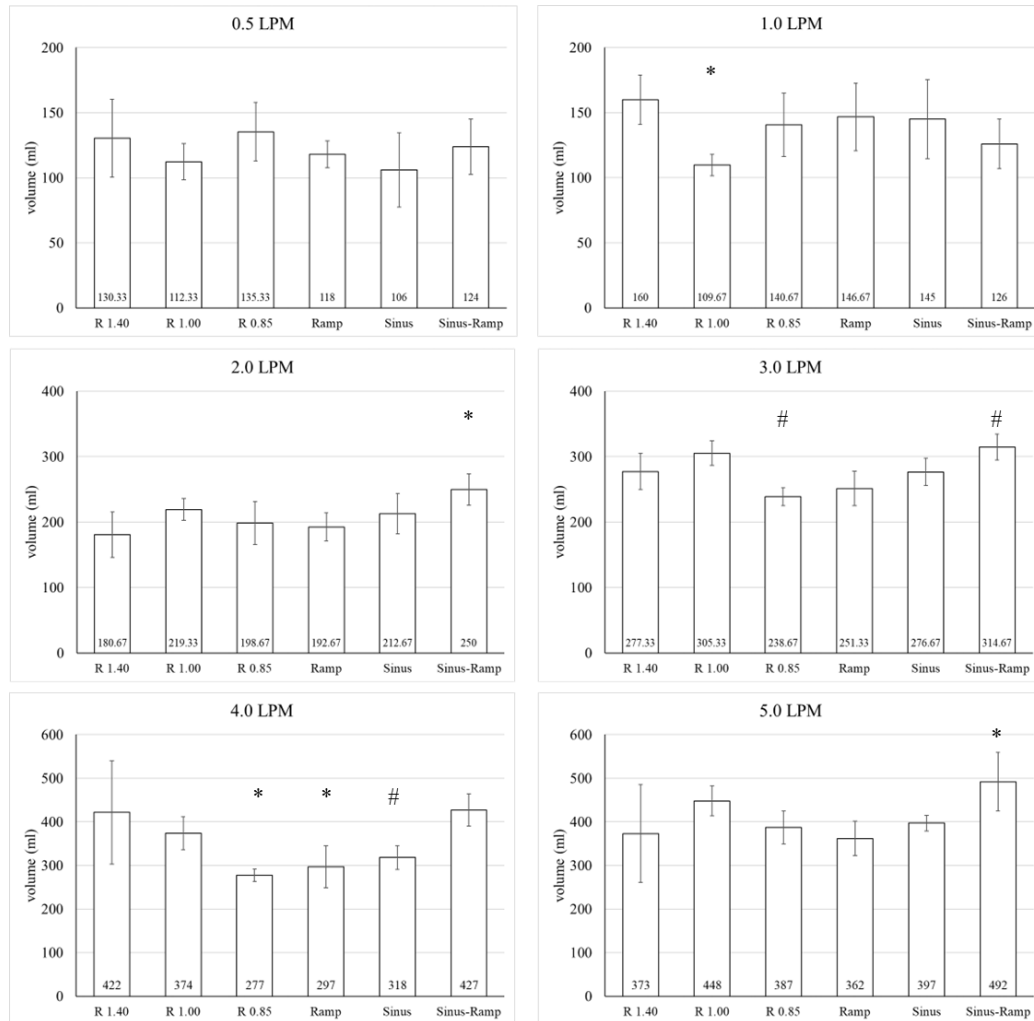


Figure 5.11 Volume output from the secondary lumen compared with the 1st iteration cannula.

One-way ANOVA with post-test comparison tested for the volume output: Data presents in mean \pm SD: * significant p -value < 0.01 ; # significant p -value < 0.05 , $n = 6$. (1st iteration: R 1.40 mm; 2nd iteration: R 1.00 mm; 3rd iteration: R 0.85 mm; 4th iteration: Ramp; 5th iteration: Sinus and; 6th iteration: Sinus-ramp)

Figure 5.11 presents the volume measurement at the secondary lumen. There were no significant differences among all the prototypes compared to the R 1.40 cannula (1st iteration) at a flow rate of 0.5 LPM. In the R 1.00 and R 0.85, ramp and sinus versions, in compared to the 1st iteration cannula, were found to have significantly lower values in different given flows. R 1.00 found significantly lower values while observed at 1.0 LPM (160 ± 18.89 ml vs 110 ± 8.24 ml, control vs R 1.00, respectively, $p < 0.05$). In R 0.85 version had significantly lower output volumes at 3 and 4 LPM compared to control (277.33 ± 27.67 ml vs 276.67 ± 20.77 ml, $p < 0.05$; and 422 ± 118.47 ml vs 318 ± 27.1 ml $p < 0.01$; control vs R 0.85, respectively). The ramp and sinus versions had significantly lower output volumes at 4 LPM compared to control (422 ± 118.47 ml vs 297 ± 48.11 ml and 318 ± 27.1 ml, $p < 0.01$ and $p < 0.05$, control vs ramp and sinus, respectively).

Notably, only the sinus-ramp version demonstrated significantly increased volume output compared with the R 1.40 cannula (1st iteration), at flow rates of 2, 3, and 5 LPM (180.67 ± 34.82 ml vs 250 ± 23.83 ml, $p < 0.01$; 277.33 ± 27.67 ml vs 314.67 ± 19.87 ml, $p < 0.05$; 373 ± 112.21 ml vs 492 ± 67.14 ml, $p < 0.01$, respectively).

5.4 CHAPTER SUMMARY

The pressure-flow characteristics, in combined with the flow direction as discussed in the previous chapter, can be defined as the estimated maximum flow of a cannula, which is associated with reduced blood and vessel trauma. This chapter also presents experiments designed to ensure adequate systemic and distal perfusion, characterised by predictability and balance to facilitate bi-directional organ perfusion.

This chapter includes measurements of the bi-directional cannula's volume and pressure gradient from both lumens in comparison to the 1st iteration cannula (Chapter 2, Session 2.2).

- The pressure-flow measurement in session 5.2.2 demonstrated an increasing trend across all cannula versions. The 1st iteration cannula had a pressure gradient of less than 100 mmHg at flow rates ranging from 0.5 to 4 LPM.
- All cannula versions observed a pressure gradient of less than 100 mmHg at 3 LPM. Therefore, this indicates the safety margin of the cannula at flow rate at about 3 LPM.
- The M-number value derived for all cannula versions was approximately 3.00, and this was non-significantly higher than the 1st iteration cannula.
- The significantly higher output volumes were found at the secondary lumen of the sinus-ramp version at flow rates of 2, 3, and 5 LPM. Although there were no significant in R 1.00 version, the volumes were found satisfactory output.

In the following stages of this thesis, animal blood was used in a mock setup for further testing in the R 1.00 and sinus-ramp versions of the prototype. This test aim to observe the haemocompatibility including depletion of RBC, WBC, and PLT.

CHAPTER 6

HAEMATOLOGICAL RESPONSES

6.1 INTRODUCTION

Non-physiological factors in extracorporeal circulation, such as mechanical blood flow, can lead to haematological reactions such as changes in endothelial cell function and blood components. As mentioned in chapter 1, the arterial cannula flow in ECMO not only may contribute to vascular damage but potentially lead to haemolysis and can interrupt the function of white blood cells, red blood cells, and platelets (Chandler, 2021; Hellums et al., 1987; Z. M. Ruggeri et al., 2006; Yarborough et al., 1966). Therefore, the haematological response is important when evaluating the effectiveness of the cannula.

To monitor haematological parameters in clinical practice, the status of haemolysis can be measured via plasma-free haemoglobin (PFH) level. The presence of free haemoglobin in the plasma can be associated with mechanical trauma to red blood cells, and possibly related to turbulent flow and shear stress in the circuit and a substantial increase in pressure gradient across the cannula (Kameneva et al., 2004; Vercaemst, 2008). Omar HR et al. report that the severe haemolysis in ECMO which a 24-hr PFH more than 50 mg/dL potentially a predictor of mortality of ECMO (Omar et al., 2015). Physiologically, high levels of PFH indicate a depletion of red cells increases the potential for free radical generation in the bloodstream. A previous study found that the increases in PFH can impair multiple organs and can be especially damaging to the kidneys – contributory factors such as inadequate perfusion can increase incidence of acute kidney failure (Ricci, 2018).

ECMO deployment has also shown an alteration in the levels of white blood cells and platelets. Interruption to WBC could potentially be associated with the development of infection and pulmonary dysfunction during ECMO, (P. M. Siegel et al., 2022). Similarly, a decrease in PLT count can indicate haemostatic changes, which are blood clotting and bleeding in patients undergoing ECMO. Thrombotic events on ECMO may

lead to emboli and contribute to ischaemia, particularly in peripheral organs and the brain. Furthermore, clot formation may interfere with gas exchange via the membrane oxygenator (Hastings et al., 2017).

Haematological testing is typically conducted for new prototypes of extracorporeal circulation components, such as arterial cannulae for ECMO and CPB (De Wachter & Verdonck, 2002). Alongside the previous tests in this project, interaction with blood can guide effectiveness of arterial cannula performance (Gourlay et al., 1990; Paulsen et al., 2013). Following the completion of this experiment, the prototypes may proceed to the next stage, which involves testing in animal and clinical trials (beyond the remit of the current project).

Therefore, in this chapter, as outlined in phase 5 of the thesis workflow (see Chapter 2), the tests will examine haemocompatibility via depletion of red cells, white blood cells, and platelets using a close-loop mock circulation system with fresh bovine blood.

6.2 MATERIALS AND METHODS

Cannula selection and flow

Based on the results of Chapters 3 to 5, there were two selected cannula versions and the 1st iteration cannula to undergo blood experiments. These cannulae were tested along with the control which is the experimental circuit without the cannulae prototype.

Regarding the cannula selection and flow for this chapter, the decision was based on the following rationales.

- In the CFD test (Chapter 3), all versions, when compared with the 1st iteration cannula (R 1.40), showed significant improvements in flow, including flow direction to the centre line, and less impact WSS, especially for the sinus-ramp versions.

- In Chapter 4, the dye injection showed positive results in R 1.00, ramp, and sinus-ramp version, indicating a symmetrical, central flow trajectory. Furthermore, the particle tracking supported these results in the R 1.00 and the sinus-ramp version.
- In Chapter 5, the results of the pressure-flow relationship supported were configuration when the pressure gradient was less than 100 mmHg and flow rate was below 3 LPM. This finding indicated that the acceptable maximum flow was 3 LPM.
- In addition, the secondary outlet of the sinus-ramp version demonstrated greater output volumes over the 1st iteration cannula at flow rates of 2, 3, and 5 LPM, follow by the R 1.00 version (Chapter 5).

Therefore, a flow rate of 3 LPM was chosen for the haematological test which is determined by the pressure gradient with a cut-off at 100 mmHg. The R 1.00 (2nd iteration) and the sinus-ramp version (6th iteration) were selected based on outcomes from chapter 3, 4 and 5.

Circuit preparation

In figure 6.1, the circuit was set up as a closed-loop system consisting of a roller pump, soft-shell reservoir, and prototype cannula (Figure 6.2). Cannula were connected to a 7 mm PVC tube (internal diameter) to evaluate blood testing with different cannula versions (Figure 6.2A and 6.2B). Prior to testing, the roller pump was calibrated by volumetric measurement through 3/8-inch PVC tubing, as described in chapter 4. There were four experiment circuits were prepared in this study.

1. Circuit without cannula (control)
2. Circuit with R 1.40 mm cannula (1st iteration)
3. Circuit with R 1.00 mm cannula (2nd iteration)
4. Circuit with sinus-ramp cannula (6th iteration)

In these circuits, the blood flowed through a 1/4 -inch tube from the reservoir outlet to the roller pump, accommodating the 3/8 -inch tube pump loop. Beyond this, blood

passed through the inlet of the prototype cannulae and divided into the two-lumen pathways. Both outlets, separate ways, received blood into a 7.00 mm tube, and then blood was combined into a 1/4 -inch tube via a Y-connection (Figure 6.2B). Blood flowed to the 1/4 -inch tube and returned to the soft-shell reservoir. A sampling port was connected to the reservoir inlet to collect samples at the specified time (Figure 6.2C).

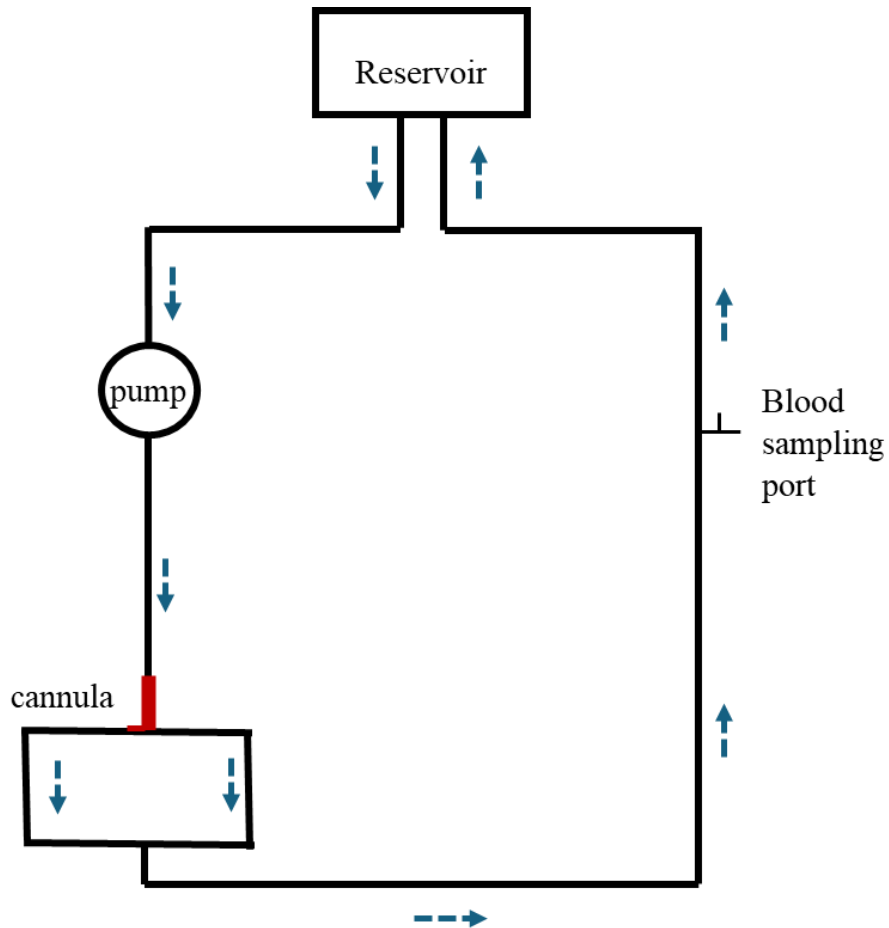


Figure 6.1 Circuit diagram for haematological test.

Dash arrow represents the flow direction, which were circulated the blood based priming solution throughout the closed loop circuit.

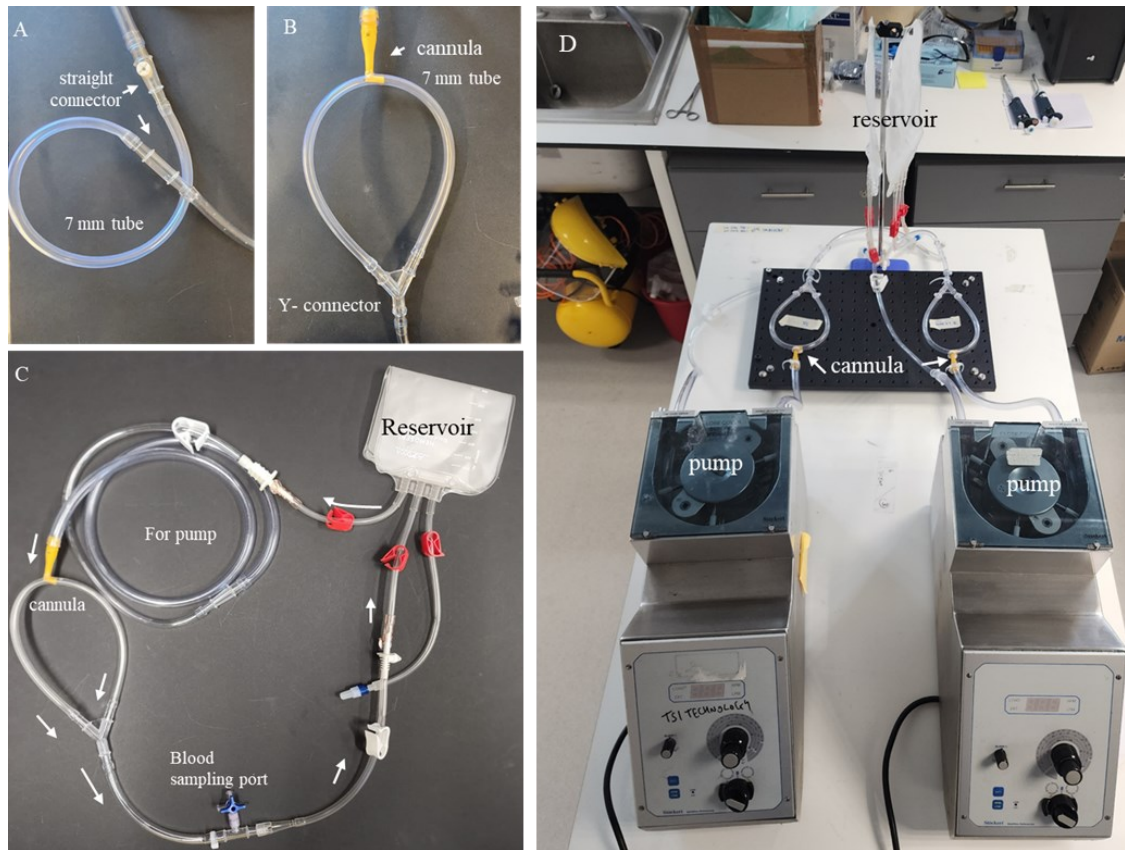


Figure 6.2 *Circuit preparation for haematological test.*

Assembled circuit for haematological test. (A: A 7.0 mm tube for control circuit; B: A 7.0 mm tube for prototype cannula; C: Circuit tubing with prototype cannula and soft-shell reservoir; D: Installed circuit system to the roller pump, arrow → blood flow direction)

Preparing of blood and priming solution

The priming solution was prepared by adding 20000 units of heparin to 4.5 litres of fresh bovine blood. Then, 400 ml of heparinized bovine blood was mixed with 300 ml of Lactated Ringer's solution (Vet Care Hartmann's Lactated Ringers, B. Braun Melsungen AG, UK). The blood-based priming solution is shown in Figure 6.3. Then, blood-based priming solution was circulated using the roller pump. The total priming volume of the circuit, including the reservoir, was approximately 300 ml.



Figure 6.3 Blood-based priming solution.

Blood sample collection

Flow was measured over 30 minutes. All selected cannula and control were tested in three cycles (n=3) and following testing, the circuit was flushed for 5 minutes using the ringier lactate solution and then replaced with the priming fluid in preparation for the repeated test.

For testing, the pump speed was slowly increased until flow reached 3 LPM and this was maintained throughout. Blood samples were collected at 0, 15, and 30 minutes. The samples were collected into 1 ml tubes for centrifugation, and 3 ml collected for the blood analysis (Ethylenediaminetetraacetic acid tubes; EDTA). Heparinized blood samples were centrifuged at 6000x RPM for 3 minutes. The plasma was then extracted with pipettes, which was prepared for a PFH assay with spectrophotometry.

The 3 ml blood in the EDTA tubes were refrigerated prior to delivery to the University of Glasgow Veterinary School, Glasgow, UK. A complete blood count was conducted to evaluate the levels of red blood cells, haemoglobin, white blood cells, and platelets. Figure 6.4 presents the overall blood collection and preparation procedure throughout this experiment.

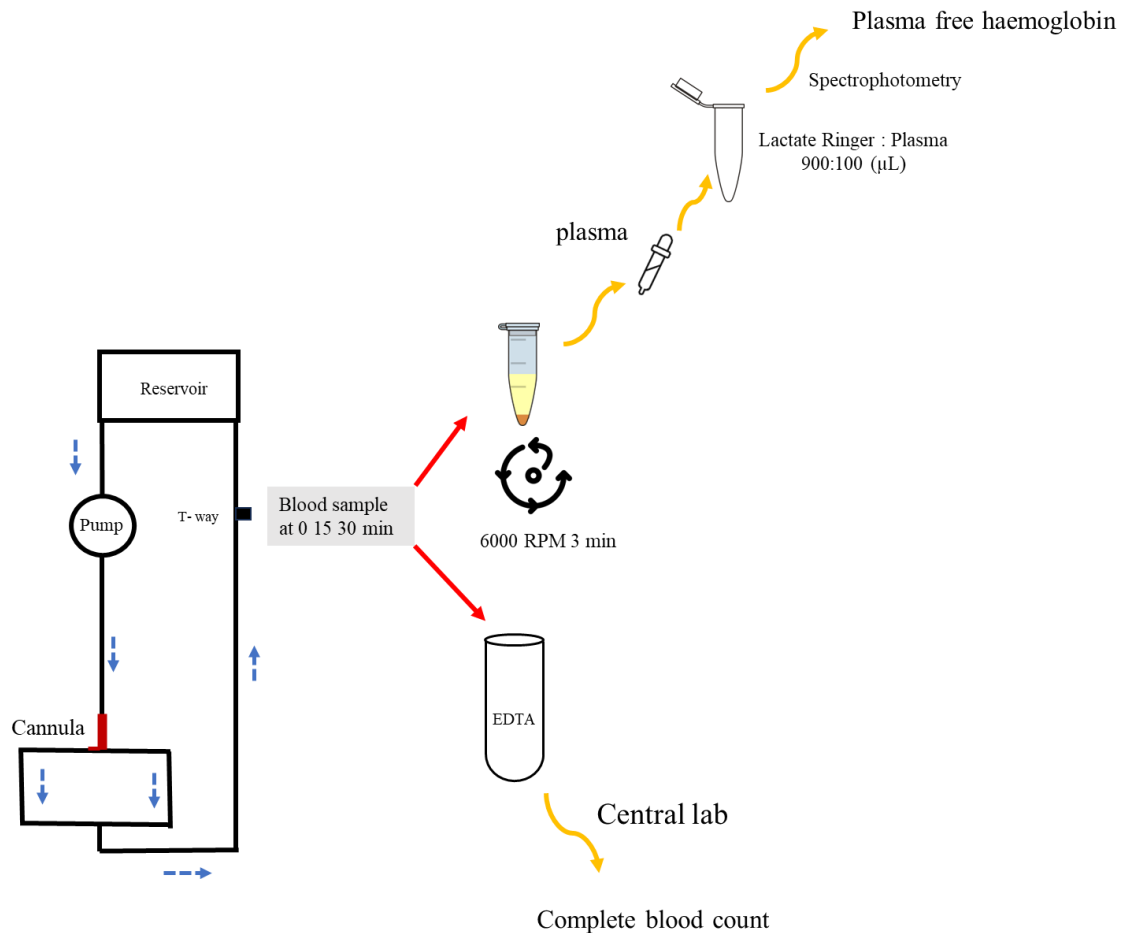


Figure 6.4 Illustrated blood sample collection and preparation process.

Blood samples were collected at 0, 15 and 30 min, then prepared to be sent to Glasgow University Veterinary School and tested with spectrophotometry. Complete blood count includes red cells, haemoglobin, white blood cells, and platelets count.

Plasma-free haemoglobin (PFH) measurement

The PFH measurement in this study was performed with spectrophotometry. The plasma was diluted with ringer lactate solution at ratio of 9:1 (Ringer solution to plasma, respectively). A 96 wells plate was prepared for plasma samples and tests were carried out in duplicate (Noe et al., 1984).

The plate was measured by spectrophotometry with the absorbance wavelengths as 380, 415 and 450 nm, as the method in previous study by Noe and colleague. The absorbance readings were collected using the Multiskan Go spectrophotometer (Thermo Scientific, Massachusetts, USA). Then, the PFH concentration was calculated based on the Allen correlation by following the equation (Harboe, 1959; Noe et al., 1984).

$$\text{Haemoglobin concentration (mg/L)} = 1.68A_{415} - 0.84A_{380} - 0.84A_{450}$$

Where: A_{415} , A_{380} and A_{450} are the absorbance value which equal to the wavelengths as 380, 415 and 450 nm, respectively.



Figure 6.5 Spectrophotometer and 96 well plate.

Spectrophotometry with the absorbance wavelengths of 380, 415, and 450 nm.

Calculation of normalised index of haemolysis (NIH)

The normalised index of haemolysis (NIH) is the reference standard for measuring haemolysis. The protocol and calculation used in this study were adapted from the American Society for Testing and Materials (ASTM), a widely accepted standard recommended for assessing haemolysis in continuous-flow blood pumps (Kameneva et al., 2006). In this protocol, the testing process includes

- Blood preparation and sample collection
- Performed with mock loop circulation
- Measuring PFH
- Calculating the normalized index of haemolysis (NIH)
- Conducting a six-hour test (Woelke et al., 2021),

However, the goal of this study was to observe the trend of haemolysis and haematological change, which has also been done in other studies using a short protocol. The trend of haematological parameters decrease from the baseline within 90 minutes as shown in previous experiments (Gourlay et al., 1990). Moreover, a recent study performed in the mocked ECMO circuit, found that PLT and WBC were decreased within the first 30 minutes, which then became a constant value, whilst RBCs showed a slight decrease until 360 minutes (Chan et al., 2021). Therefore, it is reasonable to conduct the experiment within a 30-minute timeframe.

The normalised Index of Haemolysis (NIH) was calculated based on the following formulae (Lawson et al., 2005).

$$NIH (g/100 L) = \Delta \text{ free Hb} \times V \times \frac{100-Hct}{100} \times \frac{100}{Q \times T}$$

Where: $\Delta \text{ free Hb}$ = increase of plasma free haemoglobin concentration (g/L) over the sampling time interval; V = circuit volume (L); Q = flow rate (L/min); Hct = haematocrit (%) and T = sampling time interval (min).

However, in this study the plasma free haemoglobin concentration was measured in mg/L unit. Therefore, the normalized milligram index of haemolysis (mg.N.I.H.) was used which was calculated from;

$$mg. NIH (mg/100 L) = \Delta free Hb \times V \times \frac{100-Hct}{100} \times \frac{100}{Q \times T}$$

*Where: $\Delta free Hb$ = increase of plasma free haemoglobin concentration (mg/L),
 Q = flow rate was fixed at 3 L/min, V = circuit volume was 0.3 L, T = sampling time interval was 15 and 30 minutes, respectively.*

Statistical analysis

Changes in red cell count, haemoglobin, white blood cell count, platelet count, PFH and the mg.NIH were analysed. All parameters were expressed as mean \pm standard deviation (mean \pm SD).

The comparisons of relative depletion rate of these parameters were tested using Kruskal-Wallis Test and post-test comparison. The relative depletion rate for the specific cell types, RBC, Hb, WBC, PLT and PFH were presented as a mean percentage of the initial value. The following equation was used for determining the value change throughout the test (Gourlay et al., 1990) .

$$(Measured\ value / Initial\ value) \times 100$$

Regarding the mg. NIH, the calculated value was compared by the 2-sample t-test to determine the trend at 15- and 30-minute period. Also, the one-way ANOVA were tested to compare the mg. NIH value among the group of cannulas. All results which were presented with a p-value of less than 0.05 were considered statistically significant.

6.3 RESULTS

Depletion of red blood cells

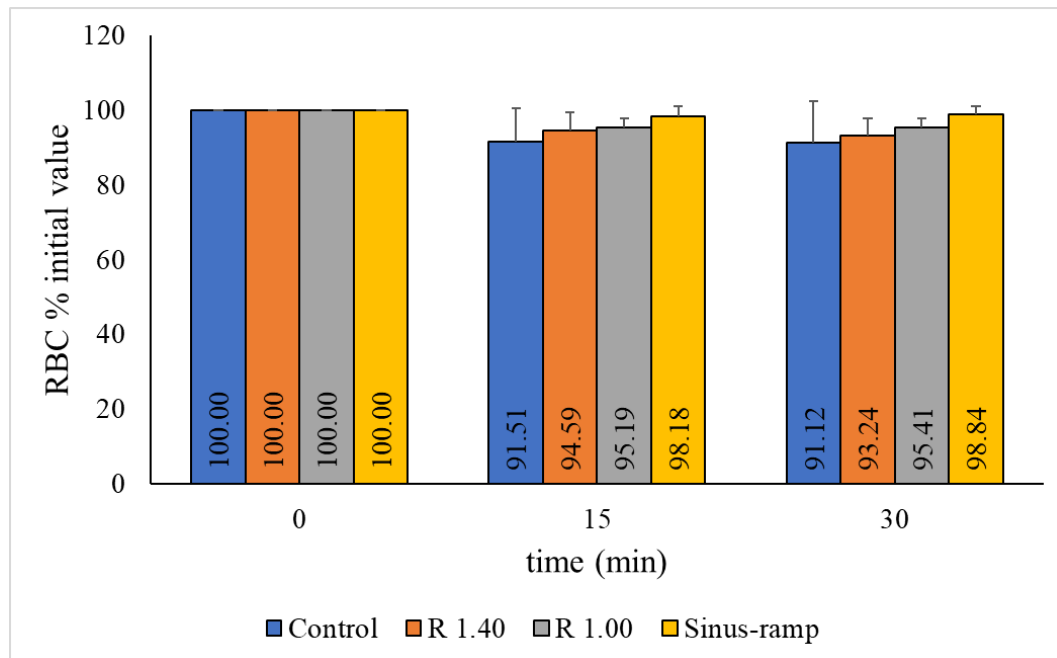


Figure 6.6 Red blood cell depletion over 30 min under four protocols.

(1st iteration: R 1.40 mm; 2nd iteration: R 1.00 mm; and: 6th iteration: Sinus-ramp; n = 3: data presents in mean ± SD)

Figure 6.6 shows the averaged percentage of the red blood cell value over 30 minutes. There was an approximate 5-10% reduction in RBC after 15 and 30 mins, with most reductions evident in the control and 1st iteration group (control: 91.51 ± 9.04 % and 91.12 ± 11.15 %; 1st iteration: 94.59 ± 4.69 % and 93.24 ± 4.56 %, respectively). However, there were no statistically significant changes found in any of the cannula prototypes. The largest alterations of RBC were found in the control circuit, which was decreased to 91.12 ± 11.15 %. The sinus ramp shows the smallest change to 98.84 ± 2.22 %.

Depletion of haemoglobin

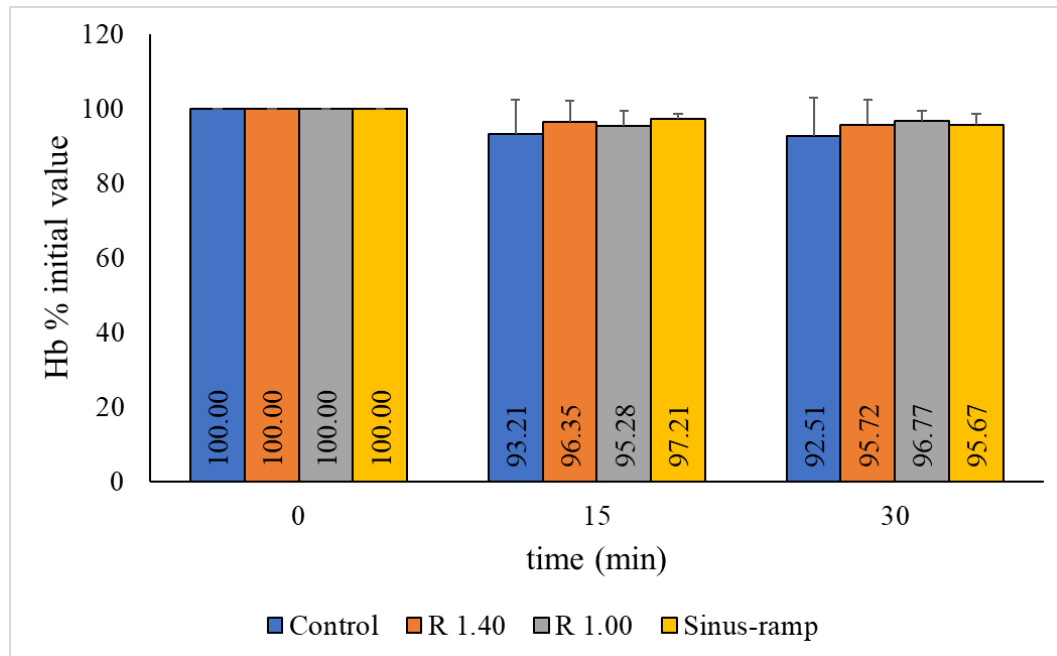


Figure 6.7 Depletion of haemoglobin over 30 min under four protocols.

(1st iteration: R 1.40 mm; 2nd iteration: R 1.00 mm; and: 6th iteration: Sinus-ramp; n = 3: data presents in mean ± SD)

The results of the Hb change are shown in Figure 6.7 and this shows a very similar profile to RBC loss. There were no statistically significant changes found in the amount of depleted Hb in each cannula group. Notably, the largest reduction in Hb was found in the control group. In this group, the value decreased to 93.21% ± 9.11 at 15 min and 92.51% ± 10.34 at 30 min, respectively). In contrast, the 1st iteration, R 1.00, and sinus-ramp versions found the percentage of Hb depletion was approximately 5% at both 15 and 30 minutes (1st iteration: 96.35 ± 5.67 % and 95.72 ± 6.68 %; R 1.00: 95.28 ± 4.10 % and 96.77 ± 2.60 %, respectively).

Depletion of white blood cells

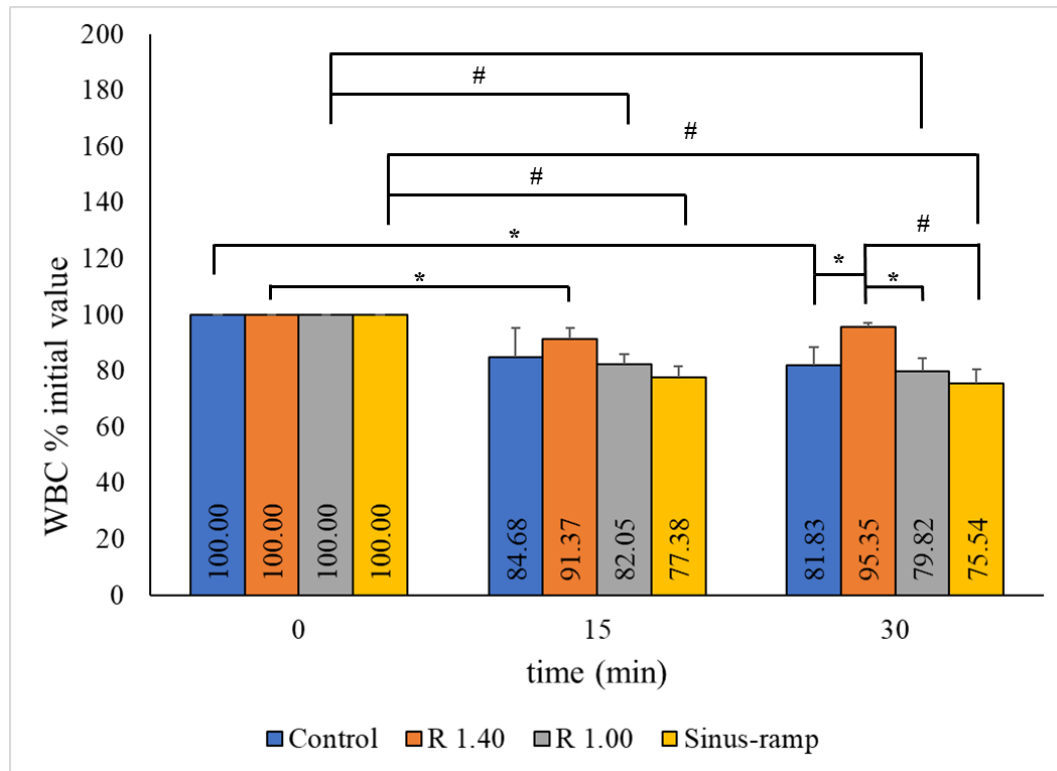


Figure 6.8 Depletion of white blood cells over 30 min under four protocols.

*(1st iteration: R 1.40 mm; 2nd iteration: R 1.00 mm; and: 6th iteration: Sinus-ramp; n = 3: data presents in mean ± SD; * significant p-value < 0.05, # significant p-value < 0.01)*

The graph in figure 6.8 illustrates the changes in WBC values. Whilst there were evident percentage change reductions in WBC among the control, R 1.00 and sinus-ramp group of approximately 15% (control: 84 ± 10.56 % and 81.83 ± 6.48 %; R 1.00: 82.05 ± 3.72 % and 79.82 ± 4.52 %; Sinus-ramp: 77.38 ± 4.28 % and 75.54 ± 4.81 %, respectively), 1st iteration group data fluctuated from approximately 10% at 15 minutes to approximately 3% at 30 minutes.

There were significant statistical differences between group found in 30 min which were control vs. 1st iteration cannula (81.83 ± 6.48 % vs. 95.35 ± 1.65 %, p-value < 0.05, respectively), 1st iteration cannula vs. R 1.00 (95.35 ± 1.65 % vs. 79.82 ± 4.52 %, p-value < 0.05, respectively), and control vs. sinus-ramp (81.83 ± 6.48 % vs. 75.54 ± 4.81 %, p-

value < 0.01, respectively). Moreover, within each group, significant statistical differences found in control at 0 vs.30 min ($100.00 \pm 0\%$ vs. $81.83 \pm 6.48\%$, p-value < 0.05, respectively), 1st iteration cannula at 0 vs. 15 min ($100.00 \pm 0\%$ vs. $91.37 \pm 3.67\%$, p-value < 0.05, respectively), R 1.00 at 0 vs. 15 min ($100.00 \pm 0\%$ vs. $79.82 \pm 4.52\%$, p-value < 0.01, respectively), sinus-ramp at 0 vs. 15 min ($100.00 \pm 0\%$ vs. $77.38 \pm 4.28\%$, p-value < 0.01, respectively), and sinus-ramp at 15 vs. 30 min ($77.38 \pm 4.28\%$ vs. $75.54 \pm 4.81\%$, p-value < 0.01, respectively).

Depletion of platelets

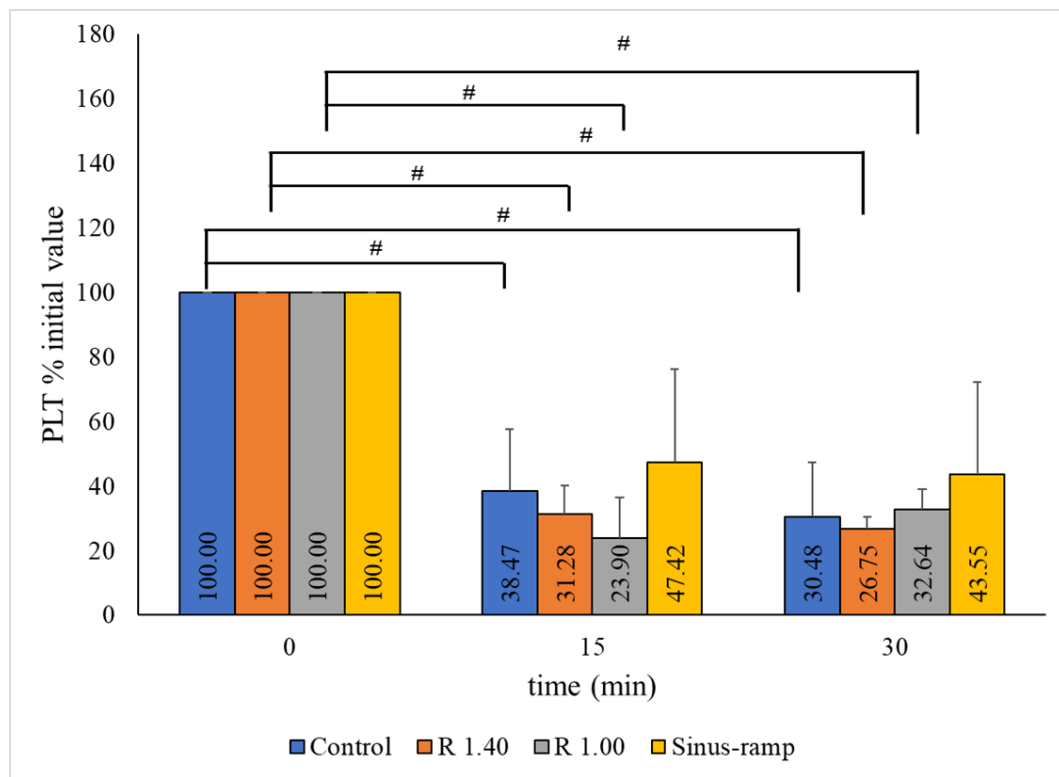


Figure 6.9 Depletion of platelets over 30 min under four protocols.

*(1st iteration: R 1.40 mm; 2nd iteration: R 1.00 mm; and: 6th iteration: Sinus-ramp; n = 3: data presents in mean ± SD; * significant p-value < 0.05, # significant p-value < 0.01)*

The rate of platelet depletion of each cannula group is shown in figure 6.9. All prototypes showed a sharp decline at 15 minutes to 30 minutes.

At the 15-minute, the percentage of platelets remaining ranged from 23.9 ± 12.40 % in the R 1.00 version to 31.28 ± 8.98 % in the 1st iteration group, 38.47 ± 19.17 % in control, and 47.42 ± 28.70 % in the sinus ramp. At the 30-minute, platelet depletion of all cannula prototypes had decreased to around 30% (control: 30.48 ± 16.83 %, 1st iteration group: 26.75 ± 3.78 %, R 1.00 32.64 ± 6.30 %, respectively), except for the Sinus-ramp version, which dropped to 43.55 ± 28.78 %.

The significant difference in PLT change found in control at 15 and 30 minutes (100 ± 0.00 % vs. 38.47 ± 19.17 % and 30.48 ± 16.83 %, respectively, p-value < 0.01), 1st iteration cannula at 15 and 30 minutes (100 ± 0.00 % vs. 31.28 ± 8.98 % and 26.75 ± 3.78 %, respectively, p-value < 0.01), and version R 1.00 at 15 and 30 minutes (100 ± 0.00 % vs. 47.47 ± 28.67 % and 43.35 ± 28.78 %, respectively, p-value < 0.01).

Haemolysed plasma

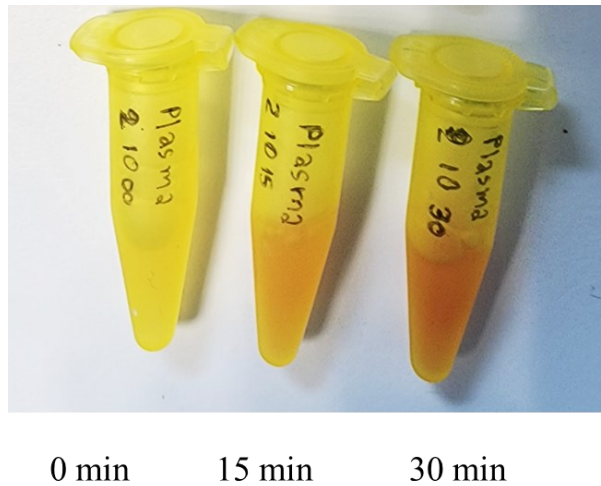


Figure 6.10 Compared the haemolysed plasma colour.

The plasma sample collected from: base line (0 min), 15 min and 30 min

The centrifuged plasma from all prototypes (shown in Figure 6.10) displays varying degrees of haemolysis. All samples show an increase in redness over time which is representative of increases in haemolysis.

Change in plasma-free haemoglobin (PFH)

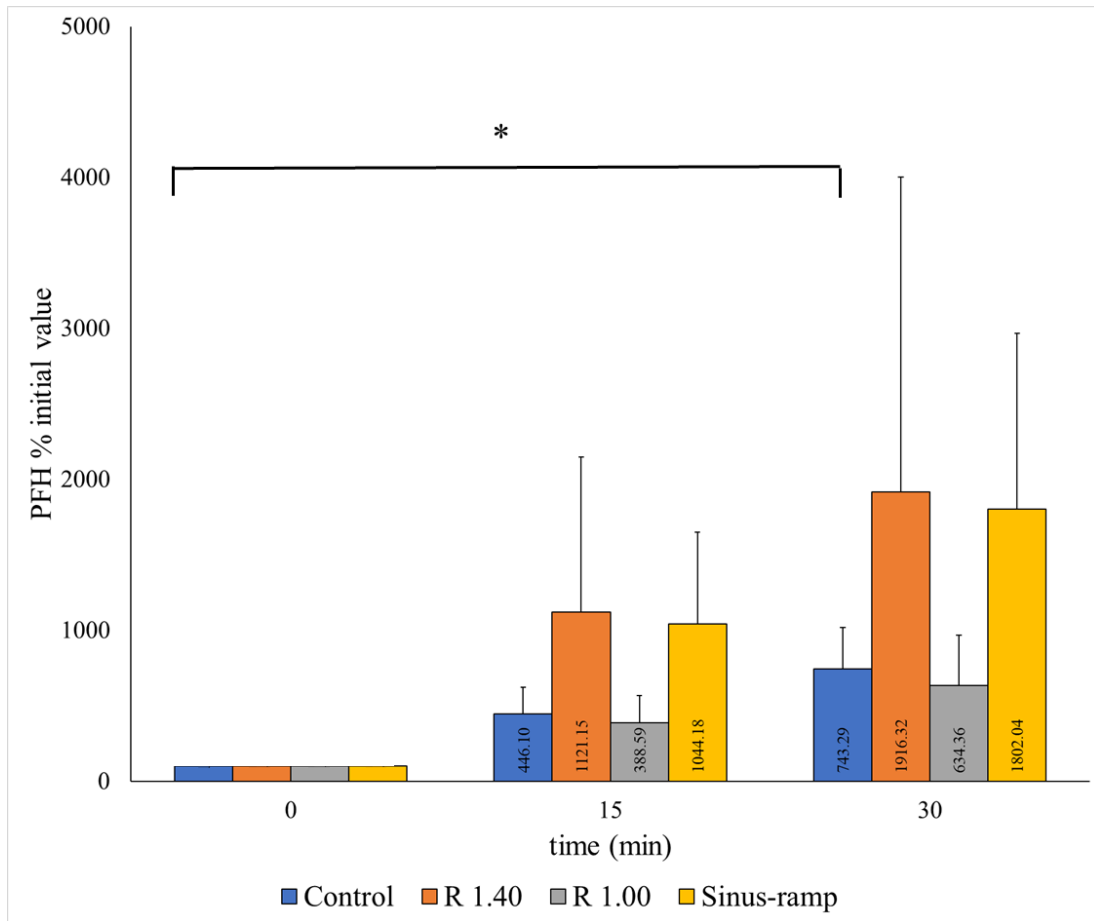


Figure 6.11 Compared the haemolysed in plasma.

(1st iteration: R 1.40 mm; 2nd iteration: R 1.00 mm; and: 6th iteration: Sinus-ramp; n = 3: data presents in mean ± SD; * significant p-value < 0.05)

The percent change in PFH is presented in Figure 6.11. PFH increased in all samples at 15 and 30 minutes. Notably, the control and version R 1.00 found in similar changes, with percentage rates ranging to nearly 500% at 15 minutes to approximately 700-800% at 30 minutes (control: 100 ± 0.00 %, 446.10 ± 176.76 % and 743.29 ± 274.57 %; R 1.00: 100 ± 0.00 , 388.59 ± 181.29 % and 634.36 ± 334.05 %, respectively). On the other hand, the Sinus-ramp version and 1st iteration cannula yielded parallel results, with the percentage rates increasing by approximately 1000% and ultimately reaching around 1800%. There was only control group had a significant difference in percent change at 0

and 30 minutes ($100 \pm 0.00 \%$, $446.10 \pm 176.76 \%$ and $743.29 \pm 274.57 \%$, p -value < 0.05 , respectively).

Normalised index of haemolysis (NIH)

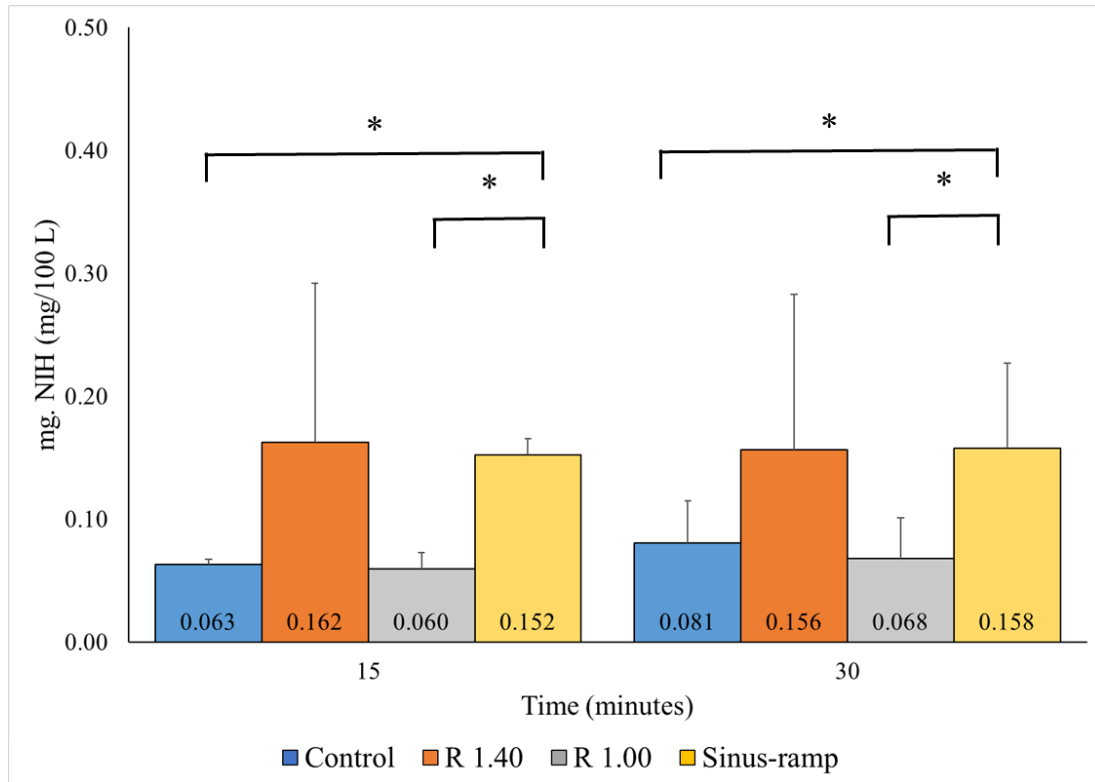


Figure 6.12 Compared the normalised index of haemolysis.

(1st iteration: R 1.40 mm; 2nd iteration: R 1.00 mm; and: 6th iteration: Sinus-ramp; n = 3; data presents in mean \pm SD; * significant p -value < 0.05)

Figure 6.12 displays the normalized index of haemolysis. On average, the value of mg.NIH increased for all cannula groups except for the 1st iteration cannula group. However, no significant difference was observed between the 15 and 30-minute intervals during the experiment. Significantly lower estimated mg.NIH values were observed in the control and R 1.00 groups compared to the control and sinus-ramp cannula groups at the 15-minute interval (p -value < 0.05), (control: 0.063 ± 0.005 , 1st iteration group: 0.162 ± 0.13 , R 1.00: 0.06 ± 0.013 , Sinus-ramp: 0.152 ± 0.013 , respectively). As well, during

the 30-minute interval, the control and R 1.00 groups showed significant lower values than 1st iteration and sinus-ramp cannula groups, control and sinus-ramp (0.081 ± 0.034 vs. 0.158 ± 0.069 , p-value < 0.05, respectively) and R 1.00 vs. sinus-ramp (0.068 ± 0.033 vs. 0.158 ± 0.069 , p-value < 0.05, respectively).

6.4 LIMITATIONS

This investigation is limited by the duration of the experiment. The following section will address the limitations that may affect the results.

- As per the ASTM recommendation, the experiment should be conducted for a duration of 6 hours. Nevertheless, in order to accommodate time constraints, this study decided on a shortened testing period of 30 minutes. This duration was considered appropriate for observing the haematological response trend. The shorter period was also used to conduct experiments in previous research (Chan et al., 2021; Gourlay et al., 1990)
- The experiment was conducted in three cycles. This issue may be related to the statistical analysis, as the presence of large error bars is evident in the majority of the results. It may be therefore warranted to increase the number of experimental cycles to ascertain more robust data.

6.5 CHAPTER SUMMARY

In this chapter, these tests attempt to examine haematological responses, particularly in relation to haemolysis, with expected improvements compared to those observed in the 1st iteration cannula (R 14.0), the result demonstrated haematological in selected cannulas as purposed in phase 5 (Chapter 2, Session 2.2).

- Regarding the outcome of chapters 4 and 5, two versions of the cannula were chosen, including version R 1.00 and sinus-ramp. Both were tested with mock circulation using bovine blood and compared with a 1st iteration cannula and a control circuit.

- The levels of RBC, Hb, WBC, and PLT counts were all reduced in all groups. However, the majority of notable distinctions were observed in WBC and PLT counts. This suggests that extracorporeal circulation can cause changes in the levels of both components.
- Levels of PFH and mg.NIH increased over a 30-minute period in all groups, with the original (R 1.40: 1st iteration) and sinus-ramp groups showing the most significant increases. This indicates a higher likelihood of impairment to the RBC compared to the R 1.00 version.

CHAPTER 7

DISCUSSION

7.1 INTRODUCTION

During peripheral VA-ECMO, arterial cannulation may limit blood flow to distal tissues, resulting in tissue ischemia and subsequent loss of function. Possible consequences may involve limb ischemia and neurological complications. As mentioned in Chapter 1, two of the most common cannulation techniques, the use of femoral artery and carotid artery access, can lead to limb ischemia and neurological complications respectively.

The current techniques for maintaining distal flow involve utilising a secondary catheter, implementing a graft, and employing a smaller cannula size. Additionally, there are commercial product offerings for bi-directional arterial cannulation for peripheral approach in cardiopulmonary bypass. However, there is still potential for complications, particularly vascular injury. This thesis presents a cannula design with a novel bi-directional flow structure that has the potential to reduce complications and offers the following device attributes.

- Single inlet bi-directional cannula.
- Single vascular access.
- Providing adequate flow in both directions.
- Outflows aligned with the central line to eliminate jetting to the vascular wall.

Following review of the current status of ECMO and in particular cannulation approaches and associated technologies, the experimental work that forms and core of the current thesis are described in chapters 3, 4, 5 and 6, all of which is focused on meeting the objectives proposed in chapter 2. The achieved objective has been met the following:

1. The CFD in Chapter 3 helped design and improve a single input bi-directional cannula with an adequate and proportional flow distribution profile, as described in Chapter 5.
2. The CFD analysis in Chapter 3, the flow visualisation in Chapter 4, and the haemodynamic test in Chapter 5 provide evidence that the cannulation approach exhibits favourable fluid dynamic properties that enable observed jetting towards the vascular wall in either output aspect.
3. The findings from chapters 5 on pressure-flow properties and chapter 6 on haematological measurement indicate that the cannula design exhibits satisfactory haemodynamic properties.

In the current chapter, the methodology and results used in this work will be discussed in four sections, with reference to the appropriate literature. The focus for discussion is as follows:

- CFD serves as a tool in the design process.
- Validation of design with flow visualisation.
- Haemodynamic measurement to assess the performance of the cannula.
- Haematological response to blood handling test.

7.2 CFD SERVES AS A TOOL IN THE DESIGN PROCESS

The concept of a single input bi-directional cannula, originally designed by T. Gourlay et al., as mentioned in Chapter 3, is of potential clinical significance. This study has re-investigated a series of prototype cannula designs using CFD in an iterative manner to enhance their configuration and design. The CFD initially analysed the flow paths of a single input bi-directional cannula with a 1.4 mm curved secondary lumen, showing an increase in flow velocity, sandblasting against the vessel wall, and elevated shear stress. Then the second lumen was subsequently optimised for flow direction by adjusting the radian curve to 1.00 mm and 0.85 mm and adding ramp, sinus, and sinus-ramp.

In this study, size of cannula was increased from 14 to 16 Fr (5.33 mm), a size more reflective of clinical setting and thought suitable for blood flows of up to 4 LPM. As well as study by Kim J et al. (2019) examined CPB outcomes with varying cannula sizes. The 16 Fr was suited for patients with a body surface area (BSA) of 1.6 - 1.7 m², which required ECMO flow of about 3.84 - 4.08 LPM (Blood flow = BSA x 2.4). Moreover, the authors found that the incidence of limb ischemia was associated with the ratio of cannula size to BSA of more than 11. This current study's calculated ratio would be 9.4 - 10, lower than the cut-off value (Kim et al., 2019).

Paulsen et al. (2013), found that 16 Fr Sarns cannula (Model No. 813578, Terumo, Japan) can provide flow of up to 4 LPM with a pressure gradient at up to 100 mmHg. Other cannula types of similar size, in common use in ECMO, have similar pressure/flow relationships, for example the 15-17 Fr Maquet arterial HLS cannulae (Arterial HLS cannulae model PAS 1715 and PAS 1515, Getinge, Rastatt, Germany) can carry a flow at 3.5 - 4.0 LPM with a pressure gradient of less than 100 mmHg. (Paulsen et al., 2013). Broman et al. (2019) found that the 15-17 Fr. arterial cannulae are typically associated with a pressure gradient of around 100 mmHg at 4 LPM and that pressure gradients varied depending on cannula model, size and length (Broman et al., 2019).

In this present work, physiological CFD conditions were used to simulate the flow from the arterial cannula to the blood vessel. The fluid conditions in this study follow the previous report by Nezami et al. (2021) and Gramigna et al. (2023), which uses Newtonian and incompressible fluid and the shear stress transport turbulent model (transition-SST). These researchers suggest that expressing blood as a Newtonian fluid is a valid approximation which offers accuracy and computational efficiency. Also, a transition-SST model was utilised to capture the turbulent flow patterns resulting from the ECMO cannula to the blood vessel precisely (Gramigna et al., 2023; Nezami et al., 2021).

The residual value is a measurement used to assess the convergence of an iterative solution in the CFD. Following the Ansys Fluent manual, the calculations in this study

reached a criterion below $10E-4$. A default criterion for the residuals is considered acceptable below $10E-3$. Furthermore, Kaufmann et al. (2014) conducted CFD in arterial blood flow via cardiopulmonary bypass to assess cerebral blood flow. Their study showed that the convergence criterion for the residuals can be addressed at time step less than $10E-4$ (Kaufmann et al., 2014).

The finest meshing at the near-vascular wall region was recommended to be prepared for the WSS prediction to investigate the impact of jet flow. This mesh resolution is associated with improving the accuracy and efficiency of the CFD solutions (Keshmiri & Andrews, 2015). The inflation layer mesh of the vascular wall needs to be created with consideration for the balance between convergence rate, solution accuracy, and computation time (Gramigna et al., 2023). This study adapted the protocol from Wickramarachchi et al. (2024), which calculated the layer of the finest mesh at vascular wall. Based on a y^+ value of approximately 1, the first layer's thickness was set at 0.077 mm. with inflation growth factor rate of 1.2 and five layer.

There are five versions of the new cannula design that were investigated in this thesis, and the results of primary lumen flow investigation indicated that there was no difference in this aspect of performance across the range of prototypes. Therefore, the study of flow was largely focused on the secondary lumen. The results of the CFD study demonstrated that flow direction is critically influenced by the configuration of the lumen. When compared to the 1st iteration cannula, which has no flow directing architecture, the R 1.00 mm, Sinus, Ramp, and Sinus-Ramp configurations were associated with improved blood flow direction and wall shear.

The high-velocity jet from the 1st iteration cannula is directed towards the inferior wall of the vessel, leading to high shear stress values at the point of impact. The increased arterial WSS caused by the arterial cannula flow can induce endothelial damage, as described in a previous report by Schnürer, C. et al (2011). This is a significant concern, as the study found that there was an endothelium lesion caused by the jet flow in a porcine model with cardiopulmonary bypass (Schnürer et al., 2011b). These results are

similar to the study by Assmann A. et al. (2014), which used the CFD to investigate the flow and WSS from the four aortic cannulas; the report found that the cannula tip design and flow were related to the values of aortic WSS (Assmann et al., 2015). Moreover, this study was supported by clinical evidence which indicated that increasing the WSS value could cause plaques to rupture and lead to embolism issues (Groen et al., 2007; Tang et al., 2009).

In the present study, we found high pressures, exceeding 100 Pa, in the secondary lumen of the 1st iteration cannula (see Figure 3.8). This finding suggests the potential for vascular damage. Sameshima et al. (2014) studied the flow using CFD and an animal model, and discovered a correlation between high WSS (as high as 100 Pa) and the likelihood of endothelium layer injury and plaque erosion (Sameshima et al., 2014). The control of flow direction and associated wall shear was a key element of the present study in an effort to produce a bi-directional cannula design that was a safe and effective solution to the challenges of providing tissue supportive bi-directional flow in ECMO.

7.3 VALIDATION DESIGN WITH FLOW VISUALISATION

Flow visualization is a useful tool in understanding the flow characteristics of a novel blood flow device. Through this technique it is possible to visualise the complex nature of fluid flow in the device environment and any structural interactions. In the present study two distinct techniques were employed: dye injection and particle tracking. The use of both techniques was crucial for validating CFD, as it allowed a comprehensive comparison of the flow distribution pattern and velocity contours resulting from both techniques.

The dye injection technique has been used to observe the distribution of stain and angle measurement, which produced precise results and provided a simple approach. Also, in this study, the recording process, using a high-speed camera, improved the measurement of dye distribution in each captured and analysed frame. The finding of dye distribution permits the comparison of flow behaviour associated with each version of the cannula. In version R 1.00, the ramp and sinus-ramp provided superior outcomes over all versions

(see Figure 4.9, 4.11 and 4.13), in which the distribution pattern was found to be narrow with a symmetrical angle.

A prior *in-vitro* study focusing on two different arterial cannulas analysed the ink-stained outflow jet (Hugenorth et al, 2021). The angle of the outflow jet was found to be different compared with the reference cannula (Hugenroth et al., 2021). In this work the ink-stained outflow jet can be observed by measuring the angle. However, there was no measurement of symmetrical angle of the dye stain as proposed in the present work. In the current work we found that measuring the symmetrical angle can differentiate the flow characteristic of each cannula configuration. The jet dispersion of arterial cannula was also tested in a study by White et al. (2009). The experiment performed dye injection and MRI to measure the velocity of five cannulas. The cannulae were inserted into a tube for dye dispersion testing. The results suggested that the cannula, which provided flow distribution into the middle lumen of the tube, was associated with a lower sand-blasting effect on the tube wall. In the MRI, the high-velocity jet to the tube wall was found in only the cannula that gave flow direction to the vessel (White et al., 2009). In the present study, a key objective was to attain a central flow distribution to prevent vascular wall interactions, in line with the critical findings of other investigators.

Ura et al. (2000) examined the vascular complications associated with arterial cannulation in ten cardiac surgery patients. The aortic wall lesion was measured using ultrasonography before and after the operation. Interestingly, the study revealed that 3 out of 10 patients exhibited a new lesion at the posterior wall of the aorta on the opposite side of the cannulation wall. The author proposed that the likely cause resulted from the cannula jet (Ura et al., 2000).

The particle distribution techniques, PIV and particle tracking velocimetry (PTV) have been used in several studies. For example, McDonald et al. (2016) used PIV to test commercial arterial cannula and to compare their flow characteristics. The study showed that different cannula configurations were associated with different flow patterns and velocities (McDonald et al., 2016). Minakawa et al. (2007) also suggested that where

possible, high velocity flow from the cannula tip should be avoided due to possible effects of the vessel wall and turbulence flow (Minakawa et al., 2007). In VA-ECMO, Haymet et al. (2020) used PIV to evaluate the potential for aortoiliac vascular injury associated with cannula outflow (Haymet et al., 2021).

Particle tracking is a complex process and has a number of limitations. In this study, the limitation of the lighting system affected the processing and result of flow tracking and velocity measurement. The particle tracking focused largely on defining the flow characteristics via investigations of flow distribution rather than velocity measurement. The results were presented by vector and magnitude of velocity. The limitations of the lighting system affected the ability to capture subtle particle movement. Fast particles produced a long streak and disappeared from the region of interest (Nobach & Bodenschatz, 2009). Therefore, in this study, the flow was set at 0.5 LPM instead of 4 LPM, as in the CFD and dye injection test. Normalisation of velocity and flow vectors was applied to this study, and they were utilised to validate the CFD and particle tracking for arterial cannula elsewhere (Lemétayer et al., 2021; Rasooli & Pekkan, 2019).

The PIV and PTV were utilised to validate the CFD test. The centreline velocity of the arterial cannula was applied to compare the different techniques to validate the flow observed in the CFD modelling as reported by Rasooli & Pekkan (2019). They measured the centreline velocity decay, which can describe how distance from the outflow relates to the velocity decrease. This parameter was utilised to validate the flow patterns associated with CFD and PIV in the newly designed arterial cannula (Rasooli & Pekkan, 2019). In this current study, we adapted and applied the result from two planes' velocities to compare particle tracking and CFD. The results found that there was a high correlation between the two techniques. Moreover, when flow visualisation and CFD findings have been compared (see Figure 4.27), the flow patterns were similar. These techniques were central to the development of the arterial cannula that was the focus of the present work and produced highly valuable data that influenced the design process.

7.4 HAEMODYNAMIC MEASUREMENT TO ASSESS THE PERFORMANCE OF THE CANNULA

Awareness and monitoring of the haemodynamic environment in extracorporeal perfusion circuits is of importance if safe and effective clinical delivery is to be achieved. Pressure gradient across the arterial cannula is an extremely important parameter in CPB and ECMO. In designing arterial canulae, it is critical to determine the pressure drop associated with the device and how this varies over a range of flow rates. In this way, it is possible to ascertain the optimal cannulae dimensions and understanding of its safe flow range (Broman et al., 2019; Kohler et al., 2012). This study illustrates experiments aimed at achieving adequate systemic and distal perfusion, characterised by predictability and balance that allow bi-directional organ perfusion. It also determines the estimated maximum flow of a cannula, which correlates with decreased blood and vessel trauma.

In a study conducted by Wang S et al. (2018), an in vitro investigation was carried out to assess arterial cannula for ECMO by measuring aspects of haemodynamic. The test system consisted of a pump, cannula, reservoir, and oxygenator, which is primed with human blood at room temperature. The pressure drop and haemodynamic energy were measured and compared to the published manufacturer's data. The manufacturer's data was obtained using a water prime. The authors suggest that there may be variations in the outcomes between the two priming solutions (Wang et al., 2018).

Montoya and colleagues (1991) proposed a standard circuit and measurement technique to determine the pressure/flow relationship in cannula. The system consisted of a cannula, water reservoir, and pump. In this system, the pressure difference between the cannula and the water reservoir was compared at different flow rates within the clinical range (Montoya et al., 1991). Similarly, Gerdes A et al. (2002) conducted an experiment in which they used room temperature water (20°C) to test the arterial cannula. The experiment was performed with the mock circuit and identified the pressure gradient of the arterial cannula (Gerdes et al., 2002).

It is clear that clinically appropriate data can be achieved through the use of water based perfusates in studying the fluid dynamics of cannula design, and in the present study we chosen to use a water prime to measure the pressure gradient across the cannula. The flow was conducted at a range of 0.5 to 5 LPM, and it was observed that the pressure gradient was around 80-100 mmHg at a flow rate of approximately 3-4 LPM. According to recommendation, the safety envelope for pressure gradient in the cannula is below 100 mmHg. (Gajkowski et al., 2022; Hessel & Hill, 1993).

From the haemodynamic perspective previous work by Menon P.G. et al. (2013) demonstrated the importance of the arterial cannula pressure gradient in terms of velocity jet and turbulence flow (Menon et al., 2013). As previously reported, the destruction of red blood cells and platelets was found in conditions of high turbulence in animal models (Tangelder et al., 1986). Vascular injury has also been reported in association with jetting and turbulence (Grooters et al., 2003; Schnürer et al., 2011a; Swaminathan et al., 2007).

In this study, all of the cannula configurations were associated with pressure gradients of less than 100 mmHg at flows of 3 LPM or less (see Figure 5.5). This finding indicated that the maximum blood flow for this cannulae is in the region of 3 LPM, which is in line with the original objective of developing a cannula for patients weighing about 40-50 kg (Brown et al., 2021; Gajkowski et al., 2022). For this reason, the testing of the haematological response associated with the cannulae in Chapter 6 was maintained at 3 LPM, the upper limit of the cannula flow range. The findings from bench experiments showed that the upper limit of flow, associated with a sub-100 mmHg pressure gradient flow in hydrodynamic experiment were not correlated to the flow that set in the CFD (4 LPM).

Pressure-flow relationship is also related to the calculated M-number, which is an important parameter for the arterial cannula. Fluid viscosity, diameter of cannula, length of cannula are the influences to calculate the M-number. Ganushchak, Y. M, et. al (2020) tested arterial cannula of different length and diameter for ECMO applications. They also performed experiments with different fluid viscosity, using water and water-glycerol

solutions. The M-number in the cannula with diameter size 15 - 17 Fr was around 3.03 to 3.3 and were similar in both perfusate solutions (Ganushchak et al., 2020). In the present study, the calculated M-number with water as a fluid at a room temperature of 22°C was found to be in the region of about 3.01 - 3.06 (see Figure 5.7), which was closely similar to the previous published study (Ganushchak et al., 2020).

This study found that the fluid dynamic response of the R 1.00 and sinus-ramp cannulae were superior to another cannula configurations tested. The maximum flow of both, as assessed by a sub-100 mmHg pressure gradient was 3 LPM, while the distal flow requirement was met.

Clearly the distal flow is a critical aspect of the engaging in bi-directional cannula design and the investigation of this aspect of the device configuration was a strong focus of the work. Studies of the blood flow to the resting leg underpin this aspect of the work Holland C.K. et al. (1998) used doppler ultrasonography to determine the normal values for volumetric blood flow in the leg at rest. According to the authors' findings, the blood flow in the superficial femoral artery of a leg at rest is estimated to be around 150 mL/min (Christy K. Holland et al., 1998).

The previous study by Foltan M et al (2019) measured the distal perfusion cannula blood flow in 18 ECMO cases using 15 and 17 Fr cannula with adding distal catheter. ECMO flow of 3 to 4 LPM can provide the distal flow at 200 to 400 ml/min, depending on the cannula size. The finding indicated that the blood flow via the distal perfusion cannula corresponds to about 10% of the blood flow within the ECMO system (Foltan et al., 2019). The measured volumetric blood flow in the lower extremities of healthy subjects was demonstrated by CK Holland and colleagues. The flow values of the popliteal, common femoral (CFA), superficial femoral (SFA), and dorsalis pedis were 284 ± 21 mL/min, 152 ± 10 mL/min, and 72 ± 5 mL/min, respectively (C. K. Holland et al., 1998). Furthermore, Chen et al. (2017) conducted blood flow measurements in 7 patients by utilising the distal superficial femoral artery to measure the current bi-directional cannula in CPB, LIVA

NOVA Bi-flow. The study revealed that the blood flow to distal perfusion was measured at 100-150 ml/min, whereas the ECMO flow ranged from 1-4 LPM (Chen et al., 2017).

In the present work, measurement on secondary lumen volume were represented by distal blood flow. The secondary lumen's volume production ranged from 231 to 314 ml/min at 3 LPM to 277 to 427 ml/min at 4 LPM, which distal flow was approximately 10% of the primary flow and in range of previous studies. Thus, this study demonstrates that there was potential of effective flow proportion to preserve the distal tissues.

7.5 HAEMATOLOGICAL RESPONSE TO BLOOD HANDLING TEST

As cannulae versions R 1.00 and sinus-ramp were associated with the best fluid dynamic characteristics (Chapters 4 and 5), and they were chosen for further study of the haematological response. Both cannulas were compared with the 1st iteration cannula and control. The haematological response to extracorporeal circulation with the cannulae in this study was performed in a close loop mock circulation. The circuit was primed with bovine blood-based priming solution. RBC, Hb, WBC, PLT and haemolysis were measured in this study.

The findings demonstrated a decrease in RBC, Hb, WBC, and PLT levels across all groups. The sinus-ramp and 1st iteration cannula markedly enhance PFH and NIH across all groups after a duration of 30 minutes. The R 1.00 cannula and control circuit exhibited similar values of PFH and NIH, which were less than those observed in the sinus-ramp and 1st iteration. This result indicates a reduced impairment of RBC, consistent with the aimed design.

The *in-vitro* mock circulation technique is utilised in several studies to evaluate the blood handling of the extracorporeal components. For example, Gourlay, et al. (1990) measured the haematological response of new ECMO components. The experiment utilised a priming solution derived from bovine blood and was carried out over a 90-minute recirculation period. The study collected samples at the beginning, middle, and end of the test to evaluate the levels of plasma-free haemoglobin, red blood cells, white blood cells,

and platelets (Gourlay et al., 1990). Chan CHH, et al. (2021), performed similar the *in-vitro* haemolysis testing of ECMO. Their experiments considering various additional factors such as the gender of human blood used, and the heparinization methods. Haematological parameters, such as the RBC count, haematocrit levels, and WBC count, were observed within a 360-minute timeframe, along with the assessment of haemolysis status (Chan et al., 2021).

In some studies, RBC destruction associated with a decrease of RBC and Hb in ECMO and CPB was possibly found to be related to mechanical trauma by several circuit components, for example, the pump and oxygenator (Appelt et al., 2020; Chan et al., 2021). Regarding the cannula, Appelt H et al. (2020) found that the small arterial cannula size in ECMO showed slightly higher RBC destruction and haemolysis (Appelt et al., 2020). Also, Vercaemst L. (2008) suggested that the haemolysis may not directly relate to the arterial cannula in CPB. However, shear force augmented by cannula flow possibly results in RBC damage (Vercaemst, 2008).

ECMO cases also report an alteration in the levels of white blood cells (Ki et al., 2020; Millar et al., 2016). These factors could be linked to the circuit material, blood flow rate, and non-physiological shear stress, and possible complications include thrombolysis, infection, and organ impairment. In addition, platelet aggregation is commonly observed in ECMO. Platelet and coagulation parameters are possibly activated in the early period of ECMO, as found by Wurzinger LJ et al. (1985) (Wurzinger et al., 1985). This shear stress may be induced by the ECMO flow (Zaverio M. Ruggeri et al., 2006). Siegel PM et al. (2022) report that patients who underwent ECMO with associated platelet dysfunction has the potential for bleeding and poor outcomes (Patrick Malcolm Siegel et al., 2022).

In the present study, all haematological parameters tended to decrease from baseline. This finding is similar to that of several *in-vitro* studies. In the previous study by Gourlay et al. (1990), the trend of haematological parameters decreased from the baseline within a time frame of 90 minutes (Gourlay et al., 1990). Also, a report by Chan CHH et al. (2021)

experimented for 360 minutes. However, within 30 minutes, the results showed a slight change in RBC and Hb, while a more remarkable decrease was found in PLT and WBC (Chan et al., 2021).

The haemolysis status is one parameter utilized for monitoring the extracorporeal circuit function. High haemolysis is considered a mechanical effect on RBC. The plasma-free haemoglobin (PFH) has become a fairly standard method for detection of haemolysis. The cut point of PFH in normal human is 50 mg/dl (Omar et al., 2015), while in some study in ECMO this remains controversial, with some investigators suggesting that a level of less than 100 mg/dl is acceptable (Kim-Campbell & Bayir, 2018).

In current experiment, blood from different animals were used which results in different initial Hb. This factor may affect the haemolysis measurement in the procedure. Jenks CL, et al (2019) compared the different degree of Hb during ECMO, and found that higher Hb was associated with an increased risk of haemolysis. These findings indicate the possibility of inconsistent results, highlighting the need for further investigation to ensure the reliability of haemolysis measurements. However, the normalised value compared with the initial percent change to eliminate the confounding factor (Jenks et al., 2019).

The 30 min test was used to observe trend of haemolysis and PFH in this current report. This procedure contrasts with Chan CHH et al. (2021) that performed experiment in ECMO to test haemolysis for 6 hr. (Chan et al., 2021). However, there was a similar trend of the values for the first 30 minutes. In this study we used the short test period to observe trends in haemolytic processes in a similar manner to that employed by Gourlay et al. in previous experiment in ECMO circuits. In his study, focused on the testing of blood handling effect in close loop circuits, and suggested that it is adequate to observe the trend of haematological response over a short time period (Gourlay et al., 1990). In addition, the degree of PFH can be seen in change in the colour of centrifuged plasma (see Figure 6.9). However, the calculated NIH in this study found at 0.063 to 0.162 mg/100L, which is within the recommend value of less than 0.1 g/100L (Fu et al., 2021).

CHAPTER 8

CONCLUSION AND FUTURE WORK

8.1 CONCLUSION

Peripheral VA-ECMO arterial cannulation has the risk of limiting blood supply to distal organs, which might result in organ ischemia and consequent loss of function. Possible outcomes may include limb ischemia and neurological problems. This study set out to develop an arterial cannula design featuring a particular bi-directional flow structure that potentially reduces or prevents these detrimental clinical issues. The objectives of this thesis were achieved through the use of CFD analysis, which enabled the design and creation of a single input bi-directional cannulae with a suitable and proportionate flow distribution profile. Furthermore, the performance difference among the various cannula versions were determined by examining pressure-flow properties and haematological measurements.

Compared with the 1st iteration cannula, the *in-silico* and *in-vitro* experiment results show that the sinus-ramp and version R 1.00 cannula effectively demonstrated favourable fluid dynamic characteristics without the potential issues of blood flow jets projecting to the vascular wall. Additionally, in version R 1.00, the haematological measurements indicate a satisfactory outcome, suggesting the potential to improve arterial cannulation in the peripheral VA-ECMO.

8.2 LIMITATIONS

There are the limitations that may influence the results of this research:

1. Patient-specific vascular geometries for CFD:
 - The accuracy of the CFD could be affected by using straight cylindrical tubes rather than patient-specific vascular geometry. This condition could result in a lack of flow characteristics in the complex vascular system.

2. Light sources in particle tracking:
 - In this study, the particle tracking experiment used LED light instead of a synchronised laser sheet system (the synchronised Nd:YAG lasers). Therefore, the unspecific visualisation plane and high flow rate made particles non-circular shape and invisible from the camera. This abnormal particle structure observed affected velocity processing. A synchronised laser sheet system can enhance particle imaging when analysing high flow through pumps in PIV or PTV analysis (Nobach & Bodenschatz, 2009; Shuib et al., 2011).
3. Velocity measurement in the particle tracking experiment:
 - The particle tracking experiment was performed at a flow rate of 0.5 LPM, and this flow was not used in the CFD (Chapter 3). Therefore, to validate flow analysis among the CFD and particle tracking in this study, the direction of flow, vector, and flow paths were assessed instead of the velocity profile.
4. Using square tube as the vasculature for particle tracking:
 - To eliminate the effect of distortion of the circular tube, in this study using the square tube as the vasculature. Therefore, the flow characteristics could be different depending on the shape.
5. The haematological experiment was conducted in three cycles.
 - Large statistical error found in the experiment, this may be because small number of experimental cycles, and this was as a result of time constraints. Further study requires repeating the cycle of experiments to generate more robust data.

8.3 FUTURE WORK

The research project has successfully developed an arterial cannula with a bi-directional flow structure, which aligns with the aim of this study. This work has been carried out *in-silico* and under benchtop conditions. Efforts have been made to ensure that the investigations informing the design and development process have been carried out under

conditions that, as far as possible, reflect the clinical setting. However, future work will need to progress these studies through the utilization of appropriate animals and ultimately, clinical models to ensure that the results gained from the present work are reflected under truly clinical conditions.

- In the animal model, it is possible to rescale the cannula to a suitable animal size and test it under clinical conditions whilst integrated into a representative ECMO circuit. This will enable the comparison of performance, critically the degree of preservation it offers to distal tissues, with other conventional cannulae types and configurations and techniques for minimising peripheral ischemia.
- Furthermore, additional experiments are necessary to explore a wider range of cannula sizes that can be used for patients across different age groups, including neonates, paediatric patients, and both small and large adults. Exploring the potential for expanding the application of these novel cannulas.

REFERENCES

- Abdel-Sayed, S., Ferrari, E., Abdel-Sayed, P., Wilhelm, M., Halbe, M., von Segesser, L. K., Maisano, F., & Berdajs, D. (2020). New bidirectional arterial perfusion device. *Int J Artif Organs*, *43*(7), 433-436. <https://doi.org/10.1177/0391398820901842>
- Abdel-Sayed, S., Ferrari, E., Abdel-Sayed, P., Wilhelm, M., von Segesser, L. K., & Berdajs, D. (2021). Design optimization of bidirectional arterial perfusion cannula. *J Cardiothorac Surg*, *16*(1), 114. <https://doi.org/10.1186/s13019-021-01500-3>
- Ahmed, T., Safdar, A., & Chahal, D. (2020). Axillary Approach for Venoarterial Extracorporeal Membrane Oxygenation Cannulation. *Cureus*, *12*(4), e7788. <https://doi.org/10.7759/cureus.7788>
- Ailawadi, G., & Zacour, R. K. (2009). Cardiopulmonary Bypass/Extracorporeal Membrane Oxygenation/Left Heart Bypass: Indications, Techniques, and Complications. *Surgical Clinics of North America*, *89*(4), 781-796. <https://doi.org/https://doi.org/10.1016/j.suc.2009.05.006>
- Allou, N., Lo Pinto, H., Persichini, R., Bouchet, B., Braunberger, E., Lugagne, N., Belmonte, O., Martinet, O., Delmas, B., Dangers, L., & Allyn, J. (2019). Cannula-Related Infection in Patients Supported by Peripheral ECMO: Clinical and Microbiological Characteristics. *ASAIO J*, *65*(2), 180-186. <https://doi.org/10.1097/mat.0000000000000771>
- ANZECMO. (2009). Extracorporeal Membrane Oxygenation for 2009 Influenza A(H1N1) Acute Respiratory Distress Syndrome. *JAMA*, *302*(17), 1888-1895. <https://doi.org/10.1001/jama.2009.1535>
- Appelt, H., Philipp, A., Mueller, T., Foltan, M., Lubnow, M., Lunz, D., Zeman, F., & Lehle, K. (2020). Factors associated with hemolysis during extracorporeal membrane oxygenation (ECMO)—Comparison of VA- versus VV ECMO. *PLoS One*, *15*(1), e0227793. <https://doi.org/10.1371/journal.pone.0227793>

- Assmann, A., Gül, F., Benim, A. C., Joos, F., Akhyari, P., & Lichtenberg, A. (2015). Dispersive Aortic Cannulas Reduce Aortic Wall Shear Stress Affecting Atherosclerotic Plaque Embolization. *Artificial Organs*, 39(3), 203-211. <https://doi.org/https://doi.org/10.1111/aor.12359>
- Au, S. Y., Chan, K. S., Fong, K. M., & Ng, G. W. Y. (2019). Clot formation between the ECMO catheter and the reperfusion catheter in a patient supported by peripheral VA-ECMO. *Intensive Care Med*, 45(11), 1657. <https://doi.org/10.1007/s00134-019-05659-1>
- Banfi, C., Pozzi, M., Brunner, M.-E., Rigamonti, F., Murith, N., Mugnai, D., Obadia, J.-F., Bendjelid, K., & Giraud, R. (2016). Veno-arterial extracorporeal membrane oxygenation: an overview of different cannulation techniques. *Journal of Thoracic Disease*, 8(9), E875-E885. <https://jtd.amegroups.org/article/view/9290>
- Banfi, C., Pozzi, M., Brunner, M. E., Rigamonti, F., Murith, N., Mugnai, D., Obadia, J. F., Bendjelid, K., & Giraud, R. (2016). Veno-arterial extracorporeal membrane oxygenation: an overview of different cannulation techniques. *J Thorac Dis*, 8(9), E875-E885. <https://doi.org/10.21037/jtd.2016.09.25>
- Bartlett, R. H. (2005). Extracorporeal life support: history and new directions. *Semin Perinatol*, 29(1), 2-7. <https://doi.org/10.1053/j.semperi.2005.02.002>
- Bartlett, R. H. (2017a). Esperanza: The First Neonatal ECMO Patient. *ASAIO J*, 63(6), 832-843. <https://doi.org/10.1097/MAT.0000000000000697>
- Bartlett, R. H. (2017b). Physiology of Gas Exchange During ECMO for Respiratory Failure. *Journal of intensive care medicine*, 32(4)(1525-1489 (Electronic)), 6. <https://doi.org/https://doi.org/10.1177/0885066616641383>
- Bauer, H. K., & Malone, M. P. (2022). Friend or Foe? Venoarterial ECMO via Carotid Artery "Jump Graft": A Case Series. *J Extra Corpor Technol*, 54(1), 67-72. <https://doi.org/10.1182/ject-67-72>
- Bazan, V. M., Taylor, E. M., Gunn, T. M., & Zwischenberger, J. B. (2021). Overview of the bicaval dual lumen cannula. *Indian J Thorac Cardiovasc Surg*, 37(Suppl 2), 232-240. <https://doi.org/10.1007/s12055-020-00932-1>

- Berdajs, D., Ferrari, E., Michalis, A., Burki, M., Pieterse, C. W., Horisberger, J., & von Segesser, L. K. (2011). New prototype of femoral arterial SmartCannula with anterograde and retrograde flow. *Perfusion*, 26(4), 271-275.
<https://doi.org/10.1177/02676591111399953>
- Berdajs, D. A., Bernandi, E., Burki, M., Hurni, M., Tozzi, P., Horisberger, J., & von Segesser, L. K. (2010). Self-expanding mini-cannula for remote perfusion with pediatric scenarios. *Interactive CardioVascular and Thoracic Surgery*, 10(6), 873-876. <https://doi.org/10.1510/icvts.2010.233080>
- Berdajs, D. A., de Stefano, E., Delay, D., Ferrari, E., Horisberger, J., Ditmar, Q., & von Segesser, L. K. (2011). The new advanced membrane gas exchanger. *Interact Cardiovasc Thorac Surg*, 13(6), 591-596.
<https://doi.org/10.1510/icvts.2011.276873>
- Berndtson, A., & Doucet, J. (2021). Travel and Transport. In J. M. Galante & R. Coimbra (Eds.), *Thoracic Surgery for the Acute Care Surgeon* (pp. 299-318). Springer International Publishing. https://doi.org/10.1007/978-3-030-48493-4_21
- Bessonov, N., Sequeira, A., Simakov, S., Vassilevskii, Y., & Volpert, V. (2016). Methods of Blood Flow Modelling [10.1051/mmnp/201611101]. *Math. Model. Nat. Phenom.*, 11(1), 1-25. <https://doi.org/10.1051/mmnp/201611101>
- Blanco, P. (2015). Volumetric blood flow measurement using Doppler ultrasound: concerns about the technique. *J Ultrasound*, 18(2), 201-204.
<https://doi.org/10.1007/s40477-015-0164-3>
- Boettcher, W., Merkle, F., & Weitkemper, H.-H. (2003). History of Extracorporeal Circulation: The Conceptual and Developmental Period [10.1051/ject/2003353172]. *J Extra Corpor Technol*, 35(3), 172-183.
<https://doi.org/10.1051/ject/2003353172>
- Bonicolini, E., Martucci, G., Simons, J., Raffa, G. M., Spina, C., Lo Coco, V., Arcadipane, A., Pilato, M., & Lorusso, R. (2019). Limb ischemia in peripheral veno-arterial extracorporeal membrane oxygenation: a narrative review of incidence, prevention, monitoring, and treatment. *Crit Care*, 23(1), 266.
<https://doi.org/10.1186/s13054-019-2541-3>

- Bradić, J., Andjić, M., Novaković, J., Jeremić, N., & Jakovljević, V. (2023). Cardioplegia in Open Heart Surgery: Age Matters. *Journal of Clinical Medicine*, 12(4).
- Brain, M. J., Butt, W. W., & MacLaren, G. (2022). Physiology of Extracorporeal Life Support (ECLS). In G. A. Schmidt (Ed.), *Extracorporeal Membrane Oxygenation for Adults* (pp. 1-61). Springer International Publishing. https://doi.org/10.1007/978-3-031-05299-6_1
- Bramson, M. L., Hill, J. D., Osborn, J. J., & Gerbode, F. (1969). Partial veno-arterial perfusion with membrane oxygenation and diastolic augmentation. *Trans Am Soc Artif Intern Organs*, 15, 412-416.
- Bramson, M. L., Osborn, J. J., Beachley Main, F., O'Brien, M. F., Wright, J. S., & Gerbode, F. (1965). A new disposable membrane oxygenator with integral heat exchange. *The Journal of Thoracic and Cardiovascular Surgery*, 50(3), 391-400. [https://doi.org/https://doi.org/10.1016/S0022-5223\(19\)33194-0](https://doi.org/https://doi.org/10.1016/S0022-5223(19)33194-0)
- Bramson, M. L., Osborn, J. J., Main, F. B., O'Brien, M. F., Wright, J. S., & Gerbode, F. (1965). A NEW DISPOSABLE MEMBRANE OXYGENATOR WITH INTEGRAL HEAT EXCHANGE. *J Thorac Cardiovasc Surg*, 50, 391-400.
- Brockaert, T., Ferreira, I., Laplante, A., Fogel, P., Grimbert, D., & Mordant, P. (2023). Preventing Acute Limb Ischemia during VA-ECMO-In Silico Analysis of Physical Parameters Associated with Lower Limb Perfusion. *J Clin Med*, 12(18). <https://doi.org/10.3390/jcm12186049>
- Brodman, R., Siegel, H., Lesser, M., & Frater, R. (1985). A comparison of flow gradients across disposable arterial perfusion cannulas. *Ann Thorac Surg*, 39(3), 225-233. [https://doi.org/10.1016/s0003-4975\(10\)62584-2](https://doi.org/10.1016/s0003-4975(10)62584-2)
- Broman, L. M., Prah Wittberg, L., Westlund, C. J., Gilbers, M., Perry da Camara, L., Swol, J., Taccone, F. S., Malfertheiner, M. V., Di Nardo, M., Vercaemst, L., Barrett, N. A., Pappalardo, F., Belohlavek, J., Muller, T., Belliato, M., & Lorusso, R. (2019). Pressure and flow properties of cannulae for extracorporeal membrane oxygenation I: return (arterial) cannulae. *Perfusion*, 34(1_suppl), 58-64. <https://doi.org/10.1177/0267659119830521>

- Brown, G., Moynihan, K. M., Deatrck, K. B., Hoskote, A., Sandhu, H. S., Aganga, D., Deshpande, S. R., Menon, A. P., Rozen, T., Raman, L., & Alexander, P. M. A. (2021). Extracorporeal Life Support Organization (ELSO): Guidelines for Pediatric Cardiac Failure. *ASAIO Journal*, 67(5).
https://journals.lww.com/asaiojournal/fulltext/2021/05000/extracorporeal_life_support_organization_elso_1.aspx
- Burrell, A. J. C., Ihle, J. F., Pellegrino, V. A., Sheldrake, J., & Nixon, P. T. (2018). Cannulation technique: femoro-femoral. *J Thorac Dis*, 10(Suppl 5), S616-s623.
<https://doi.org/10.21037/jtd.2018.03.83>
- Calderon, D., El-Banayosy, A., Koerner, M. M., Reed, A. B., & Aziz, F. (2015). Modified T-Graft for Extracorporeal Membrane Oxygenation in a Patient with Small-Caliber Femoral Arteries. *Tex Heart Inst J*, 42(6), 537-539.
<https://doi.org/10.14503/thij-14-4728>
- Chamogeorgakis, T., Lima, B., Shafii, A. E., Nagpal, D., Pokersnik, J. A., Navia, J. L., Mason, D., & Gonzalez-Stawinski, G. V. (2013). Outcomes of axillary artery side graft cannulation for extracorporeal membrane oxygenation. *J Thorac Cardiovasc Surg*, 145(4), 1088-1092. <https://doi.org/10.1016/j.jtcvs.2012.08.070>
- Chan, C. H., Ki, K. K., Zhang, M., Asnicar, C., Cho, H. J., Ainola, C., Bouquet, M., Heinsar, S., Pauls, J. P., Li Bassi, G., Suen, J., & Fraser, J. F. (2021). Extracorporeal Membrane Oxygenation-Induced Hemolysis: An In Vitro Study to Appraise Causative Factors. *Membranes*, 11(5).
- Chandler, W. L. (2021). Platelet, Red Cell, and Endothelial Activation and Injury During Extracorporeal Membrane Oxygenation. *ASAIO J*, 67(8), 935-942.
<https://doi.org/10.1097/MAT.0000000000001320>
- Chen, Y., Tutungi, E., McMillan, J., Tayeh, S. M., Underwood, J. K., Wells, A. C., Smith, J. A., & Moshinsky, R. A. (2017). Pressure and Flow Characteristics of a Novel Bidirectional Cannula for Cardiopulmonary Bypass. *Innovations (Phila)*, 12(6), 430-433. <https://doi.org/10.1097/imi.0000000000000424>

- Cleland, W. P., & Melrose, D. G. (1955). THE ARTIFICIAL HEART-LUNG AND ITS PRACTICAL APPLICATION TO CARDIAC SURGERY. *British Medical Bulletin*, 11(3), 236-239. <https://doi.org/10.1093/oxfordjournals.bmb.a069501>
- Clowes Gh Jr Fau - Hopkins, A. L. H. A. F.-N., W. E., & Neville, W. E. (1956). An artificial lung dependent upon diffusion of oxygen and carbon dioxide through plastic membranes. *Journal of Thoracic Surgery*, 32(5), 630-637. <https://doi.org/D> - CLML: 5731:14384 OTO - NLM
- Clowes, G. H. A., Hopkins, A. L., & Neville, W. E. (1956). AN ARTIFICIAL LUNG DEPENDENT UPON DIFFUSION OF OXYGEN AND CARBON DIOXIDE THROUGH PLASTIC MEMBRANES. *Journal of Thoracic Surgery*, 32(5), 630-637. [https://doi.org/https://doi.org/10.1016/S0096-5588\(20\)30575-4](https://doi.org/https://doi.org/10.1016/S0096-5588(20)30575-4)
- Clowes, G. H. A., Jr., & Neville, W. E. (1957). FURTHER DEVELOPMENT OF A BLOOD OXYGENATOR DEPENDENT UPON THE DIFFUSION OF GASES THROUGH PLASTIC MEMBRANES. *ASAIO Journal*, 3(1). https://journals.lww.com/asaiojournal/fulltext/1957/04000/further_development_of_a_blood_oxygenator.14.aspx
- Condello, I., Santarpino, G., Nasso, G., Moscarelli, M., Fiore, F., & Speziale, G. (2020). Associations between oxygen delivery and cardiac index with hyperlactatemia during cardiopulmonary bypass. *JTCVS Tech*, 2, 92-99. <https://doi.org/10.1016/j.xjtc.2020.04.001>
- Crişan, S. (2012a). Ultrasound examination of the femoral and popliteal arteries. (2066-8643 (Electronic)).
- Crişan, S. (2012b). Ultrasound examination of the femoral and popliteal arteries. *Med Ultrason*, 14(1), 74-77.
- Daniel, J. M. t., Bernard, P. A., Skinner, S. C., Bhandary, P., Ruzic, A., Bacon, M. K., & Ballard, H. O. (2018). Hollow Fiber Oxygenator Composition Has a Significant Impact on Failure Rates in Neonates on Extracorporeal Membrane Oxygenation: A Retrospective Analysis. *J Pediatr Intensive Care*, 7(1), 7-13. <https://doi.org/10.1055/s-0037-1599150>

- De Wachter, D., & Verdonck, P. (2002). Numerical Calculation of Hemolysis Levels in Peripheral Hemodialysis Cannulas. *Artificial Organs*, 26(7), 576-582.
<https://doi.org/https://doi.org/10.1046/j.1525-1594.2002.07079.x>
- Elmously, A., Bobka, T., Khin, S., Afzal, A., de Biasi, A. R., DeBois, W. J., Guy, T. S., D'Ayala, M., Gulkarov, I., Salemi, A., & Worku, B. (2018). Distal Perfusion Cannulation and Limb Complications in Venoarterial Extracorporeal Membrane Oxygenation. *J Extra Corpor Technol*, 50(3), 155-160.
- Extracorporeal Life Support Organization, E. (2017). *ELSO International Summary January 2017*.
- Extracorporeal Life Support Organization, E. (2023). *International report october 2023*
<https://www.elseo.org/registry/internationalsummaryandreports/reports.aspx>
- Featherstone, P. J., & Ball, C. M. (2018). The Early History of Extracorporeal Membrane Oxygenation. *Anaesthesia and Intensive Care*, 46(6), 555-557.
<https://doi.org/10.1177/0310057X1804600601>
- Ficial, B., Vasques, F., Zhang, J., Whebell, S., Slattery, M., Lamas, T., Daly, K., Agnew, N., & Camporota, L. (2021). Physiological Basis of Extracorporeal Membrane Oxygenation and Extracorporeal Carbon Dioxide Removal in Respiratory Failure. *Membranes (Basel)*, 11(3). <https://doi.org/10.3390/membranes11030225>
- Fiusco, F., Broman, L. M., & PrahL Wittberg, L. (2022). Blood Pumps for Extracorporeal Membrane Oxygenation: Platelet Activation During Different Operating Conditions. *ASAIO J*, 68(1), 79-86.
<https://doi.org/10.1097/mat.0000000000001493>
- Foltan, M., Philipp, A., Gobolos, L., Holzamer, A., Schneckenpointner, R., Lehle, K., Kornilov, I., Schmid, C., & Lunz, D. (2019). Quantitative assessment of peripheral limb perfusion using a modified distal arterial cannula in venoarterial ECMO settings. *Perfusion*, 34(6), 503-507.
<https://doi.org/10.1177/0267659118816934>
- Fraser, C. D., 3rd, Kovler, M. L., Guzman, W., Jr., Rhee, D. S., Lum, Y. W., Alais, S. M., & Garcia, A. V. (2019). Pediatric Femoral Arterial Cannulations in Extracorporeal Membrane Oxygenation: A Review and Strategies for

- Optimization. *ASAIO J*, 65(7), 636-641.
<https://doi.org/10.1097/mat.0000000000000884>
- Fu, M., Liu, G., Wang, W., Gao, B., Ji, B., Chang, Y., & Liu, Y. (2021). Hemodynamic evaluation and in vitro hemolysis evaluation of a novel centrifugal pump for extracorporeal membrane oxygenation. *Ann Transl Med*, 9(8), 679.
<https://doi.org/10.21037/atm-21-1135>
- Gajkowski, E. F., Herrera, G., Hatton, L., Velia Antonini, M., Vercaemst, L., & Cooley, E. (2022). ELSO Guidelines for Adult and Pediatric Extracorporeal Membrane Oxygenation Circuits. *ASAIO J*, 68(2), 133-152.
<https://doi.org/10.1097/MAT.0000000000001630>
- Ganushchak, Y. M., Kurniawati, E. R., Maessen, J. G., & Weerwind, P. W. (2020). Peripheral cannulae selection for veno-arterial extracorporeal life support: a paradox. *Perfusion*, 35(4), 331-337. <https://doi.org/10.1177/0267659119885586>
- Garcia-Rinaldi, R., Vaughan, G. D., 3rd, Revuelta, J. M., Goiti, J. J., & Gomez-Durán, C. (1983). Simplified aortic cannulation. *Ann Thorac Surg*, 36(2), 226-227.
[https://doi.org/10.1016/s0003-4975\(10\)60463-8](https://doi.org/10.1016/s0003-4975(10)60463-8)
- Gehrmann, L. P., Hafner, J. W., Montgomery, D. L., Buckley, K. W., & Fortuna, R. S. (2015). Pediatric Extracorporeal Membrane Oxygenation: An Introduction for Emergency Medicine Physicians. *J Emerg Med*, 49(4), 552-560.
<https://doi.org/10.1016/j.jemermed.2015.02.010>
- Gerbode, F., & Melrose, D. (1958). The use of potassium arrest in open cardiac surgery. *The American Journal of Surgery*, 96(2), 221-227.
[https://doi.org/https://doi.org/10.1016/0002-9610\(58\)90906-1](https://doi.org/https://doi.org/10.1016/0002-9610(58)90906-1)
- Gerdes, A., Hanke, T., & Sievers, H. H. (2002). Hydrodynamics of the new Medos aortic cannula. *Perfusion*, 17(3), 217-220.
<https://doi.org/10.1191/0267659102pf574oa>
- Gourlay, T., Fleming, J., Taylor, K. M., & Aslam, M. (1990). Evaluation of a range of extracorporeal membrane oxygenators. *Perfusion*, 5(2), 117-133.
<https://doi.org/10.1177/026765919000500206>

- Gramigna, V., Palumbo, A., Rossi, M., & Fragomeni, G. (2023). A Computational Fluid Dynamics Study to Compare Two Types of Arterial Cannulae for Cardiopulmonary Bypass. *Fluids*, 8(11).
- Groen, H. C., Gijssen, F. J., van der Lugt, A., Ferguson, M. S., Hatsukami, T. S., van der Steen, A. F., Yuan, C., & Wentzel, J. J. (2007). Plaque rupture in the carotid artery is localized at the high shear stress region: a case report. *Stroke*, 38(8), 2379-2381. <https://doi.org/10.1161/strokeaha.107.484766>
- Grooters, R. K., Ver Steeg, D. A., Stewart, M. J., Thieman, K. C., & Schneider, R. F. (2003). Echocardiographic comparison of the standard end-hole cannula, the soft-flow cannula, and the dispersion cannula during perfusion into the aortic arch. *The Annals of Thoracic Surgery*, 75(6), 1919-1923. [https://doi.org/https://doi.org/10.1016/S0003-4975\(03\)00018-3](https://doi.org/https://doi.org/10.1016/S0003-4975(03)00018-3)
- Gu, K., Zhang, Y., Gao, B., Chang, Y., & Zeng, Y. (2016). Hemodynamic Differences Between Central ECMO and Peripheral ECMO: A Primary CFD Study. *Med Sci Monit*, 22, 717-726. <https://doi.org/10.12659/msm.895831>
- Guglin, M., Zucker, M. J., Bazan, V. M., Bozkurt, B., El Banayosy, A., Estep, J. D., Gurley, J., Nelson, K., Malyala, R., Panjrath, G. S., Zwischenberger, J. B., & Pinney, S. P. (2019). Venoarterial ECMO for Adults: JACC Scientific Expert Panel. *J Am Coll Cardiol*, 73(6), 698-716. <https://doi.org/10.1016/j.jacc.2018.11.038>
- Gunaydin, S., Babaroglu, S., Budak, A. B., Sayin, B., Cayhan, V., & Ozisik, K. (2021). Comparative clinical efficacy of novel bidirectional cannula in cardiac surgery via peripheral cannulation for cardiopulmonary bypass. *Perfusion*, 38(1), 44-50. <https://doi.org/10.1177/02676591211033945>
- Hager, A., Kaemmerer, H., Rapp-Bernhardt, U., Blucher, S., Rapp, K., Bernhardt, T. M., Galanski, M., & Hess, J. (2002). Diameters of the thoracic aorta throughout life as measured with helical computed tomography. *J Thorac Cardiovasc Surg*, 123(6), 1060-1066. <https://doi.org/10.1067/mtc.2002.122310>

- Haines, N., Wang, S., Myers, J. L., & Undar, A. (2009). Comparison of two types of neonatal extracorporeal life support systems with pulsatile and nonpulsatile flow. *Artif Organs*, 33(11), 958-966. <https://doi.org/10.1111/j.1525-1594.2009.00934.x>
- Haines, N., Wang, S., Myers, J. L., & Ündar, A. (2009). Comparison of Two Types of Neonatal Extracorporeal Life Support Systems With Pulsatile and Nonpulsatile Flow. *Artificial Organs*, 33(11), 958-966. <https://doi.org/https://doi.org/10.1111/j.1525-1594.2009.00934.x>
- Harboe, M. (1959). A Method for Determination of Hemoglobin in Plasma by Near-Ultraviolet Spectrophotometry. *Scandinavian Journal of Clinical and Laboratory Investigation*, 11(1), 66-70. <https://doi.org/10.3109/00365515909060410>
- Harvey, C. (2018). Cannulation for Neonatal and Pediatric Extracorporeal Membrane Oxygenation for Cardiac Support. *Front Pediatr*, 6, 17. <https://doi.org/10.3389/fped.2018.00017>
- Hastings, S. M., Ku, D. N., Wagoner, S., Maher, K. O., & Deshpande, S. (2017). Sources of Circuit Thrombosis in Pediatric Extracorporeal Membrane Oxygenation. *ASAIO J*, 63(1), 86-92. <https://doi.org/10.1097/MAT.0000000000000444>
- Haymet, A. B., Boone, A., Vallely, M. P., Malfertheiner, M. V., Pauls, J. P., Suen, J. Y., & Fraser, J. F. (2021). Assessing potential for aortoiliac vascular injury from venoarterial extracorporeal membrane oxygenation cannulae: An in vitro particle image velocimetry study. *Artif Organs*, 45(2), E14-E25. <https://doi.org/10.1111/aor.13807>
- Hedayati, N., Sherwood, J. T., Schomisch, S. J., Carino, J. L., & Markowitz, A. H. (2004). Axillary artery cannulation for cardiopulmonary bypass reduces cerebral microemboli. *J Thorac Cardiovasc Surg*, 128(3), 386-390. <https://doi.org/10.1016/j.jtcvs.2004.01.013>
- Hellums, J. D., Peterson, D. M., Stathopoulos, N. A., Moake, J. L., & Giorgio, T. D. (1987, 1987//). Studies on the Mechanisms of Shear-Induced Platelet Activation. *Cerebral Ischemia and Hemorheology*, Berlin, Heidelberg.
- Hessel, E., & Hill, A. (1993). *Cardiopulmonary Bypass: Principles and Practice*.

- Hessel, E. A., 2nd. (2014). A Brief History of Cardiopulmonary Bypass. *Semin Cardiothorac Vasc Anesth*, 18(2), 87-100.
<https://doi.org/10.1177/1089253214530045>
- Hill, J. D. (1982). John H. Gibbon, Jr. Part I. The development of the first successful heart-lung machine. *Ann Thorac Surg*, 34(3), 337-341.
[https://doi.org/10.1016/s0003-4975\(10\)62507-6](https://doi.org/10.1016/s0003-4975(10)62507-6)
- Hill, J. D., O'Brien Thomas, G., Murray James, J., Dontigny, L., Bramson, M. L., Osborn, J. J., & Gerbode, F. (1972). Prolonged Extracorporeal Oxygenation for Acute Post-Traumatic Respiratory Failure (Shock-Lung Syndrome). *New England Journal of Medicine*, 286(12), 629-634.
<https://doi.org/10.1056/NEJM197203232861204>
- Hippelheuser, J. E., Lauric, A., Cohen, A. D., & Malek, A. M. (2014). Realistic non-Newtonian viscosity modelling highlights hemodynamic differences between intracranial aneurysms with and without surface blebs. *Journal of Biomechanics*, 47(15), 3695-3703.
<https://doi.org/https://doi.org/10.1016/j.jbiomech.2014.09.027>
- Holland, C. K., Brown, J. M., Scutt, L. M., & Taylor, K. J. (1998). Lower extremity volumetric arterial blood flow in normal subjects. *Ultrasound Med Biol*, 24(8), 1079-1086. [https://doi.org/10.1016/s0301-5629\(98\)00103-3](https://doi.org/10.1016/s0301-5629(98)00103-3)
- Holland, C. K., Brown, J. M., Scutt, L. M., & Taylor, K. J. W. (1998). Lower extremity volumetric arterial blood flow in normal subjects. *Ultrasound in Medicine & Biology*, 24(8), 1079-1086. [https://doi.org/https://doi.org/10.1016/S0301-5629\(98\)00103-3](https://doi.org/https://doi.org/10.1016/S0301-5629(98)00103-3)
- Horton, S., Thuys, C., Bennett, M., Augustin, S., Rosenberg, M., & Brizard, C. (2004). Experience with the Jostra Rotaflow and QuadroxD oxygenator for ECMO. *Perfusion*, 19(1), 17-23. <https://doi.org/10.1191/0267659104pf702oa>
- Huang, S. C., Yu, H. Y., Ko, W. J., & Chen, Y. S. (2004). Pressure criterion for placement of distal perfusion catheter to prevent limb ischemia during adult extracorporeal life support. *J Thorac Cardiovasc Surg*, 128(5), 776-777.
<https://doi.org/10.1016/j.jtcvs.2004.03.042>

- Hugenroth, K., Borchardt, R., Ritter, P., Gross-Hardt, S., Meyns, B., Verbelen, T., Steinseifer, U., Kaufmann, T. A. S., & Engelmann, U. M. (2021). Optimizing cerebral perfusion and hemodynamics during cardiopulmonary bypass through cannula design combining in silico, in vitro and in vivo input. *Sci Rep*, *11*(1), 16800. <https://doi.org/10.1038/s41598-021-96397-2>
- Hwang, J. Y. (2017). Doppler ultrasonography of the lower extremity arteries: anatomy and scanning guidelines. *Ultrasonography*, *36*(2), 111-119. <https://doi.org/10.14366/usg.16054>
- Imamura, M., & Caldarone, C. A. (2019). Venoarterial Extracorporeal Membrane Oxygenation Neck Cannulation: A Fixation Strategy Without Tourniquets. *Operative Techniques in Thoracic and Cardiovascular Surgery*, *24*(4), 256-266. <https://doi.org/https://doi.org/10.1053/j.optechstcvs.2019.09.003>
- Iwahashi, H., Yuri, K., & Nosé, Y. (2004). Development of the oxygenator: past, present, and future. *Journal of Artificial Organs*, *7*(3), 111-120. <https://doi.org/10.1007/s10047-004-0268-6>
- Jayaraman, A. L., Cormican, D., Shah, P., & Ramakrishna, H. (2017). Cannulation strategies in adult veno-arterial and veno-venous extracorporeal membrane oxygenation: Techniques, limitations, and special considerations. *Ann Card Anaesth*, *20*(Supplement), S11-s18. <https://doi.org/10.4103/0971-9784.197791>
- Jegier, W., Sekelj, P., Auld, P. A. M., Simpson, R., & McGregor, M. (1963). THE RELATION BETWEEN CARDIAC OUTPUT AND BODY SIZE. *British Heart Journal*, *25*(4), 425. <https://doi.org/10.1136/hrt.25.4.425>
- Jenks, C. L., Zia, A., Venkataraman, R., & Raman, L. (2019). High Hemoglobin Is an Independent Risk Factor for the Development of Hemolysis During Pediatric Extracorporeal Life Support. *J Intensive Care Med*, *34*(3), 259-264. <https://doi.org/10.1177/0885066617708992>
- Johnson, K. N., Carr, B., Mychaliska, G. B., Hirschl, R. B., & Gadepalli, S. K. (2022). Switching to centrifugal pumps may decrease hemolysis rates among pediatric ECMO patients. *Perfusion*, *37*(2), 123-127. <https://doi.org/10.1177/0267659120982572>

- Kaluza, M., May, B., & Doenst, T. (2022). Using a roller pump for establishing extra-corporal membrane oxygenation (ECMO) - technical considerations for times of crisis. *Perfusion*, 37(3), 229-234. <https://doi.org/10.1177/0267659121996182>
- Kameneva, M., Marascalco, P., Snyder, T., & Antaki, J. (2006). VALIDITY OF NORMALIZED INDEX OF HEMOLYSIS IN PEDIATRIC MECHANICAL CIRCULATORY ASSIST DEVICES. *ASAIO Journal*, 52(2). https://journals.lww.com/asaiojournal/fulltext/2006/03000/validity_of_normalized_index_of_hemolysis_in.179.aspx
- Kameneva, M. V., Burgreen, G. W., Kono, K., Repko, B., Antaki, J. F., & Umezu, M. (2004). Effects of turbulent stresses upon mechanical hemolysis: experimental and computational analysis. *ASAIO J*, 50(5), 418-423. <https://doi.org/10.1097/01.mat.0000136512.36370.b5>
- Kammermeyer, K. (1957). Silicone Rubber as a Selective Barrier. *Industrial & Engineering Chemistry*, 49(10), 1685-1686. <https://doi.org/10.1021/ie50574a024>
- Kaufmann, T. A., Neidlin, M., Busen, M., Sonntag, S. J., & Steinseifer, U. (2014). Implementation of intrinsic lumped parameter modeling into computational fluid dynamics studies of cardiopulmonary bypass. *J Biomech*, 47(3), 729-735. <https://doi.org/10.1016/j.jbiomech.2013.11.005>
- Kazmi, S. O., Sivakumar, S., Karakitsos, D., Alharthy, A., & Lazaridis, C. (2018). Cerebral Pathophysiology in Extracorporeal Membrane Oxygenation: Pitfalls in Daily Clinical Management. *Crit Care Res Pract*, 2018, 3237810. <https://doi.org/10.1155/2018/3237810>
- Kemaloğlu, C. (2018). Percutaneous versus Side Graft Perfusion for Peripheral Extracorporeal Membrane Oxygenation Therapy; A Single Center Experience. *Akdeniz Medical Journal*. <https://doi.org/10.17954/amj.2018.139>
- Keshmiri, A., & Andrews, K. (2015). Vascular Flow Modelling Using Computational Fluid Dynamics. In M. Slevin & G. McDowell (Eds.), *Handbook of Vascular Biology Techniques* (pp. 343-361). Springer Netherlands. https://doi.org/10.1007/978-94-017-9716-0_27

- Ki, K. K., Millar, J. E., Langguth, D., Passmore, M. R., McDonald, C. I., Shekar, K., Shankar-Hari, M., Cho, H. J., Suen, J. Y., & Fraser, J. F. (2020). Current Understanding of Leukocyte Phenotypic and Functional Modulation During Extracorporeal Membrane Oxygenation: A Narrative Review. *Front Immunol*, *11*, 600684. <https://doi.org/10.3389/fimmu.2020.600684>
- Kim-Campbell, N., & Bayir, H. (2018). Extracorporeal Membrane Oxygenation and Hemolysis-Still a Challenge. *Pediatr Crit Care Med*, *19*(11), 1089-1090. <https://doi.org/10.1097/pcc.0000000000001728>
- Kim, J., Cho, Y. H., Sung, K., Park, T. K., Lee, G. Y., Lee, J. M., Song, Y. B., Hahn, J. Y., Choi, J. H., Choi, S. H., Gwon, H. C., & Yang, J. H. (2019). Impact of Cannula Size on Clinical Outcomes in Peripheral Venoarterial Extracorporeal Membrane Oxygenation. *ASAIO J*, *65*(6), 573-579. <https://doi.org/10.1097/MAT.0000000000000858>
- Kohler, K., Valchanov, K., Nias, G., & Vuylsteke, A. (2012). ECMO cannula review. *Perfusion*, *28*(2), 114-124. <https://doi.org/10.1177/0267659112468014>
- Kolff, W. J., Berk, H. T., ter Welle, M., van der, L. A., van Dijk, E. C., & van Noordwijk, J. (1997). The artificial kidney: a dialyser with a great area. 1944. *J Am Soc Nephrol*, *8*(12), 1959-1965. <https://doi.org/10.1681/asn.V8I21959>
- Kolff, W. J., Effler, D. B., Groves, L. K., Peereboom, G., & Moraca, P. P. (1956). Disposable membrane oxygenator (heart-lung machine) and its use in experimental surgery. *Cleve Clin Q*, *23*(2), 69-97. <https://doi.org/10.3949/ccjm.23.2.69>
- Kolobow, T., & Bowman, R. L. (1963). Construction and evaluation of an alveolar membrane artificial heart-lung. *Trans Am Soc Artif Intern Organs*, *9*, 238-243.
- Kolobow, T., Spragg, R. G., Pierce, J. E., & Zapol, W. M. (1971). Extended term (to 16 days) partial extracorporeal blood gas exchange with the spiral membrane lung in unanesthetized lambs. *Trans Am Soc Artif Intern Organs*, *17*, 350-354.
- Kozik, D. (2020). Neurodevelopmental Outcomes in Pediatric Extracorporeal Membrane Oxygenation. *ASAIO J*, *66*(1), 89-90. <https://doi.org/10.1097/MAT.0000000000001112>

- Krementsov, N. (2009). Off with your heads: isolated organs in early Soviet science and fiction. *Stud Hist Philos Biol Biomed Sci*, 40(2), 87-100.
<https://doi.org/10.1016/j.shpsc.2009.03.001>
- Kumar, N., A, G., H, G., Kumar, S., & Shenoy B, G. (2023). Advances in the application of computational fluid dynamics in cardiovascular flow. *Cogent Engineering*, 10(1), 2178367. <https://doi.org/10.1080/23311916.2023.2178367>
- Kurusz, M. (2012). May 6, 1953: the untold story. *ASAIO J*, 58(1), 2-5.
<https://doi.org/10.1097/MAT.0b013e31823ccfe7>
- Lamb, K. M., DiMuzio, P. J., Johnson, A., Batista, P., Moudgill, N., McCullough, M., Eisenberg, J. A., Hirose, H., & Cavarocchi, N. C. (2017). Arterial protocol including prophylactic distal perfusion catheter decreases limb ischemia complications in patients undergoing extracorporeal membrane oxygenation. *J Vasc Surg*, 65(4), 1074-1079. <https://doi.org/10.1016/j.jvs.2016.10.059>
- Lawson, D. S., Ing, R., Cheifetz, I. M., Walczak, R., Craig, D., Schulman, S., Kern, F., Shearer, I. R., Lodge, A., & Jagers, J. (2005). Hemolytic characteristics of three commercially available centrifugal blood pumps. *Pediatric Critical Care Medicine*, 6(5).
https://journals.lww.com/pccmjournal/fulltext/2005/09000/hemolytic_characteristics_of_three_commercially.13.aspx
- Lee, B. K. (2011). Computational fluid dynamics in cardiovascular disease. *Korean Circ J*, 41(8), 423-430. <https://doi.org/10.4070/kcj.2011.41.8.423>
- Lee, E. H., Lee, K. H., Lee, S. J., Kim, J., Baek, Y. J., Ahn, J. Y., Jeong, S. J., Ku, N. S., Choi, J. Y., Yeom, J.-S., Song, Y. G., & Kim, J. H. (2022). Clinical and microbiological characteristics of and risk factors for bloodstream infections among patients with extracorporeal membrane oxygenation: a single-center retrospective cohort study. *Scientific Reports*, 12(1), 15059.
<https://doi.org/10.1038/s41598-022-19405-z>
- Lemétayer, J., Broman, L. M., & PrahL Wittberg, L. (2021). Flow Dynamics and Mixing in Extracorporeal Support: A Study of the Return Cannula [Original Research].

Frontiers in Bioengineering and Biotechnology, 9.

<https://doi.org/10.3389/fbioe.2021.630568>

Lequier, L., Horton, S. B., McMullan, D. M., & Bartlett, R. H. (2013). Extracorporeal membrane oxygenation circuitry. *Pediatr Crit Care Med*, 14(5 Suppl 1), S7-12.

<https://doi.org/10.1097/PCC.0b013e318292dd10>

Lim, M. W. (2006). The history of extracorporeal oxygenators*. *Anaesthesia*, 61(10), 984-995. <https://doi.org/https://doi.org/10.1111/j.1365-2044.2006.04781.x>

Link, M. S., Berkow, L. C., Kudenchuk, P. J., Halperin, H. R., Hess, E. P., Moitra, V. K., Neumar, R. W., O'Neil, B. J., Paxton, J. H., Silvers, S. M., White, R. D., Yannopoulos, D., & Donnino, M. W. (2015). Part 7: Adult Advanced Cardiovascular Life Support: 2015 American Heart Association Guidelines Update for Cardiopulmonary Resuscitation and Emergency Cardiovascular Care. *Circulation*, 132(18 Suppl 2), S444-464.

<https://doi.org/10.1161/cir.0000000000000261>

Lo Coco, V., Lorusso, R., Raffa, G. M., Malvindi, P. G., Pilato, M., Martucci, G., Arcadipane, A., Zielinski, K., Suwalski, P., & Kowalewski, M. (2018). Clinical complications during veno-arterial extracorporeal membrane oxygenation in post-cardiotomy and non post-cardiotomy shock: still the achille's heel. *J Thorac Dis*, 10(12), 6993-7004. <https://doi.org/10.21037/jtd.2018.11.103>

Lorusso, R., Shekar, K., MacLaren, G., Schmidt, M., Pellegrino, V., Meyns, B., Haft, J., Vercaemst, L., Pappalardo, F., Bermudez, C., Belohlavek, J., Hou, X., Boeken, U., Castillo, R., Donker, D. W., Abrams, D., Ranucci, M., Hryniewicz, K., Chavez, I., . . . Whitman, G. (2021). ELSO Interim Guidelines for Venoarterial Extracorporeal Membrane Oxygenation in Adult Cardiac Patients. *ASAIO Journal*, 67(8).

https://journals.lww.com/asaiojournal/fulltext/2021/08000/else_interim_guidelines_for_venoarterial.2.aspx

Magovern, J. A., Fonger, J. D., Wang, D. H. J., Kopilec, D., Trumble, D. R., & Smith, D. E. (2005). A femoral artery cannula that allows distal blood flow. *The Journal*

of Thoracic and Cardiovascular Surgery, 130(3), 684-686.

<https://doi.org/10.1016/j.jtcvs.2005.03.022>

Makdisi, G., Makdisi, T., & Wang, I. W. (2017). Use of distal perfusion in peripheral extracorporeal membrane oxygenation. *Ann Transl Med*, 5(5), 103.

<https://doi.org/10.21037/atm.2017.03.01>

Makdisi, G., & Wang, I. W. (2015). Extra Corporeal Membrane Oxygenation (ECMO) review of a lifesaving technology. *J Thorac Dis*, 7(7), E166-176.

<https://doi.org/10.3978/j.issn.2072-1439.2015.07.17>

Manole, A. M., Iliescu, D. M., Rusali, A., & Bordei, P. (2013). Morphometry of the aortic arch and its branches. *ARS Medica Tomitana*, 19(3), 154-159.

<https://doi.org/10.2478/arsm-2013-0027>

Marasco, S. F., Tutungi, E., Vallance, S. A., Udy, A. A., Negri, J. C., Zimmet, A. D., McGiffin, D. C., Pellegrino, V. A., & Moshinsky, R. A. (2018). A Phase 1 Study of a Novel Bidirectional Perfusion Cannula in Patients Undergoing Femoral Cannulation for Cardiac Surgery. *Innovations (Phila)*, 13(2), 97-103.

<https://doi.org/10.1097/imi.0000000000000489>

Maratta, C., Potera, R. M., van Leeuwen, G., Castillo Moya, A., Raman, L., & Annich, G. M. (2020). Extracorporeal Life Support Organization (ELSO): 2020 Pediatric Respiratory ELSO Guideline. *ASAIO Journal*, 66(9).

https://journals.lww.com/asaiojournal/fulltext/2020/09000/extracorporeal_life_support_organization_elso_1.aspx

Matsui, Y., Shimura, S., Suto, Y., Fukase, S., Tanaka, A., & Sasaki, S. (2006). A Novel Femoral Arterial Cannula to Prevent Limb Ischemia During Cardiopulmonary Support: Preliminary Report of Experimental and Clinical Experiences. *Artificial Organs*, 30(7), 557-560. [https://doi.org/https://doi.org/10.1111/j.1525-](https://doi.org/https://doi.org/10.1111/j.1525-1594.2006.00259.x)

[1594.2006.00259.x](https://doi.org/https://doi.org/10.1111/j.1525-1594.2006.00259.x)

McDonald, C. I., Bolle, E., Lang, H. F., Ribolzi, C., Thomson, B., Tansley, G. D., Fraser, J. F., & Gregory, S. D. (2016). Hydrodynamic evaluation of aortic cardiopulmonary bypass cannulae using particle image velocimetry. *Perfusion*, 31(1), 78-86. <https://doi.org/10.1177/0267659115586282>

- McGough, E. C., McGough, S., & Hawkins, J. A. (1993). Subclavian artery cannulation for infant extracorporeal membrane oxygenation. *Ann Thorac Surg*, 55(3), 787-788. [https://doi.org/10.1016/0003-4975\(93\)90301-w](https://doi.org/10.1016/0003-4975(93)90301-w)
- McLean, J. A. Y. (1959). The Discovery of Heparin. *Circulation*, 19(1), 75-78. <https://doi.org/10.1161/01.CIR.19.1.75>
- Melrose, D. G. (1953). A mechanical heart-lung for use in man. *Br Med J*, 2(4827), 57-62. <https://doi.org/10.1136/bmj.2.4827.57>
- Melrose, D. G., Bassett, J. W., Beaconsfield, P., & Graber, I. G. (1953). Experimental physiology of a heart-lung machine in parallel with normal circulation. *Br Med J*, 2(4827), 62-66. <https://doi.org/10.1136/bmj.2.4827.62>
- Menon, P. G., Antaki, J. F., Undar, A., & Pekkan, K. (2013). Aortic Outflow Cannula Tip Design and Orientation Impacts Cerebral Perfusion During Pediatric Cardiopulmonary Bypass Procedures. *Annals of Biomedical Engineering*, 41(12), 2588-2602. <https://doi.org/10.1007/s10439-013-0857-8>
- Merzkirch, W. (2007). Flow Visualization. In C. Tropea, A. L. Yarin, & J. F. Foss (Eds.), *Springer Handbook of Experimental Fluid Mechanics* (pp. 857-870). Springer Berlin Heidelberg. https://doi.org/10.1007/978-3-540-30299-5_11
- Migdady, I., Rice, C., Deshpande, A., Hernandez, A. V., Price, C., Whitman, G. J., Geocadin, R. G., & Cho, S. M. (2020). Brain Injury and Neurologic Outcome in Patients Undergoing Extracorporeal Cardiopulmonary Resuscitation: A Systematic Review and Meta-Analysis. *Crit Care Med*, 48(7), e611-e619. <https://doi.org/10.1097/CCM.0000000000004377>
- Millar, J. E., Fanning, J. P., McDonald, C. I., McAuley, D. F., & Fraser, J. F. (2016). The inflammatory response to extracorporeal membrane oxygenation (ECMO): a review of the pathophysiology. *Critical Care*, 20(1), 387. <https://doi.org/10.1186/s13054-016-1570-4>
- Minakawa, M., Fukuda, I., Yamazaki, J., Fukui, K., Yanaoka, H., & Inamura, T. (2007). Effect of Cannula Shape on Aortic Wall and Flow Turbulence: Hydrodynamic Study During Extracorporeal Circulation in Mock Thoracic Aorta. *Artificial*

Organs, 31(12), 880-886. <https://doi.org/https://doi.org/10.1111/j.1525-1594.2007.00481.x>

- Moller, P. W., Hana, A., Heinisch, P. P., Liu, S., Djafarzadeh, S., Haenggi, M., Bloch, A., Takala, J., Jakob, S. M., & Berger, D. (2019). The Effects of Vasoconstriction And Volume Expansion on Venous-Arterial ECMO Flow. *Shock*, 51(5), 650-658. <https://doi.org/10.1097/SHK.0000000000001197>
- Montoya, J. P., Merz, S. I., & Bartlett, R. H. (1991). A standardized system for describing flow/pressure relationships in vascular access devices. *ASAIO Trans*, 37(1), 4-8. <https://doi.org/10.1097/00002480-199101000-00003>
- Morris, P. D., Narracott, A., von Tengge-Kobligk, H., Silva Soto, D. A., Hsiao, S., Lungu, A., Evans, P., Bressloff, N. W., Lawford, P. V., Hose, D. R., & Gunn, J. P. (2016). Computational fluid dynamics modelling in cardiovascular medicine. *Heart*, 102(1), 18. <https://doi.org/10.1136/heartjnl-2015-308044>
- Mosier, J. M., Kelsey, M., Raz, Y., Gunnerson, K. J., Meyer, R., Hypes, C. D., Malo, J., Whitmore, S. P., & Spaite, D. W. (2015). Extracorporeal membrane oxygenation (ECMO) for critically ill adults in the emergency department: history, current applications, and future directions. *Crit Care*, 19, 431. <https://doi.org/10.1186/s13054-015-1155-7>
- Mosquera, V. X., Solla-Buceta, M., Pradas-Irun, C., & Fernandez-Arias, L. (2014). Lower limb overflow syndrome in extracorporeal membrane oxygenation. *Interact Cardiovasc Thorac Surg*, 19(3), 532-534. <https://doi.org/10.1093/icvts/ivu165>
- Mueller, X. M., Mallabiabrena, I., Mucciolo, G., & von Segesser, L. K. (2002). Optimized venous return with a self-expanding cannula: from computational fluid dynamics to clinical application. *Interactive CardioVascular and Thoracic Surgery*, 1(1), 23-27. [https://doi.org/10.1016/S1569-9293\(02\)00006-3](https://doi.org/10.1016/S1569-9293(02)00006-3)
- Naruka, V., Hartley, P., Kyriazis, P. G., Liu, G., Chacko, J., Afoke, J., & Punjabi, P. P. (2022). Chapter 3 - Progress in Cardiovascular Perfusion and Technology. In J. H. Karimov, K. Fukamachi, & M. Gillinov (Eds.), *Advances in Cardiovascular*

Technology (pp. 23-40). Academic Press.

<https://doi.org/https://doi.org/10.1016/B978-0-12-816861-5.00024-1>

National Institutes of Health, N. (2024). *COVID-19 Treatment Guidelines Panel.*

Coronavirus Disease 2019 (COVID-19) Treatment Guidelines. Retrieved 23
from <https://www.covid19treatmentguidelines.nih.gov/>

Neidlin, M., Jansen, S., Moritz, A., Steinseifer, U., & Kaufmann, T. A. (2014). Design modifications and computational fluid dynamic analysis of an outflow cannula for cardiopulmonary bypass. *Ann Biomed Eng*, 42(10), 2048-2057.

<https://doi.org/10.1007/s10439-014-1064-y>

Nezami, F. R., Khodae, F., Edelman, E. R., & Keller, S. P. (2021). A Computational Fluid Dynamics Study of the Extracorporeal Membrane Oxygenation-Failing Heart Circulation. *ASAIO J*, 67(3), 276-283.

<https://doi.org/10.1097/MAT.0000000000001221>

Nguyen Thi, B. P., Duy Nguyen, B. T., Jeong, I.-S., & Kim, J. F. (2022).

Hemocompatibility challenge of membrane oxygenator for artificial lung technology. *Acta Biomaterialia*, 152, 19-46.

<https://doi.org/https://doi.org/10.1016/j.actbio.2022.09.003>

Nguyen, T. P., Phan, X. T., Nguyen, T. H., Huynh, D. Q., Tran, L. T., Pham, H. M., Nguyen, T. N., Kieu, H. T., & Ngoc Pham, T. T. (2022). Major Bleeding in Adults Undergoing Peripheral Extracorporeal Membrane Oxygenation (ECMO): Prognosis and Predictors. *Crit Care Res Pract*, 2022, 5348835.

<https://doi.org/10.1155/2022/5348835>

Nobach, H., & Bodenschatz, E. (2009). Limitations of accuracy in PIV due to individual variations of particle image intensities. *Experiments in Fluids*, 47(1), 27-38.

<https://doi.org/10.1007/s00348-009-0627-4>

Noe, D. A., Weedn, V., & Bell, W. R. (1984). Direct spectrophotometry of serum hemoglobin: an Allen correction compared with a three-wavelength polychromatic analysis. *Clin Chem*, 30(5), 627-630.

O'Brien, C., Monteagudo, J., Schad, C., Cheung, E., & Middlesworth, W. (2017). Centrifugal pumps and hemolysis in pediatric extracorporeal membrane

- oxygenation (ECMO) patients: An analysis of Extracorporeal Life Support Organization (ELSO) registry data. *J Pediatr Surg*, 52(6), 975-978.
<https://doi.org/10.1016/j.jpedsurg.2017.03.022>
- Omar, H. R., Mirsaeidi, M., Socias, S., Sprenger, C., Caldeira, C., Camporesi, E. M., & Mangar, D. (2015). Plasma Free Hemoglobin Is an Independent Predictor of Mortality among Patients on Extracorporeal Membrane Oxygenation Support. *PLoS One*, 10(4), e0124034. <https://doi.org/10.1371/journal.pone.0124034>
- Park, D., Kim, Y.-C., Cho, S. H., Kim, J., & Ahn, J. H. (2022). Interrupted Incision Fasciotomy for Acute Compartment Syndrome After Extracorporeal Membrane Oxygenation: Surgical Technique with a Report of Two Cases. *Orthopaedic Surgery*, 14(1), 169-173. <https://doi.org/https://doi.org/10.1111/os.13177>
- Patel, K., Palanzo, D., Brehm, C., Myers, J. L., & Ündar, A. (2023). Hemodynamic evaluation of cannulas for ECMO. In *Cardiopulmonary Bypass* (pp. 847-865). <https://doi.org/10.1016/b978-0-443-18918-0.00054-1>
- Paulsen, M. J., Orizondo, R., Le, D., Rojas-Pena, A., & Bartlett, R. H. (2013). A simple, standard method to characterize pressure/flow performance of vascular access cannulas. *ASAIO J*, 59(1), 24-29.
<https://doi.org/10.1097/MAT.0b013e3182746401>
- Pavlushkov, E., Berman, M., & Valchanov, K. (2017). Cannulation techniques for extracorporeal life support. *Ann Transl Med*, 5(4), 70.
<https://doi.org/10.21037/atm.2016.11.47>
- Peek, G. J., Clemens, F., Elbourne, D., Firmin, R., Hardy, P., Hibbert, C., Killer, H., Mugford, M., Thalanany, M., Tiruvoipati, R., Truesdale, A., & Wilson, A. (2006). CESAR: conventional ventilatory support vs extracorporeal membrane oxygenation for severe adult respiratory failure. *BMC Health Serv Res*, 6, 163.
<https://doi.org/10.1186/1472-6963-6-163>
- Peek, G. J., Mugford, M., Tiruvoipati, R., Wilson, A., Allen, E., Thalanany, M. M., Hibbert, C. L., Truesdale, A., Clemens, F., Cooper, N., Firmin, R. K., & Elbourne, D. (2009). Efficacy and economic assessment of conventional ventilatory support versus extracorporeal membrane oxygenation for severe adult

- respiratory failure (CESAR): a multicentre randomised controlled trial. *Lancet*, 374(9698), 1351-1363. [https://doi.org/10.1016/s0140-6736\(09\)61069-2](https://doi.org/10.1016/s0140-6736(09)61069-2)
- Peek, G. J., Wong, K., Morrison, C., Killer, H. M., & Firmin, R. K. (1999). Tubing failure during prolonged roller pump use: a laboratory study. *Perfusion*, 14(6), 443-452. <https://doi.org/10.1177/026765919901400607>
- Polito, A., Barrett, C. S., Wypij, D., Rycus, P. T., Netto, R., Cogo, P. E., & Thiagarajan, R. R. (2013). Neurologic complications in neonates supported with extracorporeal membrane oxygenation. An analysis of ELSO registry data. *Intensive Care Med*, 39(9), 1594-1601. <https://doi.org/10.1007/s00134-013-2985-x>
- Pooboni, S. K., & Gulla, K. M. (2021). Vascular access in ECMO. *Indian J Thorac Cardiovasc Surg*, 37(Suppl 2), 221-231. <https://doi.org/10.1007/s12055-020-00999-w>
- Post, F. H., & van Walsum, T. (1993). Fluid Flow Visualization. In H. Hagen, H. Müller, & G. M. Nielson (Eds.), *Focus on Scientific Visualization* (pp. 1-40). Springer Berlin Heidelberg. https://doi.org/10.1007/978-3-642-77165-1_1
- Pozo Álvarez, A. (2021a). Cardiac Flow Visualization Techniques. In A. Pozo Álvarez (Ed.), *Fluid Mechanics Applied to Medicine: Cardiac Flow Visualization Techniques* (pp. 45-58). Springer International Publishing. https://doi.org/10.1007/978-3-030-60389-2_4
- Pozo Álvarez, A. (2021b). Techniques for the Validation of Numerical Models. In A. Pozo Álvarez (Ed.), *Fluid Mechanics Applied to Medicine: Cardiac Flow Visualization Techniques* (pp. 59-88). Springer International Publishing. https://doi.org/10.1007/978-3-030-60389-2_5
- Punjabi, P. P., & Taylor, K. M. (2013). The science and practice of cardiopulmonary bypass: From cross circulation to ECMO and SIRS. *Glob Cardiol Sci Pract*, 2013(3), 249-260. <https://doi.org/10.5339/gcsp.2013.32>
- Rabby, M. G., Shupti, S. P., & Molla, M. M. (2014). Pulsatile Non-Newtonian Laminar Blood Flows through Arterial Double Stenoses. *Journal of Fluids*, 2014, 757902. <https://doi.org/10.1155/2014/757902>

- Radakovic, D., Hamouda, K., Penov, K., Bening, C., Sayed, S., Gietzen, C., Leyh, R. G., & Aleksic, I. (2021). Central Versus Peripheral Arterial Cannulation for Venous-Arterial Extracorporeal Membrane Oxygenation in Post-Cardiotomy Patients. *ASAIO J*, 67(1), 67-73. <https://doi.org/10.1097/MAT.0000000000001202>
- Raffa, G. M., Kowalewski, M., Brodie, D., Ogino, M., Whitman, G., Meani, P., Pilato, M., Arcadipane, A., Delnoij, T., Natour, E., Gelsomino, S., Maessen, J., & Lorusso, R. (2019). Meta-Analysis of Peripheral or Central Extracorporeal Membrane Oxygenation in Postcardiotomy and Non-Postcardiotomy Shock. *Ann Thorac Surg*, 107(1), 311-321. <https://doi.org/10.1016/j.athoracsur.2018.05.063>
- Rasooli, R., & Pekkan, K. (2019). Heart valve inspired and multi-stream aortic cannula: Novel designs for cardiopulmonary bypass improvement in neonates. *Artif Organs*, 43(10), E233-E248. <https://doi.org/10.1111/aor.13462>
- Reeb, J., Olland, A., Renaud, S., Lejay, A., Santelmo, N., Massard, G., & Falcoz, P. E. (2016). Vascular access for extracorporeal life support: tips and tricks. *J Thorac Dis*, 8(Suppl 4), S353-363. <https://doi.org/10.21037/jtd.2016.04.42>
- Reed, W. A., & Kittle, C. F. (1958). Survival rate and metabolic acidosis after prolonged extracorporeal circulation with total cardiopulmonary bypass. *Ann Surg*, 148(2), 219-225. <https://doi.org/10.1097/00000658-195808000-00010>
- Ricci, Z. (2018). Hemolysis during pediatric cardiac surgery: an old issue with renewed concerns. *Journal of Laboratory and Precision Medicine*, 3, 13-13. <https://doi.org/10.21037/jlpm.2018.01.13>
- Roch, A., Lepaul-Ercole, R., Grisoli, D., Bessereau, J., Brissy, O., Castanier, M., Dizier, S., Forel, J.-M., Guervilly, C., Gariboldi, V., Collart, F., Michelet, P., Perrin, G., Charrel, R., & Papazian, L. (2010). Extracorporeal membrane oxygenation for severe influenza A (H1N1) acute respiratory distress syndrome: a prospective observational comparative study. *Intensive Care Medicine*, 36(11), 1899-1905. <https://doi.org/10.1007/s00134-010-2021-3>
- Roeleveld, P. P., & Mendonca, M. (2019). Neonatal Cardiac ECMO in 2019 and Beyond. *Front Pediatr*, 7, 327. <https://doi.org/10.3389/fped.2019.00327>

- Ruggeri, Z. M., Orje, J. N., Habermann, R., Federici, A. B., & Reininger, A. J. (2006). Activation-independent platelet adhesion and aggregation under elevated shear stress. *Blood*, *108*(6), 1903-1910. <https://doi.org/10.1182/blood-2006-04-011551>
- Ruggeri, Z. M., Orje, J. N., Habermann, R., Federici, A. B., & Reininger, A. J. (2006). Activation-independent platelet adhesion and aggregation under elevated shear stress. *Blood*, *108*(6), 1903-1910. <https://doi.org/10.1182/blood-2006-04-011551>
- Rupprecht, L., Lunz, D., Philipp, A., Lubnow, M., & Schmid, C. (2015). Pitfalls in percutaneous ECMO cannulation. *Heart Lung Vessel*, *7*(4), 320-326.
- Ruszel, N., Kiełbowski, K., Piotrowska, M., Kubisa, M., Grodzki, T., Wójcik, J., & Kubisa, B. (2021). Central, peripheral ECMO or CPB? Comparison between circulatory support methods used during lung transplantation. *Journal of Cardiothoracic Surgery*, *16*(1), 341. <https://doi.org/10.1186/s13019-021-01719-0>
- Sameshima, N., Yamashita, A., Sato, S., Matsuda, S., Matsuura, Y., & Asada, Y. (2014). The values of wall shear stress, turbulence kinetic energy and blood pressure gradient are associated with atherosclerotic plaque erosion in rabbits. *J Atheroscler Thromb*, *21*(8), 831-838. <https://doi.org/10.5551/jat.23093>
- Schnürer, C., Hager, M., Györi, G., Velik-Salchner, C., Moser, P. L., Laufer, G., Lorenz, I. H., & Kolbitsch, C. (2011a). Evaluation of aortic cannula jet lesions in a porcine cardiopulmonary bypass (CPB) model. *The Journal of cardiovascular surgery*, *52*(1), 105-109. <http://europepmc.org/abstract/MED/21224818>
- Schnürer, C., Hager, M., Györi, G., Velik-Salchner, C., Moser, P. L., Laufer, G., Lorenz, I. H., & Kolbitsch, C. (2011b). Evaluation of aortic cannula jet lesions in a porcine cardiopulmonary bypass (CPB) model. *J Cardiovasc Surg (Torino)*, *52*(1), 105-109.
- Schwarz, E. L., Pegolotti, L., Pfaller, M. R., & Marsden, A. L. (2023). Beyond CFD: Emerging methodologies for predictive simulation in cardiovascular health and disease. *Biophysics Reviews*, *4*(1), 011301. <https://doi.org/10.1063/5.0109400>
- Seldinger, S. I. (1953). Catheter Replacement of the Needle in Percutaneous Arteriography: A new technique. *Acta Radiologica*, *39*(5), 368-376. <https://doi.org/10.3109/00016925309136722>

- Severinghaus, J. W. (1979). Simple, accurate equations for human blood O₂ dissociation computations. *J Appl Physiol Respir Environ Exerc Physiol*, 46(3)(0161-7567 (Print)). <https://doi.org/10.1152/jappl.1979.46.3.599>
- Shoskes, A., Migdady, I., Rice, C., Hassett, C., Deshpande, A., Price, C., Hernandez, A. V., & Cho, S. M. (2020). Brain Injury Is More Common in Venoarterial Extracorporeal Membrane Oxygenation Than Venovenous Extracorporeal Membrane Oxygenation: A Systematic Review and Meta-Analysis. *Crit Care Med*, 48(12), 1799-1808. <https://doi.org/10.1097/CCM.0000000000004618>
- Shuib, A., Hoskins, P., & Easson, W. (2011). Experimental investigation of particle distribution in a flow through a stenosed artery. *Journal of Mechanical Science and Technology*, 25(2), 357-364. <https://doi.org/10.1007/s12206-010-1232-4>
- Siegel, P. M., Chalupsky, J., Olivier, C. B., Bojti, I., Pooth, J.-S., Trummer, G., Bode, C., & Diehl, P. (2022). Early platelet dysfunction in patients receiving extracorporeal membrane oxygenation is associated with mortality. *Journal of Thrombosis and Thrombolysis*, 53(3), 712-721. <https://doi.org/10.1007/s11239-021-02562-9>
- Siegel, P. M., Chalupsky, J., Olivier, C. B., Bojti, I., Pooth, J. S., Trummer, G., Bode, C., & Diehl, P. (2022). Early platelet dysfunction in patients receiving extracorporeal membrane oxygenation is associated with mortality. *J Thromb Thrombolysis*, 53(3), 712-721. <https://doi.org/10.1007/s11239-021-02562-9>
- Simon, F., Oberhuber, A., Floros, N., Busch, A., Wagenhäuser, M. U., Schelzig, H., & Duran, M. (2018). Acute Limb Ischemia-Much More Than Just a Lack of Oxygen. *Int J Mol Sci*, 19(2). <https://doi.org/10.3390/ijms19020374>
- Simons, J., Doddema, A. R., Körver, E. P. J., di Mauro, M., Agricola, S., Smets, J., Metz, R., Mariani, S., De Piero, M. E., Matteucci, M., Romeo, J., Ravaux, J. M., van Mook, W. N. K. A., Mees, B. M. E., & Lorusso, R. (2023). Novel cannulation strategy with a bidirectional cannula for distal limb perfusion during peripheral veno-arterial extracorporeal life support: A preliminary, single-centre study. *Perfusion*, 38(1_suppl), 44-53. <https://doi.org/10.1177/02676591231159565>

- Simons, J., Mees, B., MacLaren, G., Fraser, J. F., Zaaqoq, A. M., Cho, S.-M., Patel, B. M., Brodie, D., Bělohávek, J., Belliato, M., Jung, J.-S., Salazar, L., Meani, P., Mariani, S., Di Mauro, M., Yannopoulos, D., Broman, L. M., Chen, Y.-S., Riera, J., . . . Lorusso, R. (2024). Evolution of distal limb perfusion management in adult peripheral venoarterial extracorporeal membrane oxygenation with femoral artery cannulation. *Perfusion*, *39*(1_suppl), 23S-38S. <https://doi.org/10.1177/02676591241236650>
- Sinard, J. M., Merz, S. I., Hatcher, M. D., Montoya, J. P., & Bartlett, R. H. (1991). Evaluation of extracorporeal perfusion catheters using a standardized measurement technique--the M-number. *ASAIO Trans*, *37*(2), 60-64.
- Singh, S., Trikha, S. P., & Lewis, J. (2004). Acute compartment syndrome. *Current Orthopaedics*, *18*(6), 468-476. <https://doi.org/10.1016/j.cuor.2004.12.006>
- Sotiropoulos, F. (2012). Computational Fluid Dynamics for Medical Device Design and Evaluation: Are We There Yet? *Cardiovascular Engineering and Technology*, *3*(2), 137-138. <https://doi.org/10.1007/s13239-012-0095-5>
- Stanley, T. H. (2013). A tribute to Dr Willem J. Kolff: innovative inventor, physician, scientist, bioengineer, mentor, and significant contributor to modern cardiovascular surgical and anesthetic practice. *J Cardiothorac Vasc Anesth*, *27*(3), 600-613. <https://doi.org/10.1053/j.jvca.2012.11.011>
- Stephens, N. A., Chartan, C. A., Gazzaneo, M. C., Thomas, J. A., Das, S., Mallory, G. B., Jr., Melicoff, E., Vogel, A. M., Parker, A., Hermes, E., Heinle, J. S., McKenzie, E. D., & Coleman, R. D. (2023). Use of Berlin EXCOR cannulas in both venovenous and venoarterial central extracorporeal membrane oxygenation configurations overcomes the problem of cannula instability while bridging infants and young children to lung transplant. *JTCVS Tech*, *18*, 111-120. <https://doi.org/10.1016/j.xjtc.2023.02.004>
- Stoney, W. S. (2009). Evolution of Cardiopulmonary Bypass. *Circulation*, *119*(21), 2844-2853. <https://doi.org/10.1161/CIRCULATIONAHA.108.830174>
- Swaminathan, M., Grocott, H. P., Mackensen, G. B., Podgoreanu, M. V., Glower, D. D., & Mathew, J. P. (2007). The “Sandblasting” Effect of Aortic Cannula on Arch

- Atheroma During Cardiopulmonary Bypass. *Anesthesia & Analgesia*, 104(6).
https://journals.lww.com/anesthesia-analgesia/fulltext/2007/06000/the_sandblasting_effect_of_aortic_cannula_on_7.aspx
- Takayama, H., Landes, E., Truby, L., Fujita, K., Kirtane, A. J., Mongero, L., Yuzefpolskaya, M., Colombo, P. C., Jorde, U. P., Kurlansky, P. A., Takeda, K., & Naka, Y. (2015). Feasibility of smaller arterial cannulas in venoarterial extracorporeal membrane oxygenation. *J Thorac Cardiovasc Surg*, 149(5), 1428-1433. <https://doi.org/10.1016/j.jtcvs.2015.01.042>
- Tang, D., Teng, Z., Canton, G., Yang, C., Ferguson, M., Huang, X., Zheng, J., Woodard, P. K., & Yuan, C. (2009). Sites of rupture in human atherosclerotic carotid plaques are associated with high structural stresses: an in vivo MRI-based 3D fluid-structure interaction study. *Stroke*, 40(10), 3258-3263.
<https://doi.org/10.1161/strokeaha.109.558676>
- Tangelder, G. J., Slaaf, D. W., Muijtjens, A. M., Arts, T., oude Egbrink, M. G., & Reneman, R. S. (1986). Velocity profiles of blood platelets and red blood cells flowing in arterioles of the rabbit mesentery. *Circulation Research*, 59(5), 505-514. <https://doi.org/10.1161/01.RES.59.5.505>
- Thielicke, W., & Sonntag, R. (2021). Particle Image Velocimetry for MATLAB: Accuracy and enhanced algorithms in PIVlab. *Journal of Open Research Software*, 9(1). <https://doi.org/10.5334/jors.334>
- Thomas, S. A., Empaling, S., Darlis, N., Osman, K., Dillon, J., Taib, I., & Md Khudzari, A. Z. (2017). Computational modelling of flow and tip variations of aortic cannulae in cardiopulmonary bypass procedure. *IOP Conference Series: Materials Science and Engineering*, 243(1), 012021.
<https://doi.org/10.1088/1757-899X/243/1/012021>
- Tonna, J. E., Abrams, D., Brodie, D., Greenwood, J. C., Rubio Mateo-Sidron, J. A., Usman, A., & Fan, E. (2021). Management of Adult Patients Supported with Venovenous Extracorporeal Membrane Oxygenation (VV ECMO): Guideline from the Extracorporeal Life Support Organization (ELSO). *ASAIO Journal*,

67(6).

https://journals.lww.com/asaiojournal/fulltext/2021/06000/management_of_adult_patients_supported_with.1.aspx

Tonna, J. E., Boonstra, P. S., MacLaren, G., Paden, M., Brodie, D., Anders, M., Hoskote, A., Ramanathan, K., Hyslop, R., Fanning, J. J., Rycus, P., Stead, C., Barrett, N. A., Mueller, T., Gómez, R. D., Malhotra Kapoor, P., Fraser, J. F., Bartlett, R. H., Alexander, P. M. A., . . . on behalf of the Extracorporeal Life Support Organization Member Centers, G. (2024). Extracorporeal Life Support Organization Registry International Report 2022: 100,000 Survivors. *ASAIO Journal*, 70(2).

https://journals.lww.com/asaiojournal/fulltext/2024/02000/extracorporeal_life_support_organization_registry.9.aspx

Trieu, N. H. K., Phan, X. T., Tran, L. T., Pham, H. M., Huynh, D. Q., Nguyen, T. M., Mai, A. T., Du, Q. Q. M., Nguyen, B. X., & Pham, T. T. N. (2023). Risk factors for cannula-associated arterial thrombosis following extracorporeal membrane oxygenation support: a retrospective study. *Acute Crit Care*, 38(3), 315-324.

<https://doi.org/10.4266/acc.2023.00500>

Ündar, A., Wang, S., Özyüksel, A., & Rossano, J. W. (2018). Chapter 9 - Pediatric devices. In S. D. Gregory, M. C. Stevens, & J. F. Fraser (Eds.), *Mechanical Circulatory and Respiratory Support* (pp. 271-297). Academic Press.

<https://doi.org/https://doi.org/10.1016/B978-0-12-810491-0.00009-6>

Ura, M., Sakata, R., Nakayama, Y., & Goto, T. (2000). Ultrasonographic demonstration of manipulation-related aortic injuries after cardiac surgery. *Journal of the American College of Cardiology*, 35(5), 1303-1310.

[https://doi.org/https://doi.org/10.1016/S0735-1097\(00\)00548-9](https://doi.org/https://doi.org/10.1016/S0735-1097(00)00548-9)

Vercaemst, L. (2008). Hemolysis in cardiac surgery patients undergoing cardiopulmonary bypass: a review in search of a treatment algorithm. *J Extra Corpor Technol*, 40(4), 257-267.

von Segesser, L., Marinakis, S., Berdajs, D., Ferrari, E., Wilhelm, M., & Maisano, F. (2016). Prevention and therapy of leg ischaemia in extracorporeal life support

- and extracorporeal membrane oxygenation with peripheral cannulation. *Swiss Medical Weekly*, 146(1718), w14304. <https://doi.org/10.4414/smw.2016.14304>
- Vuylsteke, A., Brodie, D., Combes, A., Fowles, J.-a., & Peek, G. (2017). A brief history of ECMO. In A. Vuylsteke, D. Brodie, A. Combes, J.-a. Fowles, & G. Peek (Eds.), *ECMO in the Adult Patient* (pp. 1-8). Cambridge University Press. [https://doi.org/DOI: 10.1017/9781139088251.002](https://doi.org/DOI:10.1017/9781139088251.002)
- Wang, J., Wang, S., Song, Y., Huang, M., Cao, W., Liu, S., Chen, S., Li, X., Liu, M., & He, Y. (2023). The Preventive Effect of Distal Perfusion Catheters on Vascular Complications in Patients Undergoing Venous Artery Extracorporeal Membrane Oxygenation. *J Multidiscip Healthc*, 16, 963-970. <https://doi.org/10.2147/jmdh.S398704>
- Wang, S., Moroi, M., Brehm, C. E., Kunselman, A. R., & Undar, A. (2018). In Vitro Hemodynamic Evaluation of an Adult Pulsatile Extracorporeal Membrane Oxygenation System. *Artif Organs*, 42(9), E234-E245. <https://doi.org/10.1111/aor.13156>
- White, J. K., Jagannath, A., Titus, J., Yoneyama, R., Madsen, J., & Agnihotri, A. K. (2009). Funnel-tipped aortic cannula for reduction of atheroemboli. *Ann Thorac Surg*, 88(2), 551-557. <https://doi.org/10.1016/j.athoracsur.2009.04.108>
- Wickramarachchi, A., Gregory, S. D., Burrell, A. J. C., & Khamooshi, M. (2024). Flow characterization of Maquet and Bio-Medicus multi-stage drainage cannulae during venoarterial extracorporeal membrane oxygenation. *Computers in Biology and Medicine*, 171, 108135. <https://doi.org/https://doi.org/10.1016/j.compbiomed.2024.108135>
- Wild, K. T., Rintoul, N., Kattan, J., & Gray, B. (2020). Extracorporeal Life Support Organization (ELSO): Guidelines for Neonatal Respiratory Failure. *ASAIO Journal*, 66(5). https://journals.lww.com/asaiojournal/fulltext/2020/05000/extracorporeal_life_support_organization_elso_.1.aspx
- Woelke, E., Mager, I., Schmitz-Rode, T., Steinseifer, U., & Clauser, J. C. (2021). Validation of a Miniaturized Test Loop for the Assessment of Human Blood

- Damage by Continuous-Flow Left-Ventricular Assist Devices. *Ann Biomed Eng*, 49(12), 3165-3175. <https://doi.org/10.1007/s10439-021-02849-1>
- Wong, J. K., Melvin, A. L., Joshi, D. J., Lee, C. Y., Archibald, W. J., Angona, R. E., Tchantchaleishvili, V., Massey, H. T., Hicks, G. L., & Knight, P. A. (2017). Cannulation-Related Complications on Venous-Arterial Extracorporeal Membrane Oxygenation: Prevalence and Effect on Mortality. *Artif Organs*, 41(9), 827-834. <https://doi.org/10.1111/aor.12880>
- Wurzinger, L. J., Opitz, R., Blasberg, P., & Schmid-Schönbein, H. (1985). Platelet and coagulation parameters following millisecond exposure to laminar shear stress. *Thromb Haemost*, 54(2), 381-386.
- Yarborough, K. A., Mockros, L. F., & John Lewis, F. (1966). Hydrodynamic hemolysis in extracorporeal machines. *The Journal of Thoracic and Cardiovascular Surgery*, 52(4), 550-557. [https://doi.org/10.1016/s0022-5223\(19\)43399-0](https://doi.org/10.1016/s0022-5223(19)43399-0)
- Yeo, J. H., Sung, K. H., Chung, C. Y., Lee, K. M., Choi, Y., Kim, T. G., Kwon, S. S., Lee, S. Y., & Park, M. S. (2015). Acute compartment syndrome after extracorporeal membrane oxygenation. *J Orthop Sci*, 20(2), 444-448. <https://doi.org/10.1007/s00776-013-0484-0>
- Zimpfer, D., Heinisch, B., Czerny, M., Hoelzenbein, T., Taghavi, S., Wolner, E., & Grimm, M. (2006). Late vascular complications after extracorporeal membrane oxygenation support. *Ann Thorac Surg*, 81(3), 892-895. <https://doi.org/10.1016/j.athoracsur.2005.09.066>